FINAL REPORT

Improving Understanding of the Fate and Transport of Munitions Constituents to Enhance Sustainability of Operational Ranges

SERDP Project ER-1688

MAY 2015

Herbert Allen
Dominic Di Toro
Dave Ta Fu Kuo
Rosalina González Forero
Kyle Michelson
Andrew Miglino
University of Delaware

Ronald Checkai
Roman Kuperman
Michael Simini
U.S. Army Edgewood Chemical Biological Center

Jalal Hawari
National Research Council Canada
Biotechnology Research Institute

SERDP
DOD ▪ EPA ▪ DOE

REPORT DOCUMENTATION PAGE

Form Approved
OMB No. 0704-0188

PLEASE DO NOT RETURN YOUR FORM TO THE ABOVE ADDRESS.

1. REPORT DATE *(DD-MM-YYYY)*	2. REPORT TYPE	3. DATES COVERED *(From - To)*
02/05/2015	Final Report	June 2009 - December 2014

4. TITLE AND SUBTITLE

Improving Understanding of the Fate and Transport of Munitions Constituents to Enhance Sustainability of Operational Ranges

5a. CONTRACT NUMBER

W912HQ-09-C-0031

5b. GRANT NUMBER

5c. PROGRAM ELEMENT NUMBER

6. AUTHOR(S)

Herbert E. Allen, Dominic M. DiToro, Dave T.F. Kuo, Rosalina G. Forero, Kyle Michelson, Andrew Miglino, Ronald T. Checkai, Roman G. Kuperman, Michael Simini, and Jalal Hawari.

5d. PROJECT NUMBER

ER-1688

5e. TASK NUMBER

5f. WORK UNIT NUMBER

7. PERFORMING ORGANIZATION NAME(S) AND ADDRESS(ES)

University of Delaware
Department of Civil and Environmental Engineering
Newark, Delaware 19716

8. PERFORMING ORGANIZATION REPORT NUMBER

ER-1688

9. SPONSORING/MONITORING AGENCY NAME(S) AND ADDRESS(ES)

Strategic Environmental Research and Development Program
4800 Mark Center Drive, Suite 17D08
Alexandria, VA 22350-3605

10. SPONSOR/MONITOR'S ACRONYM(S)

SERDP

11. SPONSOR/MONITOR'S REPORT NUMBER(S)

ER-1688

12. DISTRIBUTION/AVAILABILITY STATEMENT

Approved for public release; distribution is unlimited.

13. SUPPLEMENTARY NOTES

14. ABSTRACT

The objective was to develop models supported by appropriate data. The project team generated data and developed a model for the kinetics of adsorption and desorption of 2,4-dinitrotoluene and nitroglycerin to and from the nitrocellulose matrix itself. Additionally, they developed a model for the partitioning of RDX, HMX, TNT, nitroglycerin, 2,4-dinitrotoluene, and nitroguanadine and mixtures of these munitions constituents to soils of varying physical/chemical characteristics. They developed and used a chemical probe to determine the magnitude of clay mineral binding sites and ascertained the soil composition responsible for irreversible binding. They modeled the results using polyparameter partitioning models, and models for irreversible bonding using soils spanning a variety of properties including soils typical of those found at operational ranges. They provided initial validation of the models developed in this project by comparing model results to those determined in soil column studies.

15. SUBJECT TERMS

16. SECURITY CLASSIFICATION OF:			17. LIMITATION OF ABSTRACT	18. NUMBER OF PAGES	19a. NAME OF RESPONSIBLE PERSON
a. REPORT	b. ABSTRACT	c. THIS PAGE		219	Herbert Allen
					19b. TELEPHONE NUMBER *(Include area code)* 302-831-8449

Reset

Table of Contents

List of Figures

List of Tables

List of Acronyms

n_F: Freundlich isotherm exponential constant
A: interfacial area
ACN: acetonitrile
ACS: American Chemical Society
ASTM: American Society for Testing and Materials
BRI: National Research Council Canada, Biotechnology Research Institute
C_{Ads}: aqueous concentration during adsorption
CEC: cation exchange capacity
C_0: recovery-adjusted initial concentration
C^N: normalized concentration
Cs: cesium
D: dissolved
D: desorption
D: effective diffusivity
DI: deionized (water)
2,4-DNT: 2,4-dinitrotoluene
DNT: 2,4-dinitrotoluene
DOM: dissolved organic matter
ECBC: U.S. Army Edgewood Chemical Biological Center
EDA: electron donor-acceptor
EDT: Esterline Defense Technologies
EPA: U.S. Environmental Protection Agency
FeOx: oxalate extractable iron
f_{clay}: fraction clay size particle in soil
f_d: fraction dissolved
f_{OC}: fraction of organic carbon in the soil
f_p: fraction particulate
f_{ST}: Site transformation factor
g: acceleration due to gravity at the Earth's surface
HMX: octahydro-1,3,5,7-tetranitro-1,3,5,7-tetrazocine
HPLC: high-performance liquid chromatography
IC: ion chromatography
K_{CEC}: cation exchange capacity normalized partition coefficient
K_{clay}: clay normalized partition coefficient
K_{Cs}: partition coefficient to charge sites determined by exchangeable Cs
K_F: Freundlich isotherm partition coefficient
K_{OC}: organic carbon (OC) normalized partition coefficient
K_{OW}: octanol-water partition coefficient
K_p: partition coefficient
K_{p0} or K_{hys}: resistant (hysteretic) partition coefficient
K_{px} or K_{rev}: reversible partition coefficient
l: diffusive length
M: Matapeake soil
MC: munitions constituents
m_{sw}: soil-water ratio

N: Nevada soil
NAC: nitro aromatic compound
NC: nitrocellulose
NG: nitroglycerin
NQ: nitroguanidine
nRR: normalized reversible resistant model
OC: organic carbon
OM: organic matter
PCB: polychlorinated biphenyl
q: amount of material sorbed per gram
R: Rhydtalog soil
RF: reversibility fraction
RDX: hexahydro-1,3,5-trinitro-1,3,5-triazine
RI: reversibility index
RMSE: root mean square error
R_{NC}: ratio of nitrocellulose to water
RO: reverse osmosis
rpm: revolutions per minute
RR or R/R: reversible resistant model
SERDP: Strategic Environmental Research and Development Program
SETAC: Society of Environmental Toxicology and Chemistry
SOM: soil organic matter
STM: Site Transformation Model
TNT: 2,4,6-trinitrotoluene
TOC: total organic carbon
U Del: University of Delaware
V: volume or volumetric flow rate
w/v: weight per volume ratio

Keywords

RDX, HMX, TNT, nitroglycerin, 2,4-dinitrotoluene, nitroguanidine, nitrocellulose, partitioning, reversible partitioning, resistant partitioning, hysteresis, kinetics.

Acknowledgments

The lead Principal Investigator would particularly like to thank Dave Ta Fu Kuo, Rosalina González Forero, Andrew Miglino, and Michael Simini for their assistance in preparation of this report. Substantial portions were based on the PhD dissertations of Rosalina González Forero and Andrew Miglino. Several undergraduate and graduate students and technicians at the University of Delaware contributed to the projects. We would particularly like to acknowledge Tifany Lorena Torralba Sánchez and Craig Warren Davis, PhD candidates; Craig Dsouza, Kevin Hickey, Samantha Keulmann, and Yara Alejandra Montenegro Pinto, who were students and visiting scientists at the University of Delaware, for their contributions to this project. Dr. Morgan L. Minyard, a post-doctoral research fellow at the U.S. Army Edgewood Chemical Biological Center also contributed to laboratory studies. In particular we would like to thank Mr. Joe Domanico, Ammunition Control Officer at the U.S. Army Edgewood Chemical Biological Center who secured the munition constituents needed for this research and also delivered these materials to the University of Delaware.

Abstract

Objectives. Our overall objective was to develop models supported by appropriate data. We generated data and developed a model for the kinetics of adsorption and desorption of 2,4-dinitrotoluene and nitroglycerin to and from the nitrocellulose matrix itself. Additionally, we developed a model for the partitioning of RDX, HMX, TNT, nitroglycerin, 2,4-dinitrotoluene, and nitroguanadine and mixtures of these munitions constituents to soils of varying physical/chemical characteristics. We developed and used a chemical probe to determine the magnitude of clay mineral binding sites and ascertained the soil composition responsible for irreversible binding. We modeled the results using polyparameter partitioning models, and models for irreversible bonding using soils spanning a variety of properties including soils typical of those found at operational ranges. We provided initial validation of the models developed in this project by comparing model results to those determined in soil column studies.

Technical Approach. Partitioning of a mixture of munitions constituents to soil was studied by analyzing the effect of kinetics and reversible/resistant behavior of the munitions constituents on the adsorption-desorption to soils of varying physical/chemical characteristics. The data was collected from batch experiments conducted near 1:1 (w/v) soil to solution ratios, reflecting field conditions better than the dilute soil suspensions used in most studies. Adsorption was followed by multiple desorptions simulating rainy events to quantify the resistance of munitions constituents to desorption.

Models were built by using the measured dissolved and particulate concentrations during the adsorption-desorption of munitions constituents, and the total organic carbon and other sorption phases present in the soils. Key soil properties were selected in order to use the minimal number of input parameters providing reasonable accuracy of predictions, but reflecting a wide range of soil characteristics to provide better application of the model in the field. Twenty-five soils from different places in America and Europe were used to isolate the effects of independent physical and chemical characteristics that affect sorption.

One of the models analyzed in this research was the reversible/resistant model. The innovation was to apply it to the partitioning of mixtures of munitions constituents in different soil types taking into account the effect of kinetics and the electrolyte matrix in the adsorption and desorption steps. Results indicate that the model is sufficiently simple and flexible that can be used in the adsorption/desorption of the mixture of munitions constituents studied, because the fitting of the data was excellent even given the variation of time of equilibration and desorption and of the soil matrices.

In addition to the reversible/resistant model, a multilinear sorption model was developed to predict partitioning of munitions constituents to soils by incorporating different sorption sites in addition to organic matter to improve the predictions. Clay minerals sites, cation exchange capacity and oxalate extractable iron were included in the partitioning model. The clay sites were used in the multilinear model in alternative forms: the particle size fraction, the cation exchange capacity and charge sites content. To determine the charge sites, a method based on cesium sorption was refined and applied. This is the first time that this probe has been used for a wide range of soils with various characteristics to develop a model incorporating specific sorption sites for the sorption of mixtures of munitions constituents.

To provide initial validation of the results obtained in the batch equilibration studies we conducted a flow-through column study of TNT and RDX. The major objective was to determine

if the resistant binding of TNT, but not of RDX, that was found in batch studies was also found in a flow-through column. This is the first application of the reversible-resistant theory to flow-through columns and by extension to percolation of compounds though soil in the field.

The presence of the nitrocellulose matrix complicates modeling of munitions constituents release from propellant and into soil solution. In addition to the dissolution of the soluble components, the role of adsorption to nitrocellulose, and desorption from nitrocellulose need to be taken into account. No adsorption/desorption kinetic model of munitions constituents with the nitrocellulose matrix currently exists. In this study the kinetics of sorption and desorption of 2,4-dinitrotoluene and nitroglycerin with nitrocellulose was measured. These data can then be compared to previous studies with assembled propellants to develop more appropriate models for sorption and desorption of 2,4-dinitrotoluene and nitroglycerin with nitrocellulose.

Results. Partitioning of munitions constituents to a number of soils indicated that organic matter in the soil was the dominant site responsible for their partitioning. Partitioning to clay was modeled as a second sorption site which could be modeled equally well by the clay size fraction of the soil or the cation exchange capacity. For soils containing little organic matter inclusion of clay provided significant improvement except for nitroglycerin. The cesium exchange method gave better fitting of the multilinear model, but the improvement was not enough to recommend its use due its cumbersome procedure. Further improvement was achieved by a trilinear model that incorporated partitioning to organic matter, clay and oxalate extractable iron. Modeling of partitioning reversibility showed that the reversibility of partitioning varied considerably among the munition constituents. The irreversible partitioning was related to binding to organic matter in the soil. The flow-through column study indicated that a portion of the RDX remained on the soil following lengthy passage of electrolyte not containing RDX. Although the batch equilibration tests indicated complete reversibility, a small non-zero resistant portion would not have been distinguished in the test.

Benefits. The study of partitioning to nitrocellulose provides new understanding of the mechanism that leads to prolong leaching of munition constituents from propellant particles. These results will permit new modeling of constituent release using a mechanistic rather than an observational approach.

The study of partitioning of munition constituents to soil has provided partition coefficients based on 1, 2, and 3 site models based on results for a large number of soils. The models which include partitioning to organic matter, clay, and iron oxide provide improved estimates of partitioning applicable to soils that vary widely in their properties. Consideration of both resistant partitioning as well as reversible partitioning provides constants that can be used to provide more accurate prediction of aqueous concentrations of these chemicals when coupled with hydrological software. Results of a column flow experiment show that a small irreversibly bound fraction of chemical, not observable in batch testing, may sequester a significant amount of material.

Objectives

The objectives of this project were to (1) investigate the rate of release of nitroglycerin (NG) and 2,4-dinitrotoluene (2,4-DNT) from nitrocellulose (NC), and (2) improve our understanding of the fate and transport parameters of munitions constituents in multiple soil types that typically are found at operational ranges.

Partitioning of MC to Soil. Partitioning of compounds to soil provides a primary mechanism for controlling their passage to groundwater and also controls their bioavailability. Our objective was to determine the partitioning of RDX, HMX, TNT, NG, 2,4-DNT, and NQ to soils of varying physical/chemical characteristics and to evaluate the kinetics of the sorption and desorption processes. Additionally, we wished to ascertain whether irreversible binding occurs. Modeling of the partitioning data were to use polyparameter partitioning models and models for irreversible bonding. We were to develop and use a chemical probe for determining the magnitude clay mineral binding sites. Initial validation of the models developed in this project was to be conducted by comparing model results to those determined in soil column studies.

Release of MC from NC. Because the major sources of MC are from low-order (partial) detonation and propellant discharge, the constituents are deposited as mixtures of heterogeneous particles that affect their dissolution properties. The complicating feature for propellant particle release modeling is the presence of the NC matrix that can interact with the MC and water. In addition to the dissolution of the soluble components, the role of adsorption to, and desorption from, the NC and the swelling due to the presence of water need to be taken into account. No adsorption/desorption kinetic model of the MC to NC presently exists. Our objective was to perform experiments to characterize the sorption-desorption of MC to NC, and analyze the results using appropriate diffusion and partitioning models.

Background

The fate of contaminants in the environment has been studied intensely since pollution became a public health problem. For this reason, many researchers have devoted their efforts to studying the physicochemical mechanisms of fate and transport phenomena. one group of these contaminants is the munitions constituents (MC). One cause of the contamination by MC is the result of incomplete detonation of explosives at operational ranges resulting in the heterogeneous dispersion of particulates. The toxic and mutagenic effects observed for many MC indicate a danger to biological receptors at down gradient sites [Kaplan and Kaplan, 1982; Robidoux et al., 2001; Sunahara et al., 2009]. More than 2000 sites have been identified as potentially contaminated by energetic chemicals and millions of acres of land in the United States are believed to be contaminated by MC with the costs of assessment and remediation estimated to be in the billions of dollars [U.S. General Accounting Office 2003]. In Canada military training sites are known to be associated with activities involving RDX, HMX, and TNT [Hawari and Halasz 2002]. The degree of contamination is extremely varied at these sites and the distribution is heterogeneous [Jenkins et al. 1997; Pennington 2002; Thiboutot et al. 2003]. Some MC, such as TNT, inhibit microbial activities in contaminated soil [Gong et al. 1999] and denitrifying activity decreases in response to TNT contamination [Siciliano et al. 2000].

To minimize the environmental impact and maintain the balance between the environment, the needs of the military, and human health, it is necessary to understand the physicochemical processes that control the transport and the reactivity of the MC.

To obtain scientifically sound and enhanced risk assessments at different operational military ranges, better understanding the transport and reactivity of MC will enhance assessment, in particular the adsorption and desorption of munitions constituents MC to soil, their kinetic behavior, and resistance to desorption. Doing this is difficult. Usually only partial information at specific conditions is generated. An example is the use of unrealistic soil to solution ratios, for which the application to the field is questionable. You et al. [1999] studied the effect of soil:solution ratio on the distribution of organic matter between the dissolved and particulate phases. They found that decreasing the water:soil ratio decreases the ratio of the organic carbon concentration in soil solid phase to the organic carbon concentration in soil solution phase or the partition coefficient (K_p). As most batch studies employ greater water:soil ratios, the K_p values obtained would be larger than the values that exist in the field. The K_p determines the concentration of soluble organic matter, which in turn has dramatic effects on the mobility of pollutants in the environment.

Sorption of MC to Soil. The majority of research has focused on the adsorption of MC onto soils, but not on the more environmentally relevant desorption and resistance to desorption, which ultimately determine the environmental threat of these contaminants and their transport through the groundwater. Studies of desorption of MC, also, have been focused in specific aspects of the phenomena. For example Douglas et al. [2011] studied desorption kinetics by the observation of RDX, HMX, and TNT concentrations in detonated and undetonated soil batches, where they found that explosive compounds loaded to soils through detonation take longer to reach steady state concentrations in aqueous batches than soils loaded with explosive residues through aqueous addition due to the heterogeneous interactions between explosive residues and soil particle surfaces. White et al. [2011] investigated desorption by the degree of photo-fragmentation into NO resulting from the irradiation of the explosives RDX and HMX coated on a variety of surfaces. Desorption data is sparse in the literature for many compounds, such as

nitroglycerin which is a major propellant for many munitions used at operational ranges [ARDEC 2008].

To describe the adsorption mechanism, the solid-water distribution coefficient [Schwarzenbach et al. 2003] or partition coefficient (K_p) is usually used. It is defined as the ratio of the concentration of chemical in the soil to the concentration of chemical in the aqueous phase. The partition coefficient is calculated using the following relationship:

$$K_p = C_s/C_w \quad (1)$$

where K_p is the partition coefficient (L kg^{-1}), C_s is the concentration of the compound adsorbed to the soil (mg kg^{-1}), and C_w is the concentration in the aqueous solution (mg L^{-1}). The organic matter contained in soil is generally the most important soil constituent responsible for the sorption of organic compounds. This has led to the use of the organic carbon (OC) normalized partition coefficient, K_{OC} (L kg^{-1} OC) [Schwarzenbach et al. 2003]. It has been found that for neutral hydrophobic chemicals there is a relationship between the octanol-water partition coefficient, K_{OW} (L water/L octanol), and fraction of organic carbon in the soil, f_{OC} (g organic carbon/g soil) to predict the partition coefficient:

$$K_p = K_{OC}\,(f_{OC}) = 0.63K_{OW}\,(f_{OC}) \quad (2)$$

Partition coefficients of adsorption are commonly applied to desorption. The problem with this approach is that adsorption and desorption may follow different isotherms. One example of this is presented by Sheremata et al. [2001], where the K_p of adsorption of TNT and RDX onto surface soils were from 10 to 100 times less than the K_p of desorption. Hatzinger et al. [2004] observed desorption hysteresis for TNT, HMX and RDX. Also, Xue et al. [1995] observed that in some soils a portion of the adsorbed TNT and RDX was not desorbable. They found that extensive non-singularity or hysteretic behavior was observed in the desorption isotherms. These studies indicate that there is a resistance to desorption of these chemicals and implies that the amount that is released to groundwater after a wetting event and the environmental risk of these compounds is not a function of the total amount of the compound in the soil, but of the portion of the material that is present in a desorbable form. It is important to note that these studies presented differences of adsorption and desorption partition coefficients, but they did not study the very long term effect of desorption.

The literature suggests that organic matter (OM) and certain clay size particle types are the main soil components responsible for the adsorption of MC, especially nitro aromatic compounds (NACs), and the investigators have attributed the main effect to one of these soil components depending on the conditions used in their studies. Zhang et al. [2009] found that the soil organic matter (SOM), compared to clay minerals, was the predominant soil component controlling sorption of 2,4-DNT and nitrobenzene in three Chinese soils and that the polarity and aromaticity of soil organic matter (SOM) might have important effects on sorption of NACs. They attribute the weak sorption to clay minerals to the type of exchangeable cations on the soils. Eriksson et al. [2004] concluded that in contaminated soils characterized by continuous leaching of dissolved organic matter (DOM), the formation of TNT degradation products and their preference for specific functional groups in DOM may significantly contribute to the transport of potentially toxic compounds into surface waters and groundwater. Singh et al. [2010] reported that not all the carbon is responsible for sorption of NACs. They concluded that the composition of organic matter affects sorption. In their study TNT and 2,4-DNT were sorbed in different soil organic matter (SOM) fractions: a commercial humic acid, commercial lignin, and both humic acid and

humin extracted from a compost. Their findings showed that the order of sorption of the NACs was: humic acid-commercial > humic acid compost > humin~lignin. The aliphatic component in the SOM significantly affected the sorption of nitroaromatics. Pennington et al. [2003] reported that NACs sorb more strongly to humic acid than to lignin or humin, and to the aliphatic rather than the aromatic fractions of organic matter.

Importance of Clay and Other Soil Components to the Sorption of MC. There is also extensive literature indicating that clays strongly adsorb NACs. Sheng et al. [2001] found that in the absence of OM, clays strongly sorb NACs. Michalkova et al. [2005] studied the adsorption of 2,4-DNT on tetrahedral and octahedral surfaces of dickite. They found that adsorption on the tetrahedral surface was more significant because the orientation of 2,4-DNT was coplanar with the surface plane and on the octahedral surface the 2,4-DNT molecule was placed with an inclination about 30 degrees to the surface plane. In another study montmorillonite was found to sorb up to 10 percent NACs by weight indicating a strong affinity of NACs to clay surfaces [Johnson et al., 2001]. The largest adsorption and the smallest desorption of the RDX and TNT explosives was reported to occur in peat [Falone et al. 2006]. Weissmahr et al. [1998] studied two factors controlling the ability of phyllosilicates to form complexes with nitroaromatic explosives: the N-donor properties of their siloxane oxygens and the accessibility of such sites for pi-acceptors. They found that the donor properties of siloxane oxygens are augmented by isomorphic substitution, but their accessibility for pi-acceptors depended on the steric effects of hydrated exchangeable cations. Yamamoto et al. [2004] concluded that NACs also exhibit very strong binding to clay minerals although binding is weaker for surface soils. Dontsova et al. [2009a] determined that phyllosilicate clay, organic matter and two forms of extractable iron (dithionite-citrate and acid oxalate) are important in the sorption of explosives onto soil. However, Brannon and Pennington [2002] have reported that binding to surface soils is weaker than to clay minerals.

Measurement of the Clay Content of Soil. The clay fraction of soil is most commonly defined as a particle size fraction determined by sieving or by hydrodynamic settling, for instance by the Bouyoucos [1962] method. The problem of using clay determined in this manner is that it is based on particle size, not mineralogy. The clay mineral content is rarely determined and the results for clay-size particles are sometimes used as a surrogate for the content of clay minerals. Zubkov [2009] found that the clay grain-size fractions and clay minerals are not exactly equivalent, but there is a relationship between them. Morkeh and McClemore [2012] reported that numerous studies have examined the variations in composition between different particle size fractions. The papers by Lapakko et al. [1998], Dinelli et al. [2007] and Hewson et al. [2012] are examples of that. The first one reported that the mineral surface area is dependent upon the mineralogy. Dinelli et al. [2007] found that the effects of grain-size distribution on mineralogy and geochemistry are greater in sediments that have not undergone diagenesis, compaction, or lithification. In addition they showed that some chemical indices are not affected by grain size distribution, including Ni/Al, Cr/Al, and Mg/Al ratios. Hewson et al. [2012] studied the particle size fractions from Tick Hill soil samples and they observed an intimate connection between mineralogy and texture when examining FTIR spectra.

Based on these findings; we decided to use the clay size fraction information and a specific method developed by Anderson and Sposito [1991] for measuring the contribution of permanent and variable surface-charge sites to the net surface charge density, based upon the strong preference of permanent-charge sites and low affinity of most variable-charge sites for cesium.

Cesium ions form strong surface complexes with siloxane surface groups on illite [Posner and Quirk 1964; Edwards et al. 1965] vermiculite [Barshad 1948] and montmorillonite [Weiss et al. 1990]. In addition, the low affinity of lithium for the permanent-charge sites and its strong preference for the variable-sites permits using lithium to displace cesium only from variable-charge sites, which reside in the diffuse-ion swarm on siloxane surfaces [Cebula and Ottewill 1981]. This is in agreement with Benson [1982] who observed significant differences in values of exchange constants for the same reaction on different smectites, attributing this to difference in charge densities related with the type and amount of substitution on intercrystalline sites. On the other hand Van Loon et al. [2009] studied the sorption of cesium on crushed and intact sodium bentonite, finding that in intact material the exchange sites are all available and the sorption of cesium is attributed to a reduction of the interlayer space, leading to a lower ability of the interlayer water for cation hydration. As cesium has a low hydration tendency, it tends to accumulate in the interlayer space rather than in the bulk water. This information suggests that cesium is useful to determine the maximum permanent charge sites on clays.

Effect of Electrolyte on Sorption of MC to Soil. Roberts et al. [2007] determined that, in the case of smectite clays, the affinity of NACs depends on the exchangeable cation which consequently affected the bioavailability and toxicity of the NACs. Potassium smectites have strong affinity for NACs, but calcium smectites have less affinity than the potassium ones, suggesting that small amounts of potassium smectites could reduce acute toxicity substantially. The study of Haderlein et al. [1996] also supports the importance of using different electrolyte matrices. They demonstrated that when the exchangeable cations of the clays include potassium or ammonium, the adsorption of NACs to clays is high because they are weakly hydrated cations, but it is negligible when the exchangeable cations at clays are sodium, calcium, magnesium or aluminum.

Reversibility of Sorption. Standard methods for determining partitioning between phases assume that the system is at equilbrium after adsorption and desorption. These equilibrium models are hampered in their approach due to the assumption that there is no difference between the values of desorption and adsorption partition coefficients [Karickhoff et al. 1979]. However, the determination of accurate partition coefficients for long sorption times is frequently difficult because of discrepancies between the degree or rate of adsorption and desorption [Karickhoff and Morris 1985] This discrepancy between the degree of adsorption and desorption is often referred to as hysteresis [Pignatello and Xing 1996].

There are three major groups of hysteretic models currently in use. The first, suggest that the analyzed systems do not reach a true equilibrium, even for long sorption times (i.e. months to years) [Young and Ball 1999] due to transport, i.e. intra-particle diffusion [Altfelder et al. 2000; Brusseau et al. 1991; Chilom and Rice 2005; Culver et al. 1997; Farrell et al. 1999; Ho and McKay 1998; Kan et al. 1998; van Beinum et al. 2006; Wu and Gschwend 1986; Yang et al. 2008]. In these cases, slow diffusive processes cause a gradual uptake that is not symmetric with respect to adsorption and desorption since the direction of transport is determined by chemical concentration gradients, i.e. contaminants may be moving toward the center of particles even after the contaminant source is removed. Diffusive processes can take many years to reach a true equilibrium state [Sabbah et al. 2006]. In addition, these models may require site specific parameters, some of which are difficult to determine prior to study, e.g. diffusion rates, sorbent particle sizes and chemistry of the system, which limits the applicability of these models to new sites.

A second group apply differing kinetic rates to adsorption and desorption. These empirical solutions typically use a two-compartment model [Chen and Nyman 2005; Cornelissen 1997] that proposes two different sorption sites with different kinetic rate constants, one fast and one slow. There is often no relationship to sorbent and sorbate properties, limiting the use of these models for new sites. Attempts have been made to correlate the first order rates derived by the two-compartment model to an apparent diffusion rate [Birdwell et al. 2007], although results are inconsistent. Other models relating first order kinetics to multiple binding sites have been employed [Ho and McKay 1998; Huang et al. 1998; Xue et al. 1995]. The models rely on at least a single rate constant for each binding site and sorbate pair. Since no strong correlation has been observed between these rates and sorbent/sorbate properties it is not possible to apply these models to new situations without site specific experimentation.

The third group assumes adsorption and desorption behavior is described by two sets of isotherms, one for the reversibly sorbed fraction and another for the fraction that is resistant or potentially irreversibly sorbed. Although many models exist using isotherms for adsorption and desorption [Huang and Weber 1997], few describe both adsorption and desorption using a single set of isotherms. Models of this category include the Reversible/Resistant (RR) [Di Toro and Horzempa 1982] and site transformation models (STM) [Di Toro 2013]. The RR model retains a portion of the adsorbed concentration as irreversibly bound using reversible and resistant partition coefficients. The STM extends on this idea by allowing for the transformation of weakly binding sites to strongly binding sites. Hysteresis is caused by the strongly bound sites not desorbing under aqueous concentrations used for desorption. The STM explanation of the behaviour is shown in Figure 1.

As the duration of adsorption contact time increases, more soils exhibit resistant behavior as noted previously for chlorophenols (Palomo and Bhandari 2006), herbicides (Lesan and Bhandari 2003) and PAHs (Wang et al. 2012), but has not been satisfactorily explained. A possible mechanism is an increase in the binding strength of the sorbent. Work performed by Lu and Pignatello [2002], Sander and Pignatello [2005, 2009], and Chilom and Rice [2005] suggests that a transition in organic carbon binding strength, through pore filling or polymeric rearrangement, may explain the observed resistance to desorption exhibited by many chemicals. These changes may not only physically change the sorbate, but may allow access to different binding sites with different sorption energies [Huang et al. 1998; Kan et al. 1998; Gebremariam et al. 2012]. Hysteresis is due to a strongly bound portion which does not desorb under observed solute conditions. These processes are not necessarily instantaneous, suggesting kinetics may also be involved [Sander et al. 2006].

Although there are several sorption models that describe adsorption or desorption behavior, few explain the transition between the two processes. A recently developed model, the Site Transformation Model (STM) (Di Toro 2013), is based on the idea that sites change binding strength as a function of adsorption concentration, resulting in hysteresis. Moreover, the model can be applied to both linear and Langmuir isotherms, enabling modeling of nonlinear sorption.

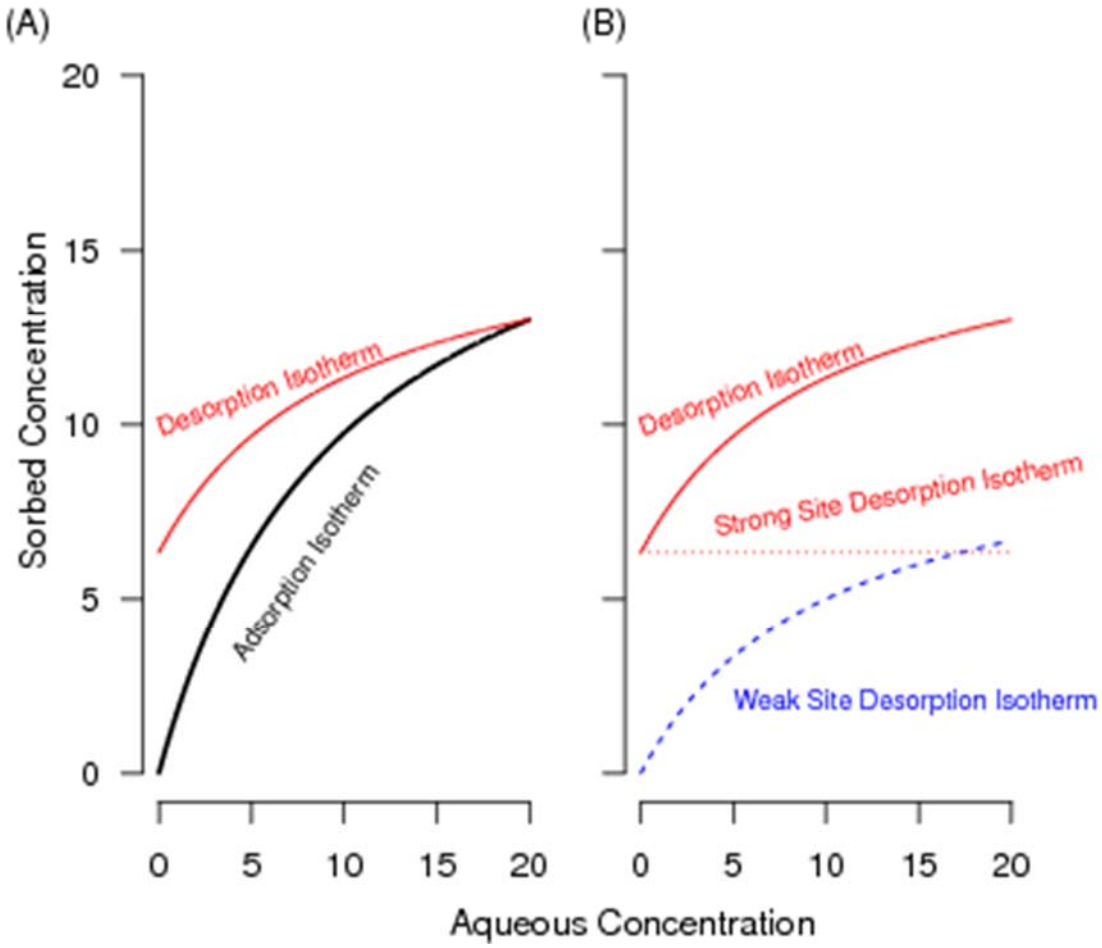

Figure 1. Illustration of STM. (A) Behavior during adsorption (black) and desorption (red). The discrepancy between the lines (hysteresis) is evident from the individual sorbed components (B). Strong sites (red) during desorption remain fixed, weak sites (blue) follow Langmuir behavior.

Transport of MC in Soil Columns. Transport of MC through the soil controls its presence in groundwater. Therefore, accurate prediction of partitioning is essentail for use in hydrodynamic models. A key parameter in hydrodynamic models is the partition coefficient which is responsible for the retardation of chemicals in the soil. There has been limited research in which the partitioning of MC in soil columns, as opposed to batch equilibrium systems, has been studied. Dontsova et al. [2006] studied the transport of RDX, TNT, and the components of Composition B in saturated flow through a soil column. For example, a flow-through soil column study conducted by Monteil-Rivera et al. [2011] confirmed high mobility of triethylene glycol dinitrate predicted from low values of K_d. However, reversible and resistant partitioning has not been incorporated into transport models of adsorption and desorption for MC or other organic compounds.

Sorption and Release of MC by Nitrocellulose. Taylor et al. (2012) measured the 2,4-DNT, NG, and NQ dissolution rates for different propellants using laboratory batch and drip tests where no soil was present, and soil column studies, which used similar propellant and residues as source terms, to determine partition coefficients and degradation rates. The surfaces of propellants and residues were studied using both light and electron microscopy. The authors found that 2,4-DNT is well bound to NC and dissolves out slowly, but that both NG and NQ

have fast initial dissolution followed by slower mass loss. The amount of NG dissolved was a function of the NG/NC ratio in the propellant and both mass loss data and microscopy results suggest that NG exists as fine liquid droplets within an NC matrix rather than as dispersed molecules. The authors theorized that NG droplets near the grain surface dissolve quickly, with diffusion rates of 3.2×10^{-14} cm^2 s^{-1} to 1.2×10^{-13} cm^2 s^{-1}, then NG diffuses through the NC matrix slowly (~10^{-14} cm^2 s^{-1}). Both 2,4-DNT and NG are added as liquids and cannot be distinguished from the NC matrix. Therefore, their distribution and movement within the nitrocellulose matrix is poorly understood. Late time-dissolution would thus be limited by molecular diffusion. The authors concluded that they had difficulty deriving a physically based dissolution model that can predict energetic losses from a variety of propellant types.

The dissolution of propellant particles is likely to be a more complex process than dissolution of particles of explosives. The reason is the presence of NC as a large fraction (~50-90%) of the propellant particles. NC can influence the dissolution in at least two ways (Brodman et al., 1975, 1982; Winkler and Starks, 1988). As the propellant incorporated within the NC matrix dissolves, it may adsorb to the NC itself. This process will retard the rate of propellant chemical release. The mechanism is analogous to hindered diffusion in soils. Depending on the magnitude of the partition coefficient, the dissolution can be much slower than would be expected from non-NC containing particles. The second mechanism is the interaction of water and compound with NC directly. NC swells in the presence of water (Cuissinat et al., 2008). The dissolving compound may also be incorporated into the pore space of the swelling NC particle. Then as the compound leaches into the surrounding media, the energetic material that was incorporated into the NC matrix during propellant processing will diffuse outward from the NC. This release is likely to be hindered by diffusion.

Materials and Methods

Chemicals. Military grade HMX, RDX, NG, NQ, TNT and 2,4-DNT in aqueous solution were provided by U.S. Army Edgewood Chemical Biological Center at Aberdeen Proving Ground, MD. Properties of MCs are presented in Table 1. HMX and RDX are considered desensitized in solution. NG was kept below 1% in aqueous solution. Calibration standards (>99% purity) for each of these MCs were obtained from AccuStandard Inc. (New Haven, CT). Calcium chloride ($CaCl_2$), potassium chloride (KCl), cesium chloride (CsCl), and HPLC grade methanol and acetonitrile were obtained from Acros Organics, through Fisher Scientific and sodium azide was obtained from Alfa Aesar through Fisher Scientific. Deionized water (18 mΩ resistance; DI) for the soil studies was provided by an E4GE Osmonics DI Water System, Model: R4 6600DLX on tap at the University of Delaware (Newark, DE).

Table 1. Physicochemical properties of the MC studied.

Physico-chemical Properties	HMX	RDX	NG	NQ	TNT	2,4-DNT
	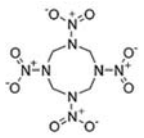	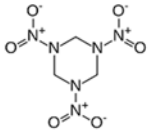	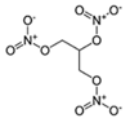	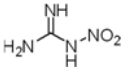	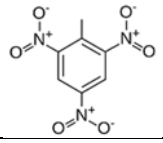	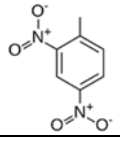
Molecular Weight (g mol^{-1})	296.16	222.26	227.11	104.07	227.13	182.15
Water Solubility at 25^0C (mg L^{-1})	4.5 [Monteil-Rivera et al., 2004]	56.3 [Monteil-Rivera et al., 2004]	1800 [HSDB, 2008]	4400 [HSDB, 2008]	130 [Chemical Properties Database, 2010]	270 [HSDB, 2008][b]
Octanol/Water Partition Coefficient (Log K_{OW})	0.17 [Monteil-Rivera et al., 2004]	0.90 [Monteil-Rivera et al., 2004]	1.62 [HSDB, 2008]	0.89 [HSDB, 2008]	1.60 [HSDB, 2008]	1.98 [HSDB, 2008]
Henry's Law Constant at 25^0C atm-m^3 mol^{-1}	2.5×10^{-14} [Chemical Properties Database, 2010][a]	1.96×10^{-11} [Sheremata et al., 2001]	3.4×10^{-6} [Chemical Properties Database, 2010][a]	4.54×10^{-16} [HSDB, 2008]	2.18×10^{-8} [HSDB, 2008]	5.40×10^{-8} [ChemID Plus Lite, 2006]

[a] At 20 °C
[b] At 22 °C

Soil Properties. This study employed 25 soils collected from the U.S., Europe and South America to identify the major influences of soil properties in the adsorption-desorption process. The soils have clay size particle content between 4.0 to 43.2%, total organic carbon content of 0.07 to 18.23%, and oxalate-extractable Fe content of 0.0053 to 1.20% as shown in Figure 2. The pH, CEC, clay size particles, OC content and major metals content (Al, Fe and Mn), were determined by the soil laboratory at the Plant and Soil Science Department at the University of

Delaware. Oxalate extractable oxides (Al, Fe and Mn) were determined at the Environmental Engineering Soils Laboratory at the University of Delaware. Table 2, in which the soils are ordered by OC, presents the relevant information of the soils. In addition Figure 3 shows a cross correlation plot of the properties of the soils studied to determine how they are correlated to build the multilinear model. As is observed in the figure, there are strong correlations between sand and clay and total nitrogen, total carbon and total organic carbon. Also cation exchange capacity is correlated with total carbon and total organic carbon. This information indicates that is possible to reduce the number of variables in the model, by using the less correlated properties of the soils.

In addition to the 25 soils indicated in Table 2, two reference materials were included in the study. These were (1) Pahokee peat obtained from the International Humic Substances Society, IHSS, and (2) kaolinite obtained from the Clay Minerals Society.

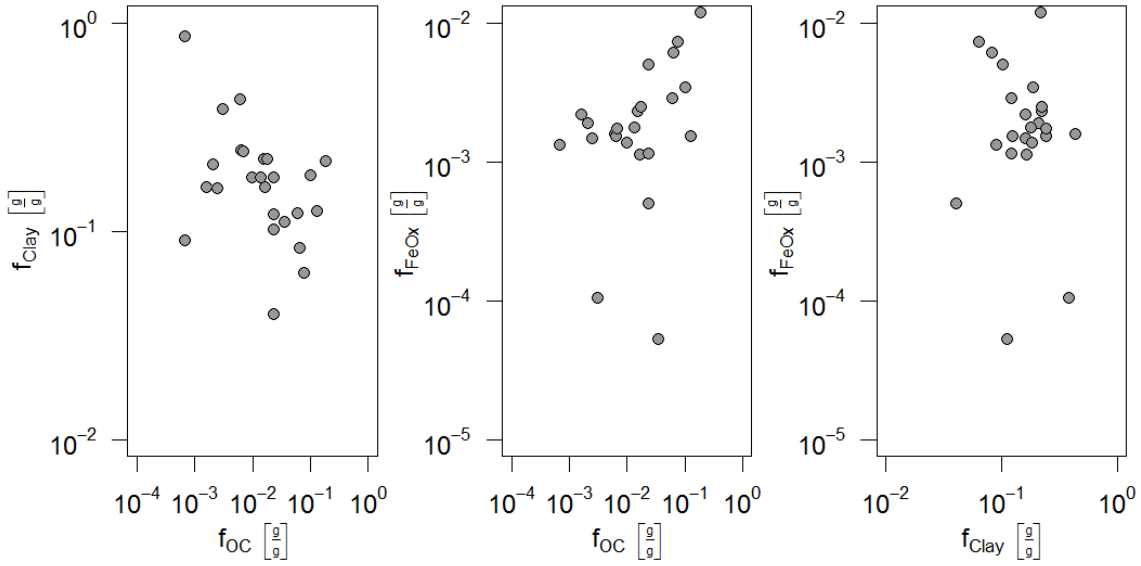

Figure 2. Relationship of fraction (f) clay, organic carbon, and oxalate-extractable iron for the 25 soils used.

Preliminary Experiments. The following set of preliminary tests were conducted to determine the conditions needed to conduct the sorption and desorption analysis.

Table 2. Soil properties.

Soil	pH[a]	CEC[b] (meq/100g)	Clay[c] (%)	TOC[d] (%)	Al[e] (mg/kg)	Fe[e] (mg/kg)	Mn[e] (mg/kg)	Al Ex.[f] (mg/kg)	Fe Ex.[f] (mg/kg)	Mn Ex.[f] (mg/kg)
Zegveld	4.8	54.8	21.7	18.23	21414	19651	389	1516	11954	148
Rhydtalog	5.0	35.9	12.5	12.83	2281	2786	113	281	1526	52
Joplin	6.5	43.8	18.7	10.12	10252	21475	484	244	3436	272
Lewis Core	5.6	37.2	6.3	7.59	27619	22270	591	15181	7269	573
Lewis Clean	5.1	31.4	8.3	6.36	27451	19410	575	13011	6130	560
Pokomoke	4.5	13.1	11.1	3.50	5037	794	16.3	888	52.6	6.22
Elliot IE	6.3	20.4	37.0	2.86	10356	19168	811	455	2541	514
Guadalajara	8.0	11.6	18.2	2.33	10630	10984	152	163	ND	31.5
Boxtel	5.4	11.0	10.2	2.32	5757	11609	269	112	5001	159
Houthalein	3.9	2.9	4.0	2.31	711	1622	3.32	111	502	ND
Annemessex	6.3	13.2	12.1	2.30	9142	11870	304	343	1153	255
Whippany	5.9	15.5	22.3	1.75	10740	11788	108	413	2496	39.7
Sassafras 1	4.4	8.5	16.4	1.63	10538	13461	83.0	276	1120	9.45
Matapeake	5.7	9.9	22.3	1.54	18068	17956	373	635	2304	238
Sassafras 2	4.5	8.8	18.1	1.35	9121	12945	73.7	422	1782	18.8
Chile Muestra	6.6	21.0	14.3	1.20	14146	25237	652	712	7083	453
Sassafras 3	4.4	5.0	18.2	0.97	8924	12609	716	336	1364	11.9
Washington 2	6.9	20.3	24.2	0.68	13565	18899	432	302	1533	199
Washington 1	6.9	17.8	24.5	0.63	14343	20777	552	334	1742	217
Souli	6.9	16.1	43.2	0.61	14769	29961	910	445	1596	630
Fort McClellan	3.8	11.0	38.6	0.31	14130	39878	30.7	557	104	2.63
Massachusetts Military Reservation B	4.3	2.5	16.2	0.24	10325	9514	85.8	659	1471	13.3
Nevada	3.4	11.2	20.9	0.20	6445	34120	220	778	1887	212
Aberdeen BA	5.5	3.8	16.2	0.16	7271	12764	88.9	250	2210	16.7
Aberdeen BT	4.8	1.9	9.1	0.07	7588	9391	59.2	153	1314	18.2

[a] *1:1 (w/v)* (*v*/*v*) soil:water
[b] Ammonium saturation buffered at pH 7.0
[c] Particle size analysis by hydrometer using the modified Bouyoucos Method [Bouyoucos 1962]
[d] Combustion using an Elementar Vario-Cube TOC Analyzer (Elementar Americas, Mt. Holly, NJ).
[e] EPA Method 3051 using a CEM MARs5 microwave digestion system (CEM, Matthews, NC). Digests were analyzed for total metals by inductively coupled plasma optical emission spectroscopy using Thermo Iris Intrepid II XSP Duo View ICP (Thermo Elemental, Madison, WI).
[f] Ex. = Extractable oxides determined by the ammonium oxalate method [McKeague and Day 1993]
ND non detected

Adsorption equilibrium time. Before adsorption and desorption isotherms could be developed it was necessary to determine the time necessary for the MCs to reach the steady state with respect to the adsorption and desorption processes. Figure 4 shows the amount of MC sorbed per gram

of Matapeake soil (q) for HMX, RDX, NG, TNT and 2,4-DNT as a function of the adsorption time. The majority of adsorption occurs within the first 2 hours. An adsorption time of 48 hours was chosen as the experimental methodology for these experiments.

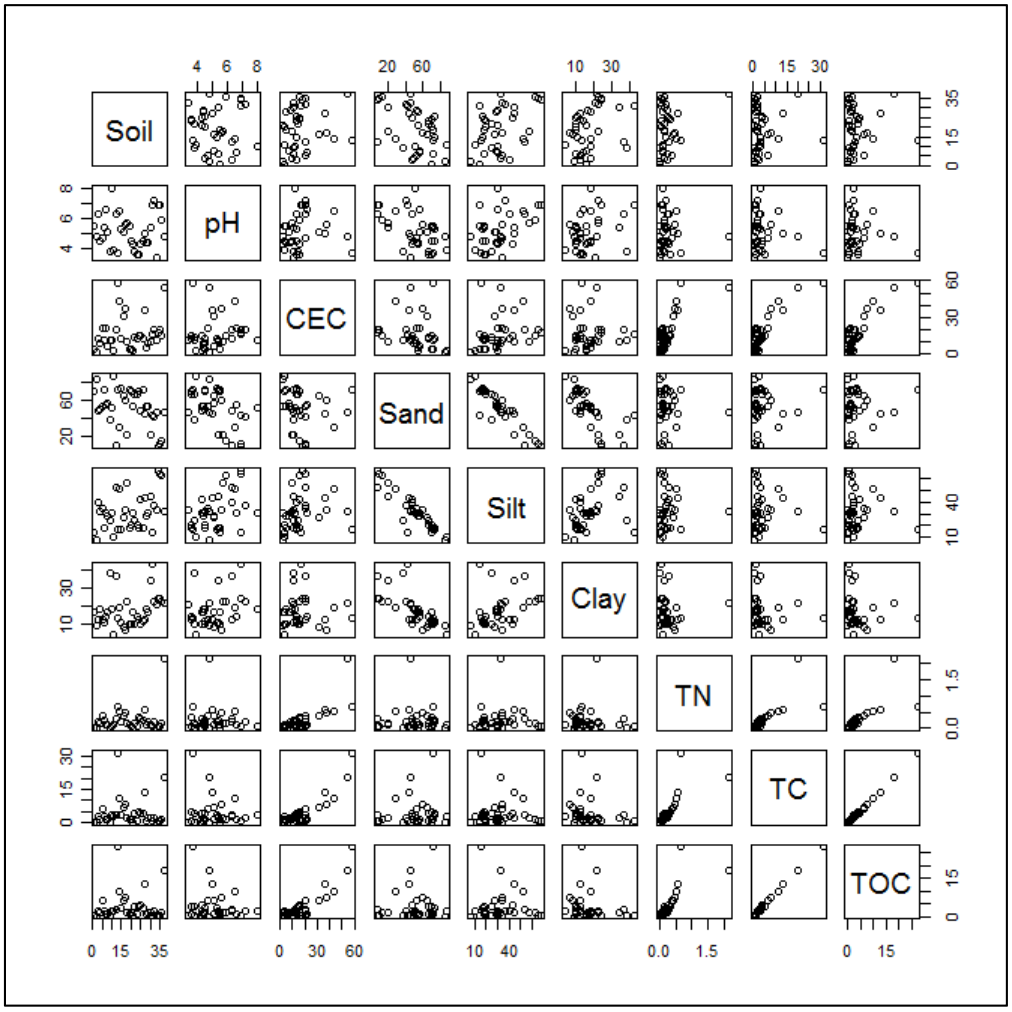

Figure 3. Cross correlation of properties of the studied soils.

Single and mixed MC. Because of the large number of experiments involved in the project, it was desirable to perform sorption experiments on a mixture of MC as opposed to each compound individually. Figure 4 presents the results from this experiment, using Matapeake soil for RDX, NG, and 2,4-DNT. Initial concentrations for RDX, NG and 2,4-DNT were from 1 and 10 mg L^{-1} for RDX and NG and from 2.3 to 23 mg L^{-1} for 2,4-DNT. At these concentrations, mixed compound adsorption is nearly identical to single compound adsorption.

Hydration volume. Soils are hydrated with a solution that is 0.01 M in both $CaCl_2$ and NaN_3 prior to the addition of MC to maintain a constant volume throughout the adsorption and desorption procedures. Therefore, effects of different volume on any adsorption or desorption step are eliminated. To determine the hydration volume, which is unique for each soil tested, triplicate samples with different volumes of hydration solution are added such that the true hydration volume will fall within the range of volumes tested. Then, additional volumes of the

same solution are added to each tube. Figure 6 shows the results from this procedure applied to two different soils: (1) Nevada which is high in clay size particles and low in organic matter, and (2) Kovlinge, which is low in clay size particles and high in organic matter. Intersection of the x-axis, at which point the full 5 mL added after hydration is recovered, is the volume necessary to hydrate the soil. Therefore, after hydration, the adsorptions and subsequent desorptions will maintain the same liquid to solid ratio after each decanting. Values for all soils are presented in Table 3.

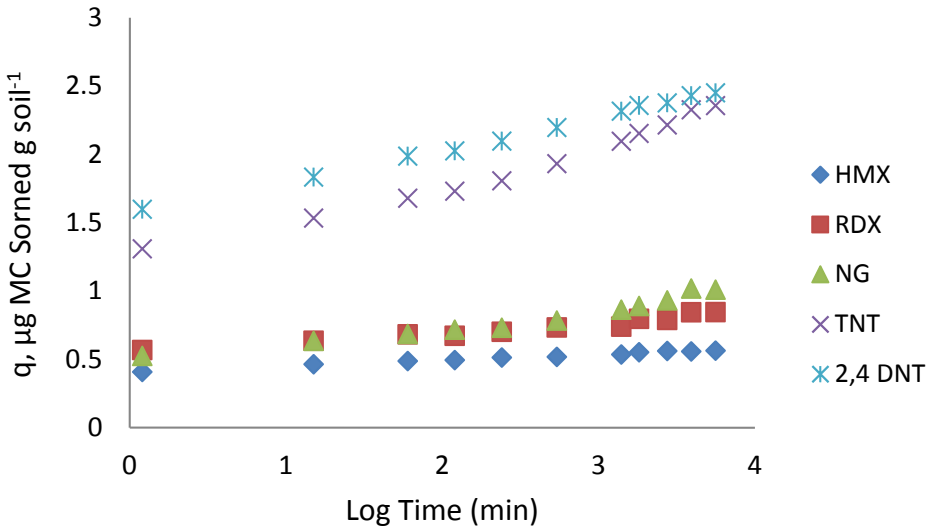

Figure 4. MC sorption as a function of equilibrium time (0 - 5 days) for HMX, RDX, NG, TNT and 2,4-DNT sorption on Matapeake soil.

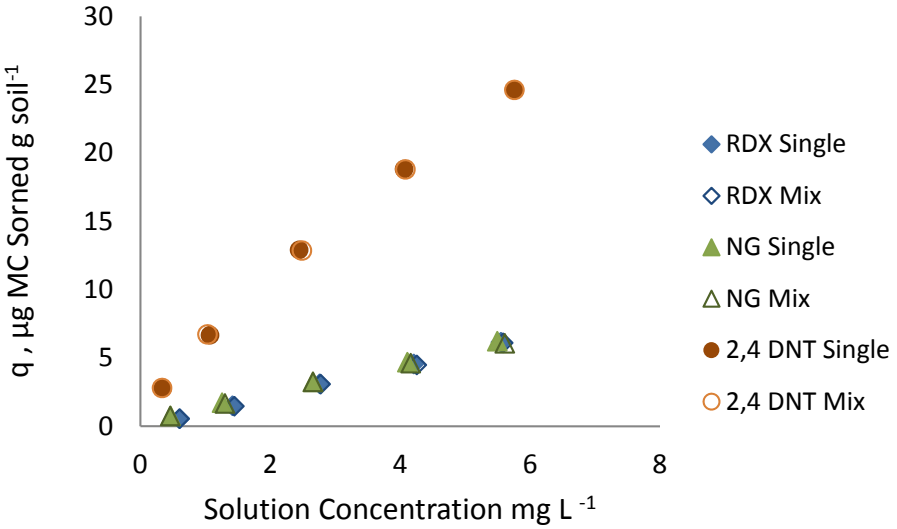

Figure 5. Relationship between single and mixed MC (RDX, NG and 2,4-DNT) sorbed by Matapeake soil and solution concentration.

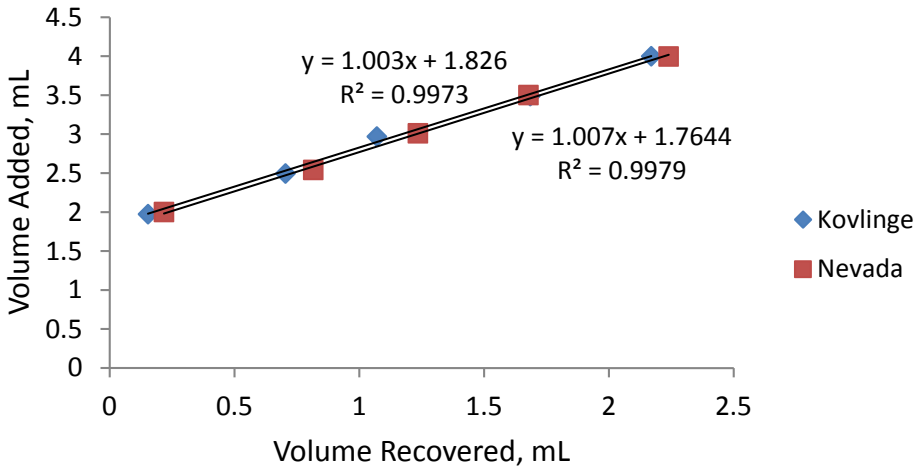

Figure 6. Hydration volume of Kovlinge and Nevada soils.

Table 3. Volume of hydration for 5 g soil.

Soil	Volume of Hydration (mL)
Zegveld	3.30
Rhydtalog	3.39
Joplin	3.40
Lewis Core	3.40
Lewis Clean	2.80
Pokomoke	2.30
Elliott	2.25
Guadalajara	2.07
Boxtel	2.33
Houthalein	1.50
Annemessex	2.30
Whippany	2.22
Sassafras 1	2.30
Matapeake	1.98
Sassafras 2	2.00
Chile Muestra	2.50
Sassafras 3	2.10
Washington 1	2.60
Washington 2	2.50
Souli	2.18
Fort McClellan	2.20
Massachusetts Military Reservation B	1.60
Nevada	1.78
Aberdeen BA	1.64
Aberdeen BT	1.64

Hydration time effect. This research also tested the hydration time effect of $CaCl_2$ and NaN_3 on sorption. The concentration of HMX, RDX, NG, TNT and 2,4-DNT in the solution was determined after two days of adsorption onto Matapeake soil at different hydration times (1, 2, 5, 10, 20 and 30 days), and the results are shown in Figure 7. A kinetic effect is observed at an initial concentration for all MC excluding RDX, and the effect is greatest in the first several days. With this information the selected time to hydrate the soils was 5 days, because at that time almost all the MC reach a steady state and the data will be reproducible.

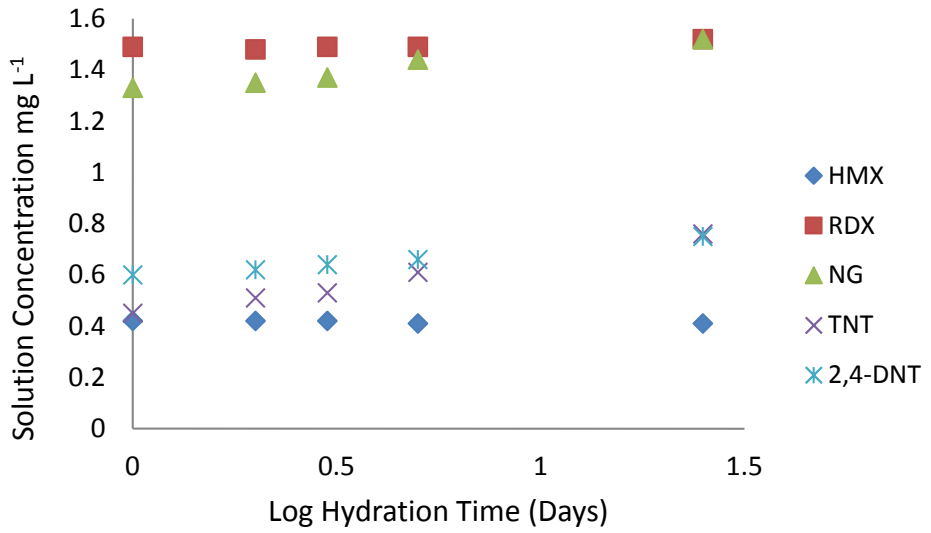

Figure 7. Effect of hydration time on a mixture of HMX, RDX, NG, TNT and 2,4-DNT sorbed by Matapeake soil after two days at different hydration times (1, 2, 5, 10, 20 and 30 days).

Effect of the addition of NQ to the mixture of MC. A final preliminary experiment was performed to compare the mixture of 5 MC: HMX, RDX, NG, TNT and 2,4-DNT with the addition of NQ, because NQ was not included in the previous experiments. Two set of samples of three concentrations of the mixture with and without NQ from 0.5 to 3 mg L^{-1} when subjected to 2 days of adsorption on Matapeake soil and the isotherm was determined. Figure 8 shows that there is no difference between 5 or 6 MC.

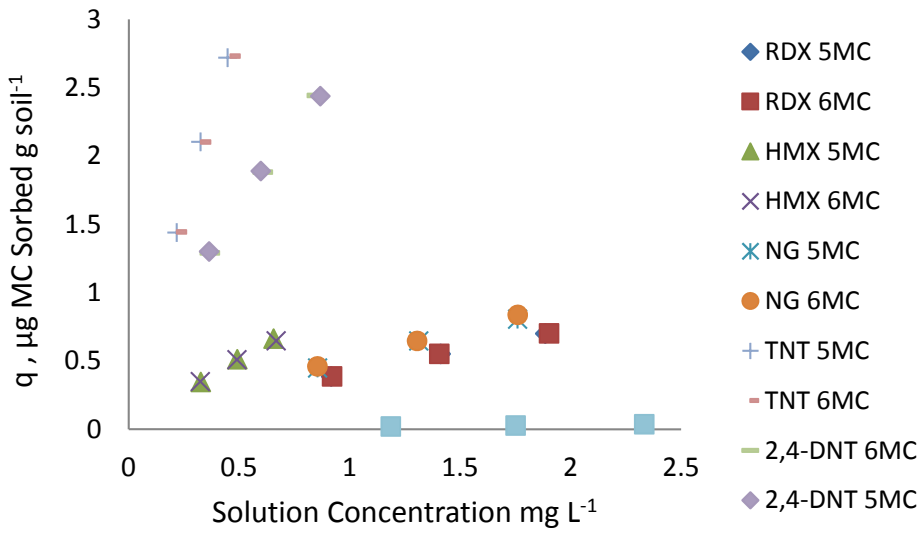

Figure 8. Effect of mixing of 5 (HMX, RDX, NG, TNT and 2,4-DNT) versus 6 MC (HMX, RDX, NG, NQ, TNT and 2,4-DNT) after 2 days of adsorption on Matapeake soil.

Sorption/Desorption Experimental Procedure. Batch sorption experiments were conducted at 1:1 (w/v) soil to solution ratio (w/v) reflecting near field conditions and at room temperature at 21°C ± 1°C. In each experiment 5 ± 0.0001 grams of soil, except as noted, were added to 12 mL borosilicate centrifuge tubes with phenolic caps and PTFE liners. Soils were hydrated for 5 days prior to the addition of MC, in a solution containing 0.01 M $CaCl_2$ and 0.01 M NaN_3. $CaCl_2$ was added to prevent flocculation of soil components and NaN_3 was added as a microbial growth inhibitor. Photodegradation was prevented by wrapping all samples and devices in aluminum foil. The pH of soil solutions was too low to result in alkaline hydrolysis of the MC [Sunahara et al. 2009].

The volume of hydration, which is the volume of solution that must be added such that any additional liquid volume after hydration will be physically separated from the soil by centrifugation, varies among the soils. Sorption of MC to soil was found to be a function of hydration time, and 5 days of hydration sufficiently minimized its effect on the extent of sorption. After the 5-day hydration time, 5 mL of MC in mixed or single component solutions was added. Triplicate samples were vortex mixed for 15 seconds to suspend the soil, and were shaken at 10 rpm in an end-over-end shaker for 2, 5, 10 or 30 days depending on the objectives of the experiment. The tubes were centrifuged for 30 min at 3000 rpm (750 × g) and the supernatant was filtered through a 0.45 µm Durapore PVDF filter (Millipore Corp., Bedford, MA). Sorption of the MC by the filter and filter apparatus was determined to be negligible. Four consecutive desorptions were then performed after each adsorption time whereby 5 mL of solution containing 0.01 M $CaCl_2$ and 0.01 M NaN_3 was added to samples that had been decanted of the preceding solution, followed by vortex mixing for 15 seconds and mixing in the end-over-end shaker for 1 day. As noted for some experiments conditions were somewhat modified particularly with respect to the MC present and their concentrations.

Extraction Procedure. For most experiments an acetonitrile extraction of the soil was performed following the desorptions so that a mass balance of the MC could be computed. The primary source of the extraction methodology was Method 8330B [U.S. EPA, 2006], but after preliminary tests it was modified to increase extraction efficiency and decrease peak tailing in

chromatograms. The extraction procedure outlined in the EPA Method involves drying of soil samples, homogenization of dry soil with a mortar and pestle, the addition of acetonitrile as the extractant, and 18 hours of sonication in a temperature controlled bath. This method was modified to increase extraction efficiency and decrease peak tailing in chromatograms. Sonication for 18 hours resulted in significant peak tailing, eliminating this step gave acceptable extraction efficiency without compromising accuracy. Extractions were performed with supernatant still wet from previous sorption experiments to simplify the process, and three consecutive extractions improved the overall extraction efficiency.

Five mL of acetonitrile (ACN) was added to each sample. Samples were vortex mixed for 15 seconds to suspend the soil in solution, and shaken at 10 rpm in an end-over-end shaker for 1 hour. This step was done three times. The tubes were centrifuged for 30 min at 3000 rpm (750 × g) and DI water was added in equal volume to the supernatant after the extraction process to decrease noise in the baseline of the chromatograms, which is particularly important at low concentrations. The solution of the supernatant and DI water was filtered through a 0.45 μm Durapore PVDF filter (Millipore Corp., Bedford, MA) and analyzed for MC by HPLC.

Analytical Methods.

MC analysis by HPLC. An HPLC method was developed to quantify the MC. The EPA Method 8330B [U.S. EPA, 2006] was modified for the analysis of MC: HMX, RDX, NG, TNT and 2,4-DNT to improve the resolution of the peaks. Conditions for both methods are presented in Table 4. In addition Tables 5 A and B show the results and the EPA method appears to outperform our method, with a lower retention time for all MC at the same 5 mg L^{-1} concentration but numerous difficulties result from the application of this method when used with a 3.5 μm C-18 column as opposed to the standard 5 μm C-18 column. A column with smaller diameter particles was chosen to decrease the time for analysis and improve peak resolution. Certified standards of MC (AccuStandard, Inc., New Haven, CT) were used in HPLC determinations.

Table 4. Chromatographic conditions in the new method vs. EPA Method 8330B.

Method	λ (nm)	T°C	Flow (mL/min)	MeOH:H_2O
New	210	16.5	2.0	Gradient
New	214	16.5	2.0	Gradient
New	254	16.5	2.0	Gradient
EPA 8330B	210	25.0	2.0	50:50
EPA 8330B	214	25.0	2.0	50:50
EPA 8330B	254	25.0	2.0	50:50

Table 5. Comparison of HPLC conditions at 10 mg/L MC concentration. (A). retention time (B). HPLC peak height.

(A)		Retention Time (min)				
		HMX	RDX	NG	TNT	2,4-DNT
New	210 nm	0.983	1.715	2.887	3.072	3.292
New	214 nm	0.979	1.708	2.884	3.071	3.292
New	254 nm	0.982	1.714	-	3.072	3.293
EPA 8330B	210 nm	0.500	0.728	1.447	1.593	1.839
EPA 8330B	214 nm	0.500	0.728	1.446	1.591	1.838
EPA 8330B	254 nm	0.500	0.728	-	1.592	1.839

(B)		Peak Height				
		HMX	RDX	NG	TNT	2,4-DNT
New	210 nm	0.983	1.715	2.887	3.072	3.292
New	214 nm	0.979	1.708	2.884	3.071	3.292
New	254 nm	0.982	1.714	-	3.072	3.293
EPA 8330B	210 nm	0.500	0.728	1.447	1.593	1.839
EPA 8330B	214 nm	0.500	0.728	1.446	1.591	1.838
EPA 8330B	254 nm	0.500	0.728	-	1.592	1.839

By introducing a gradient that used a starting water to methanol ratio greater than the 50:50 ratio in the EPA method, the retention times of all MC increased and interference with DOM was reduced significantly. A consequence of starting the gradient with a greater water to methanol ratio was lower peak resolution for HMX and RDX, but as the ratio fell below 50:50 in the course of the run, the compounds with longer retention times gained better resolution, as illustrated in Figure 9. Decreasing the temperature increased the retention time for the nitramines, and decreased the retention times for the nitroaromatics and NG. This resulted in a shorter overall run, and completely eliminated interference by DOM in the analysis of HMX and RDX.

Adsorption and desorption was quantified in 25 soils at multiple MC concentrations, so reducing the time of analysis was critical. HMX and RDX concentrations are difficult to quantify using the EPA methodology because of their low retention time, especially when they are present at low concentration. The DOM peaks have retention times that exceed 0.5 minutes in all soils, causing significant overlap of peaks and an overestimate of concentration for these compounds. NG and TNT peaks also experience some overlap in the EPA method.

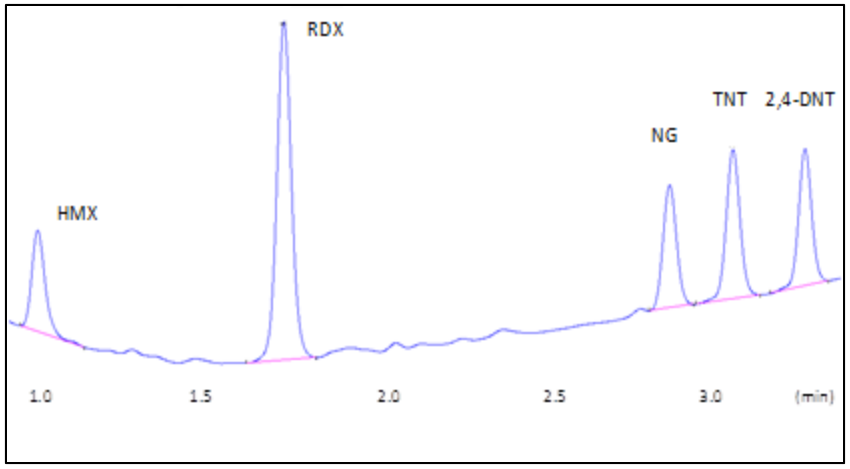

Figure 9. Peaks resolution for the MC studied (HMX, RDX, NG, TNT and 2,4-DNT) using the modified EPA 8330B Method.

After all of these tests the HPLC conditions are: Equipment Agilent 1200 Series HPLC with a Zorbax SB-C18 reversed phase column (4.6×50 mm; 3.5 µm particle size) and UV detector was used to measure MC concentrations with a methanol:water gradient of 30:70 percent to 65:35 percent from 0-2.8 minutes, and 65:35 percent to 30:70 percent from 2.8-3.2 minutes. The flow rate was 2 mL min^{-1} to achieve optimal peak resolution and separation and the UV detector was operated at a single wavelength of 214 nm.

For NQ it was necessary to use a different column because with the Zorbax column the retention time was too short, making it difficult to analyze the MC, because peaks from the dissolved organic matter (DOM) interfered with the NQ peak. A HILIC Plus column (2.1 × 100 mm) was selected for the analysis based on results of a preliminary experiment. This column is used to analyze small, polar compounds such as NQ. The analytical procedure uses a flow rate of 0.20 mL min^{-1}, an injection volume of 2 µL, a single wavelength of 263 nm, a temperature of 23 degrees Celsius, and a mobile phase of 97% acetonitrile and 3% water.

To ensure the reliability of the HPLC analytical method a cross validation was done with the Biotechnology Research Institute of Canada. Fifteen samples provided by the Biotechnology Research Institute were analyzed by both laboratories. A summary of the results, shown in Table 6, validate the method used in the subsequent experiments.

Analysis of chloride by IC. Chloride concentrations were analyzed on an ICS-2000 ion chromatography system equipped with an IonPac® AS10 anion-exchange column, an AC10 concentrator column, and a ASRS-300 suppresor (4 mm); Sample solutions, standards and blanks were run in random fashion at a flow rate of 1.2 mL min^{-1} and a column temperature of 35 °C in KOH eluent, produced by an EGC III generator; Dionex Thermo-Fisher, Sunnyvale, CA. Certified analytical standards were obtained from Dionex Thermo-Fisher (Seven Anion Standard II).

Table 6. Average of relative deviation of measured values from nominal values.

MC	BRI (%)*	U Del (%)*
HMX**	-16	-8
RDX	-4	5
NG	1	10
NQ	-2	4
TNT	-1	-1
2,4-DNT	0	1

* average of (measured value - nominal value)/nominal value × 100

** For HMX, values from two samples were excluded because HMX content was above HMX aqueous solubility at 4 °C. An additional result for BRI was excluded because it was out of range.

Determination of Charge Sites to Evaluate Clay Component of Soil. The method proposed by Anderson and Sposito [1991] was adapted and applied to the 25 soils listed in Table 2. The method is based on the sorption of cesium, which partitions almost exclusively to fixed-charge sites. The procedure is comprised of five steps that are described below. In each step the centrifuge tubes containing the soils are weighted to confirm that solids have not been lost in the process.

The first step of the procedure is the preparation of CsCl saturated soils. This is necessary because some researchers, e.g. Wanner et al. [1996], found that impurities in the clay such as sodium, potassium, magnesium and calcium, have an impact on the sorption of Cs, influencing the concentrations of competing cations. To prepare the Cs-saturated soils 0.5 ± 0.01 grams of soil sieved to <150 μm are weighted into a 50 mL polycarbonate centrifuge bottle in duplicate, then 15 mL of 0.5 M CsCl is added and equilibrated by mixing for 30 min in an end-over-end shaker. Samples are then centrifuged 15 min at 3000 rpm (750 × g) and the supernatant solution is discarded. The soils are reacted twice more with 15 mL of 0.1 M CsCl and once with 15 mL of 0.05 M CsCl. Each time, the sample is centrifuged 15 min at 3000 rpm (750 × g) and the supernatant solution is discarded.

The accessible structural charge is determined immediately after the soil saturation. This part of the procedure includes the next four steps, steps 2-5. In step 2 the CsCl saturated soils are equilibrated with 35 mL 0.05 M CsCl solution for 1 h in the end-over-end shaker at room temperature. Then the samples are centrifuged for 25 min at 3000 rpm (750 × g). Using a Pasteur pipette, the supernatant is transferred to a 50 mL plastic vial for Cs analysis.

In step 3 the soils are equilibrated with 30 mL of ethanol to reduce the concentration of entrained Cs. The Cs-saturated soils are shaken for 1 minute with 95% (v/v) ethanol because the low dielectric constant of ethanol improves ion pair formation of Cs^+ with siloxane surfaces. Anderson and Sposito [1991] found that ethanol minimized hydrolysis of adsorbed Cs which was not desorbed from exchange sites. Also, Ferris and Jepson [1975] observed that more Cs remained adsorbed on kaolinite when Cs-kaolinite was suspended in ethanol instead of water. The ethanolic suspensions are centrifuged to separate the supernatant solutions, and then transferred to glass containers. This step is done twice to assure the complete removal of entrained Cs. Our preliminary experiments showed the complete removal of Cs after two washes with ethanol. The ethanolic solutions obtained are air dried for 24 hours and the dried at 65°C to constant weight. The precipitated solid is resuspended in 25 mL of a lanthanum(III) chloride

hydrate ($LaCl_3$-$7H_2O$) solution containing 5 g La L^{-1} for Cs analysis.

Step 4 begins with drying the soils in the centrifuge tubes at 65 °C for 24 h. This step is based on the strong preference of permanent-charge sites for Cs over Li, and on the low affinity of most variable-charge sites for Cs [Anderson and Sposito 1991]. Strong surface complexes with siloxane surface groups are formed when Cs-clay is dried. Drying the Cs-saturated adsorbents enhances the formation of inner-sphere surface complexes between Cs and structural charge sites on 2:1 clay minerals. Cs that is bound to siloxane surfaces should not be displaced by lithium (Li) [Anderson and Sposito 1991]. Thus, Li should displace Cs only from variable charge sites in this step. In this step the dried soil samples are resuspended in 30 mL of 0.01 M LiCl and reacted for 1 hour in an end-over-end shaker followed by centrifugation at 3000 rpm (750 × g) for 20 minutes. The supernatant solution is saved for Cs analysis. In each step the centrifuge tubes containing the soils are weighted.

The fifth and final step involves the extraction of Cs and Li from the soils using ammonium acetate as the extractant because soft Lewis acids with low hydration energy, such as NH_4, are the best extractants for Cs adsorbed on collapsed minerals [Schultz et al. 1960; Coleman et al. 1963a; Coleman et al. 1963b]. The soils are resuspended in 30 mL of 1 M NH_4OAc, shaken for 30 minutes, and then centrifuged at 1500 rpm (375 × g) for 15 min. Two extractions are required and the supernatant solution from each extraction is saved for Cs analysis. The clay content of the soil is reported as g Cs exchanged/g soil.

Transport of MC in the Soil Column. Because the study of transport in a soil column was intended as an initial validation of the sorption information that had been developed in this project, chemicals used and procedures followed for the column study mirrored those for the batch equilibrations. The column experiments were conducted at ECBC. Analysis of chloride was performed by ECBC and analysis of MC was performed by University of Delaware.

Chemicals. The energetic materials (EM) 2,4,6-trinitrotoluene (TNT, Chemical Abstracts Service (CAS) No.: 118-96-7; 99%) and hexahydro-1,3,5-trinitro-1,3,5-triazine (RDX, CAS: 121-82-4; 99%) were obtained from Joseph A. Domanico, Ammunition Control Officer, Aberdeen Proving Ground (APG, MD 21010-5424). Stock solutions of each MC were prepared and used to prepare the final solution that was applied to the soil column. Calcium nitrate ($Ca(NO_3)_2$; CAS No. 10124-37-5) was used as an electrolyte in all solutions applied to the column. Sodium azide (NaN_3; CAS No. 26628-22-8) was used as a biocide in all solutions applied to the column. Acetonitrile (CAS No.: 75-05-8; HPLC Grade), methanol (CAS No.: 67-56-1, Chromatography Grade; 99.9%), and calcium chloride ($CaCl_2$; CAS No.: 10043-52-4; Reagent Grade), were used for the soil extractions, and in analytical determinations by HPLC. American Society for Testing and Materials (ASTM) Type I water (18 MΩ cm @ 25 ºC; ASTM D1193-99, 2004), obtained using Elix 10UV ProGard® 2 followed by Academic Q-Gard® 1 systems (Millipore®, Bedford, MA), was used throughout the study.

Sassafras sandy loam (SSL; Fine-loamy, siliceous, semiactive, mesic Typic Hapludult) collected from an open grassland field in the coastal plain on the property of the U.S. Army Aberdeen Proving Ground (Harford County, Maryland) was used to determine the sorption of TNT and RDX in the column. The soil was air-dried in an environmentally controlled greenhouse for 72-hr, passed through a 2 mm sieve and stored in bins in the dark before use. Physical and chemical characteristics of the soil are shown in Table 7.

Table 7. Mean physical and chemical characteristics of Sassafras sandy loam soil (n=3).

Soil property	Sassafras sandy loam (SSL)[a,b]
Sand (%)	55 (0.6)
Silt (%)	28 (1.1)
Clay (%)	18 (0.7)
Texture	sandy loam
CEC (cmol kg^{-1})	9.3 (0.4)
Organic Matter (%)	2.30 (0.03)
pH	4.90 (<0.01)
Water Holding Capacity (%)	18 (4)

[a] Standard error of the mean is shown in parentheses
[b] Analyses performed by Agricultural Analytical Services, College of Agricultural Sciences, Penn State University, University Park, PA.

Soil Column Description. The column consisted of a 10.0-cm-long by 2.2-cm-internal diameter glass cylinder with 1 cm glass wool and a sintered glass filter to prevent soil migration, and stopcock valve at the bottom, and a rubber cap on the top (Figure 10). The column was packed by slowly adding SSL soil (45.43 g) to a height of 10 cm. The volume of the soil column (height $\times \pi r^2$) was 37.994 cm^2. The calculated bulk density (mass/volume) was 1.196 g cm^{-3} and one pore volume (volume of water needed to saturate the soil column and produce outflow) was 18.33 cm^3, measured gravimetrically.

Two solutions were prepared:
(1) an aqueous electrolyte solution with 0.005 M $Ca(NO_3)_2$ and 0.01 M NaN_3 (biocide), and
(2) the electrolyte solution plus 5.5 mg L^{-1} RDX, 9 mg L^{-1} TNT, and 10 mg L^{-1} chloride (tracer) as sodium chloride.

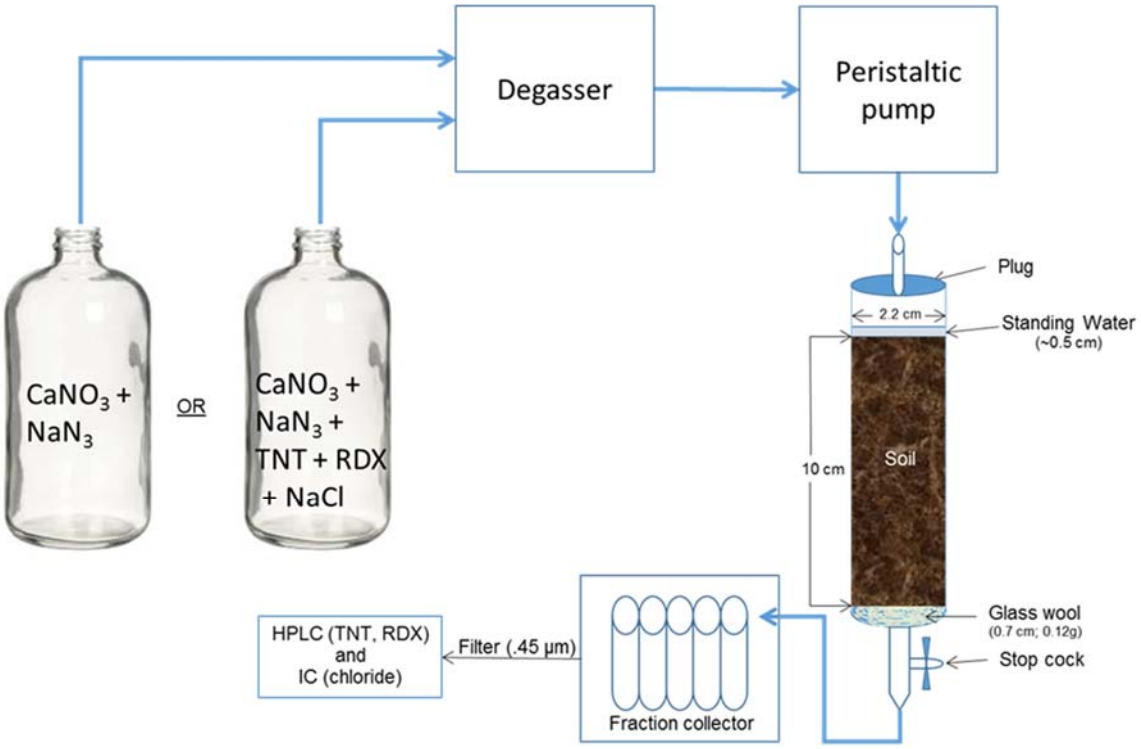

Figure 10. Soil column with delivery and collection systems.

The solutions were introduced onto the top of the column at a fixed flow rate (0.2 mL min^{-1}) using a peristaltic pump (Masterflex® Model 7523; Cole-Parmer®, Vernon Hills, IL). Outflow samples were collected continuously into 10-mL tubes using an automatic fraction collector (Spectra/Chrom® CF-1; Spectrum Laboratories, Rancho Dominguez, CA). The solutions were eluted from an acid-washed bottle (washed with detergent, rinsed 4× RO water, 1× 0.01 M HNO_3, 3× ASTM Type I H_2O) through a Gastorr online de-gassing system (Model TG-14; MicroSolv Technology Corp., Eatontown, NJ), then through the peristaltic pump and into the soil column. All tubing consisted of PTFE Teflon®. The electrolyte solution, sans MC was pumped through the tubing and column without soil into collection tubes to ensure that the MC did not adsorb to the tubing or glassware.

The soil was saturated by dripping from top to bottom with solution (1) for 32 h (~22 pore volumes), followed by solution (2) containing TNT, RDX, and NaCl for 24 h. The drip solution was then switched back to the original aqueous electrolyte solution for an additional 24 h. Outflow was collected from the bottom of the column every 30 minutes using the automatic fraction collector. Flow was continuous throughout the entire experiment. Every fourth sample was analyzed by high performance liquid chromatography (HPLC) for RDX and TNT, and by ion chromatography for chloride. Breakthrough curves of flow-through solutions were plotted for RDX, TNT, and chloride concentrations in effluent / initial solution concentrations (y axis) vs. time (x axis).

Preparation and filtration of outflow solutions and soil. Outflow solutions were removed from tubes with a glass syringe (2 mL) equipped with a 0.45 µm Millipore Durapore PVDF (polyvinylidene fluoride) filter (13 mm diam.) in a Luer filter holder attached to a stainless steel Luer-loc blunt needle (10.2 cm; 14 gauge). The filtering apparatus was first washed, sans filter, by extending the plunger into the vial, taking approximately one second to draw up the solution.

A slower pace will introduce air into the syringe, decreasing the volume of liquid obtained, and a faster pace may remove small soil particles from the sample. Half of the solution was expelled into a waste beaker and the needle was then removed and emptied. A second needle, marked to differentiate it from the first, was attached to the filter holder and the remaining solution was expelled into the waste beaker. The second needle was only used to expel the sample. The filter holder was removed and drained. More solution was drawn with the unmarked needle and filter holder as described above except the solution was not expelled. The filter holder, with needle attached, was removed and drained. A PVDF filter was inserted into the filter holder attached to the marked needle and it was attached to the syringe. The first 0.3 mL of solution was expelled into the waste beaker and the remaining solution was expelled into an amber 2 mL borosilicate HPLC vial with a PVDF snap-on cap. The filter holder was removed, the filter was discarded and the filter holder was re-assembled and washed before extracting the next sample.

RDX and TNT were extracted from the soil with acetonitrile. Wet soil was removed from each of 4 layers, (0-2 cm, 2-4 cm, 4-6 cm, and 8-10 cm). A 5 g sample was removed from each layer to which 5 mL of acetonitrile was added in duplicate. Masses were recorded on an analytical balance to the nearest 0.0001 grams. The volume of acetonitrile added was calculated according to the temperature of solution at the time of acetonitrile addition. For example, acetonitrile has a density of 0.782 g mL^{-1} at 20 degrees Celsius, and 0.776 g/mL at 25 degrees Celsius. The volume added was calculated by dividing the difference in weight by the density of acetonitrile. Each sample was then vortex mixed for 15 sec. Samples were mixed in an end-over-end mixer and rotated at 10 rpm for 24 hours, then subjected to sonication for 4 hours in a temperature controlled water bath. The temperature of the surrounding water was maintained at 18-20 degrees Celsius throughout the sonication by circulating cold water produced by a chiller beneath the water bath. Samples were then centrifuged at 3000 rpm, or approximately 750 ×g, for 30 minutes. Using glass pipettes, supernatant was transferred to the corresponding test tubes and covered with a screw cap to prevent evaporation of the acetonitrile. The caps were screwed back on the samples when finished. Masses were recorded. All extractions were performed in a fume hood. DI water (5 mL) was added to each of the test tubes containing supernatant and the new mass was recorded. The test tubes were stored in a refrigerator until analyses were performed. The water/acetonitrile solutions were removed, filtered and expelled into an amber 2 mL borosilicate HPLC vial with a PVDF snap-on cap as described above.

Study of Sorption and Release of MC by Nitrocellulose.

Chemicals. A 55-gallon drum of nitrocellulose (NC; bailed linters; grade A) was obtained by ECBC from Esterline Defense Technologies (EDT), Coachella, CA. The NC was produced by Hanwa Corporation, Seoul, South Korea and the shipment was accompanied by a Certificate of Conformity from Hanwa Corporation, which showed that the lot (Lot # HWY07L07L062) was tested and met the requirements stated in Military Specification MILSPEC MIL-DTL-244B (1996). A batch (Batch # 7032) from this lot was re-tested by EDT before shipping to ECBC and found to contain 12.55% nitrogen and 26.66% moisture. The NC was accepted and stored in a secure, climate-controlled bunker in the dark by Joe Domanico, Ammunition Control Officer, ECBC. Small quantities of NC were delivered to the ECBC Environmental Toxicology laboratory as needed and stored in the dark at room temperature until testing commenced. An aqueous stock solution (< 1%) of military grade nitroglycerine (NG; CAS # 55-63-0) was obtained from University of Delaware. Crystalline 2,4-dinitrotoluene (2,4-DNT; CAS # 121-14-2) was obtained from Sigma-Aldrich™ (97%; batch # 48896LJ). These compounds were obtained, handled, and stored IAW ECBC Safety SOP # RNG-033, Safety SOP for Handling

Small Amounts of Munitions. Sodium azide (NaN_3; CAS # 26628-22-8) was obtained from MP Biomedicals, LLC (purity unknown; lot # 6967KA). All water used in these studies was obtained from a Milipore™ purification system (Prepak; Elix 10 UV; Academic; 18 MΩ·cm resistance). HPLC grade methanol was obtained from Acros Organics through ThermoFisher Scientific. All chemicals were weighed on a Mettler Toledo balance accurate to 0.0001 grams.

Determination of experimental conditions. In order to accurately calculate the sorption / desorption kinetics of NG and 2,4-DNT with NC, three key experimental parameters were determined for nitrocellulose, 1) hydration volume, 2) hydration time, and 3) equilibration time.

The hydration volume is the volume of the NaN_3 solution that must be added to the NC to achieve full hydration prior to the addition of MC. Eight samples containing 1.0 ±.004 g NC were placed in 12 mL borosilicate centrifuge tubes with phenolic caps and PTFE liners. Volumes of purified water (18.2 MΩ·cm) ranging from 1.8 to 4.0 mL containing 0.01 M NaN_3 were placed in each tube. A series of samples containing 1.0 ± 0.1 g NC was prepared. Masses of the culture tubes with caps, and culture tubes with caps plus NC were recorded. Incremental volumes of water were added to the sample series. The samples were centrifuged at 750 × g for 30 minutes. If free water remained after centrifugation, it was drawn with a Pasteur pipette and weighed in tared tubes. Free water is a water layer observed on top of the NC layer once it has reached maximum hydration. If the free water is no longer apparent by observation, the water is being sorbed to the NC. Based on results of the initial run, the procedure was repeated with water-added volumes (mL) of 2.7, 2.8, 2.9, 3.0, 3.1, and 3.2, in duplicate. The volume of water added initially was plotted against the volume of free water recovered (if present), and extrapolated to zero to determine the volume at which no solution is recovered. The volume added at zero recovery of free water is the maximum hydration volume. A linear regression analysis was performed on all data using water added (x axis) plotted with free water collected (y axis), resulting in an x value of 2.799 g water (Figure 11). Therefore, 2.80 g water per 1 g NC was used as the hydration volume for the sorption / desorption experiments. The water mass was varied proportionally to the mass of NC used. The hydration time, the amount of time that the NC was hydrated before batch experiments, was five days. This is the hydration time required to have minimal effect on the extent of sorption of MC.

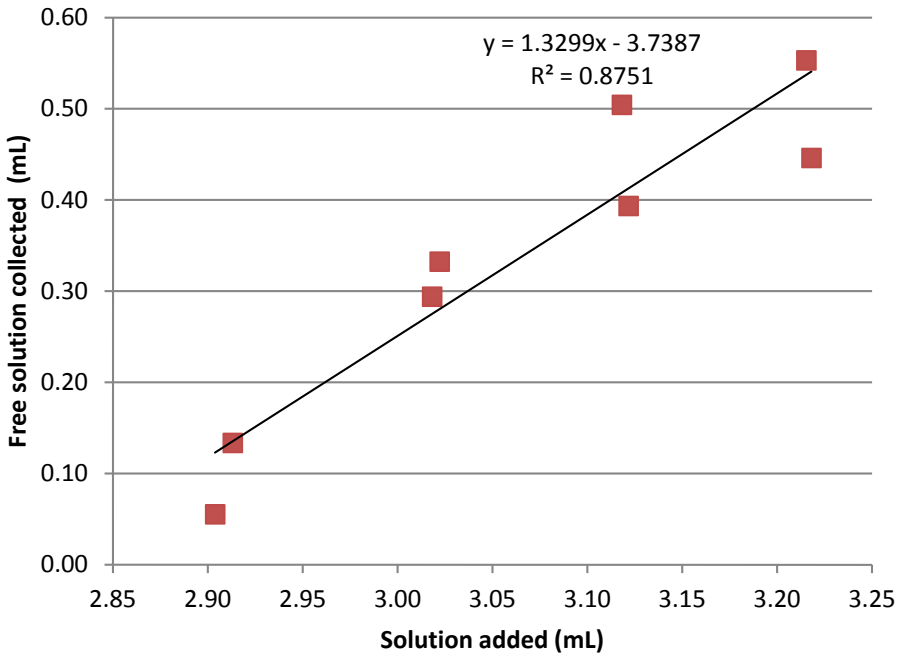

Figure 11. Volume of aqueous solution (0.01 M NaN_3) added to 1 g NC to attain full hydration. Hydration Volume (x) = 2.799 mL.

The equilibration time for sorption is the apparent time to achieve sorption steady-state concentrations of MC. The hydration volume of aqueous solution (NG or DNT + 0.01 M NaN_3) was added to each tube. Three additional tubes were prepared with the MC but without nitrocellulose, and a blank with NaN_3 solution (0.01 M) and NC. Each tube was vortex mixed for 15 s and placed in the end-over-end mixer in the dark. Samples were extracted periodically at the end of the indicated time, centrifuged for 30 min at 750×g, and drawn and filtered. All samples were analyzed by HPLC to determine their respective concentrations of MC.

A study was designed to determine the time needed to reach steady-state concentrations for sorption of NG onto NC. Five different masses of NC (0.484 g, 0.199 g, 0.099 g, 0.045 g, 0.018 g) were placed in each of 5 jars (Qorpac, 60 mL) with PTFE-lined screw-on caps. A volume of 69.08 ± 0.098 mL of solution containing 17.4 mg/L NG and 0.01 M NaN_3 was added to each jar. Two additional jars were included, one with the NG + 0.01 M NaN_3 solution sans nitrocellulose (i.e., positive control) and one with nitrocellulose with ASTM type I water only (negative control). Samples were collected 1, 4, 10, 48, 96, and 240 h following introduction of the solution into the jars. Each jar was vortex mixed for 15 s and placed on an end-over-end mixer and rotated at a rate of 30 rpm (Rotary Extractor, Lars Lande, Whitmore Lake, MI). At each time interval, approximately 5 mL of solution was extracted and placed into HPLC vials as described below. The NG concentration was determined by HPLC.

Sorption of NG onto nitrocellulose. A study was designed to determine the time needed to reach steady-state for sorption of NG onto nitrocellulose and to determine the sorption kinetics at steady-state. A solution of 20 mg L^{-1} of NG + 0.01 M NaN_3 was prepared from a stock solution containing analytically determined concentration of 453 mg L^{-1} NG. Five concentrations of NG (5, 20, 50, 200, 450 mg L^{-1}) solution were used in duplicate with 3 time points, (including three 0 time controls with no nitrocellulose and 20 mg L^{-1} NG) and 2 blanks (40 mg nitrocellulose,

water, and NaN_3 only). Nitrocellulose wet mass was weighed to 0.04 g (40 ± 0.5 mg) in all vials containing nitrocellulose. The nitrocellulose dry mass equaled nitrocellulose wet mass × 0.74 (nitrocellulose used in these studies contains 26% water by analysis) All NC was pre-wetted for five days with a solution of 0.01 M NaN_3 and 18.2 MΩ·cm H_2O (the previously determined hydration volume) for 5 days. Solutions containing 10 mL NG were auto-pipetted into pre-weighed 10 mL borosilicate glass centrifuge tubes with PTFE-lined caps and re-weighed. Each tube was vortex mixed for 15 s and placed on an end-over-end mixer and rotated at a rate of 10 rpm on a Labquake Tube Shaker Rotisserie, model no. 415110 (Thermo Fisher Scientific, Hanover Park, IL). At each time interval, solution from two tubes from each concentration of NG were pipetted from the vial, filtered, and placed in HPLC vials for analysis.

Sorption of 2,4-DNT onto NC. The experimental design to determine the sorption of 2,4-DNT onto NC consisted of five initial 2,4-DNT concentrations (1.55, 3.28, 12.8, 32.1, and 60.7 mg L^{-1}) with six timed analytical determinations (0, 48, 96, 144, 192, 384 h) for each concentration. All time/concentration pairs were replicated twice. A mass of 0.02 g (20 ± 0.5 mg) NC was wetted to the pre-determined hydration volume (mass of water as determined in the hydration time experiments) and placed in each pre-weighed 40 ml amber glass vials with PTFE-lined caps to which a solution of 2,4-DNT and 0.01 M NaN_3 was added to near the rim and re-weighed. The dry mass of nitrocellulose in each vial was determined by subtracting 26% from its wet mass. Each vial was vortex mixed for 15 s and placed on an end-over-end mixer and rotated at a rate of 30 rpm (Rotary Extractor, Lars Lande, Whitmore Lake, MI). At each time interval, 3 mL of solution was pipetted from the vial, filtered, and placed in HPLC vials for analysis. Triplicate samples of NG-only solutions for each concentration and NC-only controls were included.

Desorption of NG from NC. The experimental design to determine the desorption behavior of NG from nitrocellulose consisted of four NG concentrations (20, 50, 200, and 450 mg L^{-1}) in three volumes of desorption solution (10 mL, 40 mL, and 200 mL) containing 0.01 M NaN_3, and timed analytical determinations for each desorption solution volume / concentration combination. The NG was first sorbed onto the nitrocellulose until a steady-state concentration of NG was obtained in the solution. A mass of 0.04 g (40 ± 0.5 mg) nitrocellulose was placed in each vial. The dry mass of nitrocellulose in each vial was determined by subtracting 26% from the nitrocellulose wet mass. The nitrocellulose was wetted to the pre-determined hydration volume (volume of water as determined in the hydration time experiments) and placed in each pre-weighed 10 mL vial to which 10 mL of a solution of NG and 0.01 M NaN_3 was added with an auto-pipette and the vial was re-weighed. Each vial was vortex mixed for 15 s and placed on an end-over-end mixer and rotated at a rate of 10 rpm on a Labquake Tube Shaker Rotisserie, model no. 415110 (Thermo Fisher Scientific, Hanover Park, IL). At each time interval, solution from two tubes from each concentration of NG were pipetted from the vial, filtered, and placed in HPLC vials for analysis. Steady-state was determined when the concentrations of NG in solutions from consecutive time periods were not greater than each other.

After steady-state was obtained, the NG / NaN_3 solution was pipetted off and analyzed by HPLC to determine the solution concentration and to calculate an estimate of the NG concentration that remained sorbed to the NC. The solutions were replaced by a solution of 0.01M NaN_3 with no NG. The nitrocellulose designated for the 40 mL and 200 mL solutions were placed in respective pre-weighed 40 mL and 200 mL jars and filled to volume and re-weighed. The 10 mL solutions containing 20 mg L^{-1} NG were sampled at 1, 8, and 208 h and the solutions containing 50, 200 and 450 mg L^{-1} NG were sampled at 1, 4, 8, 48, and 208 h. The 40 mL solutions containing 20

and 50 mg L^{-1} NG were sampled at 1, 8, and 208 h, whereas solutions containing 200 and 450 mg L^{-1} were sampled at 1, 4, 8, 48, and 208 h. All replicate 10 mL and 40 mL solutions were in separate tubes. Two replicate tubes were sacrificed at each time interval for analysis. The 200 mL solutions were replicated twice per concentration and samples were taken from the same jar at each time interval. The 200 mL solutions were sampled at 1, 4, 8, 48, 100, 240, and 360 h. All samples were analyzed by HPLC.

Desorption of 2,4-DNT from NC. The experimental design to determine the desorption of 2,4-DNT from nitrocellulose consisted of three 2,4-DNT concentrations (20, 50, and 200 mg L^{-1}) in three volumes of desorption solution (10 mL, 40 mL, and 200 mL) containing 0.01M NaN_3, and timed analytical determinations for each desorption solution volume / concentration combination. The 2,4-DNT was first sorbed onto the NC until a steady-state concentration of 2,4-DNT was obtained in the solution. Steady-state was achieved when the concentration of 2,4-DNT was not different after two consecutive time intervals. A mass of 0.02 g (20 ± 0.05 mg) NC was wetted to the pre-determined hydration volume and placed in each pre-weighed 10 mL vial to which a solution of 2,4-DNT and 0.1 M NaN_3 was added with an auto-pipette to 10 mL and re-weighed. The dry mass of NC in each vial was determined by subtracting 26% (mass of water as determined in the hydration time experiments) from the nitrocellulose wet mass. Each vial was vortex mixed for 15 s and placed on an end-over-end mixer and rotated at a rate of 10 rpm on a Labquake Tube Shaker Rotisserie, model no. 415110 (Thermo Fisher Scientific, Hanover Park, IL). At each time interval, solution from two tubes from each concentration of 2,4-DNT were pipetted from the vial, filtered, and placed in HPLC vials for analysis. Steady-state was determined when the concentrations of 2,4-DNT in solutions from consecutive time periods were not greater than each other.

After steady-state was attained, the 2,4-DNT / NaN_3 solution was pipetted off and analyzed by HPLC to determine the solution concentration and to calculate an estimate of the 2,4-DNT concentration that remained sorbed to the NC. The solutions were replaced by a solution of 0.1 M NaN_3 with no 2,4-DNT. The NC designated for the 40 mL and 200 mL solutions were placed in respective pre-weighed 40 mL and 200 mL jars and filled to volume and re-weighed. Tubes containing the 10 mL solutions were vortex mixed for 15 s and placed on an end-over-end mixer. The 10 mL solutions containing 20 mg L^{-1} 2,4-DNT were sampled at 1, 8, and 208 h and the solutions containing 50, 200 and 450 mg L^{-1} 2,4-DNT were sampled at 1, 4, 8, 48, and 208 h. Jars containing the 40 mL and 200 mL solutions were vortex mixed and placed on an end-over-end mixer. The 40 mL solutions containing 20 and 50 mg L^{-1} 2,4-DNT were sampled at 1, 8, and 208 h, whereas solutions containing 200 and 450 mg L^{-1} were sampled at 1, 4, 8, 48, and 208 h. All replicate 10 mL and 40 mL solutions were in separate tubes. Two replicate tubes were sacrificed at each time interval for analysis. The 200 mL solutions were replicated twice per concentration and samples were taken from the same jar at each time interval. The 200 mL solutions were sampled at 1, 4, 8, 48, 100, 240, and 360 h. All samples were analyzed by HPLC.

Data and statistical analyses. Concentrations of NG and 2,4-DNT on nitrocellulose were determined by mass balance, following earlier sorption works [Yamamoto et al. 2004; Clausen et al. 2010] and the EPA standard guideline [US EPA 2008]. For cases where the sample vials were sacrificed upon measurement, the sorbed phase MC concentration is determined as:

$$S_t = \frac{V(C_o - C_t)}{mass_{NC}} \tag{3}$$

where S_t is the MC concentration in nitrocellulose (mg g^{-1}), V is the volume of the MC solution (L) introduced into the vial, C_o is the aqueous concentration of the introduced MC solution (mg L^{-1}), C_t is the dissolved phase concentration of the MC (mg L^{-1}) measured at time t, and $mass_{NC}$ is the total dry mass of nitrocellulose in the vial (mg, i.e., $mass_{NC}$ = wet mass NC × 0.74). In cases where samples were withdrawn without sacrificing the vials (i.e., desorption in 200-mL vial), the sorbed phase MC concentration was determined with the following expression:

$$S_t = \frac{VC_o - V_{sample}\sum C_i}{mass_{NC}} \tag{4}$$

where V_{sample} is the dissolved phase sampling volume (L) per sample, C_i is the dissolved phase MC concentration at i^{th} sampling time (mg L^{-1}). This expression is derived from mass balance on MC accounting for the fact that the amount of MC taken away from the vial varies as sorption or desorption proceeds.

All data and statistical analyses were performed in R language (version 3.1.2) using built-in functions or user-defined scripts. In addition, figures were constructed using R scripts.

Results and Discussion

Effect of Duration of Adsorption and Desorption on MC Partitioning to Soil. The effect of adsorption and of desorption duration on the partitioning of MC onto Nevada (N), Matapeake (M) and Rhydtalog (R) soils from a solution containing an initial concentration of 3 mg L^{-1} of RDX and NG and 1 mg L^{-1} of HMX (1:1 (w/v) soil to solution ratio) was studied. The sorbed concentrations were estimated by the difference in aqueous concentrations. Controls for the experiment showed no decay of the MC in the presence of NaN_3.

Adsorption time. Triplicate samples were vortex mixed for 15 seconds to suspend the soil, and were then shaken at 10 rpm in an end-over-end shaker for 2, 5, 10, and 30 days. Four consecutive desorptions were performed after each adsorption time for 1, 12, 24, and 72 hours whereby 5 mL of solution containing 0.01 M $CaCl_2$ and 0.01 M NaN_3 was added to samples that had been decanted of the preceding solution, followed by vortex mixing for 15 seconds and mixing in the end-over-end shaker for the 1, 12, 24, or 72 hour desorption time. A separate experiment with only one desorption after 30 days of adsorption time and 30 days of desorption time was conducted to identify the influence of long time on the desorption process. Each supernatant obtained from adsorption and each desorption after each adsorption time was analyzed for MC by HPLC. Each adsorption time and each desorption time was a separate treatment.

As is shown in Table 8 and Figure 12, the change in the amount of explosive sorbed per gram of soil (q) is small for HMX and RDX. Our results are in agreement with those of Monteil-Rivera et al. [2003] who observed that HMX was not significantly transformed after 7 days. For NG a continuous increase in the amount adsorbed as the time of sorption increases is observed, indicating that the amount of MC sorbed in this particular explosive is time dependent. However, because no extractions were performed, the apparent increase in the amount sorbed with time could also have been a result of degradation. Another important observation is that the behavior of all MC is consistent for these different soils, but in the case of NG the effect of kinetics is greatest in Nevada soil which is the soil with the lowest amount of organic carbon. In fact the effect is minimum with Rhydtalog soil that has 13% of OC, the highest percentage for the soils tested.

Desorption time. The concentrations of the solution after four consecutive desorptions and the desorption behavior presented a different trend than that of the adsorption [Xue et al., 1995; Sheremata et al., 2001; Hatzinger et al., 2004]. Table 9 and Figure 13 present the explosive sorbed per gram of Matapeake soil (q) after 30 days of adsorption from a solution that contained 5 mg L^{-1} for each MC except for HMX whose concentration was 2 mg L^{-1} (1:1 (w/v) soil to solution ratio) of HMX, RDX, and NG. Adsorption (A) and four consecutive desorptions (D1 to D4) for all desorption times are shown. Batch sorption/desorption simulates major processes involved in the partitioning and leaching of munition compounds in soil by rain water. The difference in the amount of MC sorbed among the various desorption times is very small even after 30 days of desorption. The figure shows that after each desorption, the explosive sorbed decreases and the data suggests that the main effect in the values of MC remaining is provided by the sorption time rather than desorption time. Desorption appears to be nearly instantaneous. Also, this figure indicates that the sorption of RDX is more reversible than the sorption of HMX and NG. This is because after the fourth desorption the concentration of RDX on the solids is nearly zero, whereas for the HMX and NG the concentration on the solids appears to reach a constant value. This behavior suggests that the resistance to desorption is greater for HMX and NG than for RDX. This finding is evidence that partition coefficients of adsorption should not be

applied to desorption confirming that the finding of Di Toro and Horzempa [1982] for PCB's, other organic chemicals [Di Toro 1985] and metals [Di Toro et al. 1986] are also observed for MCs.

Table 8. HMX, RDX and NG sorbed (µg) per gram of Nevada (N), Matapeake (M), and Rhydtalog (R) soil for 2. 5, 10, and 30 days of adsorption and 1 h desorption from a solution initially containing 3 mg L^{-1} of RDX and NG and 1 mg L^{-1} HMX.

	HMX			RDX			NG		
	q, µg MC g $soil^{-1}$								
Adsorption Time	N	M	R	N	M	R	N	M	R
2 Days	0.411	0.555	0.879	0.458	0.810	2.611	0.339	0.826	2.462
5 Days	0.498	0.518	NR*	0.442	0.851	NR	0.330	0.970	NR
10 Days	0.482	0.576	0.976	0.419	0.915	2.646	0.656	1.205	2.623
30 Days	0.535	0.647	NR	0.500	0.976	NR	0.946	1.344	NR

* 5 day and 30 day samples were not run for Rhydtalog soil.

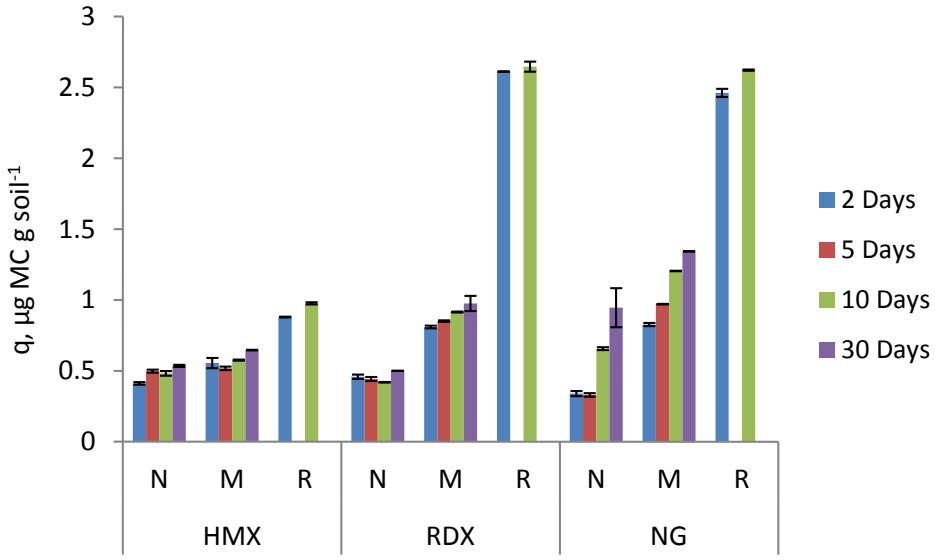

Figure 12. Effect of contact time (2, 5, 10 or 30 days) on the adsorption of MC onto Nevada (N), Matapeake (M) and Rhydtalog (R) soils from a solution initially containing 3 mg L^{-1} of RDX and NG, and 1 mg L^{-1} of HMX.

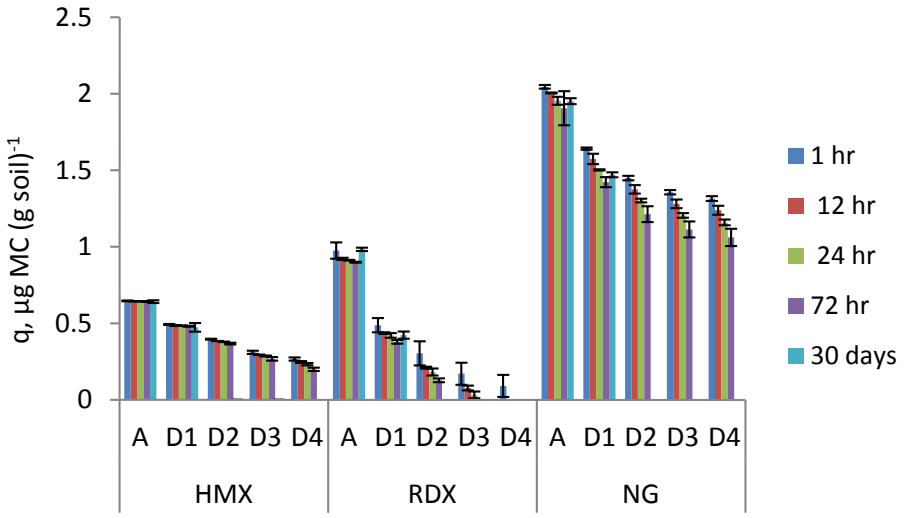

Figure 13. Effect of desorption time on adsorption (A) followed by four consecutive desorptions (D1 to D4) of HMX, RDX and NG sorbed after 30 days in Matapeake soil from a solution initially containing 5 mg L^{-1} of RDX and NG and 2 mg L^{-1} of HMX.

Table 9. HMX, RDX and NG sorbed (µg) per gram of soil following 1, 12, 24 and 72 hours of desorption after 30 days of adsorption in Matapeake soil from a solution initially containing 5 mg L^{-1} of RDX and NG and 2 mg L^{-1} of HMX.

	HMX					RDX					NG				
	q, µg MC g $soil^{-1}$														
Desorption Time	A	D1	D2	D3	D4	A	D1	D2	D3	D4	A	D1	D2	D3	D4
1 h	0.647	0.492	0.396	0.310	0.266	0.976	0.487	0.303	0.170	0.090	2.045	1.641	1.449	1.356	1.315
12 h	0.645	0.485	0.384	0.294	0.246	0.921	0.436	0.210	0.077	NA*	2.005	1.574	1.376	1.280	1.239
24 h	0.644	0.484	0.379	0.286	0.232	0.912	0.420	0.182	0.032	NA	1.954	1.502	1.302	1.205	1.159
72 h	0.642	0.481	0.367	0.267	0.199	0.899	0.379	0.128	NA	NA	1.905	1.422	1.213	1.113	1.061
30 days	0.641	0.473	NA	NA	NA	0.983	0.423	NA	NA	NA	1.952	1.470	NA	NA	NA

*NA = not analyzed

Reversible and resistant sorption model. The information presented above shows that it is not appropriate to apply the partition coefficients of sorption to desorption in studies where the MC's are investigated. There is resistance to desorption presented by some MC's such as HMX and NG compared with RDX, which is consistent with the literature [Ainsworth et al. 1993; Selim et al. 1995; Larson et al. 2008]. To account for this resistance to desorption, the reversible/resistant model of Di Toro and Horzempa [1982] was applied. This model is used because Figures 13 and 14 show that all of the sorbed compounds are not reversibly released.

In this model the overall adsorption of a chemical q ($\mu g\ g^{-1}$) is comprised of a reversible portion (q_x) and a resistant portion (q_0) as shown in Figure 13, where data (Table 10) for 30 days adsorption of a 5 mg L^{-1} initial solution concentration of NG onto Matapeake soil is presented. The resistant component can be obtained by extraction of the soil after the last desorption and, as was previously noted, the resistant behavior is chemical specific.

The resistant component, q_0, is the concentration on the particle that remains at zero dissolved concentration. It is obtained as the extrapolated intersection from adsorption followed by the consecutive desorptions plotted on the ordinate. This component shows no hysteresis [Delle, 2001]. The reversible component, q_x, is the difference between the adsorption (subscript a) and desorption (subscript D) particulate concentration and the extrapolated resistant concentration q_0:

$$q_{x\,a} = q_a - q_0 \tag{5}$$

$$q_{x\,D} = q_D - q_0 \tag{6}$$

Table 10. Solution concentration and MC sorbed (µg) per gram of soil of HMX, RDX and NG after 30 days of adsorption time for 1, 12, 24 and 72 hours of desorption time from Matapeake soil.

	HMX							
Desorption Time	1 h		12 h		24 h		72 h	
	Solution Concentration mg L^{-1}	*q*, µg MC g $soil^{-1}$	Solution Concentration mg L^{-1}	*q*, µg MC g $soil^{-1}$	Solution Concentration mg L^{-1}	*q*, µg MC g $soil^{-1}$	Solution Concentration mg L^{-1}	*q*, µg MC g $soil^{-1}$
Adsorption	0.5306	1.0320	0.5382	1.0220	0.5405	1.0177	0.5440	1.0025
Desorption 1	0.3085	0.8081	0.3142	0.7930	0.3233	0.7773	0.3267	0.7764
Desorption 2	0.2168	0.6262	0.2226	0.6052	0.2262	0.5882	0.2297	0.5820
Desorption 3	0.1349	0.5226	0.1399	0.4968	0.1467	0.4719	0.1509	0.4601
Desorption 4	0.0916	0.4475	0.0952	0.4186	0.1010	0.3884	0.1122	0.3618
	RDX							
Adsorption	2.6837	1.5750	2.7073	1.5431	2.7392	1.4975	2.7292	1.5257
Desorption 1	1.2808	0.8279	1.3117	0.7621	1.3398	0.6906	1.3228	0.7310
Desorption 2	0.6239	0.4540	0.6424	0.3742	0.6566	0.2942	0.6646	0.3132
Desorption 3	0.3153	0.2561	0.3308	0.1619	0.3407	0.0739	0.3604	0.0664
	NG							
Adsorption	2.0907	2.0451	2.1202	2.0053	2.1558	1.9541	2.2042	1.9054
Desorption 1	0.8685	1.6413	0.8963	1.5742	0.9218	1.5019	0.9543	1.4222
Desorption 2	0.3784	1.4493	0.3909	1.3755	0.3989	1.3020	0.4129	1.2134
Desorption 3	0.1717	1.3562	0.1765	1.2805	0.1806	1.2046	0.1858	1.1131
Desorption 4	0.0772	1.3150	0.0788	1.2388	0.0827	1.1591	0.0885	1.0612

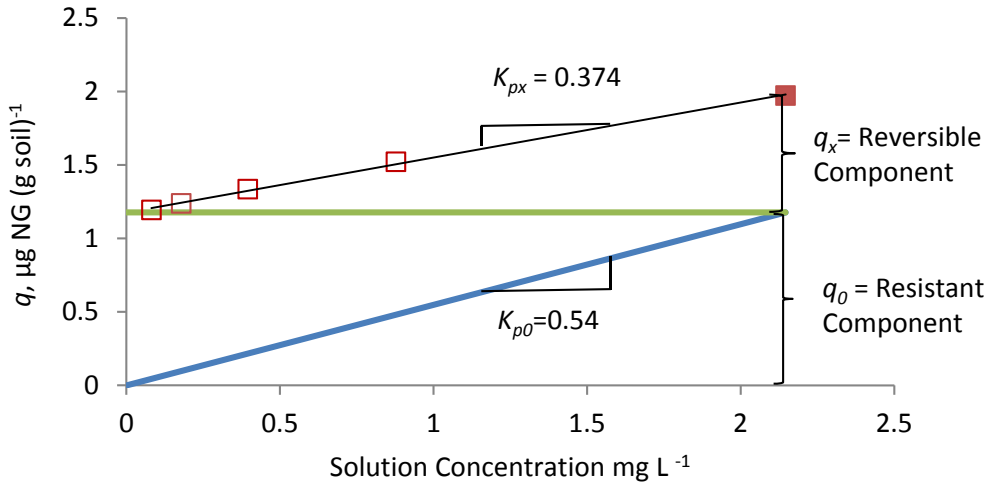

Figure 14. Reversible and resistant components of NG for 30 days adsorption onto Matapeake soil using the model proposed by Di Toro and Horzempa [1982]. The filled square represents the adsorption step and unfilled squares represent the consecutive desorption steps.

The model also defines the reversible and resistant component partition coefficients K_{px} and K_{p0} as:

$$K_{px} = q_{xD}/C_D \quad (7)$$

$$K_{p0} = q_0/C_A \quad (8)$$

where C_D is the desorption concentration and C_a is the concentration at the adsorption point. The desorption concentration of the chemical into the soil q_D, is a function of K_{px} and K_{p0}:

$$q_D = K_{p0} C_A + K_{px} C_D \quad (9)$$

where q_D is the soil concentration.

The reversible/resistant model was applied to all MC studied for samples containing initial concentrations of 5 mg L^{-1} for RDX and NG and 2 mg L^{-1} of HMX (data are in Table 11). Figures 15 A and B present the components of the model for Matapeake soil and they relate the amount of explosive sorbed per gram of soil (q) and the concentration (C). Figure 15 A shows the components after 30 days of adsorption time for each desorption time (1, 12, 24 and 72 hours) and Figure 15 B shows the components after 24 h of desorption time for each adsorption time (2, 5, 10 and 30 days). One fitted line for each chemical is presented. This indicates that the relationship between the adsorbed fraction and aqueous concentrations of MC describes the full adsorption and desorption isotherm data set by linear behavior, and the consecutive desorption data conform to desorption isotherms that can be represented by a single reversible component with partition coefficient K_{px} (Equation 9). In addition, the resistant component does not desorb after the consecutive desorptions are done. This is observed for HMX and NG rather than for RDX that is more reversible as was previously mentioned. The presence of this resistant component, especially for HMX and NG, indicates that partition coefficients of adsorption

cannot be used for desorption as was indicated previously. The model provides a good fit to the data even for variation in adsorption times as well as desorption times, so it can be used to predict adsorption and desorption concentrations of MC. The data points on Figure 15 A are more tightly grouped than are the ones on Figure 14 B, supporting the finding that adsorption time is a stronger factor on the full adsorption and desorption isotherm for these chemicals rather than is desorption time. This is seen by the fact that the separation of each data point of any chemical in Figure 15 A (desorption times) is no more than a 0.15 units of the MC sorbed (q), but in Figure 15 B (adsorption times) this separation can reach 1 unit of MC sorbed (q). On the other hand, it is important to mention that this set of data for the full adsorption and desorption isotherm of HMX, RDX and NG served to validate the reversible/resistant model [Di Toro and Horzempa 1982] because the authors suggested more experimental investigations in this area.

In addition to the results presented in Figures 14 A and B, Figure 16, 17 and 18 show the reversible component of HMX, RDX and NG for the three different soils (Matapeake, Nevada and Rhydtalog) for 2 days of adsorption time and all the desorption. The figures show that the model can be used to predict desorption of MC in soils with different characteristics because the reversible component of the MC fit with a straight line with same slope independent of the step (A, D1, D2, D3, D4), concentrations of 3-5 mg L^{-1} for RDX and NG and 1-2 mg L^{-1} for HMX, or adsorption and desorption times used . The range of the soil properties used provides evidence that the model can be applied to the MCs studied and it can be used to compute desorption concentrations of MC. Similar results are found in the literature, which have shown that as the organic matter content increases, sorption increases [Charles et al. 2008; Dontsova et al. 2009a; Zhang et al. 2009].

With the information obtained from the reversible and resistant components (Table 12), the reversible and resistant partition coefficients K_{px} and K_{p0} were calculated for each adsorption and desorption time (Figure 19). These figures show that as the desorption time increases, the reversibility for each chemical increases and the resistance decreases. RDX presents the most reversible behavior compared with HMX and NG. For RDX K_{px} is almost constant during all adsorption and desorption times and there is practically no resistant portion. For HMX and especially for NG the behavior is different. There is an adsorption time dependency for the resistance component, which decreases, as the desorption time increases. In the study of the resistance of NG, the adsorption time plays an important role as is observed in Figure 15 B; as it increases the resistance of the chemical to leave the soil increases.

To predict the concentrations of HMX and NG in the soil (q_D) in each desorption step (D1, D2, D3, and D4), a modification of the reversible/resistant model was made taking into account the effect of adsorption time.

The new assumption is that K_{p0} and the adsorption time has a first order relationship:

$$K^*_{p0} = K^*_{p0i}\ (1 - \exp(-\alpha t)) \tag{10}$$

$$q_D = K^*_{p0}\ C_A + K_{px}\ C_D \tag{11}$$

where K^*_{p0i} is the resistant partition coefficient at $t = 0$, t is the adsorption time and α is the rate constant.

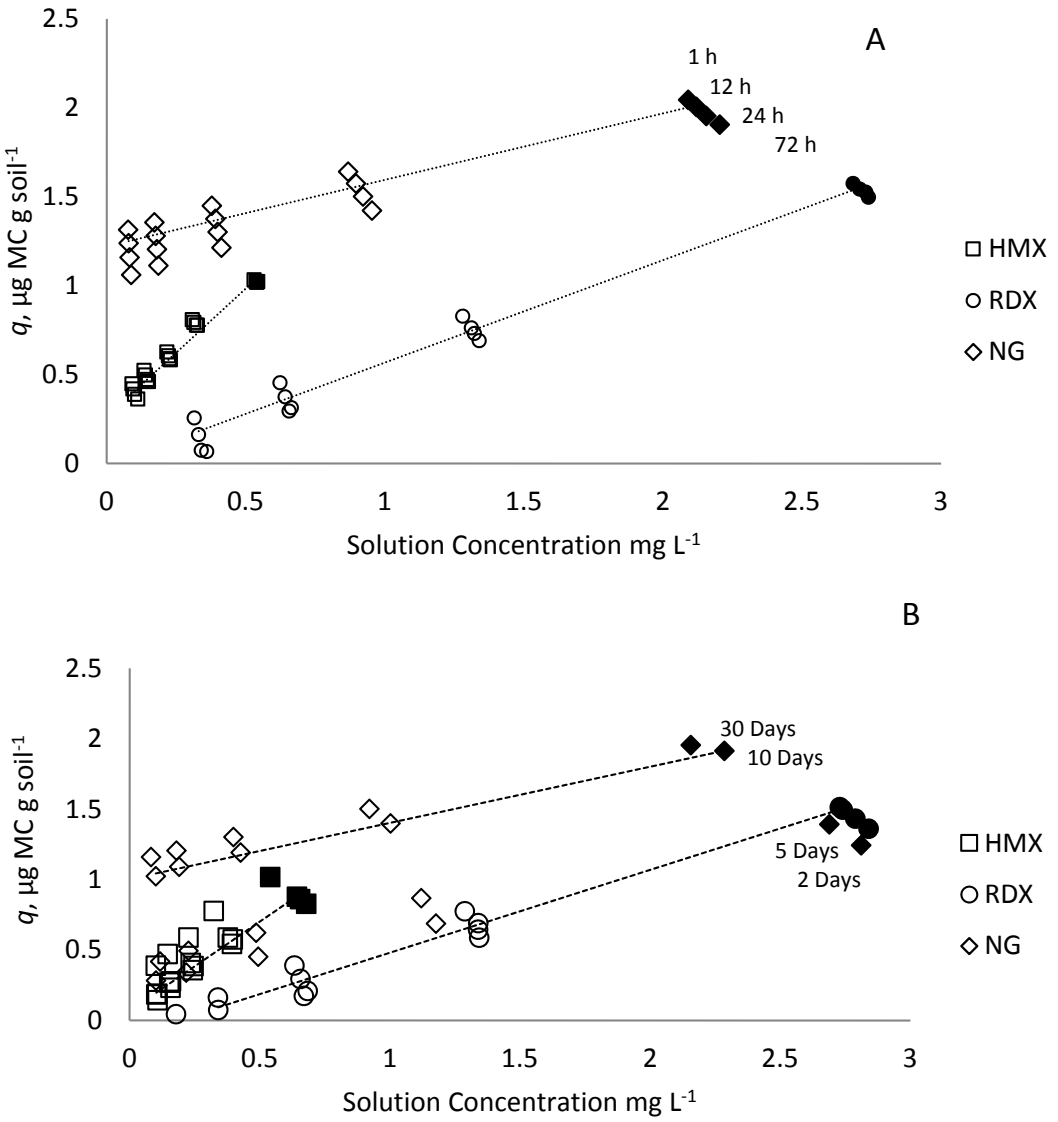

Figure 15. A. Reversible and resistant components of the model of HMX, RDX and NG after 30 days of adsorption time for 1, 12, 24 and 72 hours of desorption time from Matapeake soil. B. Reversible and resistant components of the model of HMX, RDX and NG after 24 hours of desorption time for 2, 5, 10 and 30 days of adsorption time from Matapeake soil. Initial concentrations were 5 mg L^{-1} for RDX and NG and 2 mg L^{-1} for HMX. Filled symbols represents the adsorption point and the unfilled ones the consecutive desorption steps.

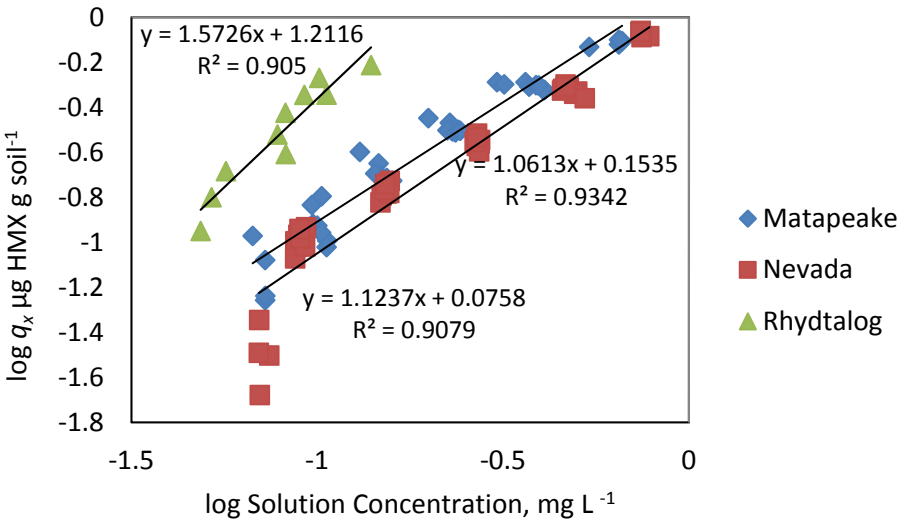

Figure 16. Reversible component (q_x, µg MC g soil^{-1}) of HMX after 2 days of adsorption time for 1, 12, 24 and 72 hours of desorption time from Matapeake soil.

Table 11. Solution concentration and MC sorbed (µg) per gram of soil of HMX, RDX and NG after 24 h of desorption time for 2, 5, 10 and 30 days of adsorption time from Matapeake soil.

Adsorption Time	30 Days		10 Days		5 Days		2 Days	
	Solution Concentration mg L^{-1}	*q*, µg MC g $soil^{-1}$	Solution Concentration mg L^{-1}	*q*, µg MC g $soil^{-1}$	Solution Concentration mg L^{-1}	*q*, µg MC g $soil^{-1}$	Solution Concentration mg L^{-1}	*q*, µg MC g $soil^{-1}$
	HMX							
Adsorption	0.5405	1.0177	0.6552	0.8607	0.6788	0.8282	0.6431	0.8776
Desorption 1	0.3233	0.7773	0.3776	0.5887	0.3938	0.5428	0.3968	0.5744
Desorption 2	0.2262	0.5882	0.2353	0.4075	0.2433	0.3567	0.2459	0.3858
Desorption 3	0.1467	0.4719	0.1595	0.2768	0.1579	0.2313	0.1527	0.2686
Desorption 4	0.1010	0.3884	0.1067	0.1902	0.1076	0.1427	0.1029	0.1845
	RDX							
Adsorption	2.7392	1.4975	2.7279	1.5150	2.7875	1.4330	2.8389	1.3622
Desorption 1	1.3398	0.6906	1.2878	0.7746	1.3389	0.6446	1.3435	0.5869
Desorption 2	0.6566	0.2942	0.6335	0.3898	0.6846	0.2086	0.6696	0.1733
Desorption 3	0.3407	0.0739	0.3392	0.1624	0.3500	NA*	0.3466	NA
Desorption 4	NA	NA	0.1786	0.0448	NA	NA	NA	NA
	NG							
Adsorption	2.1558	1.9541	2.2848	1.9141	2.6880	1.3925	2.8105	1.2442
Desorption 1	0.9218	1.5019	1.0027	1.3987	1.1206	0.8675	1.1772	0.6876
Desorption 2	0.3989	1.3020	0.4266	1.1910	0.4865	0.6220	0.4945	0.4525
Desorption 3	0.1806	1.2046	0.1905	1.0903	0.2262	0.4946	0.2175	0.3402
Desorption 4	0.0827	1.1591	0.1009	1.0235	0.1178	0.4181	0.1018	0.2824

*NA = not analyzed

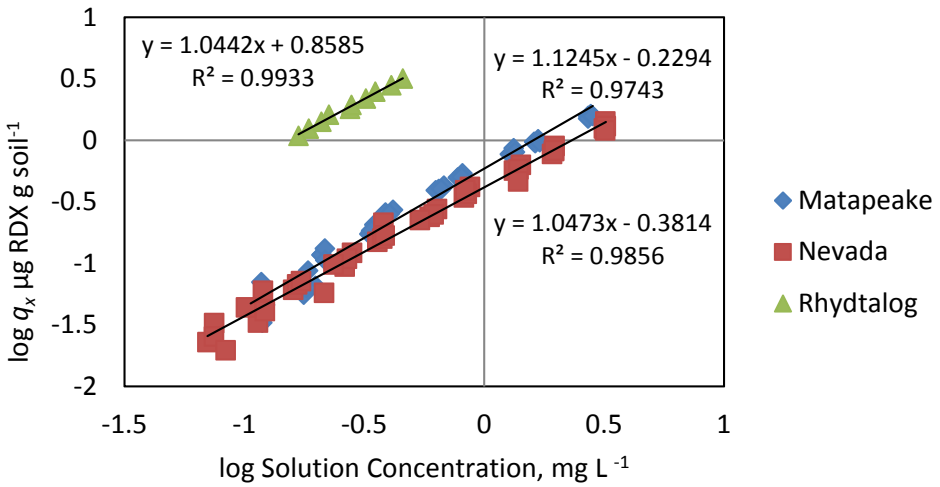

Figure 17. Reversible component (q_x, µg MC g soil^{-1}) of RDX after 2 days of adsorption time for 1, 12, 24 and 72 hours of desorption time from Matapeake soil.

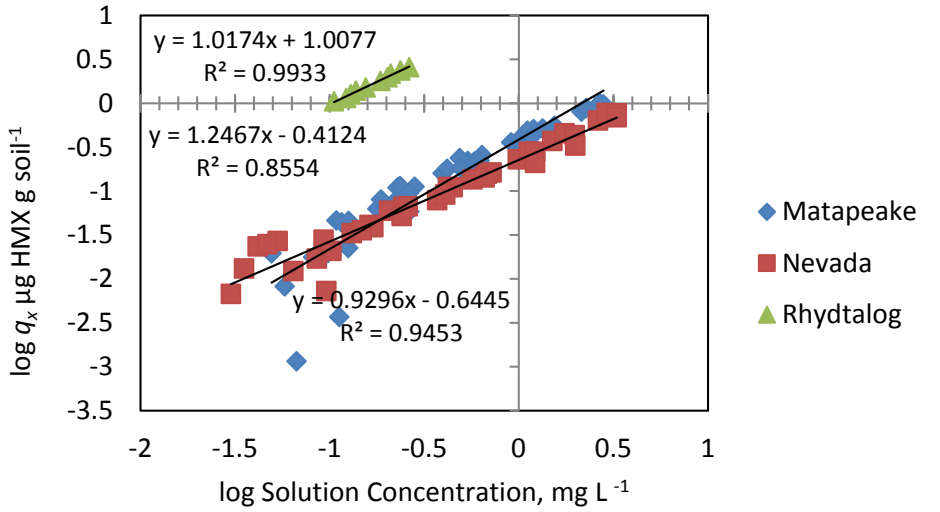

Figure 18. Reversible component (q_x, µg MC g soil^{-1}) of NG after 2 days of adsorption time for 1, 12, 24 and 72 hours of desorption time from Matapeake soil.

Table 12. Reversible and resistant partition coefficients K_{px} and K_{p0} for HMX, RDX and NG after 2, 5, 10 and 30 days of adsorption time for 1, 12, 24 and 72 hours of desorption time from Matapeake soil from a solution initially containing 5 mg L^{-1} of RDX and NG and 2 mg L^{-1} of HMX.

			HMX				RDX				NG			
			Desorption Time, Hour											
			1	12	24	72	1	12	24	72	1	12	24	72
K_{px}	Adsorption Time, days	30	1.341	1.373	1.440	1.515	0.580	0.588	0.614	0.631	0.360	0.374	0.381	0.395
		10	1.169	1.203	1.208	1.260	0.568	0.588	0.597	0.625	0.357	0.378	0.399	0.422
		5	NA*	1.156	1.182	1.201	0.603	0.618	0.624	0.635	0.348	0.367	0.370	0.447
		2	1.238	1.254	1.267	1.204	0.512	0.578	0.592	0.629	0.334	0.340	0.351	0.366
K_{p0}		30	0.647	0.571	0.488	0.488	0.035	NA	NA	NA	0.623	0.576	0.529	0.472
		10	0.289	0.190	0.144	0.144	0.006	NA	NA	NA	0.528	0.479	0.440	0.405
		5	0.244	0.126	0.069	0.069	NA	NA	NA	NA	0.221	0.190	0.155	0.043
		2	0.180	0.133	0.105	0.106	NA	NA	NA	NA	0.141	0.115	0.094	0.062

*NA = not analyzed

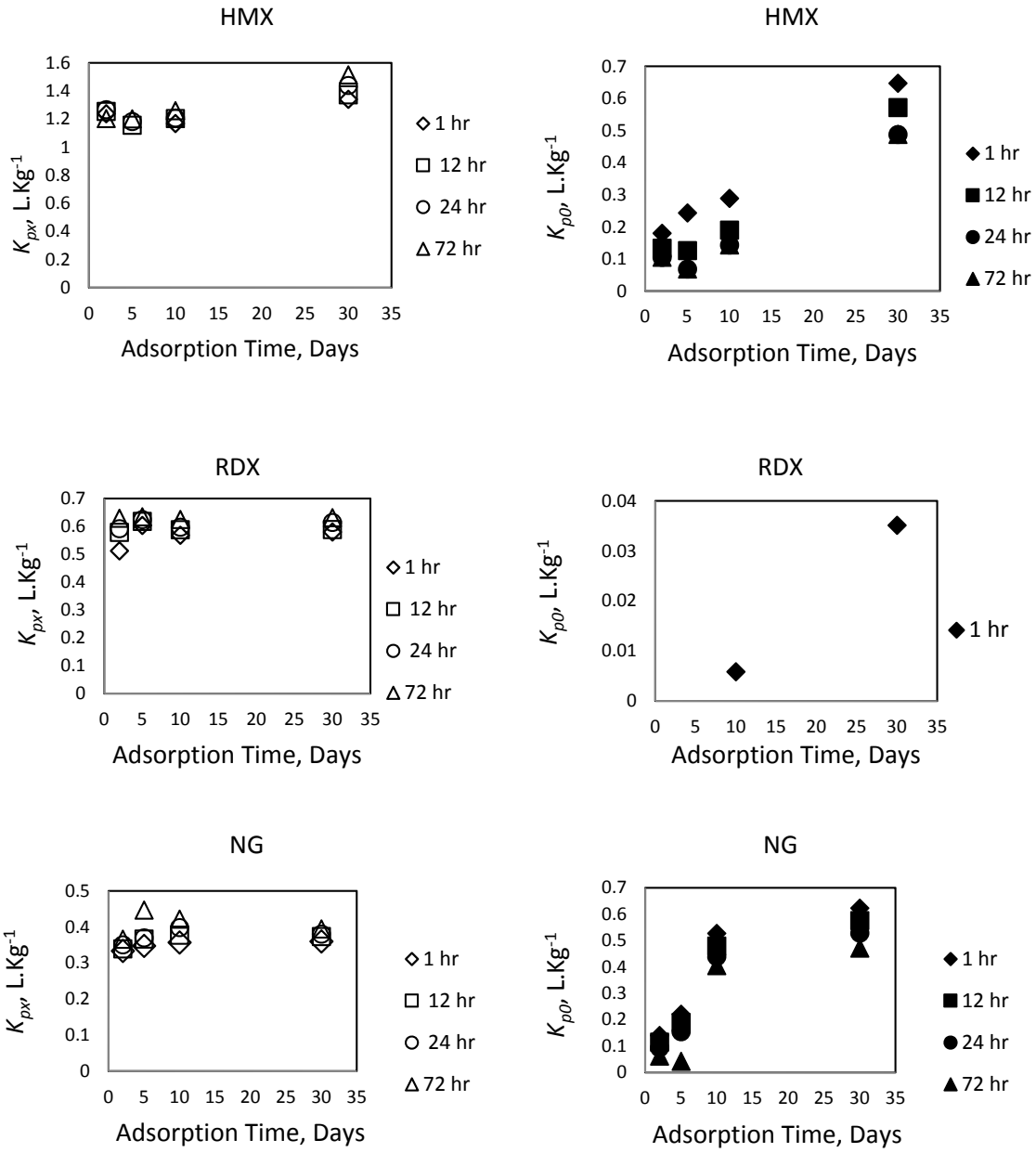

Figure 19. Reversible and resistant partition coefficients K_{px} and K_{p0} for HMX, RDX and NG after 2, 5, 10 and 30 days of adsorption time for 1, 12, 24 and 72 hours of desorption time from Matapeake soil from a solution initially containing 5 mg L^{-1} of RDX and NG and 2 mg L^{-1} of HMX.

Figure 20 shows the fitting of the K_{p0} first order model for HMX and NG to all concentrations and adsorption and desorption times. Table 13 presents the coefficients that were generated by fitting the first order model (Equation 10) by the minimization of the residuals square between the K_{p0} calculated from the model and K_{p0} obtained from the reversible/resistant model using the Excel solver tool. (Data are in Appendix D.3)

Figure 20 shows that the modification of the original reversible/resistant model (Equation 8) generates a single value of K_{p0} for each adsorption time according to Equation 10. In this way the number of parameters in the model is reduced by a factor of 4, making an improvement in the prediction because from a modeling point of view, the best scenario is to provide realistic values with the minimum number of parameters. For HMX there is an increasing trend of 0.015 L kg^{-1} per day indicating that over the period of study the maximum resistant value is not attained, whereas for NG there is a plateau which indicates that it reaches the maximum resistant concentration on the solids in around 30 days.

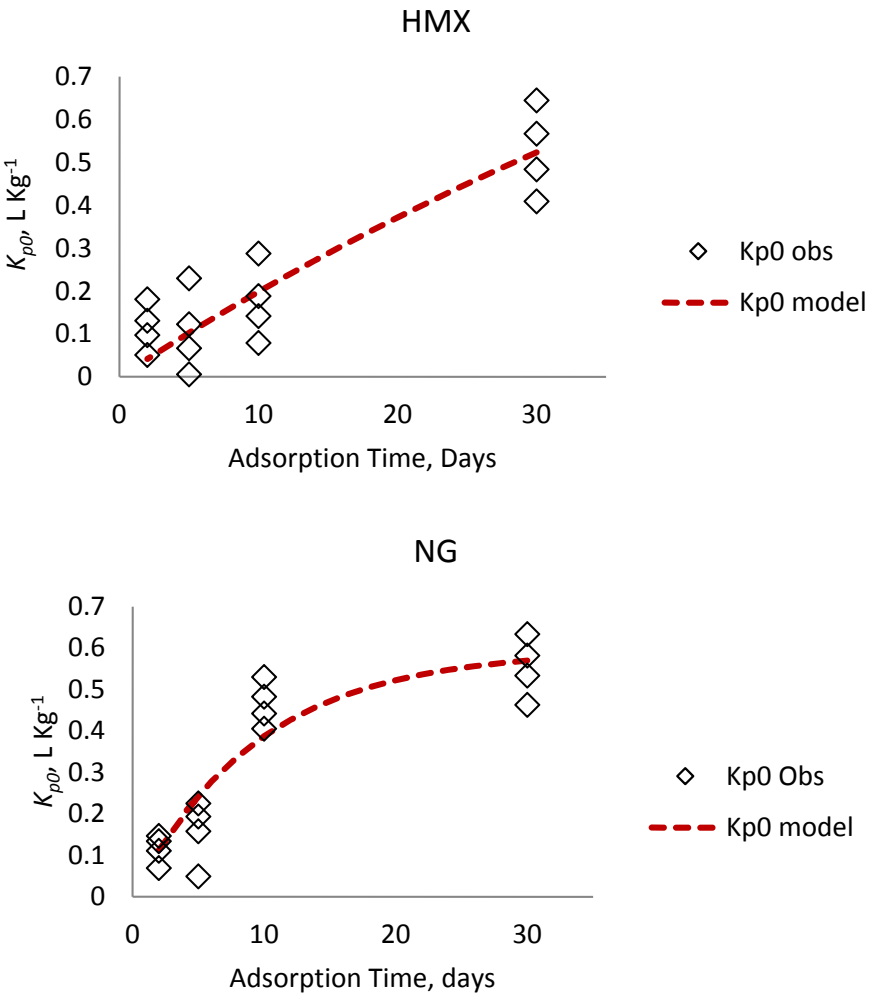

Figure 20. K_{p0} first order fitting model obtained from Equation 10 for HMX and NG.

Table 13. Parameters of the model obtained for HMX and NG from Equation 10.

Parameters	HMX	NG
K^*_{p0i} : Initial Resistant Partition Coefficient, L kg^{-1}	1.139	0.595
α: Rate Constant, $days^{-1}$	0.018	0.105

The next step in this study was to predict the concentrations of the MC in the soil according to Equation 11 and to compare them with the observed data. Table 14 shows the root mean square error, RMSE, of the predicted particulate concentrations and the particulate concentrations obtained from the measured data for HMX and NG. These RMSE values are very low, indicating that the values obtained by the model and the ones from the measurements have small differences. This is an indication that the prediction is good. On the other hand, Figure 21 shows that the predictions for HMX are within ± 0.1 of the observed values and those for NG are within 0.5 of the observed values (Appendix D.4). This supports the fact that the desorbed concentrations of MC's good predictions can be obtained using the reversible/resistant modified model of Equation 11.

Table 14. RMSE of the particulate concentration from predicted and measured particulate concentrations for HMX and NG.

	RMSE for particulate concentration µg MC g $soil^{-1}$			
	q_{D1}	q_{D2}	q_{D3}	q_{D4}
HMX	0.059	0.047	0.047	0.054
NG	0.162	0.181	0.201	0.194

Effect of Matrix Electrolyte on Adsorption and Desorption of MC. Adsorption and desorption of munitions constituents (MC) depend on the matrix in which they occur. For example, it is well known that adsorption on clay sites of nitro aromatic compounds (NACs) such as TNT is influenced by the cations on the clay [Haderlein et al. 1996]. This study involved sorption of a mixture of HMX, RDX, nitroglycerine (NG), TNT, 2,4-dinitrotoluene (2,4-DNT) and nitroguanidine (NQ) conducted by batch adsorption/desorption tests near 1:1 (w/v) soil to solution ratios, reflecting field conditions. The six soils used varied from pH 3.4 to 6.9, 4.0 to 43.2% clay size particles and 0.2 to 18.23% total organic carbon (Table 15). In addition, an agricultural peat soil of the Florida Everglades, the Pahokee peat from the International Humic Substances Society, was included. Soils were hydrated in a solution containing 0.01 M $CaCl_2$ or 0.03 M potassium chloride (KCl) or 0.03 M cesium chloride (CsCl) as electrolyte matrices for 5 days prior to the addition of MC. Each solution also contained 0.01 M NaN_3 as a microbial growth inhibitor. The ionic strengths of the potassium, cesium and calcium chloride electrolytes were 0.03 M. The concentration of each MC in the added solution was 10.0 mg L^{-1} except for HMX for which the concentration was 2.0 mg L^{-1} because it has a low solubility in water. The two adsorption times, 15 min and 48 h, were followed by four consecutive desorptions and then extraction with acetonitrile at the end.

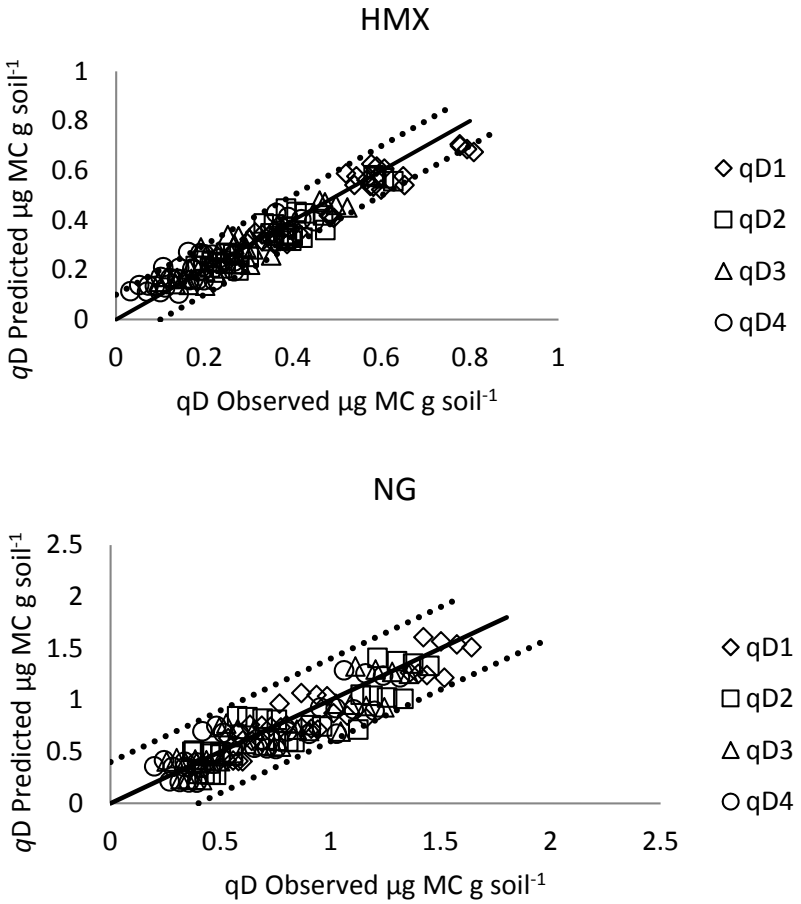

Figure 21. Relationship between observed and predicted particulate concentration in each desorption step (q_{D1} to q_{D4}) according to Equation 11 for HMX and NG.

Table 15. Soil Properties.

Soil	pH[a]	CEC[b]	Clay[c] (%)	TOC[d] (%)
Nevada	3.4	11.2	20.9	0.20
Souli	6.9	16.1	43.2	0.61
Matapeake	5.7	9.9	22.3	1.54
Houthalein	3.9	2.9	4.0	2.31
Joplin	6.5	43.8	18.7	10.12
Zegveld	4.8	54.8	21.7	18.23
Pahokee Peat	ND[e]	ND	11	28.13

[a] *1:1 (w/v)* soil:water
[b] Ammonium saturation buffered at pH 7.0
[c] Particle size analysis by hydrometer using the modified Bouyoucos Method [Bouyoucos 1961]
[d] Combustion using an Elementar Vario-Cube TOC Analyzer (Elementar Americas, Mt. Holly, NJ).
[e] ND = not determined

Sorption of MC in different electrolytes. The three different electrolytes were used to provide data from which to judge the importance of the clay fraction in the sorption of MC. The idea was to examine the influence of having Cs in the solution and to compare it to the results with K or Ca in the solution for the three groups of chemicals: nitramines HMX and RDX, aliphatics NG and NQ, and NACs TNT and 2,4-DNT. Figures 22-24 show that in most of the cases the amount of MC sorbed per gram of soil in the adsorption and consecutive desorptions for HMX, RDX, NQ, TNT and 2,4-DNT as a function of electrolyte were greater when the electrolyte used was cesium. Although NG was in the same sample it had a different behavior; for this explosive the amount of explosive sorbed per gram of soil is not dependent on the electrolyte used. The amount of MC sorbed was high in soils with high carbon content for each of the six explosives studied. Also, high values of adsorption were found for TNT and 2,4-DNT in soils with low total organic carbon content (0.2 to 2.31% of TOC) when cesium was used as electrolyte. The data shown in Figures 22-24 are in Appendix H.1. Literature suggests that the Cs^+ cation is highly adsorbed on clay minerals [Barshad 1948; Posner et al. 1964; Edwards et al. 1965], providing evidence of the importance of this soil property in the adsorption/desorption of MC. Also the amount of MC sorbed on soils with low organic carbon content was considerably greater for the nitroaromatics TNT and 2,4-DNT compared to the sorption of the nitramines HMX and RDX and the aliphatic NG and NQ.

Application of reversible and resistant model to the sorption of MC in different electrolytes. The information presented in Figures 22-24 showed decreasing concentrations for the consecutive desorptions with an approach to a plateau independent of the soil and the electrolyte used. These figures also show that it is not accurate to apply the partition coefficients of sorption to desorption because there is resistance to desorption presented by some MC's. For this reason, the reversible/resistant model was applied to all MC and electrolytes studied from the mixture of explosives of initial concentration 10 mg L^{-1} (except 2 mg L^{-1} for HMX).

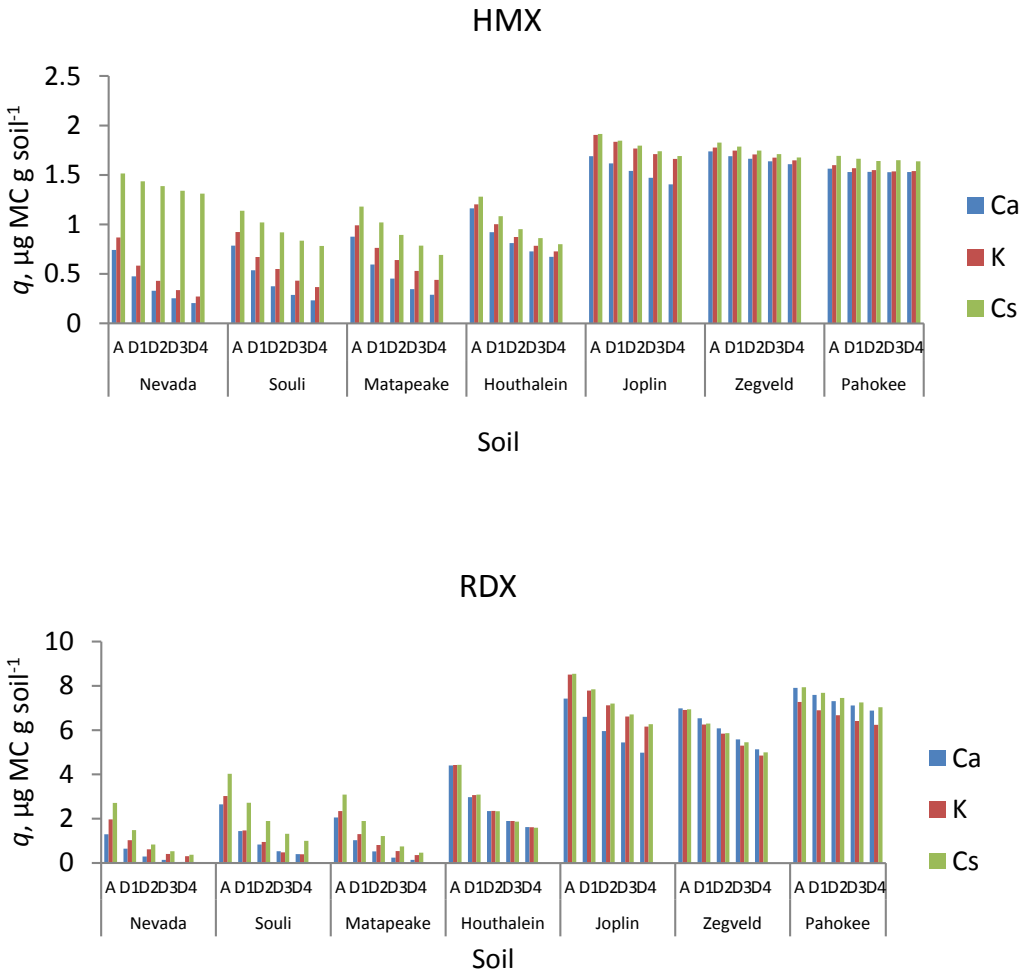

Figure 22. Amount of explosive sorbed per gram of soil (q) in the adsorption (A) – desorption (D1 to D4) of nitramines HMX and RDX for Ca, K and Cs matrix from a solution initially containing 10 mg L^{-1} of each MC except 2 mg L^{-1} for HMX.

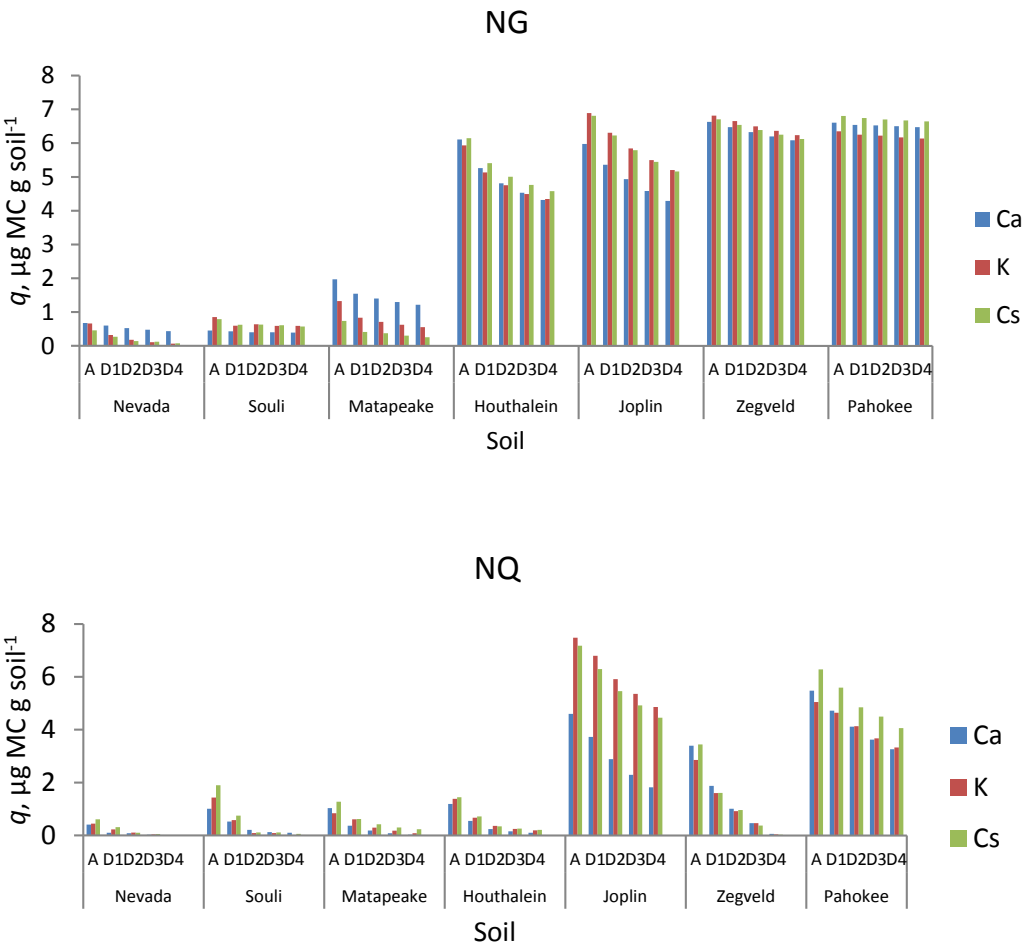

Figure 23. Amount of explosive sorbed per gram of soil (q) in the adsorption (A) – desorption (D1 to D4) for aliphatic NG and NQ for Ca, K and Cs matrix from a solution initially containing 10 mg L^{-1} of each MC except 2 mg L^{-1} for HMX.

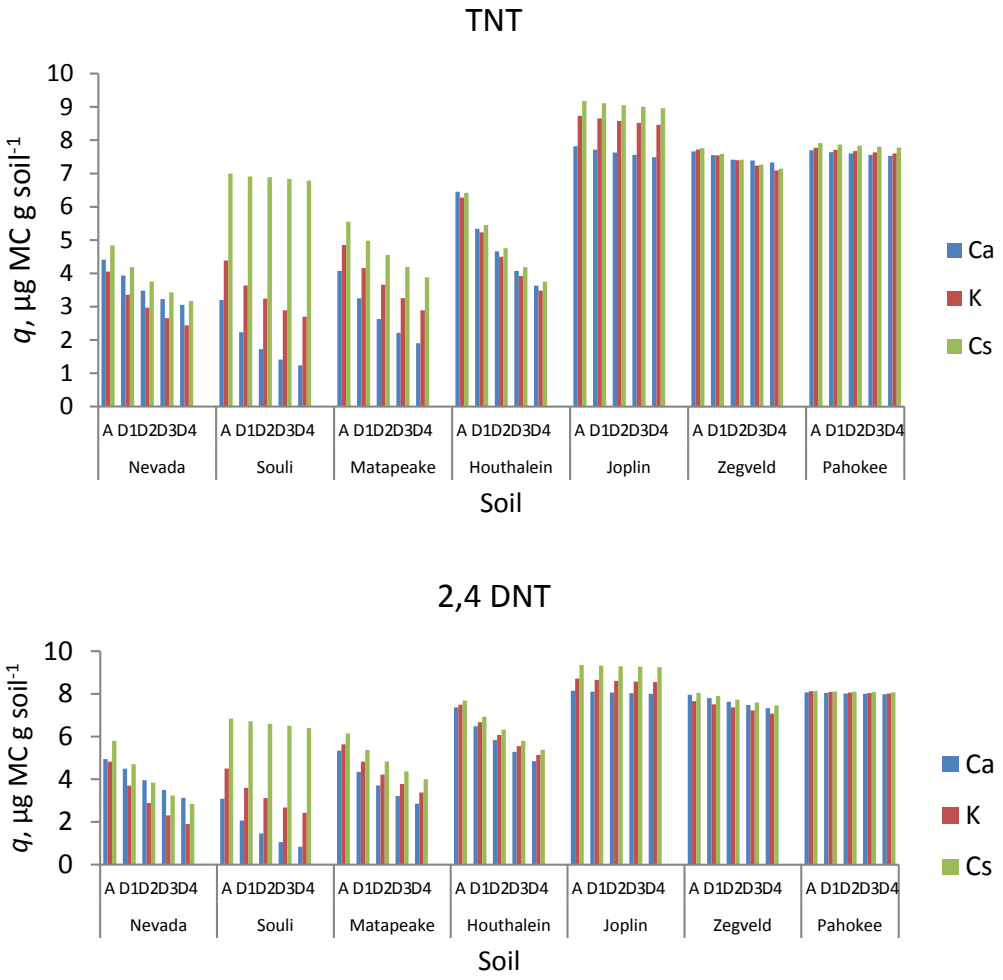

Figure 24. Amount of explosive sorbed per gram of soil (q) in the adsorption (A) – desorption (D1 to D4) for NACs TNT and 2,4-DNT for Ca, K and Cs matrix from a solution initially containing 10 mg L^{-1} of each MC except 2 mg L^{-1} for HMX.

The data were evaluated by the model in three different ways: varying electrolytes for one soil and one MC; varying the MC for one soil and one electrolyte; and varying soils for one MC and one electrolyte. Figure 25 A shows the information for sorption of RDX in Souli soil using Ca, K and Cs electrolytes; in Figure 25 B the sorption of all MC in Houthalein soil is shown for K electrolyte, and in Figure 25 C sorption of NG in all soils studied using Cs as electrolyte is shown. The complete set of evaluation for all MC, soils and electrolytes are in Appendices H.3, H.4, and H.5. The figure relates the amount of explosive sorbed per gram of soil (q) and the steady-state concentration.

Figure 25 A shows that the resistant component q_0, the amount of the MC on the particles remaining at zero dissolved concentration, varies among electrolytes. For sorption of RDX on Souli soil, this component is greater when Cs, rather than K or Ca, is the electrolyte. This is also observed for Matapeake, Nevada, Zegveld and Joplin soils in accordance with the data in Appendices H.3, H.4, and H.5 as shown previously in Figures 22-24. It is well known that RDX is poorly immobilized by soils [Sunahara et al. 2009] due its reversibility. Figure 25 A confirms

this because q_0 is very small and in the case of K and Ca electrolytes this value tends to be zero.

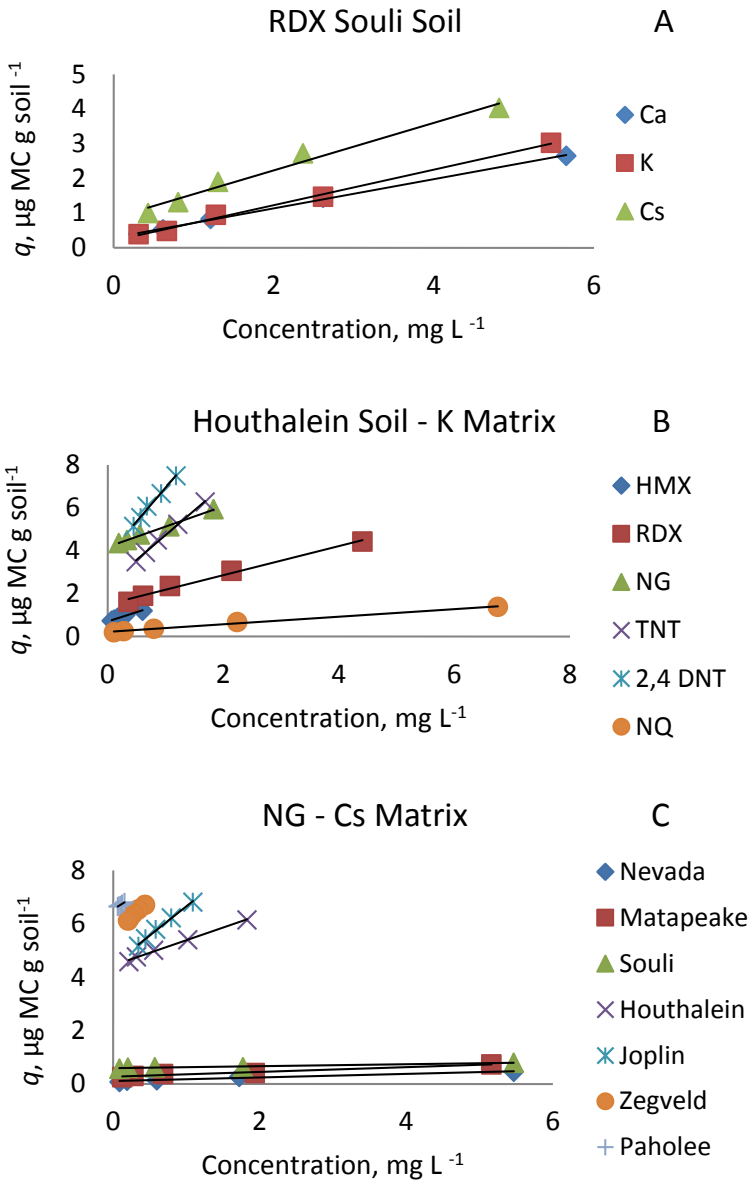

Figure 25. Reversible and resistant components of the model of MC (HMX, RDX, NG, TNT, 2,4-DNT, NQ), electrolytes (Ca, K, Cs), and soils used in the study.

Figure 25 B differs from 25 A because all MC are shown for Houthalein soil and K electrolyte. From the figure it can be seen that each MC has different reversible and resistant components. TNT and 2,4-DNT have higher values of q_0 relative to those for HMX, RDX, NG and NQ. This trend is also observed for Ca and Cs electrolytes and all soils as shown in Appendices H.3, H.4, and H.5. The chemical composition of the MC makes the difference between the components. Nitramines and NQ that are highly soluble in water are more reversible than NG and NACs that are more resistant for the same conditions of soil and electrolyte. Figure 25 C shows that the soils

with high TOC values exhibit greater resistant components, while the low TOC soils have low values of q_0 for the same MC and electrolyte (NG and Cs), indicating that soil properties are crucial in the sorption of MC. Figure 26 shows this relationship between the resistant component and TOC through graphs for each electrolyte.

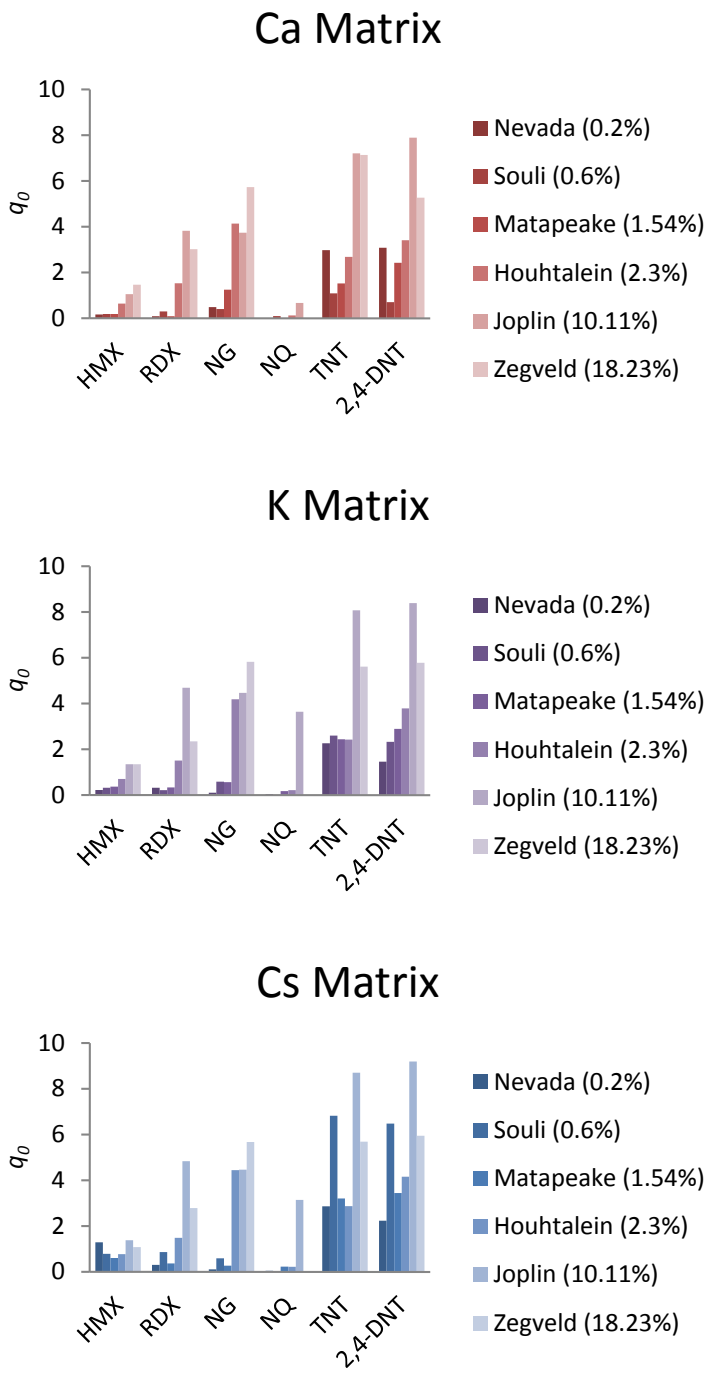

Figure 26. Relationship between the resistant component q_0 and TOC.

The data presented in Figure 25 and 26 and Appendices H.3, H.4, and H.5 indicate that the electrolyte, MC and soil properties are factors that must be taken into account when the reversible/resistant model is applied and used to make predictions and to evaluate sorption systems. From the figure it is very clear that the model can be applied to sorption of MC even for these variables studied because the relationship of the amount of explosive sorbed and the solution concentration is linear, as the model proposed.

The reversible and resistant components q_x and q_0 were computed from Figure 25 and Appendicies H.3 and H.4 and with them the reversible and resistant partition coefficients K_{px} and K_{p0} were calculated for each chemical, soil and electrolyte (Table 16). Figure 27 shows these partition coefficients for each MC. The soils are arranged from low (Nevada) to high (Pahokee) organic carbon content. The general pattern for the MC indicates that the value of K_{p0} is greater than that of K_{px}. The interactions of MC with the soil, especially with the organic carbon component, as the resistant component shown in Figure 25 are stronger than are the interactions with the aqueous phase. However, for RDX and NQ the effect of desorption produced by washing the soil (simulating rainy events as in field conditions) is greater than the resistance of the chemicals into the soil. These results are due to RDX being highly reversible [Morley et al. 2005] and NQ having high solubility in water [Sheremata et al. 2001]. So, they are removed easily even from high organic carbon content soils.

HMX, NG, TNT and 2,4-DNT exhibit resistant behavior, especially in soils with high organic carbon content. The value of K_{p0} for the nitroaromatics is greater than that of the aliphatics (NG and NQ) and for the cyclic nitramine (HMX). Sunahara et al. [2009] indicated that clays are strong sorbents for NACs, suggesting that in the present study clays have an important role in addition to that of organic carbon in the sorption of these chemicals. Schwarzenbach et al. [2003] indicated that the electronic distribution on the nitroaromatics (NACs) makes the center of the ring electropositive. The center of the ring strongly interacts with the mineral surface because it is electron rich and forms an electron Donor – Acceptor complex (EDA complex) with NAC. Another important observation is that the resistant component is greater in most of the cases when the electrolyte is cesium and this effect is larger for the nitroaromatics TNT and 2,4-DNT. This can be observed in Figure 23 and it is due to the EDA complex of NAC and the fact that cesium has a large atomic radius and low affinity to the variable-charge sites in clays [Anderson and Sposito 1991], which permits the displacement of the cation by the NAC.

Although both HMX and RDX are nitramines, their behavior is different. For HMX the resistant partition coefficient is greater than that of RDX because the immobilization of HMX is favored by the presence of clay in soils [Monteil-Rivera et al. 2003]. HMX spatial conformation may be the cause of the difference in adsorption behavior compared to RDX. They are also different because HMX has a greater crystal density than RDX and it is more resistant to high temperature than RDX [Johnson 1956].

Multilinear (*organic matter and clay size particles*) *model for sorption.* The partitioning results suggest that the variation in the amount of the MC sorbed and the reversible and resistant partition coefficients have strong dependency on TOC and clays in soils. Previous studies indicate that the influence of the characteristics of soils are very important in the adsorption/desorption of MC. These observations, and the fact that many researchers for decades have studied the influence of organic carbon and clays in the adsorption/desorption of MC in an independent manner [Eriksson et al. 2004; Hatzinger et al. 2004; Michalkova et al. 2005; Dontsova et al. 2009a], were the motivation to develop a model to predict the partition

coefficients that included these two main characteristics of the soils as parameters: the organic carbon content (f_{OC}) and clay size particle content (f_{clay}). In the proposed model, it was assumed that the partition coefficient K_p can be expressed as the sum of two partition coefficients, one for the organic carbon and the other one for the clay size particle, each incorporating the fraction of its component multiplied by their corresponding sorption coefficients. Equation 12 shows the proposed model:

$$K_{p\,s,e,m} = K_{OC\,m}\,(f_{OC\,s}) + K_{clay\,e,m}\,(f_{clay\,s}) \quad (12)$$

where $K_{OC\,m}$ = sorption coefficient to organic carbon in the soil and $K_{clay\,e,m}$ = sorption coefficient to the clay size particles in the soil, f_{OC} = fraction of the organic carbon in the soil and f_{clay} = fraction of clay size particles in the soil, and s = soil, e = electrolyte, and m = munitions constituents. Both f_{OC} and f_{clay} are properties of a soil, $K_{OC\,m}$ is only a function of the chemical, but $K_{clay\,e,m}$ is a function of the chemical and the electrolyte used. The model takes into account that the soil-specific partition coefficient for a MC depends on the electrolyte as well as the soil characteristics.

The partition coefficient K_p in L kg^{-1} was calculated from the data as the relationship between the amount of MC sorbed per mass of soil and the concentration remaining in the solution after equilibrium in the adsorption step. The fractions organic carbon and clay, f_{OC} and f_{clay}, were calculated from the properties of the soils listed in Table 2. The parameters K_{OC} and K_{clay}, which were calculated for the chemicals, soils and electrolytes, were obtained by minimization of the log residuals square between the K_p calculated from the experimental data and the K_p obtained by the model using the Excel solver tool.

In addition to K_p calculated by the multilinear model in Equation 12, K_p was estimated from only the first part of this equation that is named the organic carbon (OC) model:

$$K_{p\,s,m} = K_{OC\,m}\,(f_{OC\,s}) \quad (13)$$

Both values of K_p are presented in Figure 28. K_p from the organic carbon model was determined because the organic fraction is considered as the dominant component of the soil responsible for the sorption of organic contaminants. It is very common to use the organic carbon normalized partition coefficient, K_{OC}, and the fraction organic carbon to compute K_p [Schwarzenbach et al. 2003].

Figure 28 and Appendix H.5 relate the partition coefficient with the fraction of organic carbon and show the results of the K_p observed from the experiment, K_p calculated by the Organic Carbon Model and K_p obtained from the multilinear model. The clay size particles were taken to be the value of clay determined by particle size that is the fraction of particles with diameter less than 0.002 mm. This was done for each chemical, electrolyte and soil. The graphs in Figure 28 clearly show that the addition of clay in the model improve the fitting to the observed data.

To analyze the differences between the values predicted by the models and the observed values, the root mean square error (RMSE) was used. Values of RMSE (Table 17) for both the multilinear and the organic carbon models are presented in Figure 29. This figure shows that for all MC studied except NG, the multilinear model fits the data with a smaller RMSE than the organic carbon model, indicating that the K_p values obtained by the multilinear model are closer to the observed values than are the values obtained from the organic carbon model. This indicates that the multilinear model can more accurately predict the partition coefficients of HMX, RDX, NQ, TNT and 2,4-DNT in the soils and electrolytes used than can be done by using

the usual organic carbon approach. For NG the organic carbon approach sufficiently predicts K_p, because the RMSE obtained by the two models were the same. In fact, for NG the partition coefficient for the clay component obtained by the Excel solver tool for the multilinear model was estimated to be zero.

The results shown in Figures 28 and 29 show the importance of clay minerals in soils, because the goodness of fit increased when this component of the soil is included. For HMX and RDX the fit increased by 45%, for NQ and TNT by 24% and for 2,4-DNT by 6%. This increment is especially important for nitramines, NQ and TNT, while for NG the Organic Carbon Model is sufficient to predict the partition coefficient of adsorption although the multilinear model can be used.

Table 16. Reversible and resistant partition coefficients K_{px} L kg^{-1} and K_{p0} L kg^{-1} of HMX, RDX, NG, NQ, TNT and 2,4-DNT for the six soils studied using Ca, K and Cs as electrolytes**.**

	K_{px}			K_{p0}			K_{px}			K_{p0}		
	Ca	K	Cs	Ca	K	Cs	Ca	K	Cs	Ca	K	Cs
	HMX						RDX					
Nevada	0.738	0.886	1.166	0.201	0.289	6.290	0.190	0.269	0.430	0.012	0.050	0.053
Souli	0.815	0.941	0.694	0.235	0.472	1.434	0.421	0.512	0.684	0.053	0.038	0.179
Matapeake	1.153	1.178	1.451	0.317	0.673	1.433	0.349	0.371	0.565	0.014	0.059	0.073
Houthalein	0.848	0.869	0.904	1.028	1.155	1.308	0.647	0.679	0.685	0.339	0.342	0.335
Joplin	5.650	5.854	6.289	8.887	13.727	16.261	2.457	3.069	3.081	2.544	3.653	3.898
Zegveld	3.725	7.379	12.744	21.043	22.580	18.564	3.675	3.938	3.740	2.676	2.023	2.525
	NG						NQ					
Nevada	0.038	0.104	0.067	0.084	0.017	0.019	0.058	0.057	0.089	0.001	0.006	0.006
Souli	0.010	0.046	0.037	0.069	0.102	0.107	0.145	0.229	0.319	0.014	0.000	0.000
Matapeake	0.150	0.148	0.089	0.256	0.110	0.052	0.160	0.116	0.168	0.001	0.026	0.036
Houthalein	1.004	0.948	0.944	2.086	2.284	2.433	0.161	0.177	0.188	0.018	0.031	0.033
Joplin	1.821	2.266	2.188	2.978	4.084	4.105	2.160	2.423	2.409	0.349	2.172	1.837
Zegveld	2.031	2.298	2.443	12.481	12.939	13.015	1.652	1.195	1.635	0.000	0.000	0.000
	TNT						2,4-DNT					
Nevada	0.844	1.073	1.435	1.638	1.319	2.013	1.042	1.271	1.453	1.567	0.525	0.877
Souli	0.695	0.780	0.243	0.352	1.114	9.127	0.678	0.765	0.242	0.193	0.781	3.924
Matapeake	1.278	1.658	2.324	0.735	1.608	3.062	1.278	1.544	1.692	1.030	1.570	2.078
Houthalein	2.141	2.305	2.138	1.524	1.435	1.679	3.147	3.155	3.008	2.687	3.202	3.422
Joplin	4.152	6.389	5.358	47.608	77.250	98.299	3.940	4.536	3.192	120.590	120.341	177.173
Zegveld	1.783	7.525	7.469	25.501	19.826	20.534	10.333	7.126	8.141	19.927	21.449	22.737

Table 17. RMSE of the multilinear and organic carbon models applied to HMX, RDX, NG, NQ, TNT and 2,4-DNT for all electrolytes.

		Electrolyte		
	MC	Ca	K	Cs
Multilinear Model	HMX	0.1385	0.1503	0.2909
	RDX	0.1254	0.1487	0.1219
	NG	0.3292	0.3122	0.3895
	NQ	0.1826	0.3053	0.2498
	TNT	0.3015	0.2868	0.2753
	2, 4-DNT	0.4000	0.3210	0.3349
Organic Carbon Model	HMX	0.2406	0.2576	0.5081
	RDX	0.2067	0.2584	0.3031
	NG	0.3277	0.3112	0.3882
	NQ	0.2658	0.3646	0.3498
	TNT	0.3546	0.3443	0.4335
	2, 4-DNT	0.4124	0.3332	0.3729

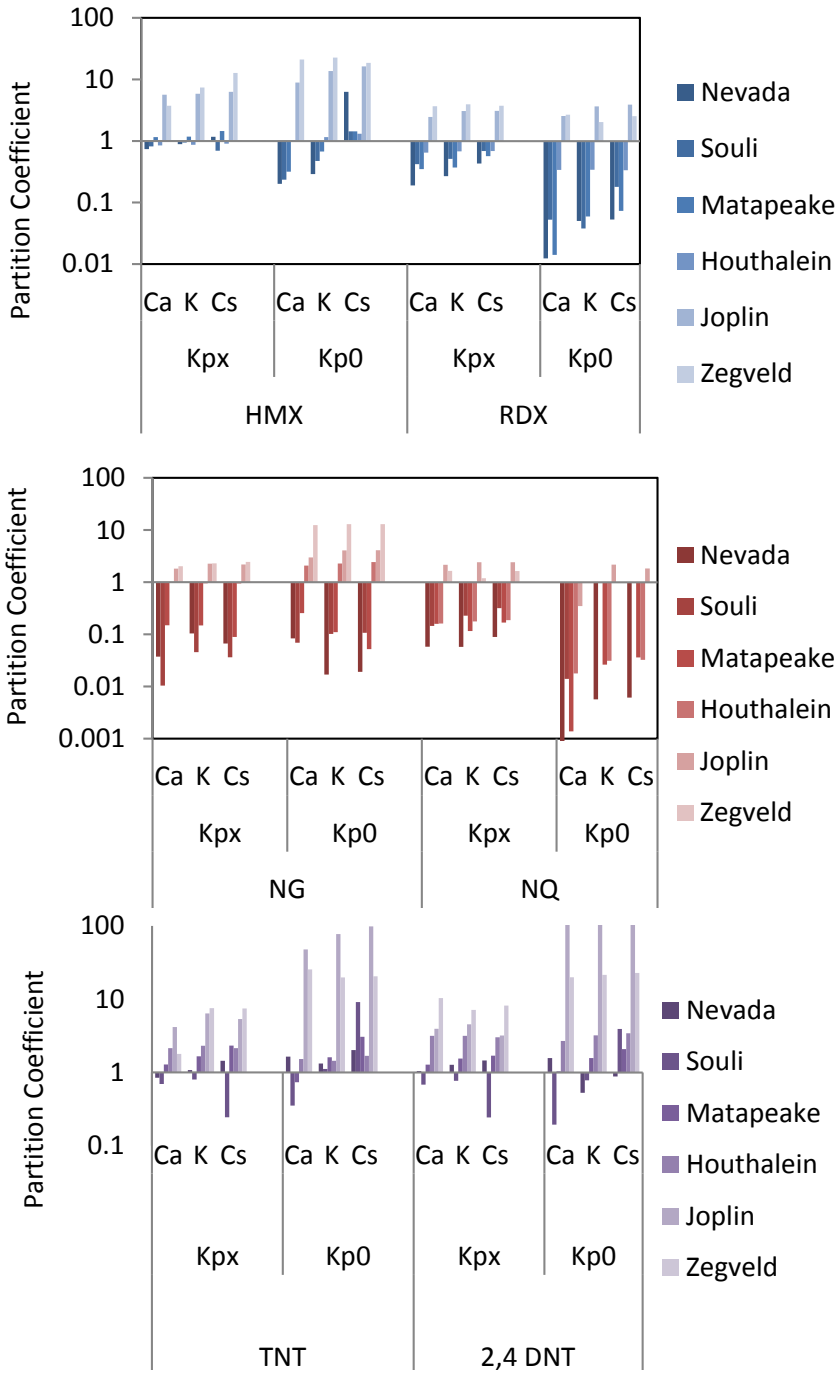

Figure 27. Reversible and resistant partition coefficients K_{px} and K_{p0} of HMX, RDX, NG, NQ, TNT and 2,4-DNT for the six soils studied using Ca, K and Cs as electrolytes.

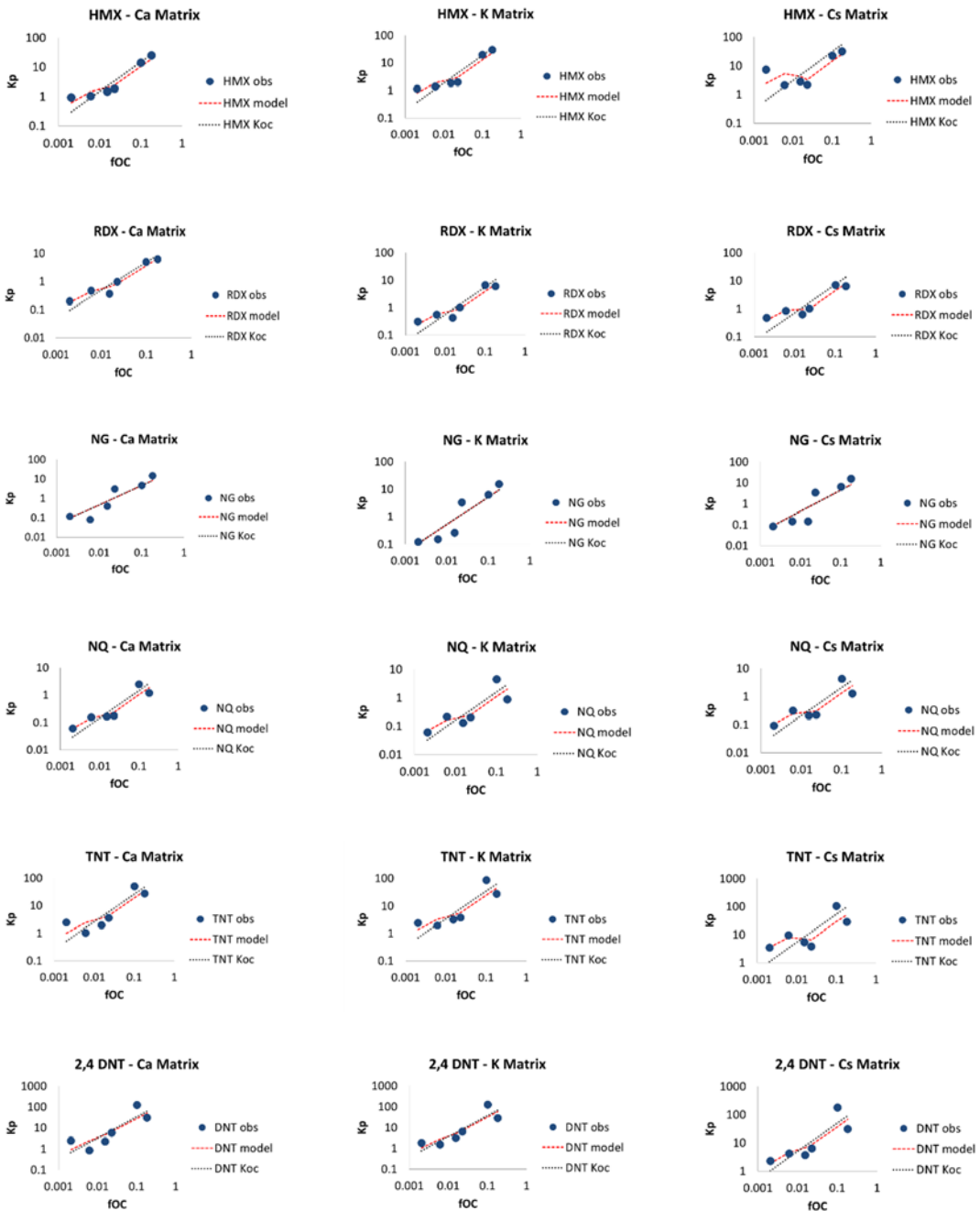

Figure 28. K_p from the observed data (obs), multilinear model (model) and Organic Carbon Model (K_{OC}) for partitioning of HMX, RDX, NG, NQ, TNT and 2,4-DNT related to the fraction of organic carbon for all electrolytes and soils.

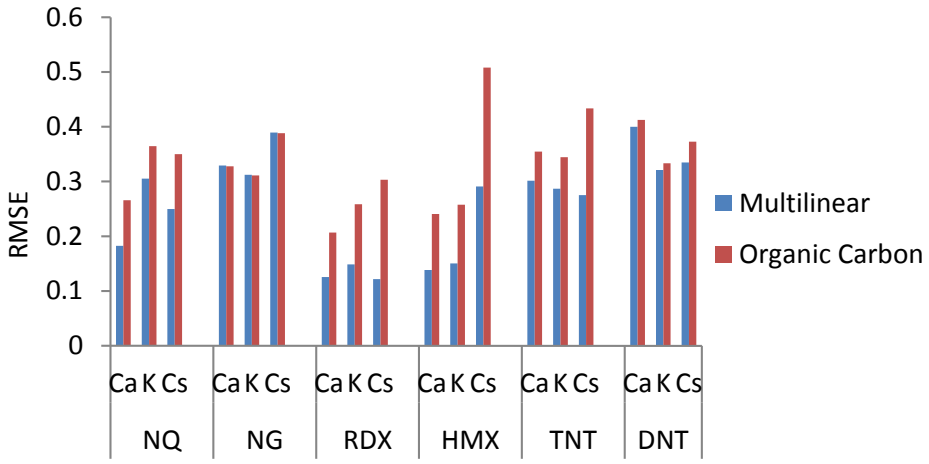

Figure 29. RMSE of the multilinear and organic carbon models applied to HMX, RDX, NG, NQ, TNT and 2,4-DNT for all electrolytes.

Partition coefficients of each component of the multilinear model (organic carbon and clay) K_{OC} and K_{clay}, were obtained by using the Excel solver tool for each chemical and electrolyte and are presented in Figure 30 and Table 18. The figure shows that the K_{OC} values are higher than the K_{clay} values, indicating that the organic carbon influences the adsorption process to a greater extent than does the clay component. This finding agrees with the literature; the multilinear model increases the goodness of fit of the data because the clay component is included in the model. Figure 30 indicates that for all MC except for NG the values of the partition coefficients are higher when the electrolyte is cesium. For NG, considering that organic carbon alone is sufficient to predict its K_p, the addition of clay in the model is unnecessary. As partitioning of NG is not influenced by clays, cesium lost importance, while for the other MC if the electrolyte is cesium, the effect of clay in the sorption of MC is increased.

The variation of the partition coefficients among the electrolytes, as shown in Figure 30, is greater for K_{clay} than for K_{OC} for HMX, RDX, NQ, TNT and 2,4-DNT. This suggests that the effect of the electrolyte in the soil is small on the sorption of these chemicals, as well as NG, due the strong interaction between the MC and organic carbon. The partitioning between clay and HMX, RDX, NQ, TNT and 2,4-DNT has more specificity depending on the electrolyte involved, as was also reported for NACs by Haderlein et al. [1996] and Roberts et al. [2007].

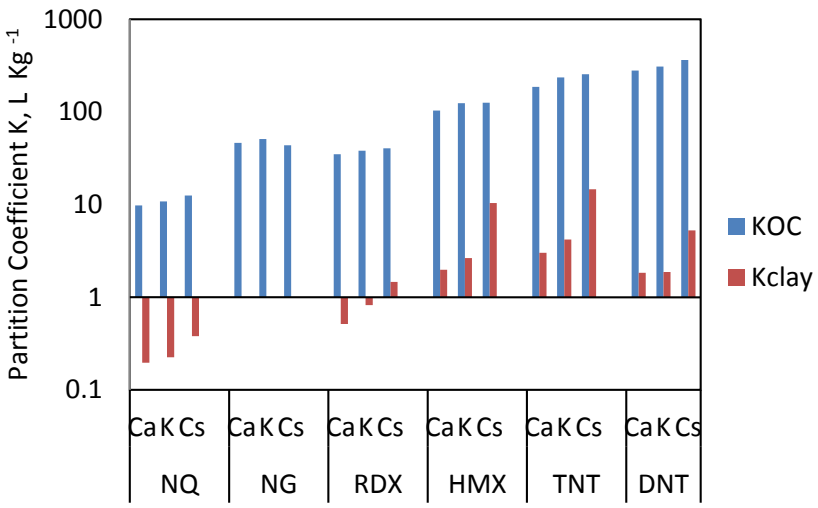

Figure 30. Partition coefficients of organic carbon and clay components, obtained by the Excel solver tool in the multilinear model, of HMX, RDX, NG, NQ, TNT and 2,4-DNT for all electrolytes and soils.

Table 18. Partition coefficients of organic carbon and clay components, L kg^{-1}, obtained using the Excel solver tool for the multilinear model, of HMX, RDX, NG, NQ, TNT and 2,4-DNT for all electrolytes and soils.

		Electrolyte		
	MC	Ca	K	Cs
K_{OC}	HMX	103.334	124.049	125.590
	RDX	34.937	38.112	40.416
	NG	46.229	50.967	43.573
	NQ	9.790	10.782	12.502
	TNT	186.072	235.245	255.055
	2, 4-DNT	278.859	308.439	363.706
K_{clay}	HMX	1.977	2.639	10.392
	RDX	0.512	0.821	1.461
	NG	0.000	0.000	0.000
	NQ	0.196	0.225	0.380
	TNT	3.015	4.191	14.578
	2, 4-DNT	1.831	1.866	5.263

The K_{OC} parameters of both models (multilinear and organic carbon) can be compared with the octanol-water partition coefficient, because this is a reference value when there are interactions between chemicals and organic phases such as the organic carbon in the soil. Figure 30 and Table 19 show that for all electrolytes, the organic carbon model approach, defined by Equation 2, can be used for NG. This is in agreement with Clausen et al. [2010] who found that the most important variable impacting the sorption of NG is organic matter. For the other MCs it is not

accurate to use only organic matter, especially for NACs such as TNT and 2,4-DNT and for cyclic nitramines as HMX and RDX due to the mechanisms explained previously.

For decades researchers have demonstrated linear relationships between K_{OC} and K_{OW} for some hydrophobic compounds. For example, Karickhoff et al. [1979] found a linear relationship between K_{OC} and K_{OW} for the hydrophobic pollutants anthracene, tetracene, and phenanthrene. But for nitro compounds this is not the case (Figure 31 and Table 20 and 21). Linear regressions were computed and the regression coefficient (R^2) obtained for Figure 31 A was between 0.16 and 0.17 and for Figure 31 B it was between 0.01 and 0.3, indicating that there was no linear behavior for the relationships between K_{OC} and K_{OW} or between K_p and K_{OW}.

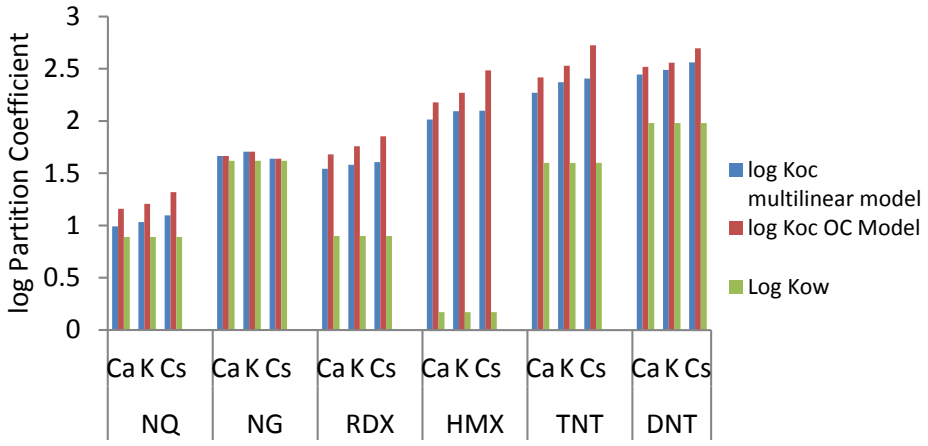

Figure 31. Log partition coefficients of K_{OC} of the multilinear model, K_{OC} model and K_{OW} of HMX, RDX. NG. NQ, TNT and 2,4-DNT for all electrolytes.

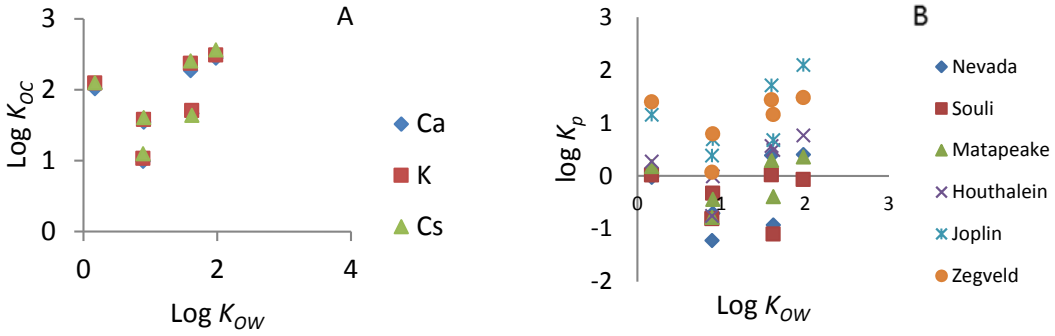

Figure 32. A. Relationship of log K_{OC} obtained by the multilinear model for all MC and electrolytes and log K_{OW} for each MC. B. Relationship of log of K_p obtained by the multilinear model for each soil used to all MC for Ca electrolyte and log K_{OW} for each MC.

Table 19. Log partition coefficients of K_{OC} of the multilinear model, K_{OC} model and K_{OW} of HMX, RDX, NG, NQ, TNT, and 2,4-DNT for all electrolytes.

		Electrolyte		
	MC	Ca	K	Cs
Log K_{OC} multilinear model	HMX	2.014	2.094	2.099
	RDX	1.543	1.581	1.607
	NG	1.665	1.707	1.639
	NQ	0.991	1.033	1.097
	TNT	2.270	2.372	2.407
	2, 4-DNT	2.445	2.489	2.561
Log K_{OC} OC Model	HMX	2.179	2.270	2.485
	RDX	1.680	1.759	1.853
	NG	1.665	1.707	1.639
	NQ	1.161	1.207	1.319
	TNT	2.417	2.528	2.726
	2, 4-DNT	2.519	2.558	2.696
Log K_{OW}	HMX	0.17	0.17	0.17
	RDX	0.90	0.90	0.90
	NG	1.62	1.62	1.62
	NQ	0.89	0.89	0.89
	TNT	1.60	1.60	1.60
	2, 4-DNT	1.98	1.98	1.98

Table 20. Log K_{OC} obtained by the multilinear model for all MC and electrolytes and log K_{OW} for each MC.

	Log K_{OW}	Log K_{OC}		
MC		Ca	K	Cs
HMX	0.17	2.014	2.094	2.099
NQ	0.89	0.991	1.033	1.097
RDX	0.90	1.543	1.581	1.607
TNT	1.60	2.270	2.372	2.407
NG	1.62	1.665	1.707	1.639
2,4-DNT	1.98	2.445	2.489	2.561

Table 21. Log K_p obtained by the multilinear model for each soil used to all MC for Ca electrolyte and log K_{OW} for each MC.

		Log K_p					
		HMX	NQ	RDX	TNT	NG	2,4-DNT
	K_{OW}	0.17	0.89	0.90	1.60	1.62	1.98
Nevada	Ca	-0.028	-1.222	-0.708	0.386	-0.929	0.401
	Cs	0.870	-1.037	-0.323	0.532	-1.078	0.358
	K	0.067	-1.217	-0.503	0.374	-0.926	0.242
Souli	Ca	0.015	-0.810	-0.329	0.017	-1.102	-0.069
	Cs	0.318	-0.510	-0.077	0.971	-0.839	0.618
	K	0.143	-0.657	-0.257	0.276	-0.823	0.181
Matapeake	Ca	0.176	-0.788	-0.446	0.294	-0.394	0.357
	Cs	0.447	-0.688	-0.207	0.725	-0.845	0.569
	K	0.262	-0.878	-0.371	0.506	-0.585	0.486
Houthalein	Ca	0.272	-0.756	-0.0095	0.565	0.489	0.765
	Cs	0.337	-0.664	0.0004	0.575	0.527	0.802
	K	0.299	-0.689	0.0019	0.570	0.511	0.802
Joplin	Ca	1.155	0.385	0.694	1.713	0.678	2.095
	Cs	1.354	0.623	0.839	2.015	0.797	2.256
	K	1.290	0.650	0.822	1.922	0.780	2.097
Zegveld	Ca	1.398	0.066	0.792	1.438	1.160	1.479
	Cs	1.497	0.102	0.800	1.447	1.187	1.488
	K	1.475	-0.053	0.776	1.436	1.181	1.454

In addition to applying the multilinear model to the adsorption partition coefficients, the multilinear model was applied to the reversible, K_{px}, and the resistant, K_{p0}, partition coefficients generated by the reversible/resistant model (Table 16) because K_p is formed from these two components as is shown in Equations 14 and 15. It is important to note that each model is applied independently from the other to determine the influence of OC and clay in the reversible and resistant partition coefficients:

$$K_{px\,s,e,m} = K_{OC\,m,x}\,(f_{OC\,s}) + K_{clay\,e,m,x}\,(f_{clay\,s}) \quad (14)$$

$$K_{p0\,s,e,m} = K_{OC\,m,0}\,(f_{OC\,s}) + K_{clay\,e,m,0}\,(f_{clay\,s}) \quad (15)$$

where $K_{OC\,m,x}$ = sorption coefficient to organic carbon in the soil for the reversible sites, $K_{OC\,m,0}$ = sorption coefficient to organic carbon in the soil for the resistant sites, $K_{clay\,m,x}$ = sorption coefficient to clay size particles in the soil for the reversible sites, and $K_{clay\,e,m,0}$ = sorption coefficient to the clay size particles in the soil for the resistant sites, f_{OC} = fraction of organic carbon in the soil, f_{clay} = fraction of the clay size particles in the soil and s = soil, e = electrolyte, and m = munitions constituents. Both f_{OC} and f_{clay} are properties of a soil, $K_{OC\,m}$ is a function of the chemical in the reversible and resistant sites and $K_{clay\,e,m}$ is a function of both the chemical and the electrolyte used in the reversible and resistant sites. The partition coefficients K_{px} and K_{p0} in L kg^{-1}, which are presented in Table 22, were estimated from the reversible and resistant model from Equations 7 and 8. The fractions organic carbon and clay, f_{OC} and f_{clay} were taken

from Table 2, and the parameters K_{OC} and K_{clay} were calculated for all the chemicals, soils and electrolytes (Table 22 and 23). They were obtained by fitting the multilinear model (Equations 14 and 15) by the minimization of the log residuals square between the K_p calculated from the experimental data and the K_p obtained by the model using the Excel solver tool.

Figures 33 and 34 relate the partition coefficient of the reversible and resistant partition coefficients with the fraction of organic carbon. They show the results of the K_{px} and K_{p0} obtained from the calculations of the reversible and resistant model and K_{px} and K_{p0} obtained from the multilinear model. This was done for each chemical, electrolyte and soil. The graphs on Figure 33 clearly show that this reversible component has a soil properties dependency, and can be expressed as a linear relationship of organic carbon and clay size particles. Figure 34 shows that K_{p0} is not dependant on the soil properties OM and clay size fraction in as strong a way as is K_{px}. Table 24 shows the values of RMSE for each MC for all electrolytes. This table indicates that the model fits the K_{px} and K_{p0} coefficients very well because the RMSE values are very low. The K_{px} values are lower than are those of K_{p0} as is expected. This provides evidence that the K_{px} partition coefficient or the reversible component from the reversible/resistant model, depends on the fractions of organic carbon and clay. The value of K_{p0} that relates the concentration on the particles that remains at zero dissolved concentration and the concentration at the adsorption point does not fit as well as K_{px} when the multilinear model is applied. Mechanisms of binding associated with the partition coefficients K_{OC} and K_{clay} from the multilinear model should be studied to understand the difference between K_{px} and K_{p0}.

The partition coefficients K_{OC} and K_{clay} generated from the multilinear model applied to K_{px} and K_{p0} are presented in Figure 35. As in the K_p analysis, the K_{OC} values are higher than the K_{clay} values, indicating that the partitioning of the MC, even in the reversible and resistant sites, are highly dependent on the organic carbon rather than the clay component of the soil. However, to get a good estimation of K_{px} and K_{p0} by the multilinear model, the clay component needs to be included for five (HMX, RDX, NQ, TNT and 2,4-DNT) of the six munitions constituents studied. This is demonstrated by using the K_{px} and K_{p0} from the data of Tables 16 and 22 to compute the low RMSE values presented in Table 24. To provide additional support, the K_{px} and K_{p0} values were determined using Equations 16 and 17. Appendix H.6 shows the standard deviation of these values and the ones obtained by Equations 14 and 15 to compare them with the K_{px} and K_{p0} values obtained from the reversible and resistant model (Table 16). The results that are shown in Appendix H.6 indicate that the clay component should be included for all electrolytes for all the MC investigated, with the exception of NG which does not require consideration of the clay size fraction.

$$K_{px\,s,e,m} = K_{OC\,m,x}\,(f_{OC\,s}) \tag{16}$$

$$K_{p0\,s,e,m} = K_{OC\,m,0}\,(f_{OC\,s}) \tag{17}$$

Conclusions regarding the electrolyte. The electrolyte matrix affected the amount of explosive sorbed per gram of soil. Adsorption was a function of the electrolyte used and the strength of sorption by the clay component depended on which electrolyte was used. Inclusion of the fraction clay in addition to the fraction organic carbon in the analysis of the adsorption of MC, as was done in the multilinear model, improved the estimation of the partition coefficient K_p for the adsorption of MC in soils with a wide range of properties rather than using the traditional approach in which only organic carbon is considered.

The data were fitted with the reversible and resistant model which can be used as a predictive

tool to determine future concentrations of the MC even with variation of MC, electrolyte, and soils, because it was found that the relationship between the particulate concentration of the MC in the soil per gram of soil and the equilibrium concentration for an adsorption step followed by multiple desorption steps had a linear behavior with a slope K_{px} as was proposed in the formulation of the model. The multilinear model provided good evidence that the use of the size clay fraction in addition to the total organic carbon to predict partitioning of MC in soils with a wide range of properties is useful to predict partition coefficients. The sorption models have been extended to predict the reversible and resistant partition coefficients parameters K_{px} and K_{p0} of the reversible/resistant model, providing new advances in this area.

Table 22. Partition coefficients K_{px} and K_{p0} L kg^{-1} from the multilinear model of K_{px} and K_{p0} for HMX, RDX, NG, NQ, TNT and 2,4-DNT for all electrolytes and soils.

	K_{px}			K_{p0}			K_{px}			K_{p0}		
	Ca	K	Cs	Ca	K	Cs	Ca	K	Cs	Ca	K	Cs
	HMX						RDX					
Nevada	0.559	0.625	0.629	0.127	0.218	1.718	0.177	0.229	0.353	0.018	0.026	0.052
Souli	1.212	1.364	1.394	0.367	0.597	3.685	0.405	0.516	0.772	0.053	0.077	0.135
Matapeake	1.008	1.193	1.349	0.864	1.256	2.831	0.472	0.552	0.683	0.125	0.187	0.246
Houthalein	0.814	1.024	1.284	1.273	1.797	2.044	0.520	0.573	0.593	0.184	0.278	0.3370
Joplin	3.594	4.519	5.660	5.586	7.884	9.044	2.288	2.522	2.617	0.808	1.220	1.479
Zegveld	6.194	7.835	9.901	10.058	14.175	15.406	4.048	4.441	4.542	1.455	2.199	2.653
	NG						NQ					
Nevada	0.026	0.045	0.034	0.071	0.054	0.050	0.057	0.068	0.103	0.0042	0.035	0.038
Souli	0.076	0.126	0.099	0.209	0.161	0.148	0.138	0.158	0.232	0.011	0.079	0.087
Matapeake	0.184	0.276	0.240	0.518	0.397	0.365	0.197	0.194	0.249	0.018	0.094	0.098
Houthalein	0.272	0.400	0.356	0.772	0.591	0.543	0.243	0.222	0.259	0.024	0.105	0.106
Joplin	1.193	1.755	1.562	3.388	2.593	2.383	1.069	0.976	1.142	0.106	0.460	0.467
Zegveld	2.148	3.157	2.814	6.104	4.670	4.292	1.906	1.731	2.011	0.189	0.814	0.824
	TNT						2,4-DNT					
Nevada	0.581	0.654	0.470	0.479	0.758	2.571	0.565	0.690	0.450	0.392	0.412	1.033
Souli	1.255	1.462	1.084	1.206	1.838	5.620	1.282	1.530	1.033	1.116	1.231	2.629
Matapeake	1.011	1.488	1.296	2.024	2.716	4.954	1.409	1.487	1.211	2.553	3.090	4.562
Houthalein	0.783	1.482	1.453	2.686	3.415	4.288	1.491	1.421	1.341	3.735	4.623	6.130
Joplin	3.461	6.526	6.390	11.796	15.003	18.920	6.562	6.262	5.897	16.388	20.282	26.918
Zegveld	5.939	11.456	11.317	21.117	26.773	32.824	11.574	10.957	10.435	29.496	36.548	48.223

Table 23. Partition coefficients K_{OC} and K_{clay} L kg^{-1} from the multilinear model of K_{px} and K_{p0} for HMX, RDX, NG, NQ, TNT and 2,4-DNT for all electrolytes and soils.

		Electrolyte				Electrolyte		
	MC	Ca	K	Cs		Ca	K	Cs
	Reversible							
K_{OC}	HMX	31.165	39.891	51.337	K_{clay}	2.366	2.593	2.501
	RDX	21.451	23.332	23.179		0.633	0.865	1.459
	NG	11.769	17.262	15.422		0.000	0.047	0.000
	NQ	10.249	9.215	10.568		0.174	0.234	0.388
	TNT	29.620	59.822	60.105		2.487	2.539	1.659
	2, 4 DNT	60.982	56.845	55.328		2.105	2.740	1.609
	Resistant							
K_{OC}	HMX	55.091	77.411	75.632	K_{clay}	0.068	0.286	7.464
	RDX	7.969	12.051	14.422		0.000	0.0078	0.108
	NG	33.468	25.605	23.532		0.000	0.000	0.000
	NQ	1.026	4.319	4.355		0.000	0.123	0.139
	TNT	114.436	144.222	167.393		1.172	2.213	10.645
	2, 4-DNT	161.441	200.460	261.682		0.296	0.000	2.380

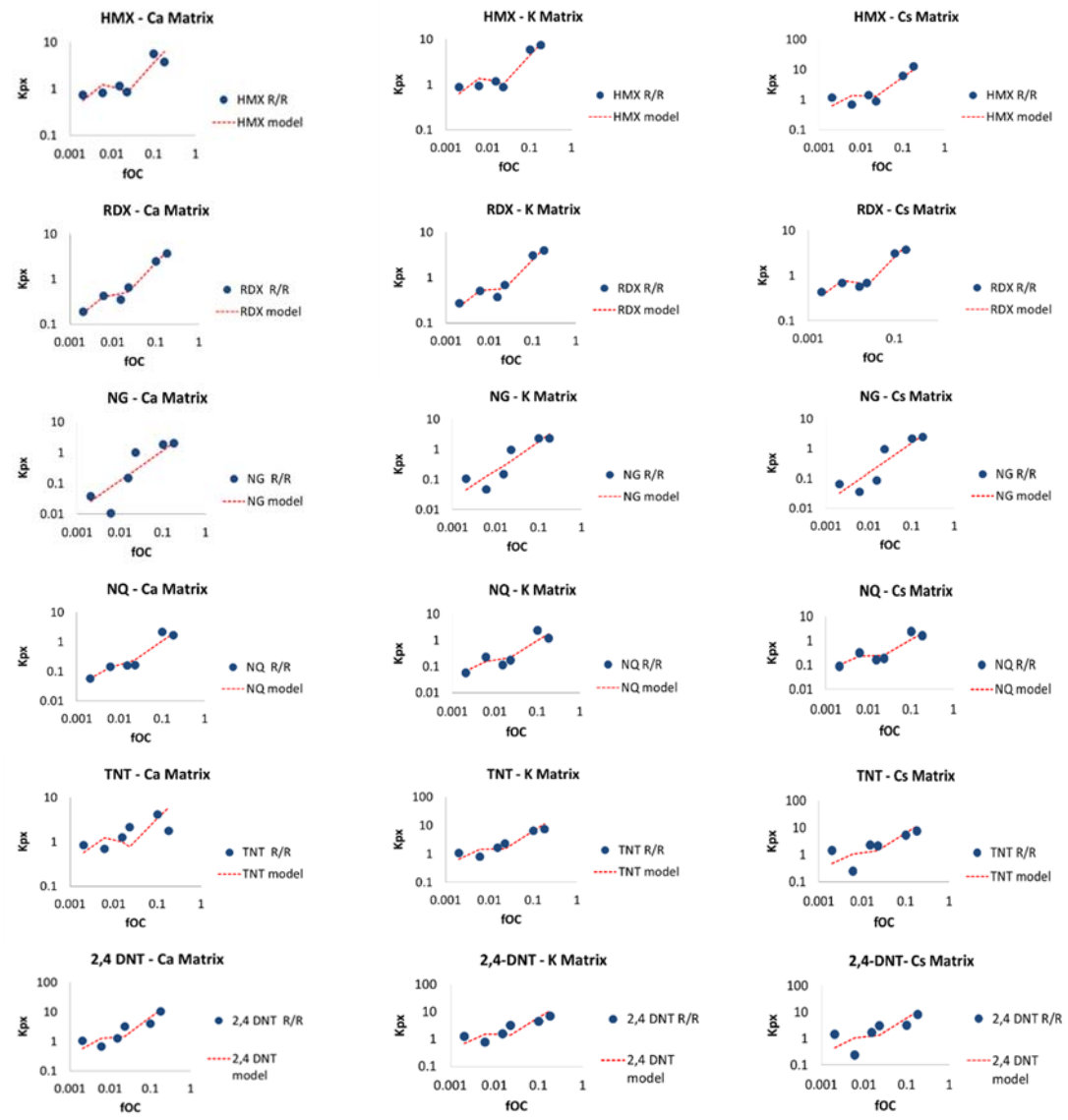

Figure 33. K_{px} from the reversible/resistant model (R/R) and multilinear model (model) of HMX, RDX, NG, NQ, TNT and 2,4-DNT related to the fraction of organic carbon for all electrolytes and soils.

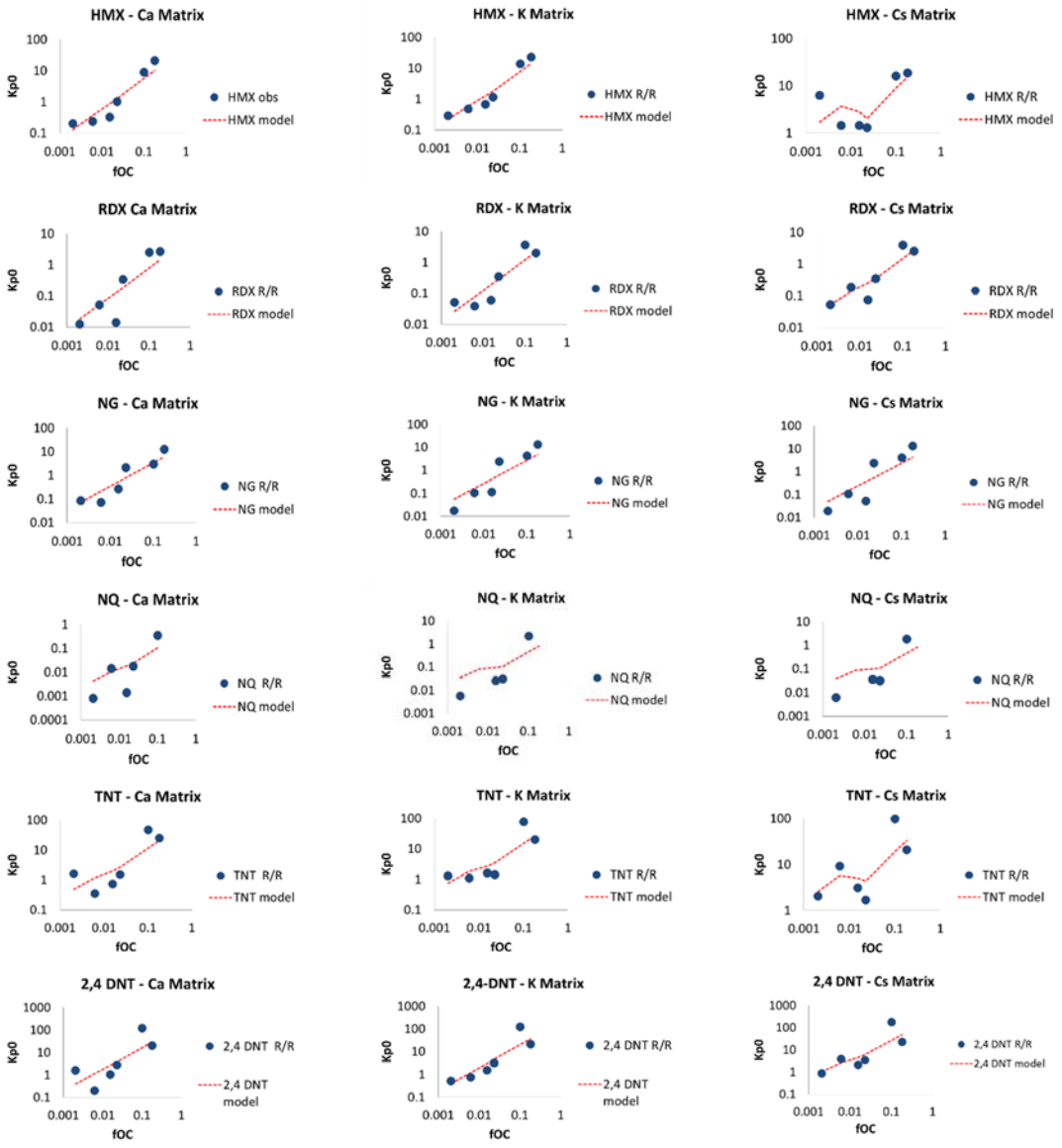

Figure 34. K_{p0} from the reversible/resistant model (R/R) and multilinear model (model) of HMX, RDX, NG, NQ, TNT and 2,4-DNT related to the fraction of organic carbon for all electrolytes and soils.

Table 24. RMSE of the reversible K_{px} and resistant K_{p0} partition coefficients, L kg^{-1}, obtained by the multilinear model from the relationships between the amount of MC sorbed q, µg MC g $soil^{-1}$ and the solution equilibrium concentration mg L^{-1} for all MC, soils and electrolytes. (K_{px} and K_{p0} values are in Table 16 and 22).

		HMX	RDX	NG	NQ	TNT	2,4-DNT
Ca	K_{px}	0.150	0.071	0.435	0.309	0.226	0.152
	K_{p0}	0.264	0.469	0.320	0.447	0.562	0.658
K	K_{px}	0.106	0.092	0.309	0.177	0.237	0.214
	K_{p0}	0.198	0.332	0.444	0.370	0.368	0.692
Cs	K_{px}	0.184	0.074	0.333	0.362	0.384	0.175
	K_{p0}	0.337	0.281	0.520	0.369	0.407	0.654

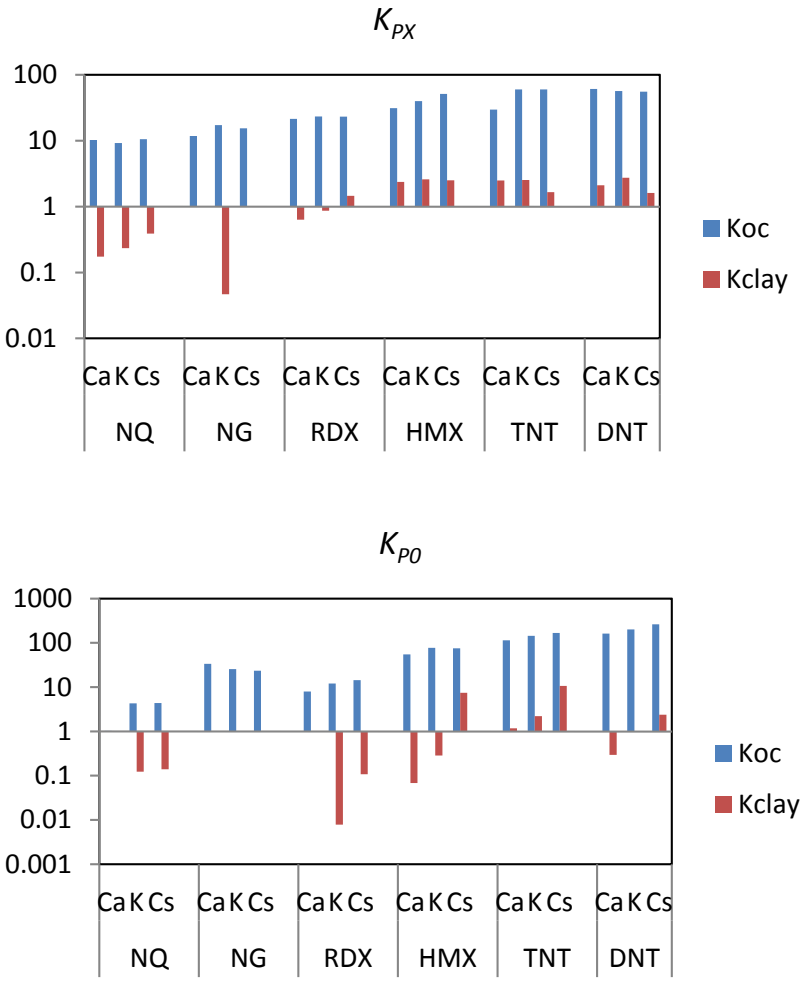

Figure 35. Partition coefficients K_{OC} and K_{clay} from the multilinear model of K_{px} and K_{p0} for HMX, RDX, NG, NQ, TNT and 2,4-DNT for all electrolytes and soils.

Multilinear Model using Cesium Exchange as the Clay Component. In this, and all subsequent portions of the research concerned with the partitioning of MC to soil, all 25 soils listed in Table 2 were used. Data for 2 day adsorption time was used except for the section titled "Normalization and Reversible Resistant Modeling of 5 MC onto 25 Soils at 4 Durations of Adsorption" for which multiple adsorption durations were included. Five MC mixtures, summarized in Table 25 were sorbed for each adsorption time. Set AL1 contained all muntions at a relatively low concentration. Set AL2 was a replicate of set AL1 and was used as an analytical and experimental check. Set AH1 contained all munitions at a relatively high concentration. Finally, two special cases were used to separate TNT from the remaining munitions. Set DH1 contained all munitions except TNT at the AH1 concentration. Set TH1 contained only TNT at the AH1 concentration.

Table 25. Nominal concentrations for the five MC mixtures used in the study of partitioning by 25 soils.

	Concentration, mg L^{-1}					
Set	HMX	RDX	NG	NQ	TNT	2,4-DNT
AL1	0.75	3	3	3	3	10
AL2	0.75	3	3	3	3	10
AH1	1.5	10	10	10	10	20
DH1	1.5	10	10	10	0	20
TH1	0	0	0	0	10	0

The model presented in Equation 12 assumed that the partition coefficient K_p can be calculated from the sum of two linear terms, one for the organic carbon and the other one for the clay size particles as the fraction of each component multiplied by their corresponding sorption coefficients. In this section, this model was modified by replacing the clay component by the fixed charge sites data obtained by the Cs method. Charge sites in soils have two major groups of sources: the dual-charge particles such as phyllosilicates and allophane, which possess both positive and negative charge simultaneously, and charged particles such as metal oxides that change their surface charge in response to changes, mainly in pH, in the soil solution [Zhu et al., 2009]. Sources of charge on clays are their edge sites and the face sites that have unsatisfied bonds. Using the charge sites instead of clay size could permit more specific information of the sites where the adsorption of MC occurred. Equation 18 shows the modified multilinear model, which was named the charge sites model:

$$K_{p\,s,m} = K_{OC\,m}\,(f_{OC\,s}) + K_{Cs\,m}\,C_{Cs\,s} \qquad (18)$$

where $K_{OC\,m}$ = sorption coefficient of the MC to organic carbon in the soil and $K_{Cs\,m}$ = sorption coefficient of the MC to the charge sites in the soil, f_{OC} = fraction of the organic carbon in the soil, C_{Cs} = concentration of the charge sites in the soil determined by Cs exchange, s = soil, and m = munitions constituents. Both f_{OC} and C_{Cs} are properties of a soil and $K_{OC\,m}$ and $K_{Cs\,m}$ are a function of the munition considered. The dependence of $K_{Cs\,m}$ on the electrolyte is not included because in this portion of the research 0.01 M $CaCl_2$ was the only electrolyte used.

The partition coefficient K_p in L kg^{-1} was calculated from the data as the relationship between the amount of MC sorbed per mass of soil and the concentration remaining in the solution after equilibration in the adsorption step. The fraction of organic carbon and of clay f_{OC} was calculated from the properties of the soils listed in Table 26, which also lists the concentration of charge

sites, C_{Cs}, which was obtained by the cesium exchange method. The parameters K_{OC}, K_{clay}, and K_{Cs} were calculated for all the chemicals and soils. They were obtained by fitting the multilinear model by the minimization of the log residuals square between the K_p, calculated from the experimental data and the K_p obtained by the model using the Excel solver tool. The measured values of K_p are presented in Table 27 and the K_p values computed using the Organic Carbon, Clay Size, and Charge Sites Models are presented in Tables 28, 29, and 30, respectively.

In addition to K_p calculated by the Charge Sites Model in Equation 18, K_p was estimated for all soils (Table 27) using the Organic Carbon (OC) Model that has been presented as Equation 13. Also, K_p was obtained by the multilinear model (Equation 12, the Clay Size Model) for the 25 soils tested. The data are presented in Table 28.

Figures 36, 37, and 38 present the relationships of the K_p values calculated by the three models (OC, clay size and charge sites) with Equations 13, 12, and 18, respectively. Figures 39, 40, and 41 are residual plots showing the fit of the three models which indicate the improved fitting using the charge sites component compared with the clay size component.

Table 26. Soil properties for the computation of multilinear partition coefficients.

Soil	pH[a]	CEC[b] (meq/100g)	Clay[c] (%)	TOC[d] (%)	Cs exchanged[e] (mg Cs g soil^{-1})	FeOx[f] (mg/kg)
Zegveld	4.8	54.8	21.7	18.23	28.23	11954
Rhydtalog	5.0	35.9	12.5	12.83	9.97	1526
Joplin	6.5	43.8	18.7	10.12	17.49	3436
Lewis Core	5.6	37.2	6.3	7.59	13.48	7269
Lewis Clean	5.1	31.4	8.3	6.36	10.53	6130
Pokomoke	4.5	13.1	11.1	3.50	5.93	53
Elliot IE	6.3	20.4	37.0	2.86	12.62	2541
Guadalajara	8.0	11.6	18.2	2.33	8.47	ND
Boxtel	5.4	11.0	10.2	2.32	6.59	5001
Houthalein	3.9	2.9	4.0	2.31	2.99	502
Annemessex	6.3	13.2	12.1	2.30	7.40	1153
Whippany	5.9	15.5	22.3	1.75	6.22	2496
Sassafras 1	4.4	8.5	16.4	1.63	4.45	1120
Matapeake	5.7	9.9	22.3	1.54	6.74	2304
Sassafras 2	4.5	8.8	18.1	1.35	4.36	1782
Chile Muestra	6.6	21.0	14.3	1.20	8.56	7083
Sassafras 3	4.4	5.0	18.2	0.97	4.31	1364
Washington 2	6.9	20.3	24.2	0.68	6.67	1533
Washington 1	6.9	17.8	24.5	0.63	6.75	1742
Souli	6.9	16.1	43.2	0.61	9.31	1596
Fort McClellan	3.8	11.0	38.6	0.31	3.50	104
Massachusetts Military Reservation B	4.3	2.5	16.2	0.24	3.19	1471
Nevada	3.4	11.2	20.9	0.20	7.20	1887
Aberdeen BA	5.5	3.8	16.2	0.16	3.31	2210
Aberdeen BT	4.8	1.9	9.1	0.07	1.97	1314

[a] *1:1 (w/v)* (*v*/*v*) soil:water

[b] Ammonium saturation buffered at pH 7.0

[c] Particle size analysis by hydrometer using the modified Bouyoucos Method [Bouyoucos 1962]

[d] Combustion using an Elementar Vario-Cube TOC Analyzer (Elementar Americas, Mt. Holly, NJ).

[e] Cesium exchange method of Anderson and Sposito [1991]

[f] FeOx = Extractable oxides determined by the Ammonium Oxalate method [McKeague and Day 1993]

Table 27. Measured values of K_p (L kg^{-1}) for 2 day equilibration for 25 soils.

	K_p Observed (L kg^{-1})					
Soil	HMX	RDX	NG	NQ	TNT	DNT
Zegveld	10.012	8.252	8.441	1.542	25.461	31.190
Rhydtalog	14.363	6.247	9.018	1.086	20.698	32.485
Joplin	10.842	4.228	3.499	2.643	33.667	79.946
Lewis Core	4.802	2.702	1.222	1.872	10.286	46.060
Lewis Clean	2.802	1.305	0.870	1.116	4.691	10.604
Pokomoke	5.033	1.828	1.393	0.523	7.494	16.983
Elliot IE	1.856	0.966	0.998	0.395	4.550	6.453
Guadalajara	0.790	0.358	0.175	0.155	0.682	0.721
Boxtel	2.984	1.075	0.388	0.218	3.446	3.499
Houthalein	2.190	0.900	1.394	0.183	2.725	3.869
Annemessex	1.647	0.937	1.211	0.304	5.172	5.812
Whippany	1.523	0.706	0.900	0.251	2.741	3.569
Sassafras 1	0.591	0.424	0.422	0.080	1.197	1.422
Matapeake	1.365	0.522	0.349	0.245	1.815	1.896
Sassafras 2	1.197	0.422	0.340	0.073	1.205	1.377
Chile Muestra	2.158	0.684	0.250	0.293	2.042	3.170
Sassafras 3	1.358	0.429	0.364	0.067	1.228	1.444
Washington 2	0.980	0.432	0.079	0.098	1.336	1.011
Washington 1	1.370	0.367	0.051	0.078	1.293	0.941
Souli	1.064	0.438	0.223	0.125	0.867	0.856
Fort McClellan	0.521	0.178	ND	0.220	0.371	0.296
Massachusetts Military Reservation B	0.345	0.119	ND	0.050	0.441	0.445
Nevada	0.918	0.283	0.263	0.158	1.052	1.231
Aberdeen BA	0.379	0.113	0.031	0.031	0.561	0.372
Aberdeen BT	0.366	0.140	0.035	0.015	0.381	0.247

ND = no data

Table 28. K_p (L kg^{-1}) calculated with the Organic Carbon Model, Equation 13 for 2 day equilibration for 25 soils.

	K_p Predicted by the OC Model (L kg^{-1})					
Soil	HMX	RDX	NG	NQ	TNT	DNT
Zegveld	20.691	8.531	6.428	2.705	28.856	35.584
Rhydtalog	14.562	6.004	4.524	1.904	20.308	25.044
Joplin	11.486	4.736	3.568	1.502	16.019	19.754
Lewis Core	8.615	3.552	2.676	1.126	12.014	14.815
Lewis Clean	7.219	2.976	2.243	0.944	10.067	12.415
Pokomoke	3.973	1.638	1.234	0.519	5.540	6.832
Elliot IE	3.246	1.338	1.008	0.424	4.527	5.583
Guadalajara	2.645	1.090	0.822	0.346	3.688	4.548
Boxtel	2.633	1.086	0.818	0.344	3.672	4.529
Houthalein	2.622	1.081	0.815	0.343	3.657	4.509
Annemessex	2.611	1.076	0.811	0.341	3.641	4.490
Whippany	1.986	0.819	0.617	0.260	2.770	3.416
Sassafras 1	1.850	0.763	0.575	0.242	2.580	3.182
Matapeake	1.748	0.721	0.543	0.229	2.438	3.006
Sassafras 2	1.532	0.632	0.476	0.200	2.137	2.635
Chile Muestra	1.362	0.562	0.423	0.178	1.900	2.342
Sassafras 3	1.101	0.454	0.342	0.144	1.535	1.893
Washington 2	0.772	0.318	0.240	0.101	1.076	1.327
Washington 1	0.715	0.295	0.222	0.094	0.997	1.230
Souli	0.692	0.286	0.215	0.091	0.966	1.191
Fort McClellan	0.352	0.145	ND	0.046	0.491	0.605
Massachusetts Military Reservation B	0.272	0.112	ND	0.036	0.380	0.469
Nevada	0.227	0.094	0.071	0.030	0.317	0.390
Aberdeen BA	0.182	0.075	0.056	0.024	0.253	0.312
Aberdeen BT	0.079	0.033	0.025	0.010	0.111	0.137

ND = no data

Table 29. K_p (L kg^{-1}) calculated with the Clay Size Model, Equation 12 for 2 day equilibration for 25 soils.

	K_p Predicted by the Clay Size Model (L kg^{-1})					
Soil	HMX	RDX	NG	NQ	TNT	DNT
Zegveld	13.174	6.208	4.810	1.940	22.550	34.473
Rhydtalog	9.219	4.355	3.382	1.360	15.832	24.256
Joplin	7.440	3.482	2.677	1.089	12.610	19.151
Lewis Core	5.433	2.570	2.000	0.803	9.351	14.347
Lewis Clean	4.610	2.170	1.679	0.678	7.877	12.028
Pokomoke	2.661	1.229	0.931	0.385	4.425	6.633
Elliot IE	2.706	1.154	0.790	0.364	4.002	5.477
Guadalajara	1.978	0.876	0.631	0.276	3.095	4.438
Boxtel	1.818	0.830	0.620	0.260	2.973	4.402
Houthalein	1.693	0.793	0.611	0.248	2.875	4.371
Annemessex	1.840	0.834	0.617	0.262	2.975	4.369
Whippany	1.650	0.705	0.483	0.222	2.444	3.351
Sassafras 1	1.453	0.633	0.445	0.199	2.216	3.112
Matapeake	1.503	0.634	0.428	0.200	2.188	2.954
Sassafras 2	1.290	0.548	0.373	0.173	1.898	2.587
Chile Muestra	1.112	0.478	0.330	0.151	1.662	2.296
Sassafras 3	1.026	0.422	0.274	0.134	1.436	1.869
Washington 2	0.937	0.357	0.204	0.114	1.165	1.334
Washington 1	0.907	0.342	0.191	0.110	1.108	1.240
Souli	1.249	0.436	0.205	0.141	1.342	1.240
Fort McClellan	0.952	0.311	ND	0.101	0.912	0.664
Massachusetts Military Reservation B	0.476	0.167	ND	0.054	0.517	0.486
Nevada	0.538	0.179	0.074	0.058	0.533	0.421
Aberdeen BA	0.420	0.140	0.059	0.046	0.419	0.335
Aberdeen BT	0.222	0.072	0.028	0.024	0.211	0.151

ND = no data

Table 30. K_p (L kg^{-1}) calculated by the Charge Sites Model, Equation 18 for 2 day equilibration for 25 soils.

	K_p Predicted by the Charge Sites Model L kg^{-1}					
Soil	HMX	RDX	NG	NQ	TNT	DNT
Zegveld	12.910	6.074	4.769	1.922	21.629	32.327
Rhydtalog	8.117	3.994	3.307	1.263	14.427	22.443
Joplin	7.344	3.423	2.656	1.083	12.153	18.002
Lewis Core	5.544	2.578	1.994	0.816	9.144	13.513
Lewis Clean	4.570	2.138	1.667	0.677	7.600	11.299
Pokomoke	2.529	1.181	0.918	0.374	4.194	6.223
Elliot IE	2.828	1.185	0.789	0.376	4.052	5.327
Guadalajara	2.126	0.914	0.633	0.290	3.155	4.283
Boxtel	1.937	0.858	0.622	0.272	2.994	4.208
Houthalein	1.578	0.753	0.601	0.238	2.693	4.078
Annemessex	2.005	0.875	0.621	0.277	3.038	4.198
Whippany	1.583	0.683	0.475	0.216	2.359	3.213
Sassafras 1	1.343	0.598	0.436	0.189	2.089	2.950
Matapeake	1.517	0.637	0.424	0.202	2.178	2.867
Sassafras 2	1.179	0.514	0.364	0.163	1.785	2.465
Chile Muestra	1.506	0.590	0.347	0.187	1.962	2.337
Sassafras 3	0.961	0.403	0.268	0.128	1.376	1.808
Washington 2	1.032	0.386	0.206	0.123	1.259	1.381
Washington 1	1.012	0.374	0.193	0.119	1.212	1.297
Souli	1.251	0.440	0.201	0.140	1.396	1.342
Fort McClellan	0.515	0.189	ND	0.0600	0.611	0.644
Massachusetts Military Reservation B	0.446	0.160	ND	0.051	0.511	0.513
Nevada	0.817	0.262	0.086	0.084	0.792	0.570
Aberdeen BA	0.414	0.140	0.057	0.045	0.436	0.379
Aberdeen BT	0.232	0.076	0.028	0.024	0.233	0.182

ND = no data

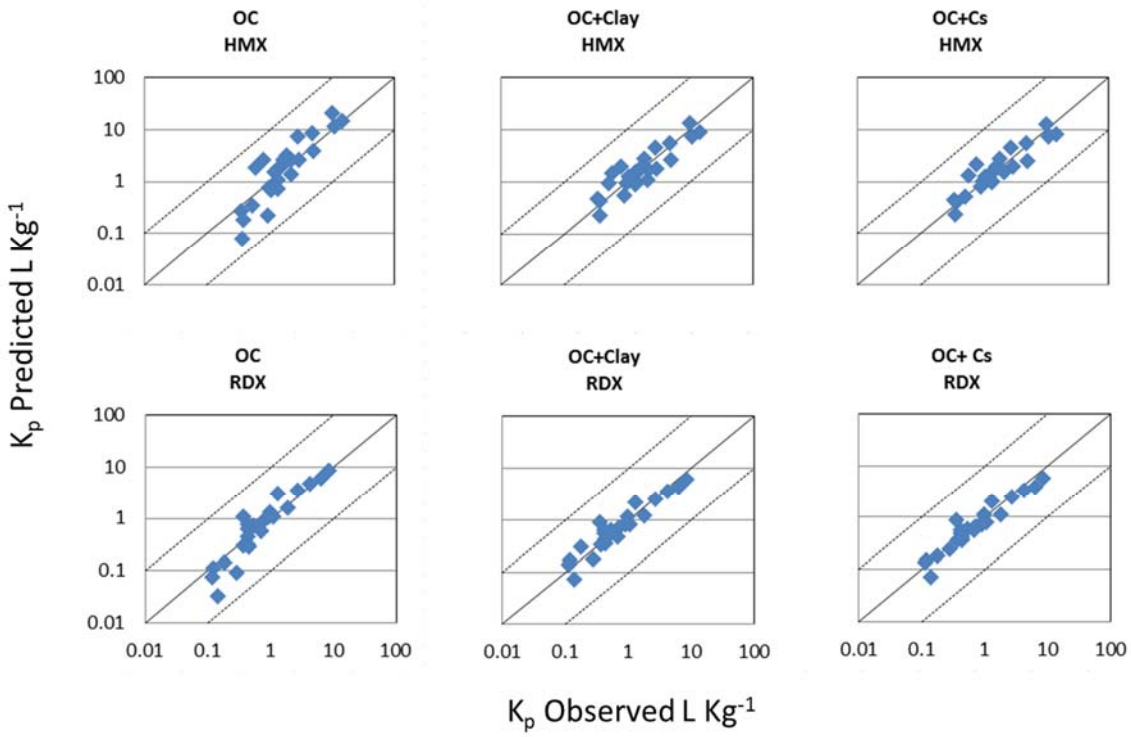

OC	$K_{p\,s,m} = K_{OC\,m}\,(f_{OC\,s})$
OC+Clay	$K_{p\,s,m} = K_{OC\,m}\,(f_{OC\,s}) + K_{clay\,m}\,(f_{clay\,s})$
OC+Cs	$K_{p\,s,m} = K_{OC\,m}\,(f_{OC\,s}) + K_{Cs\,m}\,(C_{Cs\,s})$

Figure 36. Relationship between K_p for HMX and RDX calculated with Equation 13 (Organic Carbon Model, OC), Equation 12 (Clay Size Model, OC+Clay), and Equation 18 (Charge Sites Model, OC+Cs) and measured values of K_p. The solid line represents the 1:1 ratio, and the dashed lines bracket at 1 log unit above and below the 1:1 line. Data are for 2 day equilibration for 25 soils.

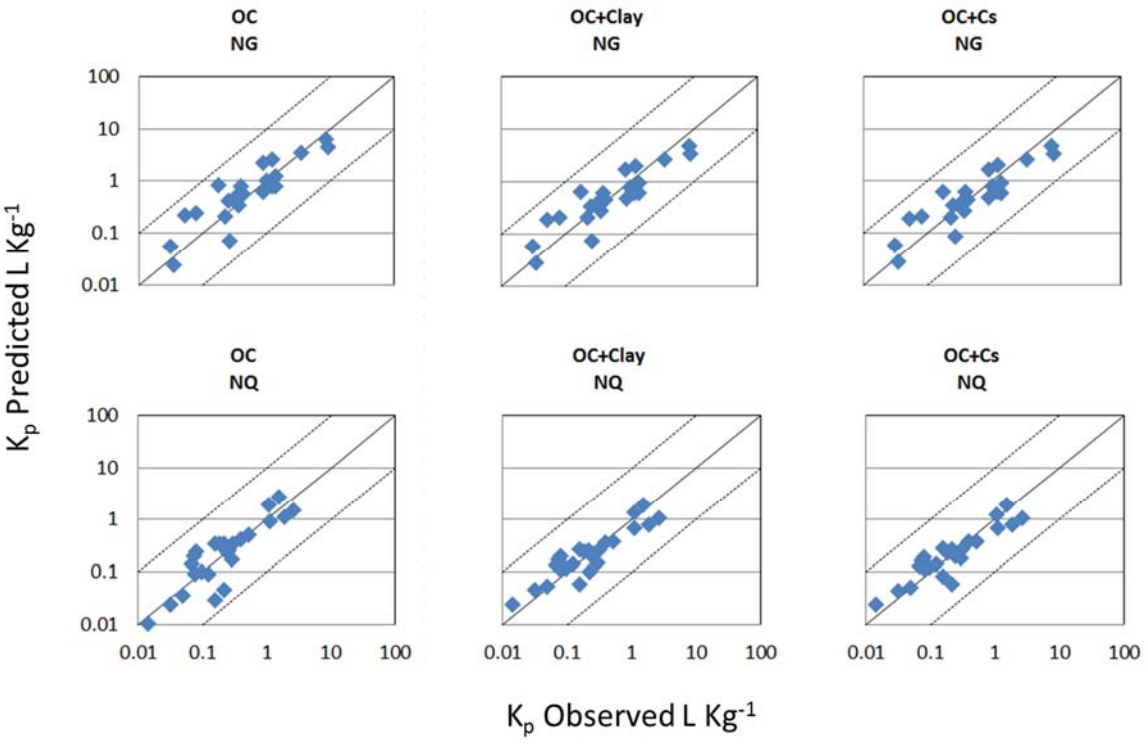

OC	$K_{p\,s,m} = K_{OC\,m}\,(f_{OC\,s})$
OC+Clay	$K_{p\,s,m} = K_{OC\,m}\,(f_{OC\,s}) + K_{clay\,m}\,(f_{clay\,s})$
OC+Cs	$K_{p\,s,m} = K_{OC\,m}\,(f_{OC\,s}) + K_{Cs\,m}\,(C_{Cs\,s})$

Figure 37. Relationship between K_p for NG and NQ calculated with Equation 13 (Organic Carbon Model, OC), Equation 12 (Clay Size Model, OC+Clay), and Equation 18 (Charge Sites Model, OC+Cs) and measured values of K_p. The solid line represents the 1:1 ratio, and the dashed lines bracket at 1 log unit above and below the 1:1 line. Data are for 2 day equilibration for 25 soils.

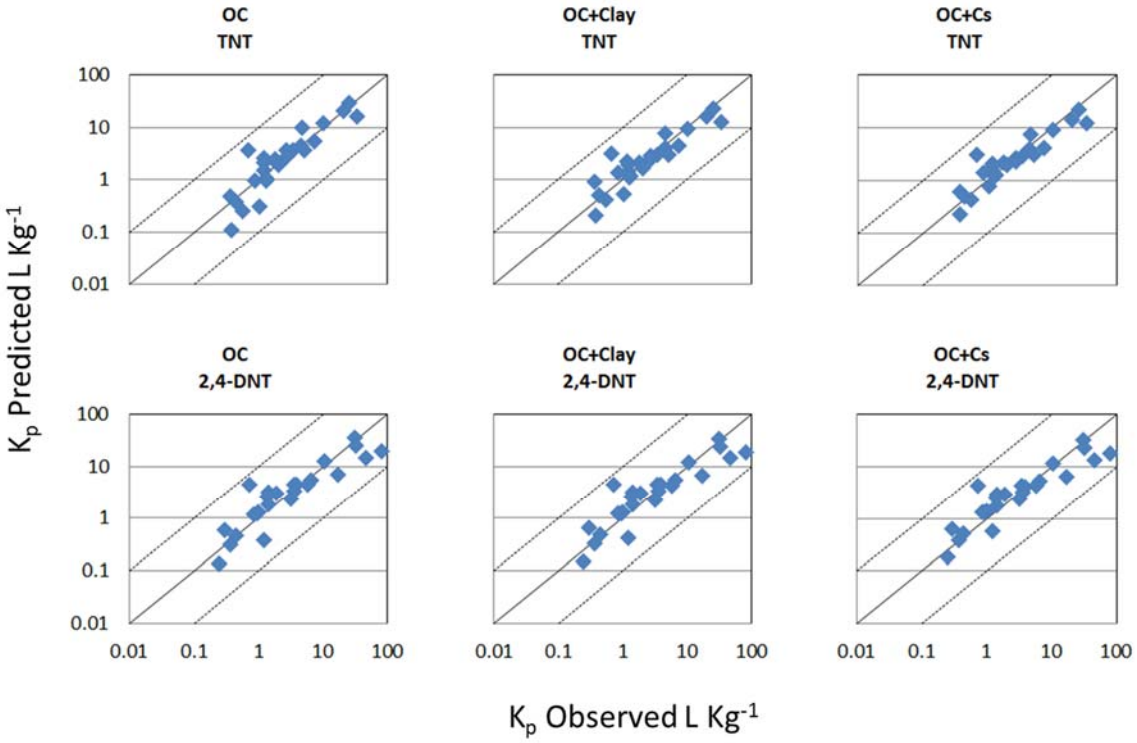

OC	$K_{p\,s,m} = K_{OC\,m}\,(f_{OC\,s})$
OC+Clay	$K_{p\,s,m} = K_{OC\,m}\,(f_{OC\,s}) + K_{clay\,m}\,(f_{clay\,s})$
OC+Cs	$K_{p\,s,m} = K_{OC\,m}\,(f_{OC\,s}) + K_{Cs\,m}\,(C_{Cs\,s})$

Figure 38. Relationship between K_p for TNT and 2,4-DNT calculated with Equation 13 (Organic Carbon Model, OC), Equation 12 (Clay Size Model, OC+Clay), and Equation 18 (Charge Sites Model, OC+Cs) and measured values of K_p. The solid line represents the 1:1 ratio, and the dashed lines bracket at 1 log unit above and below the 1:1 line. Data are for 2 day equilibration for 25 soils.

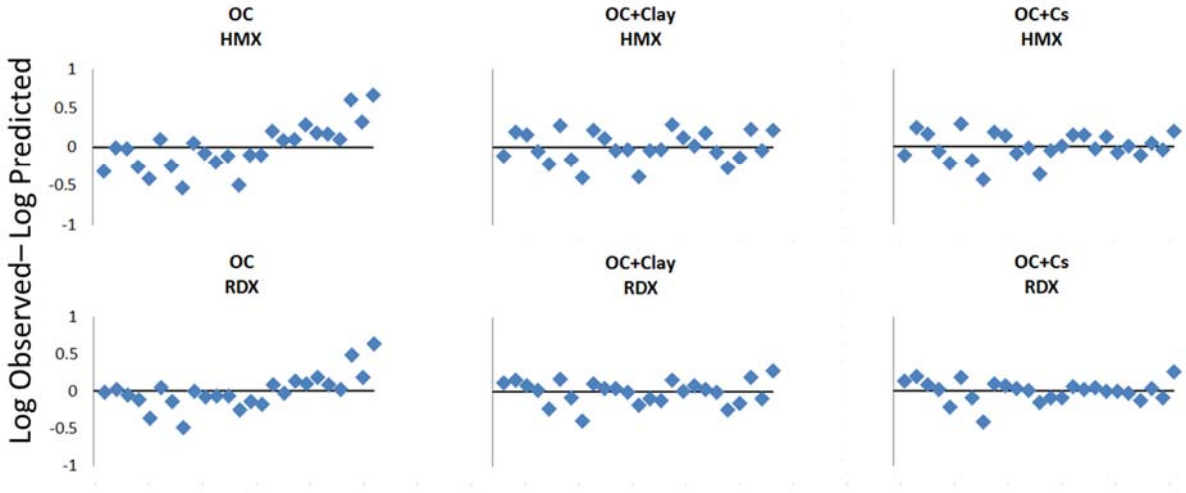

OC $K_{p\,s,m} = K_{OC\,m}\,(f_{OC\,s})$

OC+Clay $K_{p\,s,m} = K_{OC\,m}\,(f_{OC\,s}) + K_{clay\,m}\,(f_{clay\,s})$

OC+Cs $K_{p\,s,m} = K_{OC\,m}\,(f_{OC\,s}) + K_{Cs\,m}\,(C_{Cs\,s})$

Figure 39. Residuals (Log Observed – Log Predicted) of K_p for HMX and RDX calculated with Equation 13 (Organic Carbon Model, OC), Equation 12 (Clay Size Model, OC+Clay), and Equation 18 (Charge Sites Model, OC+Cs) and measured values of K_p. The x-axis is organized in decreasing OC content from 18.23% at the origin to 0.07%. Data are for 2 day equilibration for 25 soils.

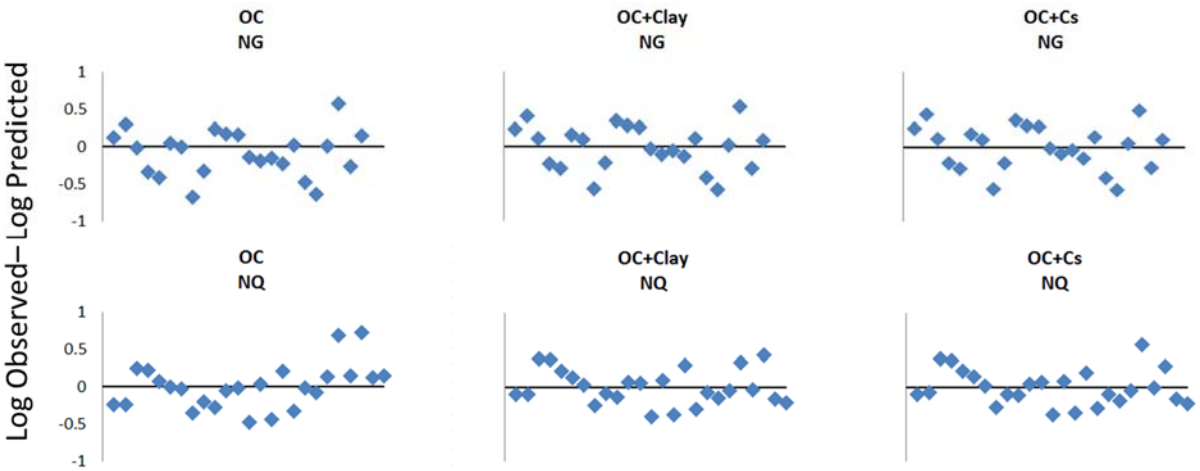

OC $K_{p\,s,m} = K_{OC\,m}\,(f_{OC\,s})$

OC+Clay $K_{p\,s,m} = K_{OC\,m}\,(f_{OC\,s}) + K_{clay\,m}\,(f_{clay\,s})$

OC+Cs $K_{p\,s,m} = K_{OC\,m}\,(f_{OC\,s}) + K_{Cs\,m}\,(C_{Cs\,s})$

Figure 40. Residuals (Log Observed – Log Predicted) of K_p for NG and NQ calculated with Equation 13 (Organic Carbon Model, OC), Equation 12 (Clay Size Model, OC+Clay), and Equation 18 (Charge Sites Model, OC+Cs) and measured values of K_p. The x-axis is organized in decreasing OC content from 18.23% at the origin to 0.07%. Data are for 2 day equilibration for 25 soils.

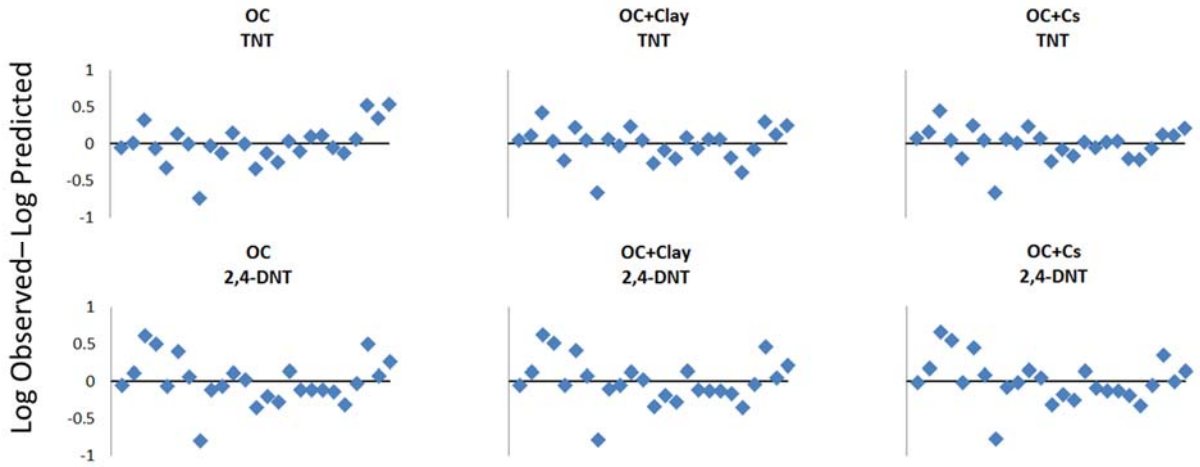

OC	$K_{p\,s,m} = K_{OC\,m}\,(f_{OC\,s})$
OC+Clay	$K_{p\,s,m} = K_{OC\,m}\,(f_{OC\,s}) + K_{clay\,m}\,(f_{clay\,s})$
OC+Cs	$K_{p\,s,m} = K_{OC\,m}\,(f_{OC\,s}) + K_{Cs\,m}\,(C_{Cs\,s})$

Figure 41. Residuals (Log Observed – Log Predicted) of K_p for TNT and 2,4-DNT calculated with Equation 13 (Organic Carbon Model, OC), Equation 12 (Clay Size Model, OC+Clay), and Equation 18 (Charge Sites Model, OC+Cs) and measured values of K_p. The x-axis is organized in decreasing OC content from 18.23% at the origin to 0.07%. Data are for 2 day equilibration for 25 soils.

The assumption used in the building of the multilinear models is that the influence of additional soil properties, rather than only organic carbon as traditionally used, is important. In Figures 36, 37, and 38 the data points are closer to the 1:1 solid line when the clay size particles or charge sites are included in the model rather than when only OC is used. The Charge Sites Model increases this closeness indicating better estimation of K_p using this model rather than the OC and Clay Size Models. This is confirmed from the residual plots on Figures 39, 40, and 41 because the closeness to the x-axis line of the data points increases when the Charge Sites Model is used for HMX, RDX, NQ, TNT and 2,4-DNT. In addition to that, the root mean square error (RMSE) of the predicted K_p data from the three K_p models OC, Clay Size and Charge Sites and the K_p obtained from the measured data was calculated and they are presented in Figure 42 for each MC confirming the increase of the fitting of the K_p observed and the K_p predicted by the multilinear Charge Sites Model. The data were subdivided into three groups organized by the organic carbon of the soil. The data, which are presented in Table 31 and Figure 43, are divided into three OC categories; low 0.07 to 0.9%, medium 1 to 3% and high 4 to 18%. The importance of considering the charged sites can be seen in the results for HMX and RDX. For these MC the Charge Sites Model has a much lower RMSE for the low OC group of data compared to the values for the medium and high OC soils. There is a lesser improvement in predictive ability for TNT and 2,4-DNT for the low OC soils and no improvement for NQ or NG for which the RMSE is independent of the OC content. Thus, for soils with a low content of OC, the use of the Charge Sites Model should be considered if data of high accuracy is required. However, in most situations the use of the Clay Size Model will likely give acceptable results. The K_{OC}, K_{clay}, and K_{Cs} parameters for the OC, Clay Size, and Charge Site Models are presented in Table 32.

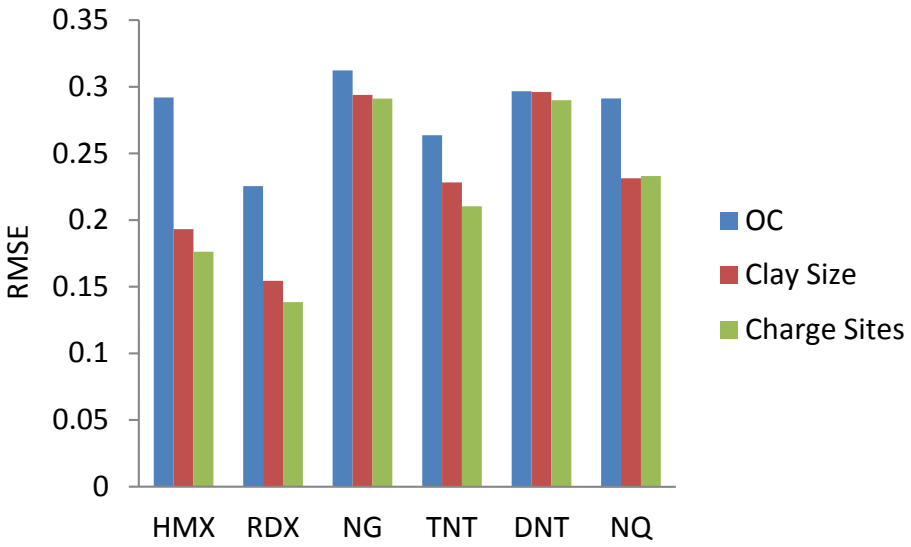

Figure 42. Comparison of the RMSE for K_p obtained by the OC, Clay Size and Charge Sites models and K_p measured data for 2 day equilibration for 25 soils.

Table 31. RMSE values obtained by the OC, Clay Size and Charge Sites models separating these values by the OC content (low 0.07 to 0.9%, medium 1 to 3% and high 4 to 18%) for 2 day equilibration for 25 soils.

	HMX		
	OC	OC+Clay	OC+Cs
OC (0.07-0.9%)	0.3469	0.1644	0.1060
OC (1-3%)	0.2655	0.2205	0.2085
OC (4-18%)	0.2394	0.1845	0.2002
	RDX		
OC (0.07-0.9%)	0.2854	0.1564	0.1059
OC (1-3%)	0.1977	0.1581	0.1522
OC (4-18%)	0.1567	0.1448	0.1561
	NG		
OC (0.07-0.9%)	0.3882	0.3586	0.3462
OC (1-3%)	0.2822	0.2596	0.2623
OC (4-18%)	0.2555	0.2622	0.2656
	NQ		
OC (0.07-0.9%)	0.3621	0.2333	0.2558
OC (1-3%)	0.2662	0.2194	0.2019
OC (4-18%)	0.1972	0.2475	0.2457
	TNT		
OC (0.07-0.9%)	0.2849	0.2040	0.1377
OC (1-3%)	0.2772	0.2499	0.2451
OC (4-18%)	0.1995	0.2247	0.2365
	2,4-DNT		
OC (0.07-0.9%)	0.2308	0.2256	0.1924
OC (1-3%)	0.3054	0.3007	0.2913
OC (4-18%)	0.3625	0.3718	0.3915

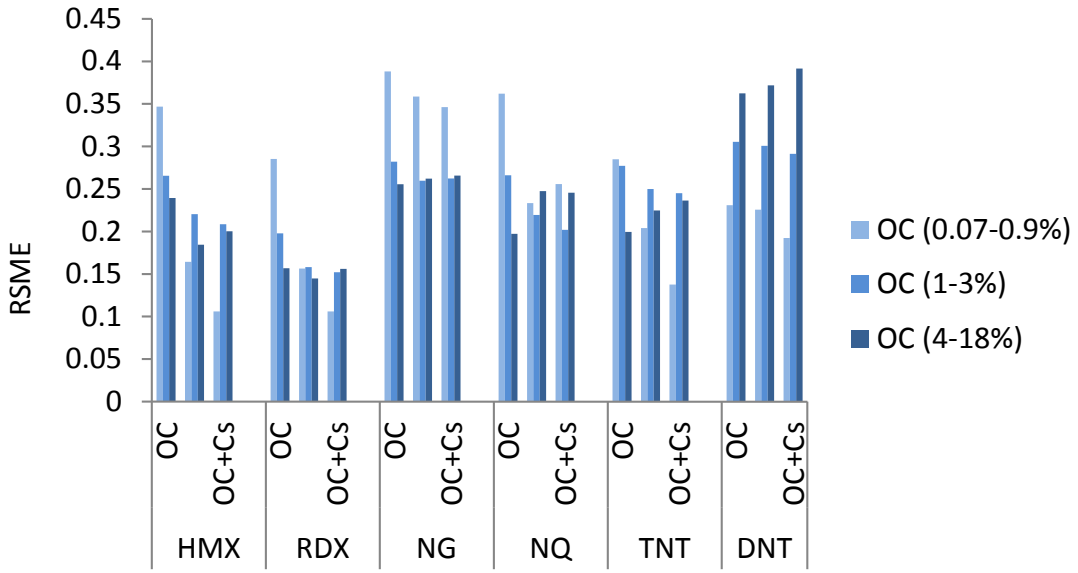

Figure 43. Comparison of the RMSE for K_p obtained by the OC, Clay Size and Charge Sites models and K_p measured data separating these values by the OC content (low 0.07 to 0.9%, medium 1 to 3% and high 4 to 4 to 18%) for 2 day equilibration for 25 soils**.**

Table 32. Parameters of the OC, Clay Size and Charge Sites Models for HMX, RDX, NG, NQ, TNT and 2,4-DNT. Data are for 2 day equilibration for 25 soils**.**

	Parameter	HMX	RDX	NG	NQ	TNT	2,4-DNT
K_p OC	K_{OC}	113.50	46.80	35.26	14.84	158.29	195.20
K_p Clay Size	K_{OC}	70.00	33.42	26.26	10.43	122.05	188.86
	K_{Clay}	1.90	0.537	0.104	0.179	1.38	0.205
K_p Charge Sites	K_{OC}	55.66	28.93	25.39	9.14	106.19	172.50
	K_{Cs}	13021	3770.7	656.09	1203.4	10697	4146.0

Multilinear Model using Cation Exchange Capacity (CEC). The charge sites method increased the goodness of fit in estimation of K_p to low OC content soils by an average of 40% for HMX, RDX, TNT and 2,4-DNT relative to the clay size method, but the determination of charge by the Cs method is not convenient because it requires many steps and is time consuming. The CEC was tested in the multilinear model because it is the sum of total exchangeable cations that a soil can adsorb [Sparks 2003] and the cations on the cation exchange sites of the soil particles are easily exchangeable with other cations. The cation exchange capacity is the maximum adsorption of readily exchangeable ions in a diffuse ion swarm and outer-sphere complexes on the soil particle surface [De Kimpe et al. 1979]. In addition it was selected because the CEC is impacted by the soil texture (amount of clay), clay type (surface areas), soil organic matter, source of charge and pH [Soil Colloids Course 2007]. The model (Equation 19), uses CEC rather than the clay component.

$$K_{p\,s,m} = K_{OC\,m}\,(f_{OC\,s}) + K_{CEC\,m}\,(CEC_s) \qquad (19)$$

where $K_{OC\,m}$ = sorption coefficient to organic carbon in the soil $K_{CEC\,m}$ = sorption coefficient to

CEC in the soil, f_{OC} = fraction of OC in the soil, CEC = cation exchange capacity of the soil, s = soil, and m = munitions constituents. The K_p values computed for the 25 soils that were tested are presented in Table 33 and the experimental values are presented in Table 24. The values of CEC for the soils are presented in Table 2.

Figures 44, 45, and 46 present the relationships of the K_p values calculated by the three multilinear models (CEC, Clay Size and Charge Sites) with Equations 19, 12 and 18, respectively, and the measured values of K_p obtained from the adsorption/ desorption experiment. Figures 47, 48, and 49 are residual plots to analyze the fit of the three multilinear models. The clay size and charge sites models are included to facilitate their comparison to the CEC model, to determine which of these three soil properties is sufficient to make decisions about the fate of MC.

From Figures 44-49 and the RMSE values for the CEC model compared with Clay Size and Charge Sites models for low organic carbon content soils presented in Table 34 it is clear that the CEC Model provides similar estimations of K_p to the Clay Size Model. Therefore, CEC clearly can replace the clay size component in the model. Table 35 shows the parameters of the CEC Model. They have the same trend as the Charge Sites Model in Table 30 because for HMX, RDX, NQ and TNT the K_{CEC} parameter has a greater effect in the partition coefficient of adsorption than does the organic carbon. This illustrates the importance of including soil properties other than only OC when studying sorption.

The results of the models obtained with clay, charge sites and CEC were compared to evaluate these soil properties as predictors of MC sorption. Figure 50 presents the relationships among the properties. The figure shows that there is no relationship between the concentration of clay sized particles and the CEC. This is in agreement with Lambooy [1984] who found for 50 soil samples that CEC differs irrespective of clay sized particles content. This difference has been attributed to the difference in clay mineralogy among some soil forms [De Kimpe et al. 1978]. Martel et al. [1978] showed that the variations in mineralogical composition, although small, were sufficient to explain nearly 50% of the variation in CEC and Miller [1970] found that the type of clay alone could explain up to 50% of the variation in CEC. There is a linear correlation between the charge sites and CEC because CEC is the maximum adsorption of readily exchangeable ions in a diffuse ion swarm and outer-sphere complexes on the soil particle surface [Sposito, 2000] and the charge sites are the ones which reside in the diffuse-ion swarm on siloxane surfaces [Cebula and Ottewill 1981]. For the 25 soils, the charge sites determined by Cs exchange vary from 15 to 65% of the charge sites determined by CEC. The CEC fits in the multilinear model because CEC is due to the electrostatic forces (outer-sphere) which permit the interaction of a counter ion in the boundary layer between the solution and a charged particle surface and the counter ions in a diffuse cloud around the charged particle [Sparks 2003].

Table 33. K_p (L kg^{-1}) calculated by the Cation Exchange Capacity (CEC) Model, Equation 19. Data are for 2 day equilibration for 25 soils.

	K_p Predicted by the CEC Model L kg^{-1}					
Soil	HMX	RDX	NG	NQ	TNT	DNT
Zegveld	12.678	6.021	5.511	21.795	33.193	1.754
Rhydtalog	8.788	4.198	3.866	15.233	23.330	1.219
Joplin	7.714	3.538	3.123	12.629	18.582	1.051
Lewis Core	6.005	2.717	2.363	9.644	13.988	0.814
Lewis Clean	5.044	2.280	1.981	8.090	11.723	0.683
Pokomoke	2.564	1.194	1.070	4.287	6.403	0.352
Elliot IE	2.585	1.118	0.921	3.886	5.345	0.344
Guadalajara	1.853	0.837	0.726	2.968	4.296	0.251
Boxtel	1.817	0.825	0.720	2.933	4.271	0.247
Houthalein	1.402	0.704	0.679	2.602	4.159	0.199
Annemessex	1.917	0.852	0.725	2.992	4.261	0.258
Whippany	1.734	0.728	0.578	2.498	3.306	0.228
Sassafras 1	1.316	0.591	0.510	2.091	3.010	0.178
Matapeake	1.337	0.586	0.491	2.050	2.865	0.179
Sassafras 2	1.178	0.515	0.431	1.802	2.513	0.158
Chile Muestra	1.713	0.651	0.445	2.123	2.388	0.217
Sassafras 3	0.780	0.351	0.303	1.242	1.791	0.105
Washington 2	1.395	0.492	0.292	1.536	1.451	0.172
Washington 1	1.242	0.441	0.266	1.383	1.333	0.153
Souli	1.145	0.410	0.252	1.294	1.277	0.142
Fort McClellan	0.724	0.250	ND	0.769	0.682	0.088
Massachusetts Military Reservation B	0.257	0.105	ND	0.357	0.458	0.033
Nevada	0.675	0.221	0.111	0.659	0.488	0.081
Aberdeen BA	0.279	0.102	0.064	0.323	0.330	0.035
Aberdeen BT	0.134	0.048	0.029	0.151	0.147	0.017

ND = No Data

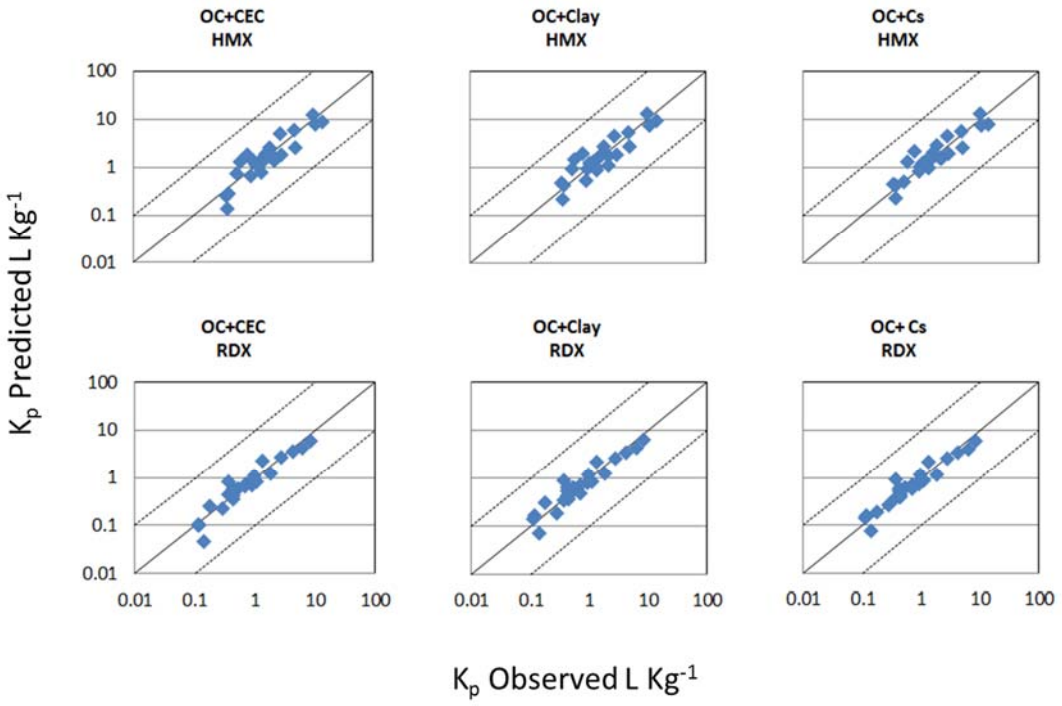

OC+CEC	$K_{p\,s,m} = K_{OC\,m}\,(f_{OC\,s}) + K_{CEC\,m}\,(CEC_s)$
OC+Clay	$K_{p\,s,m} = K_{OC\,m}\,(f_{OC\,s}) + K_{clay\,m}\,(f_{clay\,s})$
OC+Cs	$K_{p\,s,m} = K_{OC\,m}\,(f_{OC\,s}) + K_{Cs\,m}\,(C_{Cs\,s})$

Figure 44. Relationship between K_p for HMX and RDX calculated with Equation 19 (CEC Model – OC+CEC), Equation 12 (Clay Size Model - OC+Clay), and Equation 18 (Charge Sites Model - OC+Cs) and measured values of K_p. The solid line represents the 1:1 ratio, and the dashed lines bracket at 1 log unit above and below the 1:1 line. Data are for 2 day equilibration for 25 soils**.**

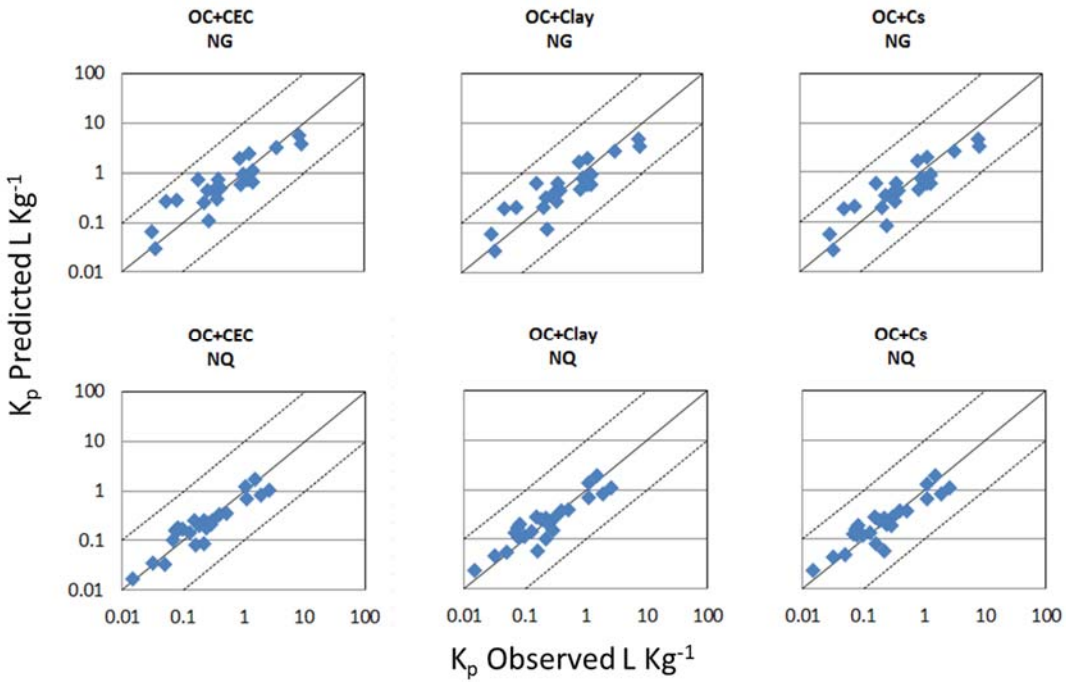

OC+CEC	$K_{p\,s,m} = K_{OC\,m}\,(f_{OC\,s}) + K_{CEC\,m}\,(CEC_s)$
OC+Clay	$K_{p\,s,m} = K_{OC\,m}\,(f_{OC\,s}) + K_{clay\,m}\,(f_{clay\,s})$
OC+Cs	$K_{p\,s,m} = K_{OC\,m}\,(f_{OC\,s}) + K_{Cs\,m}\,(C_{Cs\,s})$

Figure 45. Relationship between K_p for NG and NQ calculated with Equation 19 (CEC Model – OC+CEC), Equation 12 (Clay Size Model - OC+Clay), and Equation 18 (Charge Sites Model - OC+Cs) and measured values of K_p. The solid line represents the 1:1 ratio, and the dashed lines bracket at 1 log unit above and below the 1:1 line. Data are for 2 day equilibration for 25 soils**.**

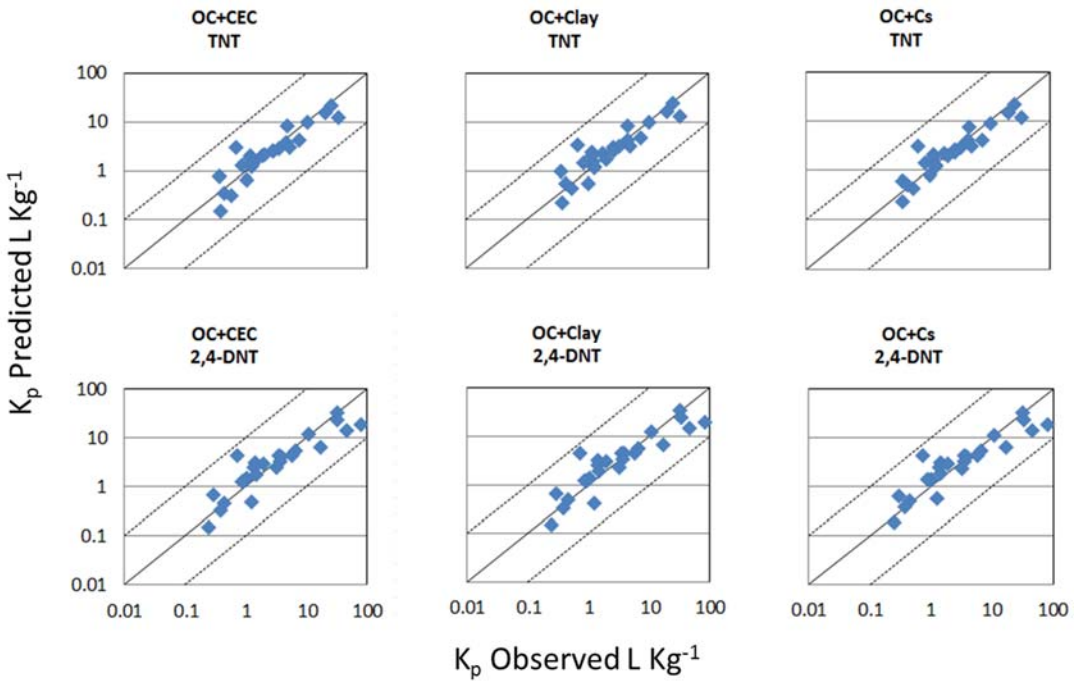

OC+CEC	$K_{p\,s,m} = K_{OC\,m}\,(f_{OC\,s}) + K_{CEC\,m}\,(CEC_s)$
OC+Clay	$K_{p\,s,m} = K_{OC\,m}\,(f_{OC\,s}) + K_{clay\,m}\,(f_{clay\,s})$
OC+Cs	$K_{p\,s,m} = K_{OC\,m}\,(f_{OC\,s}) + K_{Cs\,m}\,(C_{Cs\,s})$

Figure 46. Relationship between K_p for TNT and 2,4-DNT calculated with Equation 19 (CEC Model – OC+CEC), Equation 12 (Clay Size Model - OC+Clay), and Equation 18 (Charge Sites Model - OC+Cs) and measured values of K_p. The solid line represents the 1:1 ratio, and the dashed lines bracket at 1 log unit above and below the 1:1 line. Data are for 2 day equilibration for 25 soils**.**

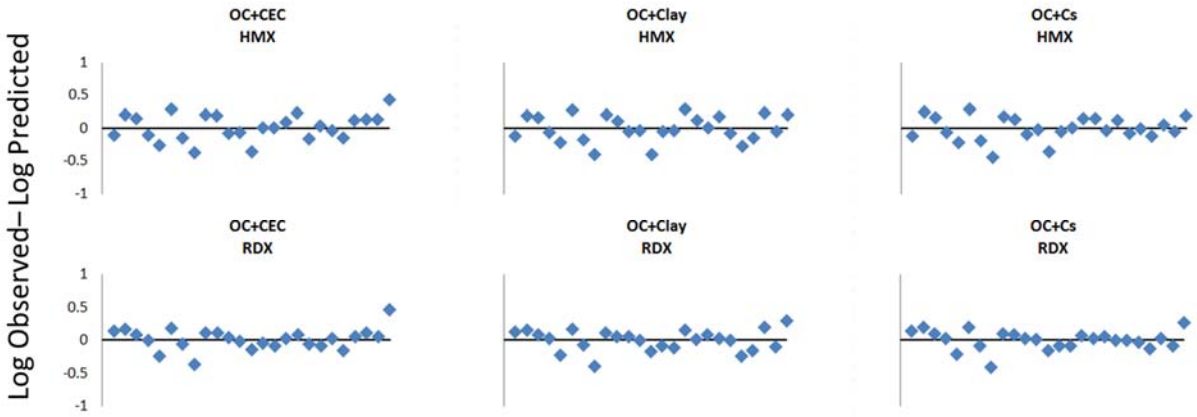

OC+CEC $K_{p\,s,m} = K_{OC\,m}\,(f_{OC\,s}) + K_{CEC\,m}\,(CEC_s)$

OC+Clay $K_{p\,s,m} = K_{OC\,m}\,(f_{OC\,s}) + K_{clay\,m}\,(f_{clay\,s})$

OC+Cs $K_{p\,s,m} = K_{OC\,m}\,(f_{OC\,s}) + K_{Cs\,m}\,(C_{Cs\,s})$

Figure 47. Residuals (Log Observed – Log Predicted) of K_p for HMX and RDX calculated with Equation 19 (CEC Model – OC+CEC), Equation 12 (Clay Size Model - OC+Clay), and Equation 18 (Charge Sites Model - OC+Cs) and measured values of K_p. The x-axis is organized in decreasing OC content from 18.23% at the origin to 0.07%. Data are for 2 day equilibration for 25 soils**.**

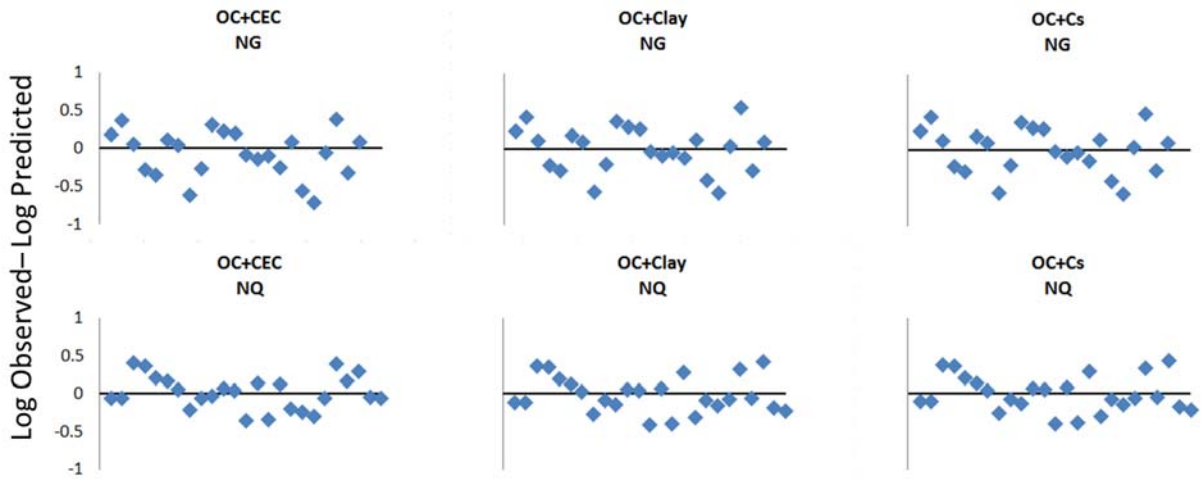

OC+CEC $K_{p\,s,m} = K_{OC\,m}\,(f_{OC\,s}) + K_{CEC\,m}\,(CEC_s)$

OC+Clay $K_{p\,s,m} = K_{OC\,m}\,(f_{OC\,s}) + K_{clay\,m}\,(f_{clay\,s})$

OC+Cs $K_{p\,s,m} = K_{OC\,m}\,(f_{OC\,s}) + K_{Cs\,m}\,(C_{Cs\,s})$

Figure 48. Residuals (Log Observed – Log Predicted) of K_p for NG and NQ calculated with Equation 19 (CEC Model – OC+CEC), Equation 12 (Clay Size Model - OC+Clay), and Equation 18 (Charge Sites Model - OC+Cs) and measured values of K_p. The x-axis is organized in decreasing OC content from 18.23% at the origin to 0.07%. Data are for 2 day equilibration for 25 soils**.**

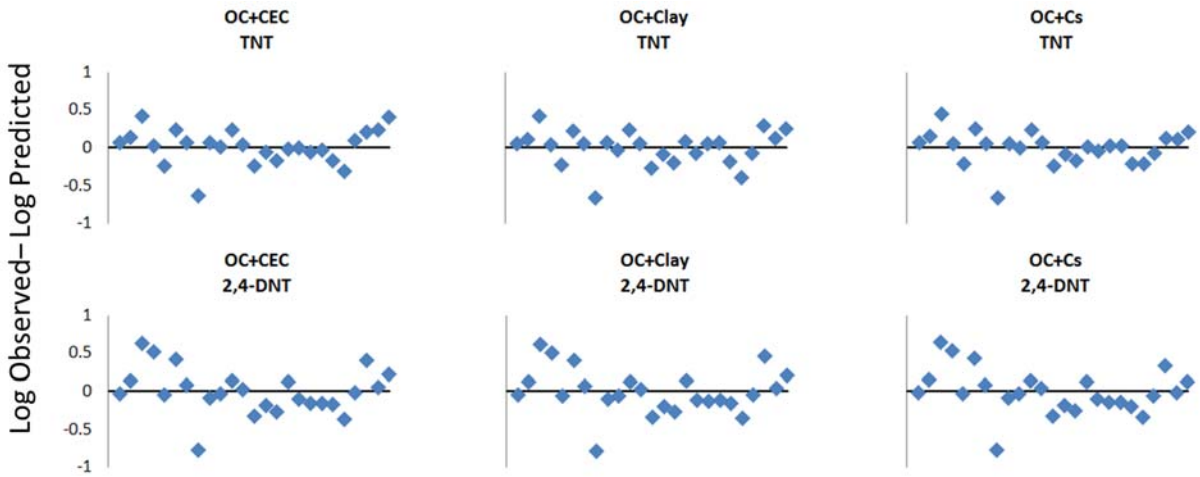

OC+CEC $K_{p\,s,m} = K_{OC\,m}\,(f_{OC\,s}) + K_{CEC\,m}\,(CEC_s)$

OC+Clay $K_{p\,s,m} = K_{OC\,m}\,(f_{OC\,s}) + K_{clay\,m}\,(f_{clay\,s})$

OC+Cs $K_{p\,s,m} = K_{OC\,m}\,(f_{OC\,s}) + K_{Cs\,m}\,(C_{Cs\,s})$

Figure 49. Residuals (Log Observed – Log Predicted) of K_p for TNT and 2,4-DNT calculated with Equation 19 (CEC Model – OC+CEC), Equation 12 (Clay Size Model - OC+Clay), and Equation 18 (Charge Sites Model - OC+Cs) and measured values of K_p. The x-axis is organized in decreasing OC content from 18.23% at the origin to 0.07%. Data are for 2 day equilibration for 25 soils**.**

Table 34. RMSE obtained by the OC, clay size, charge sites and CEC models to low organic carbon content soils (0.07-0.9%). Data are for 2 day equilibration for 25 soils.

Model	HMX	RDX	NG	NQ	TNT	DNT
OC	0.3469	0.2854	0.3882	0.2849	0.2308	0.3621
OC+Clay	0.1644	0.1564	0.3586	0.2040	0.2256	0.2333
OC+Cs	0.1060	0.1059	0.3462	0.1377	0.1924	0.2558
OC+CEC	0.1964	0.1746	0.3944	0.2120	0.2193	0.2263

Table 35. Parameters of the CEC model for HMX, RDX, NG, NQ, TNT and 2,4-DNT. Data are for 2 day equilibration for 25 soils.

CEC Model						
Parameter	HMX	RDX	NG	NQ	TNT	2,4-DNT
K_{OC}	54.360	28.624	28.803	7.870	107.656	178.577
K_{CEC}	5.625	1.631	0.528	0.648	4.407	1.297

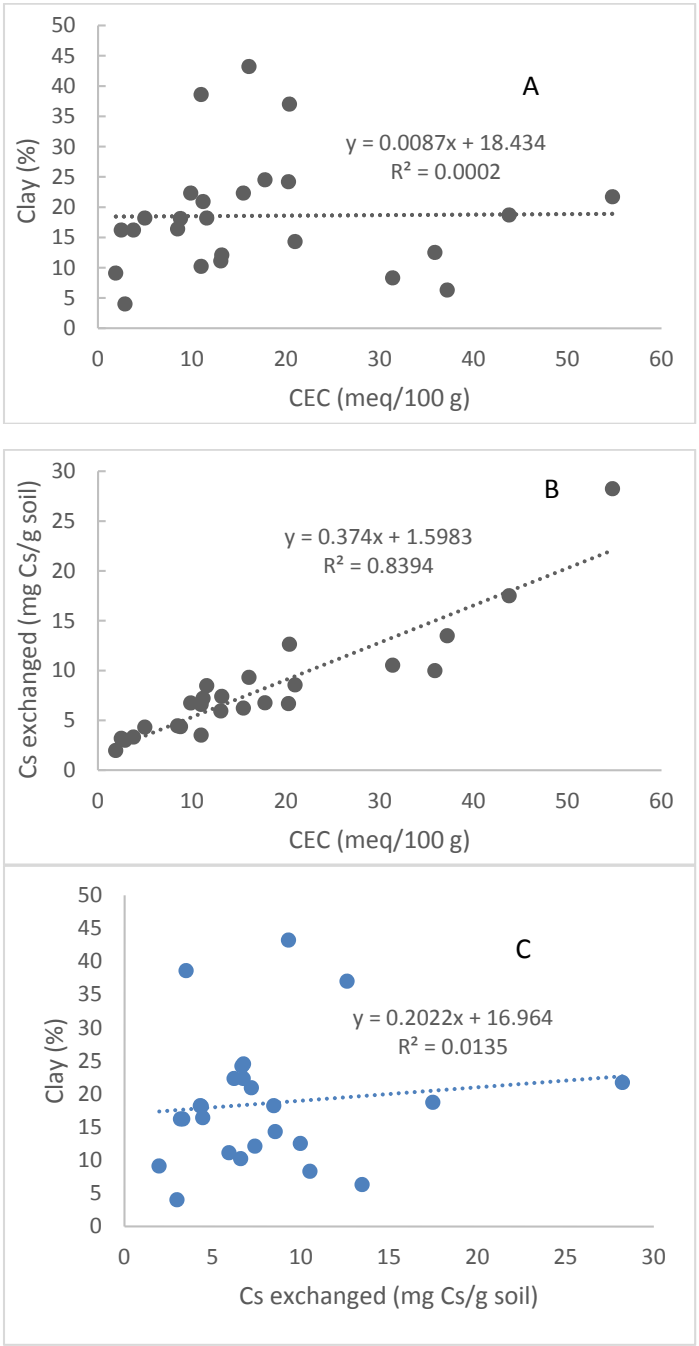

Figure 50. A. Relationship between clay sized particles and CEC. B. Relationship between Cs exchanged and CEC. C. Relationship between and clay sized particles and Cs exchanged. Data are for 2 day equilibration for 25 soils.

In addition to the relationships presented above, the relationships between clay, charge sites (Cs exchange), or CEC and organic carbon OC were evaluated and are shown in Figure 51. It is clear that the charge sites and CEC are related with OC in a linear way. This agrees with the results of Rashidi and Seilsepour [2008] who showed a linear regression model based on soil organic carbon can be used to predict soil CEC. Their R^2 was 0.74 using 75 soils from different fields and the ones in Figure 51 were 0.80 for CEC and 0.73 for Cs exchange, respectively. Charge sites and CEC present similar results because they are correlated, while clay sized particle concentration is not correlated in a linear manner with OC. However, the OC+clay model works because of the specific interactions between clay and the MC. For example, Monteil et al. [2003] found that HMX is immobilized in soils by the presence of clay. Sunahara et al. [2009] indicated that clays are strong sorbents for NACs, and Schwarzenbach et al. [2003] said that the electronic distribution on the nitroaromatics (NACs) in the center of the ring electropositive produces strongly interactions with the mineral surface because the mineral surface is electron rich and forms an electron Donor – Acceptor complex (EDA complex) with NACs.

Trilinear Model. The literature indicates that the presence of Fe in the soil influences the fate of MC in the environment. Chapell [2011] showed that the sorption distribution coefficient K_d for TNT was directly related to soil CEC and extractable soil Fe content. Pennington and Patrick [1990] reported statistically significant correlations among K_d for TNT with oxalate-extractable Fe, CEC, and percent clay, but in their study the relationship of K_d with OC was not considered. Some researchers have studied the abiotic degradation of the MC due to Fe. Nefso et al. [2005] and Sunahara et al. [2009] are examples of that. In the first case they determined that exchangeable Fe overwhelms any influence of structural ferrous iron in the degradation of TNT. In the second case it was found that Fe reduces TNT and RDX.

To determine the influence of Fe on the K_p estimation by the multilinear models, it was decided to include oxalate extractable Fe (FeOx) as an additional sorption site in the CEC Model, Equation 19, to yield the Trilinear Model, Equation 20.

$$K_{p\,s,m} = K_{OC\,m}\,(f_{OC\,s}) + K_{CEC\,m}\,(CEC_s) + K_{FeOx\,m}\,(C_{FeOx\,s}) \qquad (20)$$

where $K_{OC\,m}$ = sorption coefficient to organic carbon in the soil, $K_{CEC\,m}$ = sorption coefficient to CEC in the soil, K_{FeOx} = sorption coefficient to oxalate extractable iron in the soil, f_{OC} = fraction of OC in the soil, CEC = cation exchange capacity of the soil, C_{FeOx} = concentration of oxalate extractable iron in the soil, s = soil, and m = munitions constituents. The CEC model was selected because CEC is a soil property that is easier to measure than charge sites and it provides results that are similar to those of the Clay Model. The extractable iron was selected because, according to Keng and Uehara [1973], charge sites soils usually contain a high proportion of colloids of metal oxides, especially those of Fe and Al. The oxalate extractable Fe gives a measure of the "active" forms of the Fe [Schwertmann 1964], which are ferrihydrite and small amounts of organically bound Fe [Del Campillo and Torrent 1992]. This method is a measure of the quantity of amorphous iron oxides, or more generally as a measure of the "activity" of the iron oxides [Blume and Schwertmann 1969]. Oxalate does not dissolve a major part of the crystalline iron oxides. It attacks most silicate minerals and goethite and hematite only slightly [Schwertmann 1973]. In other words, the oxalate extractable Fe provides a measure of additional sorption sites that influence the partition coefficient for the adsorption of MC.

Figure 52 shows the relationship of K_p values calculated by the Trilinear Model with Equation 20. K_p values computed by the Trilinear Model are listed in Table 36 and measured values of K_p

obtained from the adsorption/desorption experiment are given in Table 27. The parameters of the model are given in Table 37. Figure 52 shows the improvement attained by the addition of the FeOx component in the model in comparison with Figures 44-46 without it. The plot of residuals for the Trilinear Model shown in Figure 53 can be contrasted to plots for models that do not include FeOx, which are shown in Figures 47-49. This shows the importance of FeOx on influencing the fate of MC. FeOx is an important component of the adsorption partition coefficient, particularly for soils with low OC. For HMX the percentage of the adsorption bound to FeOx is 12%, for RDX it is 8%, for NG it is 1.3%, for TNT it is 9% and for 2,4-DNT it is 3%.

Table 36. *Kp* (L kg^{-1}) calculated with Equation 20, the Trilinear Model. Data are for 2 day equilibration for 24 soils. Results for Guadalajara are not included because no oxalate extractable iron was detected.

	K_p Predicted by the Trilinear Model L kg^{-1}					
Soil	HMX	RDX	NG	NQ	TNT	2,4-DNT
Zegveld	13.827	6.463	5.389	24.460	35.534	1.821
Rhydtalog	8.835	4.288	3.763	16.150	24.508	1.266
Joplin	7.638	3.573	2.978	13.190	19.493	1.087
Lewis Core	6.405	2.876	2.254	10.640	14.961	0.840
Lewis Clean	5.377	2.413	1.889	8.923	12.539	0.706
Pokomoke	2.452	1.181	1.025	4.376	6.659	0.364
Elliot IE	2.555	1.123	0.848	4.028	5.623	0.353
Guadalajara	NC	NC	NC	NC	NC	NC
Boxtel	2.282	0.974	0.701	3.670	4.775	0.255
Houthalein	1.526	0.754	0.678	2.915	4.429	0.208
Annemessex	1.865	0.849	0.678	3.080	4.457	0.266
Whippany	1.755	0.742	0.523	2.630	3.509	0.233
Sassafras 1	1.336	0.606	0.482	2.222	3.181	0.183
Matapeake	1.460	0.630	0.461	2.302	3.096	0.184
Sassafras 2	1.255	0.545	0.403	1.983	2.697	0.162
Chile Muestra	2.117	0.772	0.382	2.696	2.797	0.219
Sassafras 3	0.877	0.385	0.290	1.427	1.944	0.109
Washington 2	1.119	0.412	0.206	1.217	1.405	0.172
Washington 1	1.049	0.386	0.192	1.168	1.325	0.154
Souli	0.976	0.362	0.186	1.109	1.276	0.143
Fort McClellan	0.484	0.180	ND	0.478	0.597	0.089
Massachusetts Military Reservation B	0.386	0.144	ND	0.534	0.563	0.034
Nevada	0.637	0.209	0.067	0.615	0.518	0.081
Aberdeen BA	0.460	0.155	0.056	0.559	0.465	0.035
Aberdeen BT	0.249	0.082	0.026	0.299	0.229	0.017

NC = Not calculable because no Fe was detected in the oxalate extraction.

ND = No Data

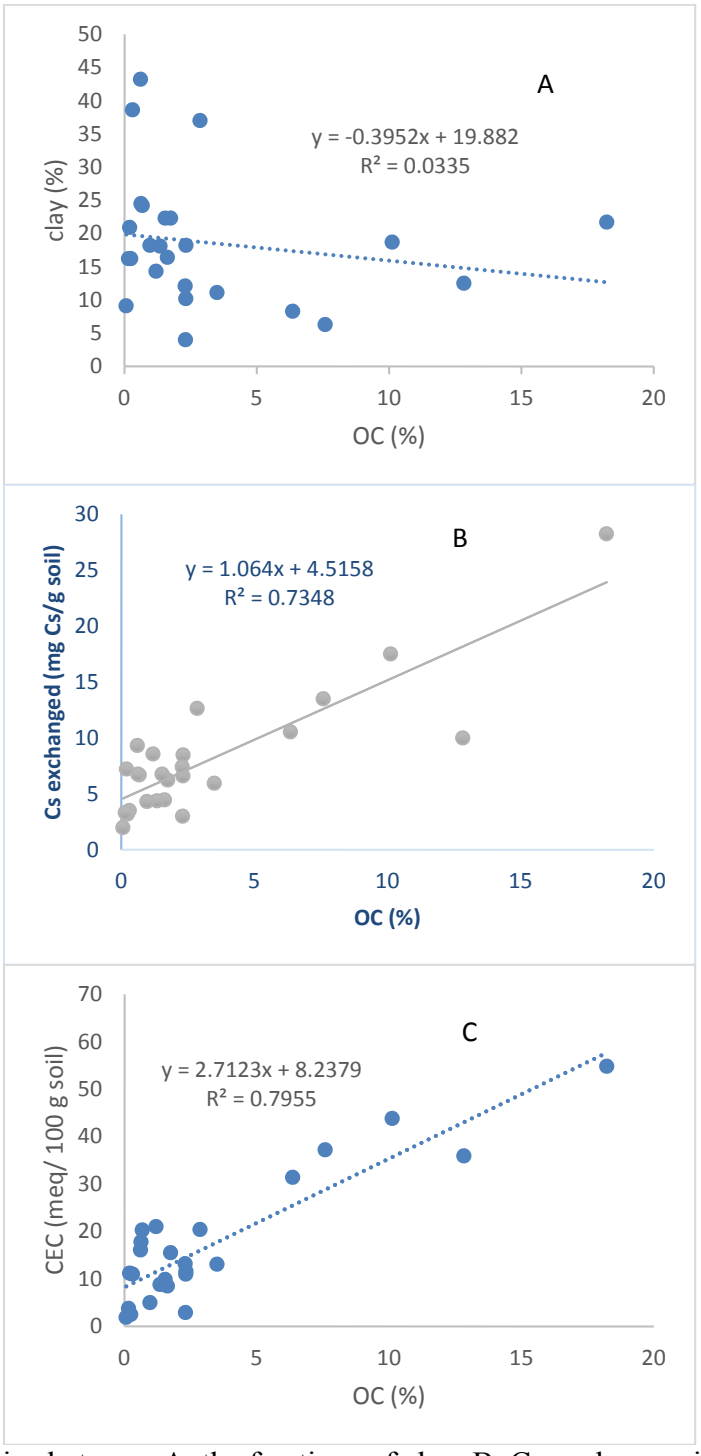

Figure 51. Relationships between A. the fractions of clay, B. Cs exchange site concentration, and C. CEC with the fraction of OC. Data are for 2 day equilibration for 25 soils.

Table 36. *Kp* (L kg^{-1}) calculated with Equation 20, the Trilinear Model. Data are for 2 day equilibration for 24 soils. Results for Guadalajara are not included because no oxalate extractable iron was detected.

	K_p Predicted by the Trilinear Model L kg^{-1}					
Soil	HMX	RDX	NG	NQ	TNT	2,4-DNT
Zegveld	13.827	6.463	5.389	24.460	35.534	1.821
Rhydtalog	8.835	4.288	3.763	16.150	24.508	1.266
Joplin	7.638	3.573	2.978	13.190	19.493	1.087
Lewis Core	6.405	2.876	2.254	10.640	14.961	0.840
Lewis Clean	5.377	2.413	1.889	8.923	12.539	0.706
Pokomoke	2.452	1.181	1.025	4.376	6.659	0.364
Elliot IE	2.555	1.123	0.848	4.028	5.623	0.353
Guadalajara	NC	NC	NC	NC	NC	NC
Boxtel	2.282	0.974	0.701	3.670	4.775	0.255
Houthalein	1.526	0.754	0.678	2.915	4.429	0.208
Annemessex	1.865	0.849	0.678	3.080	4.457	0.266
Whippany	1.755	0.742	0.523	2.630	3.509	0.233
Sassafras 1	1.336	0.606	0.482	2.222	3.181	0.183
Matapeake	1.460	0.630	0.461	2.302	3.096	0.184
Sassafras 2	1.255	0.545	0.403	1.983	2.697	0.162
Chile Muestra	2.117	0.772	0.382	2.696	2.797	0.219
Sassafras 3	0.877	0.385	0.290	1.427	1.944	0.109
Washington 2	1.119	0.412	0.206	1.217	1.405	0.172
Washington 1	1.049	0.386	0.192	1.168	1.325	0.154
Souli	0.976	0.362	0.186	1.109	1.276	0.143
Fort McClellan	0.484	0.180	ND	0.478	0.597	0.089
Massachusetts Military Reservation B	0.386	0.144	ND	0.534	0.563	0.034
Nevada	0.637	0.209	0.067	0.615	0.518	0.081
Aberdeen BA	0.460	0.155	0.056	0.559	0.465	0.035
Aberdeen BT	0.249	0.082	0.026	0.299	0.229	0.017

NC = Not calculable because no Fe was detected in the oxalate extraction.

ND = No Data

Table 37. Parameters of the trilinear model for HMX, RDX, NG, NQ, TNT and 2,4-DNT. Data are for 2 day equilibration for 24 soils. Results for Guadalajara are not included because no oxalate extractable iron was detected.

	K_p Trilinear Model					
	HMX	RDX	NG	TNT	DNT	NQ
K_{OC}	60.183	30.973	29.277	121.934	190.153	8.268
K_{CEC}	28.829	8.090	0.0000	8.522	0.000160	6.370
K_{FeOx}	120 e-4	3.50 e-5	4.36 e-6	1.51 e-5	7.27 e-5	0.000

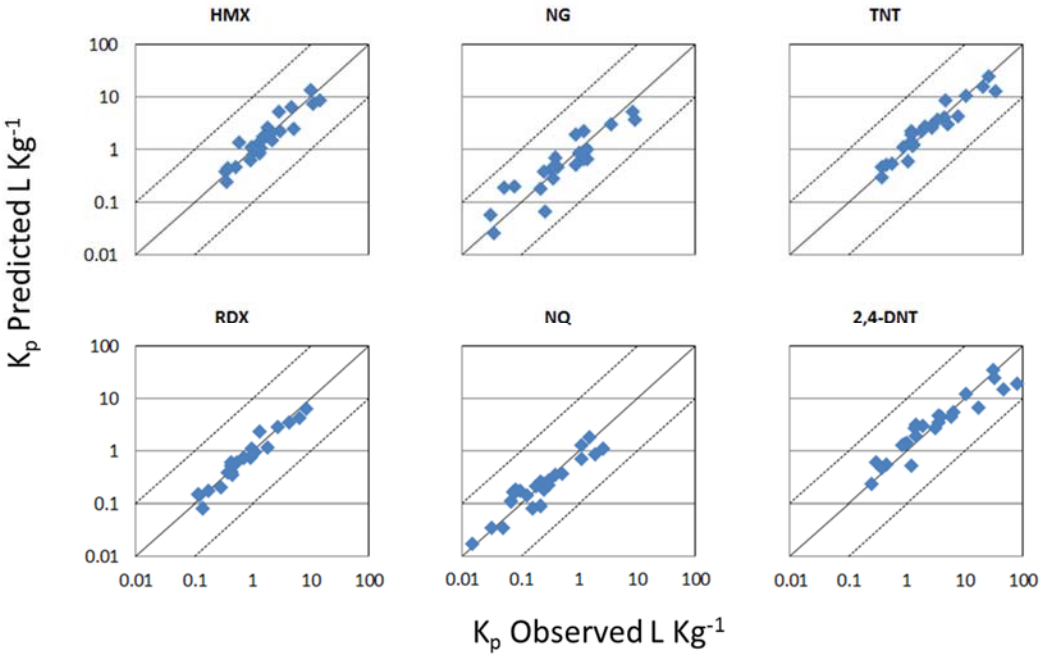

OC+CEC+FeOx $K_{p\,s,m} = K_{OC\,m}\,(f_{OC\,s}) + K_{CEC\,m}\,(CEC_s) + K_{FeOx\,m}\,(C_{FeOx\,s})$

Figure 52. Relationship between K_p calculated with Equation 20 and measured values of K_p for all MC. The solid line represents the 1:1 ratio, and the dashed lines bracket at 1 log unit above and below the 1:1 line. Data are for 2 day equilibration for 24 soils. Results for Guadalajara are not included because no oxalate extractable iron was detected.

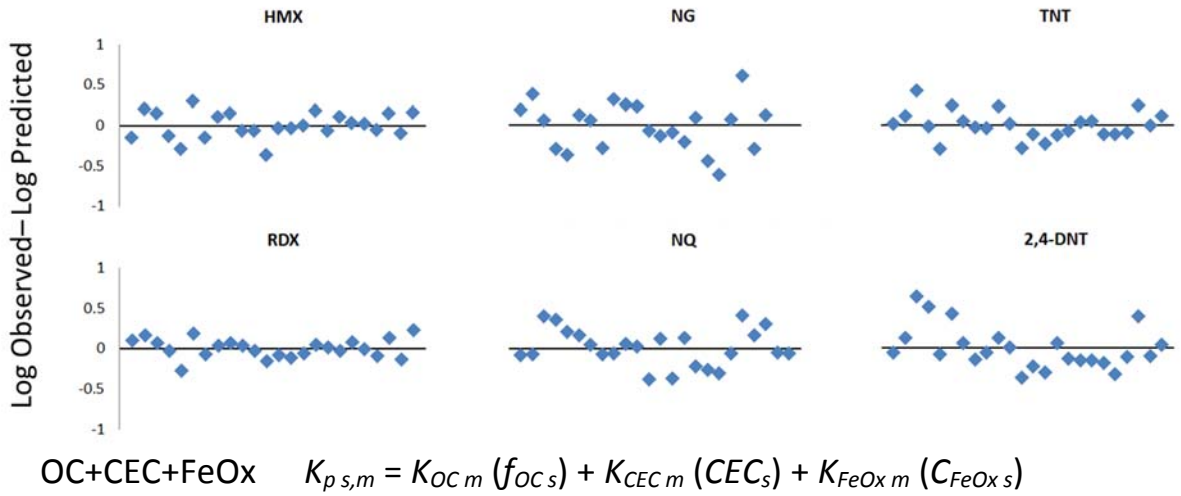

Figure 53. Residuals (Log Observed – Log Predicted) of K_p calculated with Equation 20 and measured values of K_p for all MC. The x-axes is organized in decreasing OC content from 18.23% from the origin to 0.07%. Data are for 2 day equilibration for 24 soils. Results for Guadalajara are not included because no oxalate extractable iron was detected.

Additional information is presented in Figure 54 and Table 38 which show the RSME for the OC model, the OC + CEC model, and the OC + CEC + FeOx model. This figure indicates the improvement of the models when the extractable Fe is added; all chemicals showed that improvement especially the NACs and nitramines. This confirms the influence of Fe on the partition coefficient as reported in the literature. For HMX, the average reduction of the RMSE using the trilinear model in comparison to the CEC model was 21%, for RDX 28%, for NG 13%, for TNT 30%, for DNT 18% and for NQ 2%. In soils with low organic carbon the impact of the addition of the FeOx to OC and CEC in the model was determined. The results in Table 39 show the lowest RSME values are obtained by adding the oxalate extractable Fe component to the OC + CEC model. From this table it can be seen that for HMX, TNT and 2,4-DNT in these low OC soils the lowest RSME values are obtained by adding the extractable Fe component to the model. For the other MC the values are in the second place of fitting. As in previous analyses, NG depends mainly on the OC content of the soil.

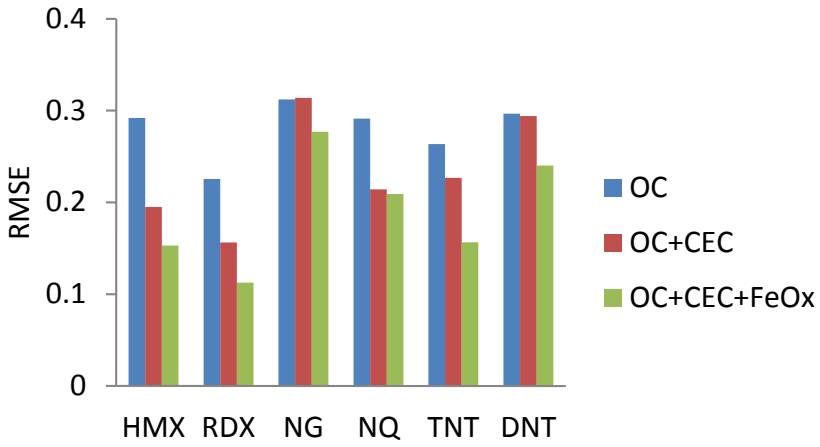

Figure 54. Comparison of the RMSE for K_p obtained by the OC Model, CEC Model, and Trilinear CEC Model. Data are for 2 day equilibration for 25 soils except for the trilinear model which includes only 24 soils. Results for Guadalajara are not included because no oxalate extractable iron was detected.

Table 38. RMSE values obtained by the OC Model, CEC Model, and Trilinear OC + CEC + FeOx Model. Data are for 2 day equilibration for 25 soils except for the trilinear model which includes only 24 soils. Results for Guadalajara are not included because no oxalate extractable iron was detected.

	RMSE					
Model	HMX	RDX	NG	NQ	TNT	2,4-DNT
OC	0.2920	0.2255	0.3123	0.2636	0.2967	0.2913
OC+CEC	0.1965	0.1574	0.3110	0.2273	0.2941	0.2152
OC+CEC+FeOx	0.1784	0.1341	0.2746	0.1649	0.2526	0.2306

Table 39. RMSE obtained by the OC, Clay Size, Charge Sites, CEC and Trilinear OC + CEC + FeOx models for low organic carbon content soils (0.07-0.9%). Data are for 2 day equilibration.

Model	HMX	RDX	NG	NQ	TNT	2,4-DNT
OC	0.3469	0.2854	0.3882	0.2849	0.2308	0.3621
OC+Clay	0.1644	0.1564	0.3586	0.2040	0.2256	0.2333
OC+Cs	0.1060	0.1059	0.3462	0.1377	0.1924	0.2558
OC+CEC	0.1964	0.1746	0.3944	0.2120	0.2193	0.2263
OC+CEC+FeOx	0.1143	0.1094	0.3693	0.1073	0.1958	0.2277

Multilinear Models Applied to the Reversible and Resistant Partition Coefficients K_{px} and K_{p0}. In addition to the application of the multilinear models (OC+Clay, OC+Cs, OC+CEC, OC+CEC+Fe) to the adsorption partition coefficient for the 25 soils for 2 day equilibration, the multilinear model was applied to the reversible K_{px} and the resistant K_{p0} partition coefficients

generated by the reversible/resistant model. The soil properties OC, CEC and extractable Fe were selected to test in the K_{px} and K_{p0} multilinear models as in the K_p models, because they showed an important influence in the adsorption partition coefficient estimation. Equations 21 and 22 show the models tested for K_{px} and K_{p0}:

$$K_{px\,s,m} = K_{OC\,m\,x}\,(f_{oc\,s}) + K_{CEC\,m\,x}\,(CEC_s) + K_{FeOx\,m\,x}\,(C_{FeOx\,s}) \quad (21)$$

$$K_{p0\,s,m} = K_{OC\,m\,0}\,(f_{oc\,s}) + K_{CEC\,m\,0}\,(CEC_s) + K_{FeOx\,m\,0}\,(C_{FeOx\,s}) \quad (22)$$

where $K_{OC\,m\,x}$ = sorption coefficient to organic carbon in the soil for the reversible sites, $K_{OC\,m\,0}$ = sorption coefficient to organic carbon in the soil for the resistant sites, $K_{CEC\,m\,x}$ = sorption coefficient to the CEC in the soil for the reversible sites, $K_{CEC\,m\,0}$ = sorption coefficient to the CEC in the soil for the resistant sites, $K_{FeOx\,m\,x}$ = sorption coefficient to the extractable Fe in the soil for the reversible sites, $K_{FeOx\,m\,0}$ = sorption coefficient to the extractable Fe in the soil for the resistant sites, f_{OC} = fraction of the organic carbon in the soil, CEC = Cation Exchange Capacity in the soil, C_{FeOx} = concentration of oxalate extractable Fe in the soil, s = soil, and m = munitions constituents.

Figures 55 and 56 show the relationship of K_{px} and K_{p0} values calculated by the Trilinear Reversible/Resistant Models with Equations 21 and 22 and the values obtained by the Reversible/Resistant model with Equations 7 and 8 for all MC. The values are given in Table 40. Figures 57 and 58 are residual plots of the difference between the observed data obtained by the Reversible and Resistant Model (Equations 7 and 8) and the predicted values from the Trilinear Model (equations 21 and 22). These figures show that the K_{px} trilinear model fit the values for HMX, RDX, NQ, TNT and 2,4-DNT better than NG, indicating that the addition of CEC and Fe for these MC improves the estimation of this partition coefficient. The contribution of the sum of the terms CEC and FeOx to the reversible partition coefficient, K_{px}, is 50% for HMX, 20% for RDX, 14% for NQ, 20% for TNT, and 10% for 2,4-DNT. For NG these terms provide no contribution to the partition coefficient because sorption of NG mainly depends on OC. For the K_{p0} portion of the model, CEC and FeOx are responsible for 7% of the value for HMX, 12% for RDX, 10% for NG, 68% for NQ, 7% for TNT, and 1% for 2,4-DNT. The effect of CEC and FeOx is greater for K_{px} than it is for K_{p0} for most of the MC (with the exception of NQ).

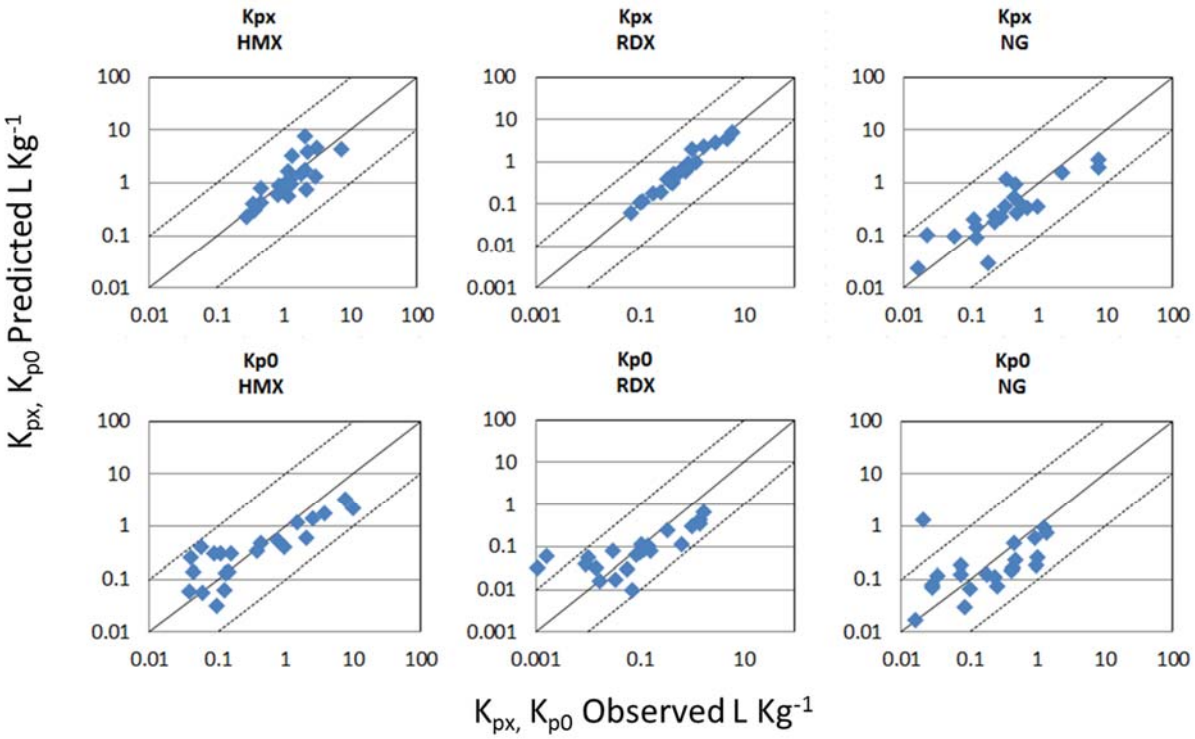

$$K_{px\,s,m} = K_{OC\,m\,x}\,(f_{oc\,s}) + K_{CEC\,m\,x}\,(CEC_s) + K_{FeOx\,m\,x}\,(C_{FeOx\,s})$$

$$K_{p0\,s,m} = K_{OCm\,0}\,(f_{oc\,s}) + K_{CEC\,m\,0}\,(CEC_s) + K_{FeOx\,m\,0}\,(C_{FeOx\,s})$$

Figure 55. Relationship between K_{px} and K_{p0} for HMX, RDX and NG calculated with Equations 21 and 22 and values of K_{px} and K_{p0} from the reversible/resistant model. The solid line represents the 1:1 ratio, and the dashed lines bracket at 1 log unit above and below the 1:1 line. Data are for 2 day equilibration for 24 soils. Results for Guadalajara are not included because no oxalate extractable iron was detected.

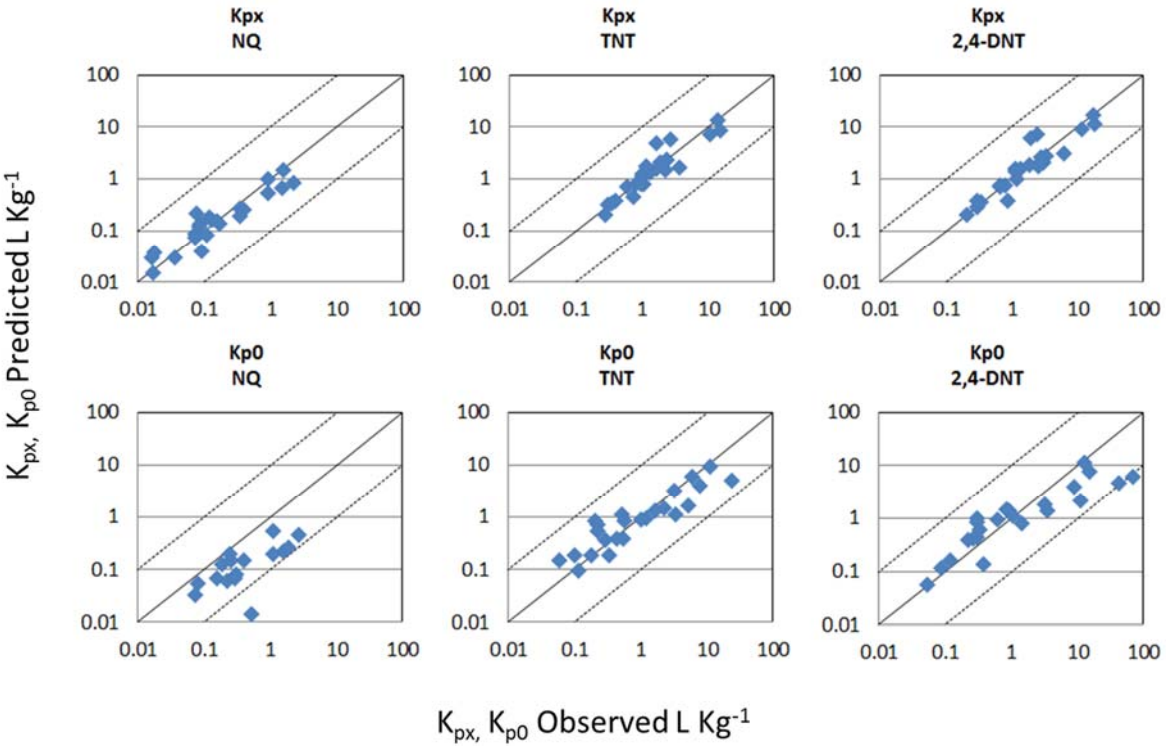

$$K_{px\,s,m} = K_{OC\,m\,x}\,(f_{oc\,s}) + K_{CEC\,m\,x}\,(CEC_s) + K_{FeOx\,m\,x}\,(C_{FeOx\,s})$$

$$K_{p0\,s,m} = K_{OC\,m\,0}\,(f_{oc\,s}) + K_{CEC\,m\,0}\,(CEC_s) + K_{FeOx\,m\,0}\,(C_{FeOx\,s})$$

Figure 56. Relationship between K_{px} and K_{p0} for NQ and TNT calculated with Equations 21 and 22 and values of K_{px} and K_{p0} from the reversible/resistant model. The solid line represents the 1:1 ratio, and the dashed lines bracket at 1 log unit above and below the 1:1 line. Data are for 2 day equilibration for 24 soils. Results for Guadalajara are not included because no oxalate extractable iron was detected.

Table 40. Reversible and resistant partition coefficients K_{px} L kg^{-1} and K_{p0} L kg^{-1} of HMX, RDX, NG, NQ, TNT and 2,4-DNT. Data are for 2 day equilibration for 24 soils. Results for Guadalajara are not included because no oxalate extractable iron was detected.

	K_{px} L kg^{-1} by the Reversible/Resistant Model Equation 7						K_{px} L kg^{-1} by the Trilinear Reversible/Resistant Model Equation 21					
Soil	HMX	RDX	NG	TNT	DNT	NQ	HMX	RDX	NG	TNT	2,4-DNT	NQ
Zegveld	2.136	5.982	7.924	13.759	17.255	1.534	7.807	5.186	2.782	13.324	17.169	1.504
Rhydtalog	3.179	4.942	7.925	14.991	17.952	0.893	4.626	3.489	1.958	8.591	11.324	1.014
Joplin	7.306	2.869	2.218	10.446	11.549	2.208	4.374	2.942	1.544	7.190	9.178	0.833
Lewis Core	2.269	1.739	0.335	2.621	2.384	1.463	3.949	2.341	1.158	5.956	7.401	0.658
Lewis Clean	1.354	1.003	0.458	1.647	1.908	0.886	3.320	1.964	0.970	4.998	6.2060	0.552
Pokomoke	3.056	1.239	0.421	2.345	6.065	0.341	1.321	0.976	0.534	2.339	3.049	0.279
Elliot IE	1.161	0.855	0.521	2.346	3.317	0.380	1.659	0.938	0.436	2.292	2.767	0.255
Guadalajara	NC	NC	NC	NC	NC	NC	NC	NC	NC	NC	NC	NC
Boxtel	1.829	0.873	0.314	1.877	2.695	0.074	1.514	0.767	0.354	2.122	2.569	0.217
Houthalein	2.191	0.751	0.965	2.215	2.936	0.119	0.751	0.599	0.353	1.533	2.064	0.179
Annemessex	1.209	0.830	0.684	3.582	2.682	0.333	1.135	0.707	0.351	1.710	2.127	0.196
Whippany	1.218	0.622	0.476	1.642	2.523	0.126	1.214	0.621	0.267	1.539	1.797	0.166
Sassafras 1	0.468	0.424	0.224	1.019	1.138	0.087	0.813	0.499	0.249	1.236	1.541	0.139
Matapeake	1.233	0.442	0.276	1.296	1.327	0.166	0.967	0.514	0.235	1.325	1.593	0.142
Sassafras 2	0.977	0.419	0.110	1.015	1.116	0.081	0.825	0.447	0.206	1.137	1.370	0.123
Chile Muestra	2.133	0.661	0.219	1.136	1.819	0.152	1.761	0.630	0.183	1.759	1.824	0.159
Sassafras 3	1.184	0.423	0.118	1.037	1.154	0.073	0.562	0.310	0.148	0.812	0.994	0.087
Washington 2	1.266	0.349	0.022	0.788	0.662	0.082	0.969	0.388	0.104	0.815	0.760	0.086
Washington 1	0.866	0.435	0.056	0.939	0.782	0.106	0.904	0.356	0.096	0.780	0.740	0.081
Souli	0.954	0.384	0.119	0.595	0.644	0.072	0.831	0.332	0.093	0.733	0.706	0.076
Fort McClellan	0.457	0.177	0.000	0.307	0.295	0.018	0.427	0.181	ND	0.325	0.281	0.038
Massachusetts Military Reservation B	0.373	0.102	0.000	0.349	0.337	0.016	0.307	0.111	ND	0.339	0.371	0.030
Nevada	0.814	0.253	0.178	0.740	0.872	0.091	0.608	0.192	0.031	0.455	0.382	0.041
Aberdeen BA	0.345	0.115	0.016	0.397	0.295	0.035	0.410	0.119	0.024	0.385	0.383	0.030
Aberdeen BT	0.275	0.069	0.002	0.280	0.202	0.017	0.226	0.061	0.011	0.209	0.206	0.015

NC = Not calculable because no Fe was detected in the oxalate extraction.
ND = No Data

Table 40 (continued). Reversible and resistant partition coefficients K_{px} L kg^{-1} and K_{p0} L kg^{-1} of HMX, RDX, NG, NQ, TNT and 2,4-DNT. Data are for 2 day equilibration for 24 soils. Results for Guadalajara are not included because no oxalate extractable iron was detected.

	K_{p0} L kg by the Reversible/Resistant Model Equation 8						K_{p0} L kg ^{1} by the Trilinear Reversible/Resistant Model Equation 22					
Soil	HMX	RDX	NG	TNT	DNT	NQ	HMX	RDX	NG	TNT	2,4-DNT	NQ
Zegveld	7.696	1.673	0.021	11.182	12.537	0.000	3.329	0.680	1.355	9.249	11.397	ND
Rhydtalog	9.991	1.425	1.223	5.938	14.817	0.221	2.241	0.439	0.950	6.174	7.960	0.327
Joplin	3.828	1.479	1.378	23.417	68.468	0.531	1.800	0.359	0.772	4.979	6.299	0.336
Lewis Core	2.480	1.043	0.935	7.800	42.867	0.465	1.420	0.296	0.586	3.962	4.765	0.298
Lewis Clean	1.521	0.350	0.445	3.171	8.815	0.266	1.190	0.248	0.491	3.322	3.993	0.251
Pokomoke	2.053	0.659	0.999	5.285	11.071	0.195	0.606	0.118	0.264	1.667	2.168	0.101
Elliot IE	0.763	0.109	0.475	2.252	3.200	0.014	0.532	0.111	0.230	1.483	1.794	0.138
Guadalajara	NC	NC	NC	NC	NC	NC	NC	NC	NC	NC	NC	NC
Boxtel	0.431	0.141	0.074	1.628	0.838	0.147	0.475	0.106	0.178	1.347	1.481	0.106
Houthalein	0.058	0.159	0.438	0.510	0.925	0.067	0.407	0.080	0.166	1.123	1.435	0.045
Annemessex	0.962	0.122	0.962	3.276	3.435	0.060	0.415	0.084	0.180	1.150	1.435	0.092
Whippany	0.385	0.101	0.424	1.184	1.068	0.127	0.340	0.073	0.145	0.954	1.106	0.102
Sassafras 1	0.111	0.002	0.179	0.199	0.301	0.000	0.298	0.061	0.127	0.830	1.020	ND
Matapeake	0.159	0.087	0.075	0.556	0.610	0.082	0.300	0.065	0.122	0.844	0.974	0.075
Sassafras 2	0.041	0.010	0.238	0.222	0.296	0.000	0.260	0.056	0.107	0.729	0.852	ND
Chile Muestra	0.090	0.030	0.034	0.994	1.432	0.147	0.313	0.081	0.115	0.916	0.806	0.145
Sassafras 3	0.000	0.009	0.254	0.223	0.325	0.000		0.040	0.075	0.528	0.613	ND
Washington 2	0.045	0.014	0.029	0.527	0.295	0.000	0.140	0.032	0.078	0.398	0.435	ND
Washington 1	0.142	0.001	0.028	0.435	0.259	0.000	0.135	0.031	0.071	0.384	0.406	ND
Souli	0.132	0.057	0.102	0.285	0.221	0.053	0.129	0.030	0.067	0.368	0.392	0.085
Fort McClellan	0.059	0.000	0.000	0.058	0.003	0.198	0.055	ND	ND	0.153	0.193	0.051
Massachusetts Military Reservation B	0.000	0.017	0.001	0.097	0.117	0.034	ND	0.017	0.021	0.186	0.162	0.022
Nevada	0.124	0.034	0.085	0.334	0.382	0.068	0.063	0.018	0.031	0.187	0.141	0.060
Aberdeen BA	0.038	0.000	0.016	0.179	0.087	0.000	0.060	ND	0.017	0.184	0.119	ND
Aberdeen BT	0.096	0.071	0.035	0.114	0.052	0.000	0.032	0.010	0.008	0.097	0.055	ND

NC = Not calculable because no Fe was detected in the oxalate extraction.
ND = No Data

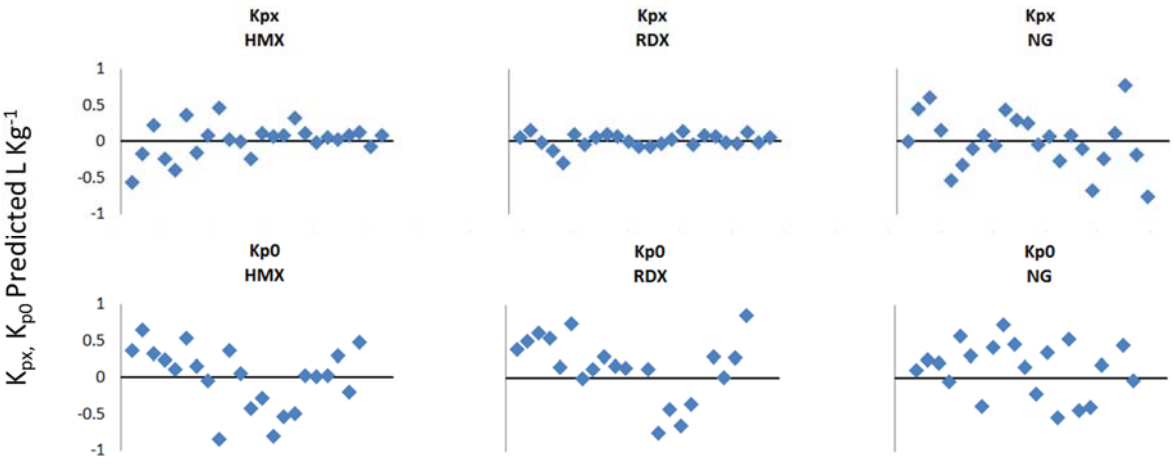

$$K_{px\,s,m} = K_{OC\,m\,x}\,(f_{oc\,s}) + K_{CEC\,m\,x}\,(CEC_s) + K_{FeOx\,m\,x}\,(C_{FeOx\,s})$$
$$K_{p0\,s,m} = K_{OC\,m\,0}\,(f_{oc\,s}) + K_{CEC\,m\,0}\,(CEC_s) + K_{FeOx\,m\,0}\,(C_{FeOx\,s})$$

Figure 57. Residuals (Log Observed – Log Predicted) of K_{px} and K_{p0} for HMX, RDX and NG calculated with the Trilinear Reversible/Resistant Model in Equations 21 and 22 and values of K_{px} and K_{p0} from the Reversible/Resistant Model in Equations 7 and 8. The x-axes is organized in decreasing OC content from 18.23% from the origin to 0.07%. Data are for 2 day equilibration for 24 soils. Results for Guadalajara are not included because no oxalate extractable iron was detected.

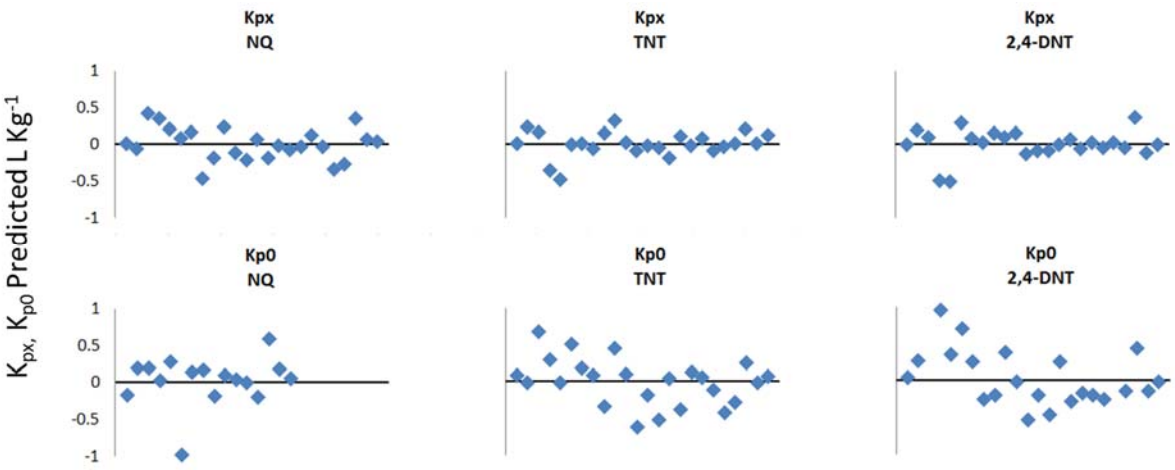

$$K_{px\,s,m} = K_{OC\,m\,x}\,(f_{oc\,s}) + K_{CEC\,m\,x}\,(CEC_s) + K_{FeOx\,m\,x}\,(C_{FeOx\,s})$$
$$K_{p0\,s,m} = K_{OC\,m\,0}\,(f_{oc\,s}) + K_{CEC\,m\,0}\,(CEC_s) + K_{FeOx\,m\,0}\,(C_{FeOx\,s})$$

Figure 58. Residuals (Log Observed – Log Predicted) of K_{px} and K_{p0} for NQ, TNT and 2,4-DNT calculated with the Trilinear Reversible/Resistant Model in Equations 21 and 22 and values of K_{px} and K_{p0} from the Reversible/Resistant Model in Equations 7 and 8. The x-axes is organized in decreasing OC content from 18.23% from the origin to 0.07%. Data are for 2 day equilibration for 24 soils. Results for Guadalajara are not included because no oxalate extractable iron was detected.

These results suggested examination of the RMSE values for the estimation of K_{px} and K_{p0} with contributions of OC, clay size, charge sites, CEC and FeOx to the model. Figure 59 and Table 41 show the RMSE values for the reversible and resistant partition coefficients for each MC. The models fit the K_{px} and K_{p0} coefficients very well as indicated by the low RMSE values. The RMSE values for K_{px} are lower than are those for K_{p0}. This provides evidence that the K_{px} partition coefficient for the reversible component from the reversible/resistant model, depends on the soil properties including organic carbon and the properties that account for the charge sites, e.g. CEC, as well as oxalate extractable Fe. For the reversible component in Figure 59 the CEC Trilinear Model which includes OC, CEC and extractable Fe provides very good fittings for HMX, RDX, NQ, TNT and 2,4-DNT. Although the RMSE values for the Trilinear Model for NG are good, the figure clearly shows that the reversible component is mainly dependent on OC because there is no variation in the RMSE values among the models. K_{p0} relates the concentration of the MC that remains on the particle at zero dissolved concentration and the concentration at the adsorption point. Figure 59 shows that the addition of the other soil properties investigated, other than OC in the K_{p0} models, does not markedly affect the RMSE values. For that reason the origin of those resistant sites may be from OC rather than the other soil properties studied. However, the value of K_{p0} that represents the resistant fraction of the soil may be affected by the type of the material comprising the organic fraction of the soil. Pignatello [2000] proposed that the soil organic matter has a composition of rubbery and glassy polymers, where the rubbery material has an expanded, flexible, and highly solvated structure and the glassy materials are condensed, rigid and less solvated structures. It is possible that K_{p0} can be

related to the glassy polymer because the resistant sites are more rigid than are the reversible ones. Singh et al. [2010] mentioned that it is not the total carbon content of the organic matter, but its chemical structure that has a profound effect on the sorption of organic contaminants. Their study indicated that aliphatic compounds in the soil organic matter significantly affected the non-specific sorption of TNT and 2,4-DNT. These mechanisms of binding associated with the chemical composition of organic carbon on the sorption of MC should be studied to determine their influence on K_{p0}.

Table 42 shows the parameters of the Trilinear Model of K_{px} and K_{p0} for the MC confirming the previous comments about the greater dependency of K_{px}, compared to K_{p0}, on the soil properties including organic carbon, CEC, and oxalate extractable Fe.

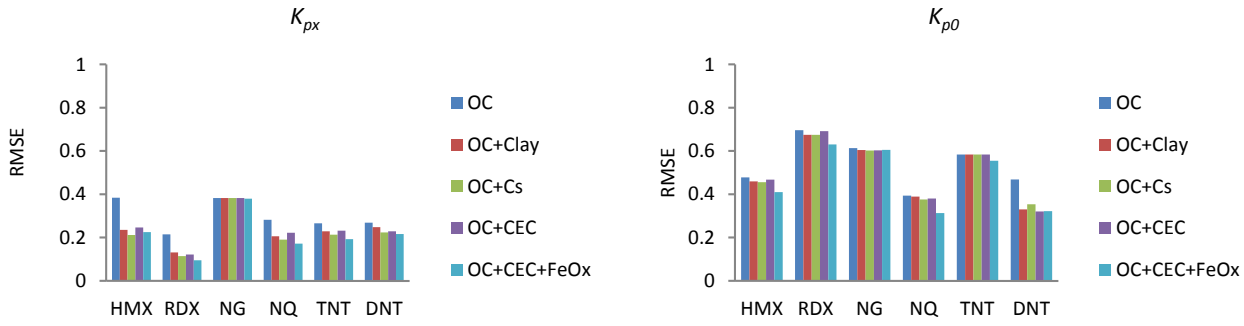

Figure 59. Comparison of the RMSE of the reversible and resistant partition coefficients K_{px} and K_{p0} for all MC obtained by the OC, OC+Clay, OC+Cs, OC+CEC and OC+CEC+FeOx models and K_{px} and K_{p0} obtained by the reversible and resistant model. Data are for 2 day equilibration for 25 soils except for the trilinear model that includes only 24 soils**.** Results for Guadalajara are not included for the trilinear model because no oxalate extractable iron was detected.

Table 41. RMSE values of the reversible and resistant partition coefficients K_{px} and K_{p0} for all MC of OC, Clay Sites, Charge Sites, CEC, and Trilinear FeOx Models. Data are for 2 day equilibration for 25 soils except for the trilinear model that includes only 24 soils**.** Results for Guadalajara are not included for the trilinear model because no oxalate extractable iron was detected.

	K_{px}					
Model	HMX	RDX	NG	NQ	TNT	2,4-DNT
OC	0.3841	0.2145	0.3825	0.2820	0.2660	0.2686
OC+Clay	0.2352	0.1315	0.3825	0.2060	0.2287	0.2482
OC+Cs	0.2119	0.1143	0.3825	0.1901	0.2132	0.2233
OC+CEC	0.2467	0.1219	0.3825	0.2220	0.2319	0.2290
OC+CEC+FeOx	0.2250	0.0948	0.3799	0.1719	0.1927	0.2160
	K_{p0}					
Model	HMX	RDX	NG	NQ	TNT	2.4-DNT
OC	0.4779	0.6955	0.6134	0.3934	0.5837	0.4680
OC+Clay	0.4592	0.6747	0.6043	0.3889	0.5837	0.3299
OC+Cs	0.4560	0.6748	0.6023	0.3757	0.5837	0.3539
OC+CEC	0.4672	0.6918	0.6030	0.3803	0.5837	0.3204
OC+CEC+FeOx	0.4101	0.6300	0.6049	0.3128	0.5544	0.3220

Table 42. K_{px} and K_{p0} parameters of the Trilinear Model, Equations 21 and 22, for HMX, RDX, NG, NQ, TNT and 2,4-DNT. Data are for 2 day equilibration for 24 soils**.** Results for Guadalajara are not included because no oxalate extractable iron was detected.

	HMX	RDX	NG	NQ	TNT	2,4-DNT
K_{px} Trilinear Model						
K_{OC}	26.207	24.311	15.258	7.470	62.608	86.951
K_{CEC}	33.775	10.527	0	1.456	12.091	0.000162
K_{FeOx}	1.14e-4	1.98e-5	0	5.86e-6	1.10e-4	1.10e-4
K_{p0} Trilinear Model						
K_{OC}	17.287	3.356	6.985	1.316	47.540	61.940
K_{CEC}	0	0	1.658	4.636	0	0.000162
K_{FeOx}	1.48e-5	5.71e-6	0	5.92e-6	4.87e-5	8.14e-6

Finally, to better understand the relationship between K_p and its components K_{px} and K_{p0} among the soil properties, a set of residual plots related with soil properties studied in the multilinear models was prepared as Figures 60 – 63. These figures show the residuals (Log Observed – Log Predicted) of K_p, K_{px}, and K_{p0} for the Trilinear Model and the log of the f_{OC}, f_{clay}, CEC, and oxalate extractable iron values for all MC. The figures show there are large residuals exceeding

one log unit only for a few instances. These are for NG, RDX, and 2,4-DNT. However, the soils for which these large residuals occurred are not the same for the different munitions. Therefore, they seem to be random and not caused by a particular soil property. If the samples with these very large residuals are ignored, the distribution of residual values is random for NG, RDX, and NQ with respect to f_{OC} in Figure 60. The residual values increase with increasing f_{OC} for HMX, TNT, and 2,4-DNT. The values of the parameters f_{clay}, CEC, and oxalate extractable iron are unrelated to the residual error as shown in Figures 61, 62, and 63 with a single exception. The residual error for 2,4-DNT increases with increasing CEC as shown in Figure 61.

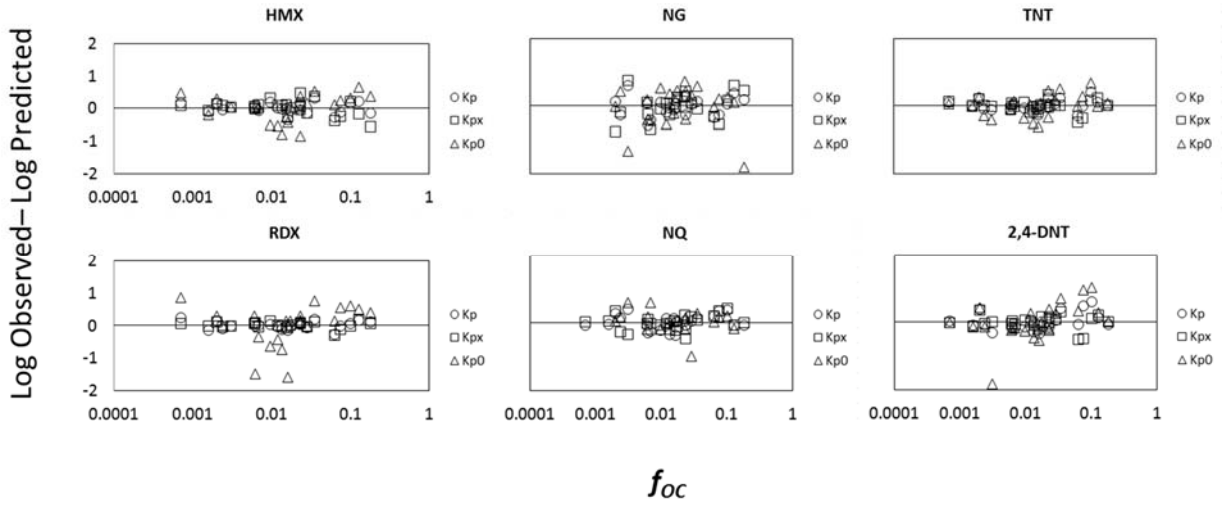

$$K_{p\,s,m} = K_{OC\,m}\,(f_{oc\,s}) + K_{CEC\,m}\,(CEC_s) + K_{FeOx\,m}\,(C_{FeOx\,s})$$
$$K_{px\,s,m} = K_{OC\,m\,x}\,(f_{oc\,s}) + K_{CEC\,m\,x}\,(CEC_s) + K_{FeOx\,m\,x}\,(C_{FeOx\,s})$$
$$K_{p0\,s,m} = K_{OC\,m\,0}\,(f_{oc\,s}) + K_{CEC\,m\,0}\,(CEC_s) + K_{FeOx\,m\,0}\,(C_{FeOx\,s})$$

Figure 60. Residuals (Log Observed – Log Predicted) of K_p, K_{px}, and K_{p0} calculated with Equation 20 and values observed for K_p and those obtained from the Reversible/ Resistant Model (Equations 21 and 22) for K_{px} and K_{p0} related to f_{OC} values. Data are for 2 day equilibration for 24 soils**.** Results for Guadalajara are not included because no oxalate extractable iron was detected.

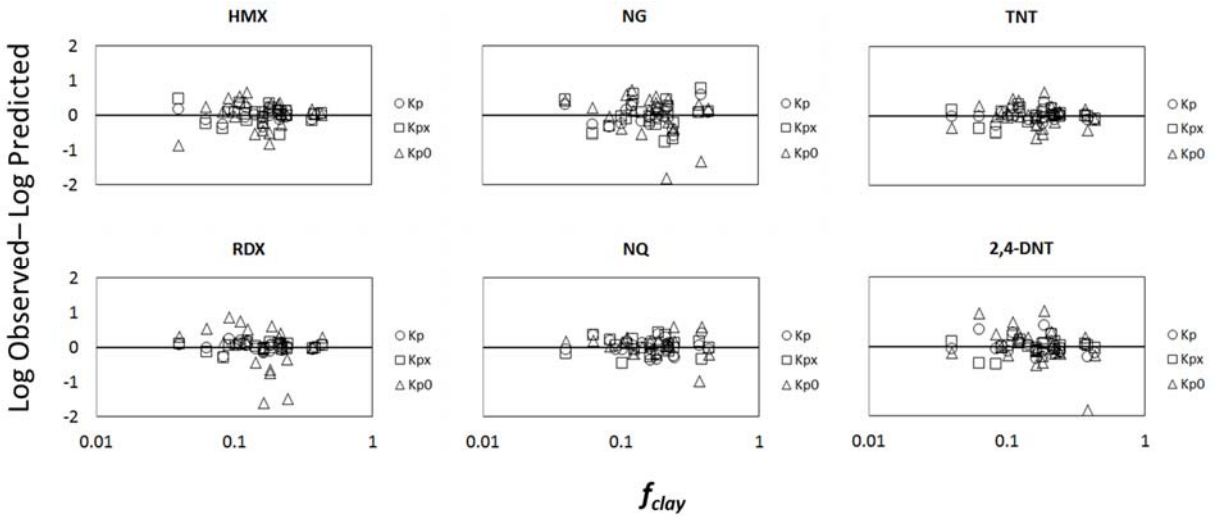

$$K_{p\,s,m} = K_{OC\,m}\,(f_{oc\,s}) + K_{CEC\,m}\,(CEC_s) + K_{FeOx\,m}\,(C_{FeOx\,s})$$

$$K_{px\,s,m} = K_{OC\,m\,x}\,(f_{oc\,s}) + K_{CEC\,m\,x}\,(CEC_s) + K_{FeOx\,m\,x}\,(C_{FeOx\,s})$$

$$K_{p0\,s,m} = K_{OC\,m\,0}\,(f_{oc\,s}) + K_{CEC\,m\,0}\,(CEC_s) + K_{FeOx\,m\,0}\,(C_{FeOx\,s})$$

Figure 61. Residuals (Log Observed – Log Predicted) of K_p, K_{px}, and K_{p0} calculated with Equation 20 and values observed for K_p and those obtained from the Reversible/ Resistant Model (Equations 21 and 22) for K_{px} and K_{p0} related to f_{clay} values. Data are for 2 day equilibration for 24 soils**.** Results for Guadalajara are not included because no oxalate extractable iron was detected.

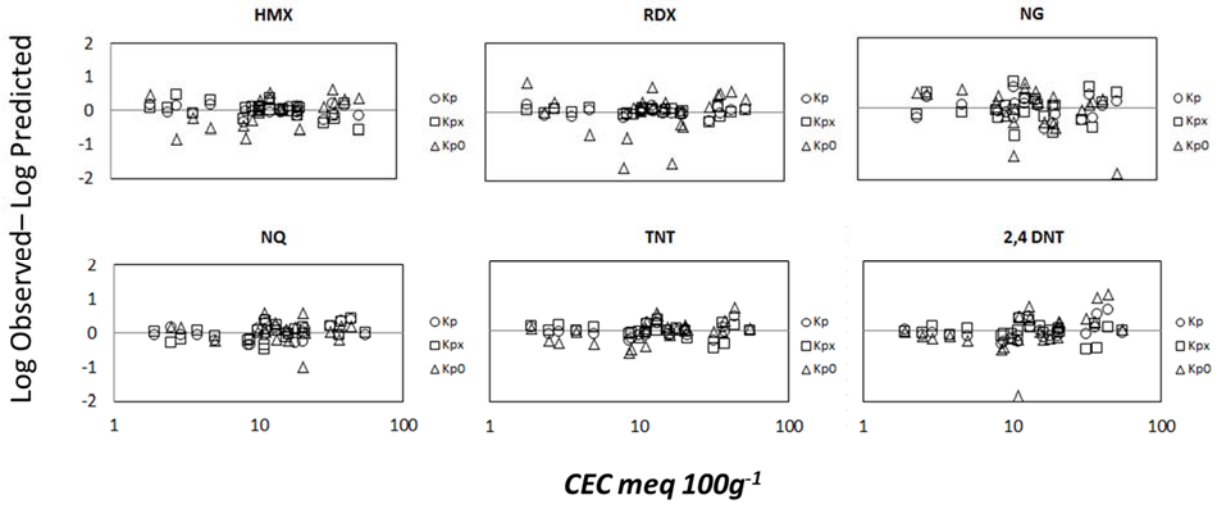

$$K_{p\,s,m} = K_{OC\,m}\,(f_{oc\,s}) + K_{CEC\,m}\,(CEC_s) + K_{FeOx\,m}\,(C_{FeOx\,s})$$

$$K_{px\,s,m} = K_{OC\,m\,x}\,(f_{oc\,s}) + K_{CEC\,m\,x}\,(CEC_s) + K_{FeOx\,m\,x}\,(C_{FeOx\,s})$$

$$K_{p0\,s,m} = K_{OC\,m\,0}\,(f_{oc\,s}) + K_{CEC\,m\,0}\,(CEC_s) + K_{FeOx\,m\,0}\,(C_{FeOx\,s})$$

Figure 62. Residuals (Log Observed – Log Predicted) of K_p, K_{px}, and K_{p0} calculated with Equation 20 and values observed for K_p and those obtained from the Reversible/ Resistant Model (Equations 21 and 22) for K_{px} and K_{p0} related to CEC values. Data are for 2 day equilibration for 24 soils**.** Results for Guadalajara are not included because no oxalate extractable iron was detected.

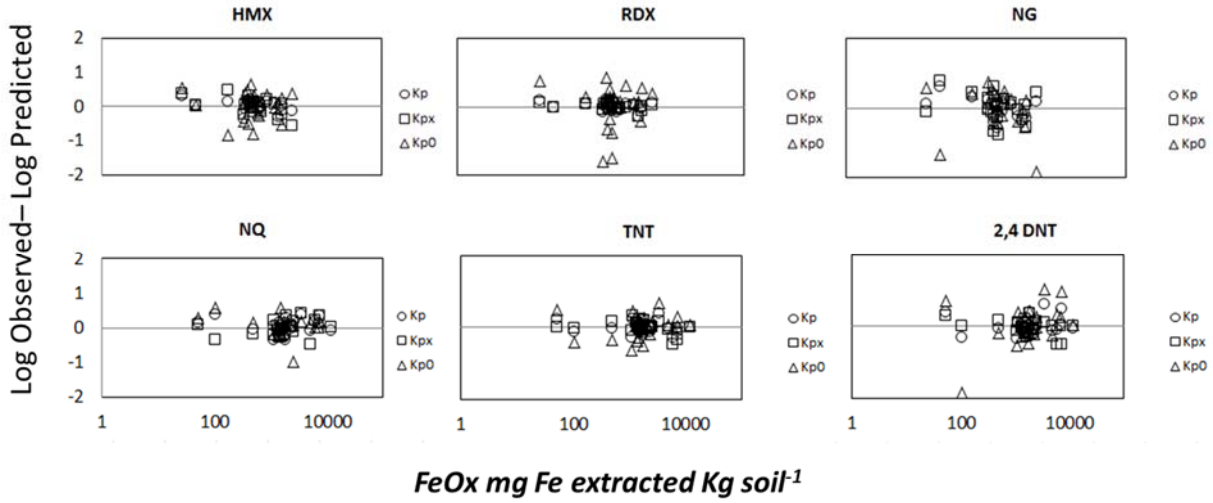

$$K_{p\,s,m} = K_{OC\,m}\,(f_{oc\,s}) + K_{CEC\,m}\,(CEC_s) + K_{FeOx\,m}\,(C_{FeOx\,s})$$
$$K_{px\,s,m} = K_{OC\,m\,x}\,(f_{oc\,s}) + K_{CEC\,m\,x}\,(CEC_s) + K_{FeOx\,m\,x}\,(C_{FeOx\,s})$$
$$K_{p0\,s,m} = K_{OC\,m\,0}\,(f_{oc\,s}) + K_{CEC\,m\,0}\,(CEC_s) + K_{FeOx\,m\,0}\,(C_{FeOx\,s})$$

Figure 63. Residuals (Log Observed – Log Predicted) of K_p, K_{px}, and K_{p0} calculated with Equation 20 and values observed for K_p and those obtained from the Reversible/ Resistant Model (Equations 21 and 22) for K_{px} and K_{p0} related to oxalate extractable Fe concentrations. Data are for 2 day equilibration for 24 soils**.** Results for Guadalajara are not included because no oxalate extractable iron was detected.

Conclusions regarding multilinear models. Modification of the clay size multilinear model by the use of sorption charge sites component determined by Cs exchange, in addition to the fraction organic carbon in the analysis of the adsorption of MC, provided some improvement on the estimation of the partition coefficient K_p for adsorption of MC in soils with a wide range of properties. However, because there are many steps required in the determination of the concentration of Cs exchange sites, its use is not warranted given the degree of improvement in parameter estimation achieved.

The multilinear model was tested using CEC as an alternative to the use of the clay size fraction and with the incorporation of the concentration of oxalate extractable Fe. The results showed that the CEC model produces results that are comparable to those for the clay size model, permitting use of CEC rather than clay size. The linear relationship between CEC and charge sites determined by Cs exchange supports the use of the CEC in the multilinear model for partitioning of MC to soil.

In addition to the multilinear models that considered two components for the sorption, a trilinear model including OC, oxalate extractable Fe and CEC was developed. This model provided good evidence that the use of CEC and extractable Fe, in addition to OC, is useful to predict partition coefficients for partitioning of MC in soils. The inclusion of the oxalate extractable Fe will not normally be required for surface soils, but is likely to be necessary for prediction of partitioning to aquifer sands given their very low concentrations of organic matter.

An important conclusion was that the reversible and resistant partition coefficients K_{px} and K_{p0} can be estimated by the multilinear models. The results indicated that the reversible coefficient K_{px} depends on the soil properties and it can be obtained by the trilinear model which includes OC, CEC and extractable Fe especially for soils with low organic carbon content. On the other hand, K_{p0} showed more dependency on OC. Mechanisms of binding associated with the chemical composition of organic carbon on the sorption of MC should be studied in relation to K_{p0}.

Normalization and Reversible/ Resistant Modeling of 5 MC onto 25 Soils at 4 Durations of Adsorption. The results for the partitioning of all MC except for NQ for all four equilibration durations were further analyzed. Samples for which the sorbent matrix material interfered with quantification of MC peaks were excluded. In addition, sequences that contained incomplete or missing samples precluding the calculation of a mass balance were removed from further analysis. Further, for several soils, the 2 and 720 h sorptions were not run due to time constraints.

Degradation was observed despite the presence of sodium azide, NaN_3, to inhibit biota. This degradation could have been abiotic [Comfort et al. 1995]. As a screening criteria, if the mass loss exceeded 20% of the initial mass the data were excluded from further analysis. The mass recovered from the two hour data set was used as the initial total mass since degradation would have been minimal in this set. If two hour data were unavailable, the two day (48 h) data were used as initial mass. After these criteria was applied, the remaining data, comprising 6,640 observations, were used in the modeling.

Modeling adsorption partitioning. Data were composed of an adsorption followed by 4 sequential desorptions. Due to observed hysteresis, separate analyses of the adsorption and desorption behavior were conducted. Linear isotherms were used to relate the sorbed concentration, q, to the aqueous concentration, C, using the partition coefficient, K_P:

$$q = K_P C \tag{23}$$

During adsorption the MC partitions between the bulk aqueous (dissolved phase) and the bulk particulate (sorbed phase). The fractionation of the MC into the phases is quantified by the fraction dissolved, f_d, and fraction particulate, f_p, parameters:

$$C_d = f_d C_{tot} \tag{24}$$

$$C_p = f_p C_{tot} \tag{25}$$

where C_p is the particulate bound concentration, and C_{tot} is the total concentration.

The fractions of the MC in each phase is related to the partition coefficient by the following equations [Schwarzenbach et al. 2002]:

$$f_d = \frac{1}{1+mK_p} \tag{26}$$

$$f_p = \frac{mK_p}{1+mK_p} = 1 - f_d \tag{27}$$

where f_d is the fraction dissolved (unitless), f_p is the fraction particulate (unitless), K_p is the partition coefficient, L water (kg soil)$^{-1}$, and m is the soil-water ratio, L water (kg soil)$^{-1}$.

Using this sorption model, the sequence of observed aqueous concentrations can be modeled as follows. At adsorption (step 0), the aqueous concentration is the fraction dissolved multiplied by the initial total concentration, $C_{tot}(0)$:

$$C_d(0) = f_d C_{tot}(0) \quad (28)$$

In the experiment under analysis, the aqueous portion was then removed and analyzed to determine $C_d(0)$. The aqueous phase was then replaced with clean liquid, allowing for desorption from the particulate phase. The total concentration for the first desorption, step 1, is the fraction particulate of the total concentration for the adsorption step:

$$C_{tot}(1) = f_p C_{tot}(0) \quad (29)$$

The corresponding dissolved concentration that results is given by

$$C_d(1) = f_d C_{tot}(1) \quad (30)$$

which can be expressed as

$$= f_d f_p C_{tot}(0) \quad (31)$$

and using Equation 27 yields

$$= f_d(1 - f_d) C_{tot}(0) \quad (32)$$

Following this sequence, for k desorption steps, the dissolved concentration is

$$C_d(k) = f_d(1 - f_d)^k C_{tot}(0) \quad (33)$$

Therefore, for a reversible adsorption-desorption model, the sequence of dissolved concentrations depends on two parameters, the fraction dissolved, f_d, and the initial concentration, $C_{tot}(0)$.

In order to account for the loss due to degradation the total mass recovered was used to estimate $C_{tot}(0)$. The total mass recovered is the sum of the adsorption and desorption concentrations multiplied by the respective volume of the aqueous phase and the total extracted mass:

$$C_{tot}(0)V(0) = \sum_{k=0}^{n} C_d(k)V(k) + M_{ext} \quad (34)$$

where $V(k)$ is the volume of the phase, *L,* at step k, and M_{ext} is the total mass recovered from extraction, *mg.*

Since Equation 33 is linear with respect to $C_{tot}(0)$, the aqueous concentration can be normalized allowing for a simultaneous analysis of all data sets in Table 25 that have different initial concentrations. This is accomplished by dividing the observed concentration by the the initial concentration:

$$C_d^N(k) = \frac{C_d(k)}{C_{tot}(0)} \quad (35)$$

where the normalized concentration is denoted by the superscript N. Substituting Equation 33 into Equation 35 yields

$$C_d^N(k) = f_d(1 - f_d)^k \quad (36)$$

Equation 36 is the reversible model used to analyzed the adsorption and sequential desorption aqueous concentration data. The normalized sorbed concentration is given by

$$q_T^N(k) = \frac{1}{m}(1 - f_d)^{(k+1)} \quad (37)$$

The reversible partitioning model, Equation 36, was fit to only the adsorption data to derive an adsorption partition coefficient. Fitting was performed by minimizing the root mean square

errors (RMSE) between normalized observed (Obs) and modeled (Mod) aqueous concentrations:

$$RMSE = \sqrt{\frac{1}{n}\sum_{i=1}^{n}\left(log_{10}C^{N}_{d,Obs,i}(k) - log_{10}C^{N}_{d,Mod,i}(k)\right)^{2}} \quad (38)$$

where n is the number of adsorption concentrations and $k = 0$ to restrict the fitting to adsorption data only. The partition coefficients were estimated for each sorbent, munition, and adsorption contact time set using R statistical software and the *nls* package [R Core Team 2014].

Modeling desorption partitioning.

Reversible model. Desorption concentrations were predicted using the reversible model, Equation 36, and the estimated adsorption partition coefficients. Adsorption partition coefficients were used since the reversible model treats adsorption and desorption identically. The reversible model predicts that the aqueous concentrations should exhibit linear behavior when plotted on a log-linear scale. This is demonstrated by taking the log of both sides of Equation 36:

$$log_{10}C^{N}_{d}(k) = log_{10}(f_d(1-f_d)^{k}) \quad (39)$$

and separating terms on the right hand side

$$log_{10}C^{N}_{d}(k) = log_{10}f_d + log_{10}(1-f_d)^{k} \quad (40)$$

which yields

$$log_{10}C^{N}_{d}(k) = log_{10}f_d + (k)log_{10}(1-f_d) \quad (41)$$

Equation 41 is linear in k with slope $log_{10}(1-f_d)$ and intercept $log_{10}f_d$.

The results are shown in Figure 64 which compares the predicted and observed normalized aqueous concentrations for two soils (the full set of comparisons is shown in Appendix J.1.3). Normalized concentrations are shown versus the experimental step: adsorption, desorption 1, desorption 2, desorption 3 and desorption 4 (A, 1, 2, 3, 4 respectively). From the plot it is evident that the model systematically over predicts desorption. This is most evident in the 720 h data for DNT where the model overpredicts the aqueous concentration by an order of magnitude. In addition, the discrepancy between observed and predicted aqueous concentrations increases as the adsorption contact time increases. This over prediction is due the reversible model allowing too much chemical to desorb. As a result, the degree to which the model overpredicts the aqueous concentration is an indication of the extent of hysteresis.

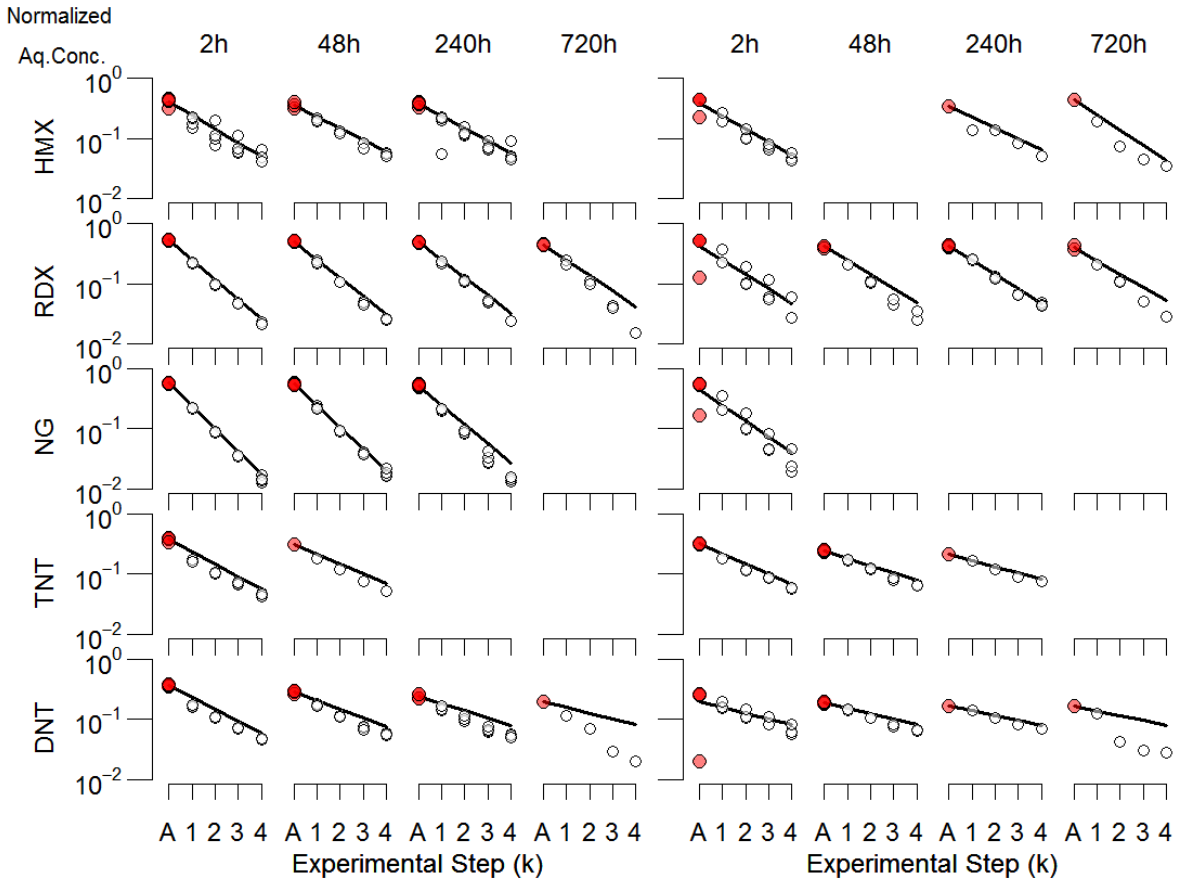

Figure 64. Comparison of reversible model (lines) with observed data (points) for Matapeake (left) and Houthalein (right) soils. Concentrations are normalized to the initial concentration $\left[\frac{mg/L}{mg/L}\right]$. Filled circles indicate adsorption concentrations. Hollow circles indicate desorption concentrations. 2h, 48h, 240h, and 720h refer to the duration of the adsorption contact time. A, 1, 2, 3, 4 refer to the adsorption and the four desorption steps ($k = 0,1,2,3,4$ in Equation 36).

To better understand the shortcomings of the reversible model, RMSE were calculated for each sorbent and each munition using Equation 38 (Figure 65A). The RMSE for all MC are < 0.2 for the majority of low f_{OC} sorbents ($f_{OC} < 0.02$), but there was a significant increase in RMSE for higher f_{OC} sorbents. This increase is especially evident for NG, TNT and DNT munitions. In addition, RMSE were determined for each adsorption contact time and each munition, Figure 65B. There appears to be an increase in RMSE as adsorption time increases. To more accurately describe the observed partitioning, the data are analyzed next using the reversible/resistant model.

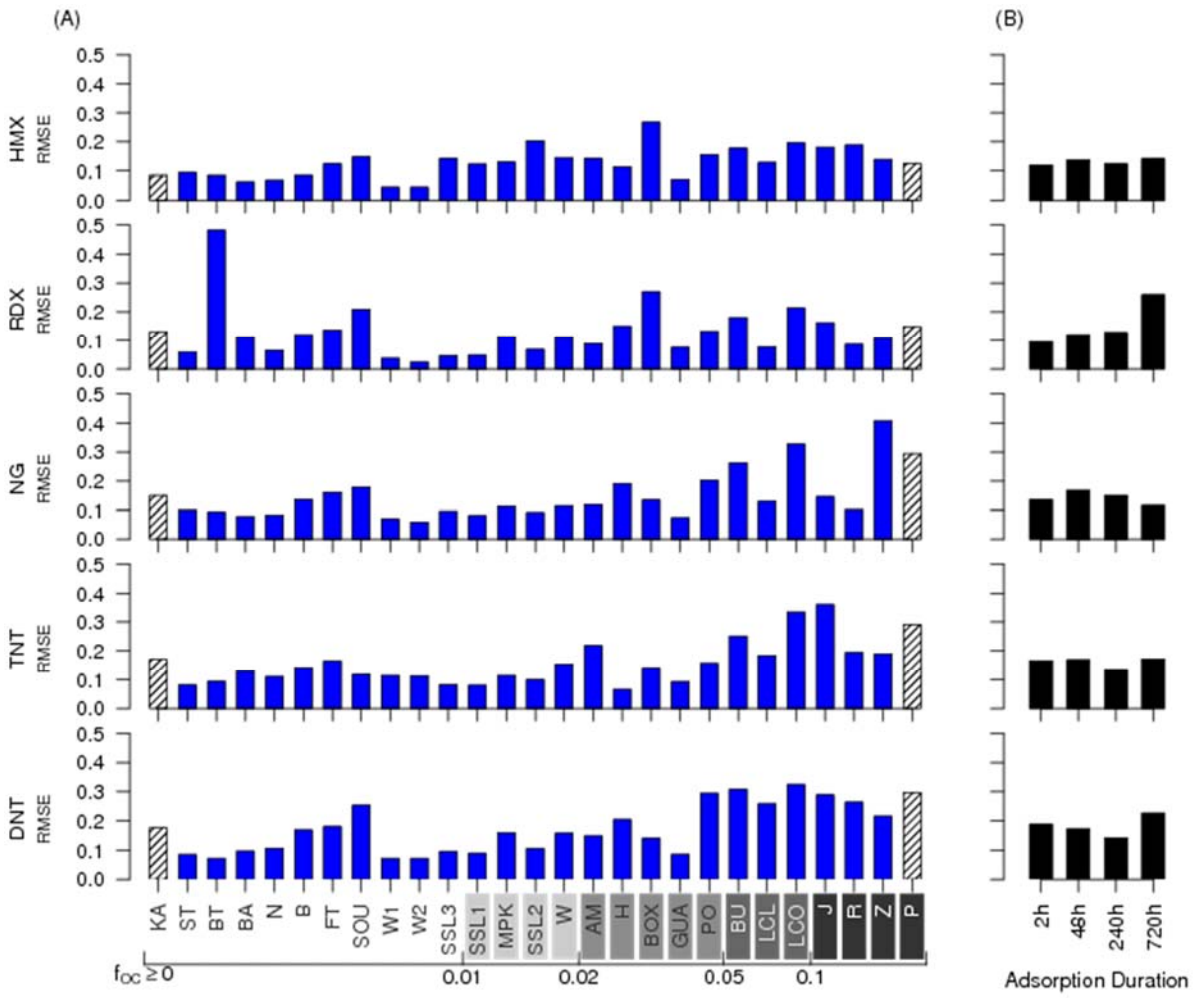

Figure 65. RMSE, Equation 38, for the reversible partitioning model aqueous concentrations, C_{aq}^{N}. (A) RMSE determined for each soil and reference sorbent. Abbreviations are defined in Appendix A Shading indicates increasing f_{OC}. Filled bars indicate soils, hashed bars indicate reference sorbents. (B) RMSE determined for each adsorption contact time.

Reversible/resistant model. To model hysteretic sorption, the reversible/resistant (RR) model is used [Di Toro and Horzempa 1982]. This model has previously been used to explain hysteretic sorption of PCBs and other chemicals [Di Toro 1985]. The RR model uses linear partition coefficients to describe the total sorbed concentration, q_T (g kg^{-1}) as the sum of the reversibly bound, q_x, and the resistantly bound, q_0, concentrations. Each of these components is defined by a partition coefficient, K_{px} (L kg^{-1}) and K_{p0} (L kg^{-1}) respectively.

At adsorption, the component sorbed concentrations are equal to the aqueous concentrations multiplied by the respective partition coefficient, Equations 42 and 43.

$$q_{x,Ads} = K_{px} C_{d,Ads} \tag{42}$$

$$q_{0,Ads} = K_{\mathrm{p0}} C_{d,Ads} \tag{43}$$

where $C_{d,Ads}$ is the aqueous concentration, mg/L, $q_{x,Ads}$ is the reversibly sorbed concentration,

mg g^{-1}, and $q_{0,Ads}$ is the resistant sorbed concentration, mg g^{-1}. The total sorbed concentration, q_T, g kg^{-1}, is the sum of these two components:

$$q_{T,Ads} = K_{px}C_{d,Ads} + K_{\mathrm{p0}}C_{Ads} \tag{44}$$

This equation can be rewritten as the sum of the reversible and resistant partition coefficients times the aqueous concentration,

$$q_{T,Ads} = \left(K_{px} + K_{\mathrm{p0}}\right)C_{d,Ads} \tag{45}$$

By defining the adsorption partition coefficient, K_P, L kg^{-1}, as the sum of K_{px} and K_{p0}, the adsorption isotherm is derived:

$$q_{T,Ads} = K_P C_{d,Ads} \tag{46}$$

The adsorption isotherm is defined by slope K_P and the intercept is at the origin.

During subsequent desorptions, however, the resistantly bound portion remains fixed at $q_{0,Ads}$ determined at the adsorption concentration, Equation 43,

$$q_{0,Des} = q_{0,Ads} = K_{\mathrm{p0}}C_{d,Ads} \tag{47}$$

where $q_{0,Des}$ is the resistant component concentration, mg g^{-1}. At desorption, the reversible component remains proportional to the aqueous concentration

$$q_{x,des} = K_{px}C_{d,Des} \tag{48}$$

Therefore, desorption occurs along an isotherm defined by slope K_{px} and intercept $K_{\mathrm{p0}}C_{d,Ads}$.

$$q_{T,Des} = K_{px}C_{d,Des} + K_{\mathrm{p0}}C_{d,Ads} \tag{49}$$

Thus, the RR model portrays hysteresis as the result of a resistantly bound concentration, $K_{\mathrm{p0}}C_{Ads}$, that does not desorb at any of the aqueous concentrations at each of the desorption steps.

For a data analysis comparable to Equation 36, a normalized version of the RR model is required. The derivation is presented in Appendix J.2.1 and the result is

$$q^N_{T,Ads} = m\left(K_{px} + K_{\mathrm{p0}}\right)C^N_{d,Ads} \tag{50}$$

$$q^N_{T,Des} = mK_{px}C^N_{d,Des} + mK_{\mathrm{p0}}C^N_{d,Des} \tag{51}$$

where q^N_T is the total sorbed concentration normalized to the initial concentration

$$q^N_T = \frac{mq_T}{C_{tot(0)}} \tag{52}$$

where m is the soil-water ratio, g mL^{-1}, and N denotes a normalized concentration.

The equations used to describe partitioning for consecutive desorptions using the RR model can be normalized in the same way as the reversible model (derivation is in Appendix J.2.2). The result is that only the reversibly bound normalized concentration, $(1 - f_0)$, desorbs:

$$C^N_d(k) = (1 - f_0)f_x(1 - f_x)^k \tag{53}$$

where $C^N_d(k)$ is the normalized aqueous concentration for experimental step k, f_0 is the fraction of the initial concentration bound to resistant sites:

$$f_0 = \frac{mK_{\mathrm{p0}}}{1+mK_{px}+mK_{\mathrm{p0}}} \tag{54}$$

and f_x is the aqueous phase fraction of the reversibly bound concentration:

$$f_x = \frac{1}{1+mK_{px}} \tag{55}$$

The normalized sorbed concentration is given by

$$q_T^N = \frac{1}{m}\left((1-f_0)(1-f_x)^{(k+1)} + f_0\right) \tag{56}$$

Equation 53 is the reversible/resistant model used for analysis. In comparison to the reversible model (Equation 36) the RR model is identical, with the exception of the adjustment to the initial concentration, $(1-f_0)$. As a result, the RR model also exhibits log-linear behavior:

$$log_{10}C_d^N(k) = log_{10}(1-f_0) + log_{10}f_x + (k)log_{10}(1-f_x) \tag{57}$$

The reversible-resistant model was applied to the data allowing for time dependent reversible, K_{px}, and resistant, K_{p0}, partition coefficients. The fit was performed in R using the *nls* non-linear least squares package [R Core Team 2014]. Sorbed concentrations were required to properly fit the resistant component. The normalized sorbed concentration for step k was computed by summing the normalized aqueous concentrations for steps k through 4 and the extracted mass, normalized to the initial mass:

$$q_{T,Obs}^N(k) = \sum_{i=k}^{4} C_d^N(i) + \frac{M_{ext}}{C_{tot}(0)V(0)} \tag{58}$$

The sum of squared residuals (ssq) between observed and modeled aqueous and sorbed concentrations were minimized to estimate the partition coefficients. In order to properly weigh the adsorption and desorption data, the adsorption residual was given a weight of 4 relative to a unity weight for the four consecutive desorptions.

$$ssq = \sum_{\substack{0\le k\le 4\\ 1\le i\le 5}} W(k)\left[\left(log_{10}C_{d,Obs,i}^N(k) - log_{10}C_{d,Mod,i}^N(k)\right)^2 + \left(log_{10}q_{T,Obs,i}^N(k) - log_{10}q_{T,Mod,i}^N(k)\right)^2\right] \tag{59}$$

where k is the experimental step, i denotes the experimental concentration group as described in Table 25, and $W(k)$ is the weighting function: for $k = 0$, $W = 4$ and for $k > 0$, $W = 1$. The estimated partition coefficients, K_{px} and K_{p0} are shown in Appendices J.2.3 and J.2.4. Application of the RR model to the data shows good agreement with observed concentration. Figure 66 presents the results for all MC and two soils (the full set of results are shown in Appendix J.2.6). The RR model accurately predicts the aqueous concentration for each sorption time, indicating that time dependent partition coefficients with a resistant component is sufficient to describe the observed concentrations.

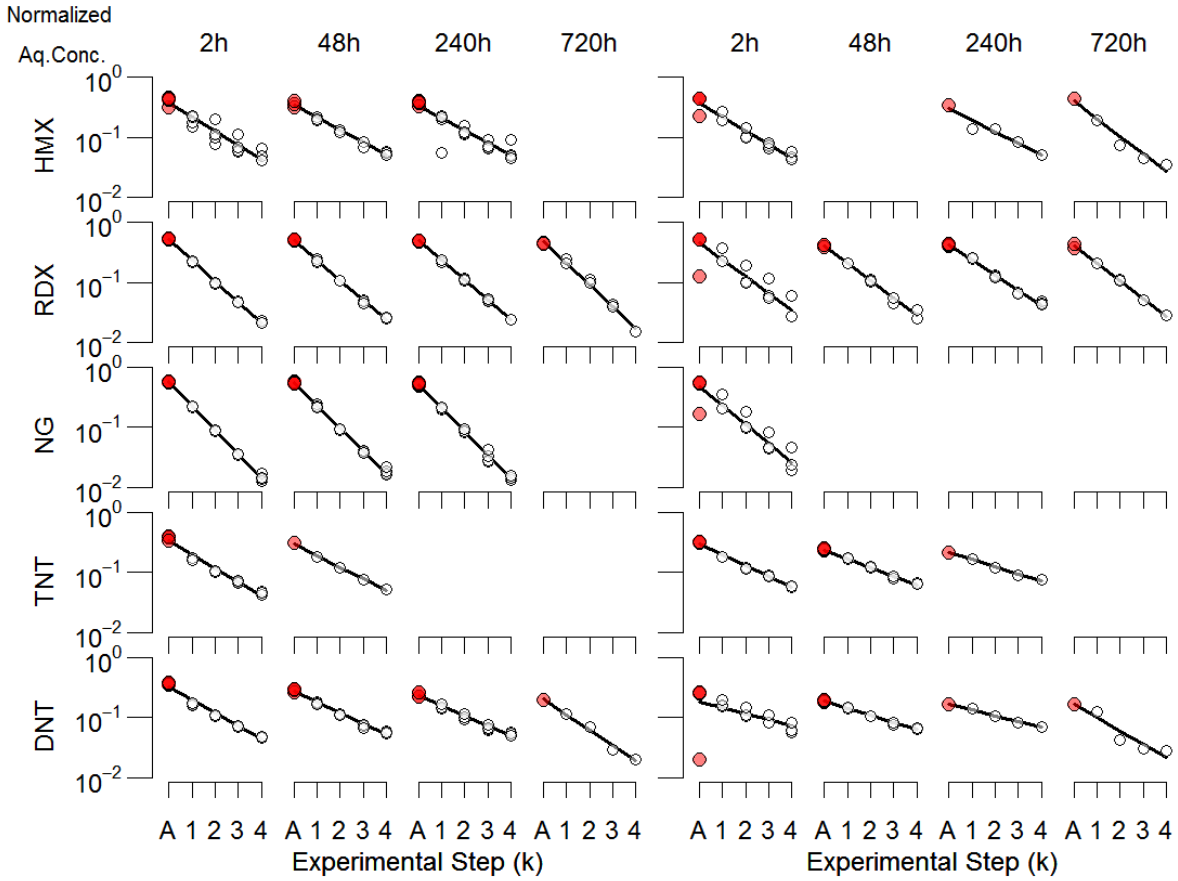

Figure 66. Comparison of RR model (lines) with observed data (points) for Matapeake (left) and Houthalein (right) soils. Concentrations are normalized to the initial concentration $\left[\frac{mg/L}{mg/L}\right]$. Filled circles indicate adsorption point. Hollow circles indicate desorption points. 2h, 48h, 240h, and 720h refer to the duration of the adsorption step. A, 1, 2, 3, 4 refer to the adsorption and the four desorption steps. ($k = 0,1,2,3,4$ in Equation 53).

To gauge the improvement obtained by using the RR model, a comparison of the reversible and RR models was conducted. The RMSE was calculated for each MC, soil and sorption time and compared in Figure 67. Throughout the range of f_{OC} the RR model is an improvement over the reversible model. For several soils, the improvement is dramatic (e.g. RDX on Aberdeen BTi soil (BT) and DNT on Lewis Core (LCO) soil). NG shows less improvement per soil which is attributed to variability within the 720 h data set. As is shown in Figure 67B, the RR model decreases RMSE for the 2, 48 and 240 h adsorption contact time for NG, indicating an overall improvement to the fit.

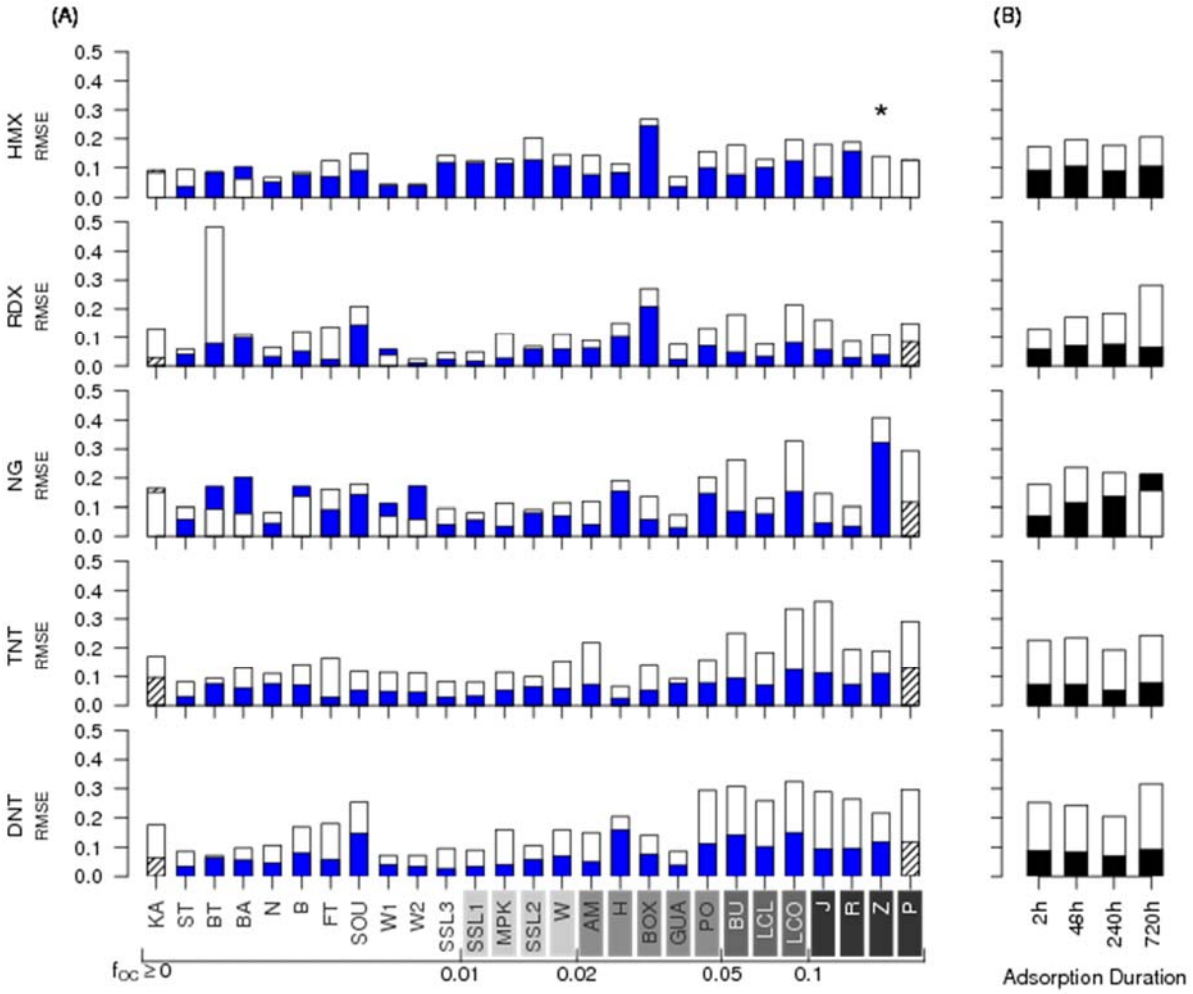

Figure 67. RMSE, Equation 38, for RR model predicted aqueous concentrations, C_{aq}^{N}, compared to reversible model aqueous concentrations. (A) RMSE determined for each soil (B) RMSE determined for each adsorption contact time. Filled bars indicate RR determined RMSE. Hollow bars indicate reversible model RMSE. Hashed bars indicate reference sorbents.∗ indicates a soil with either the reversible or RR RMSE value missing.

Residuals from the reversible and RR model fits of C_d^N were compared to illustrate the importance of including a hysteretic fraction. From the model results, shown previously in Figures 64 and 66, it was expected that the RR model would show improvement for higher f_{OC} soils. Residuals of the aqueous concentration are shown as a function of sorbent in Figure 67. It is apparent that for all MC there is bias in the reversible model residuals. Predicted aqueous concentrations are always greater than observed, indicated by the negative residual. Over-prediction of aqueous concentrations is due to the lack of resistant sorption, as is evidenced by the RR residuals where there is no bias. Aqueous concentrations are accurately portrayed by the RR model because a portion of the chemical is unable to participate in desorption.

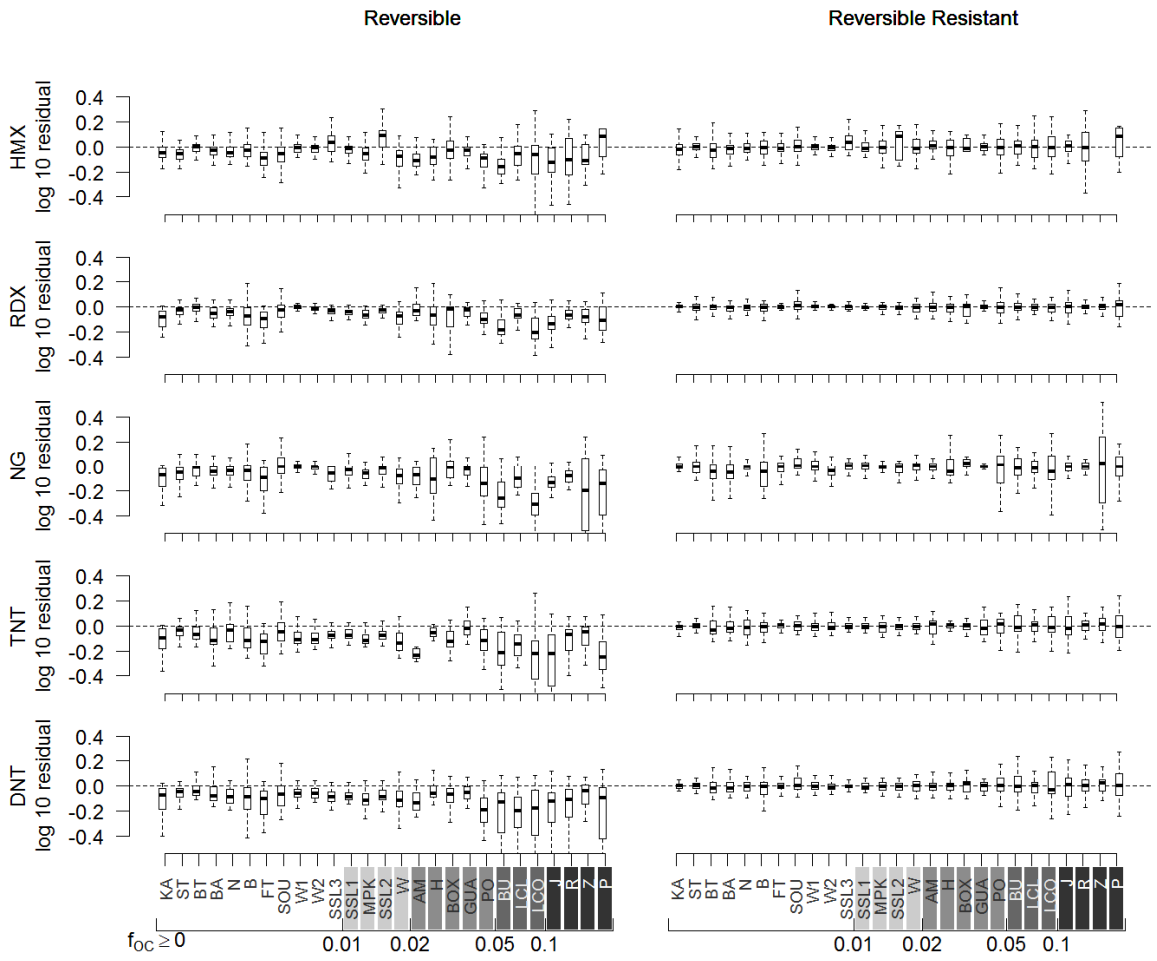

Figure 68. Comparison of log_{10} residuals (log_{10}observed $- log_{10}$predicted) for reversible and RR model aqueous concentrations as determined by the respective model. Bias shows the over-prediction of linear derived aqueous concentrations due to lack of resistant sorption. Outliers have been omitted for clarity.

Multilinear model of adsorption partition coefficients. Since the model predicts the observed concentrations well, an investigation of the partition coefficient was conducted. The adsorption partition coefficient was analyzed by using a multilinear model [González Forero 2013]. The multilinear model decomposes a partition coefficient into multi-site partitioning to the sorbent matrix using sorbent specific partition coefficients. In this analysis, the sorbent properties were organic carbon (OC) content and clay sized particle fractions:

$$K_P(i,j) = f_{OC}(i)K_{OC}(j) + f_{clay}(i)K_{clay}(j) \quad (60)$$

where $f_{OC}(i)$ is the OC mass fraction of sorbent i (g OC (g sorbent)$^{-1}$), $K_{OC}(j)$ is the partition coefficient for MC j binding to OC (L (kg OC)$^{-1}$), $f_{clay}(i)$ is the clay sized particle mass fraction of sorbent i (g clay (g sorbent)$^{-1}$), and $K_{clay}(j)$ is the partition coefficient for MC j binding to the clay sized particles (L (kg clay)$^{-1}$). It has been previously observed by González Forero [2013] that using these two sites is sufficient to accurately model the adsorption partition coefficient.

The multilinear model parameters were estimated by minimizing the RMSE, Equation 38, between RR estimated K_P and multilinear regression predicted K_P using R and the *nls* package [R Core Team 2014] contact time (columns) plotted against f_{OC} on log-log axes. The partition coefficients are shown as points with error bars of one standard error. The two reference sorbents are shown as squares. The multilinear model is shown as the solid red line. The model estimated partition coefficients are shown in Appendix J.1.2. Sorbent specific partition coefficients K_{OC} and K_{clay} are shown in Tables 43 and 44. To evaluate the contribution of clay sized particle sorption with only a single sorption site, OC:

$$K_P(i,j) = f_{OC}(i)K_{OC}(j) \tag{61}$$

is shown as the dashed red line in Figure 69.

The predicted and estimated partition coefficients are in close agreement. Behavior similar to the single sorption site partition coefficient (Equation 61) is seen for $f_{OC} > 0.01$. Below this threshold, mutltilinear predicted partition coefficients deviate from a linear relationship with f_{OC}. This non-linearity is due to the increasing importance of binding to the clay size particle fraction as f_{OC} decreases.

The multilinear partition coefficients, Figure 70, show that there is a time component to sorption to OC as K_{OC} increases with adsorption contact time. However K_{clay} does not show the same relationship. This suggests that only the OC fraction of the sorbent is changing binding strength as the adsorption contact time increases.

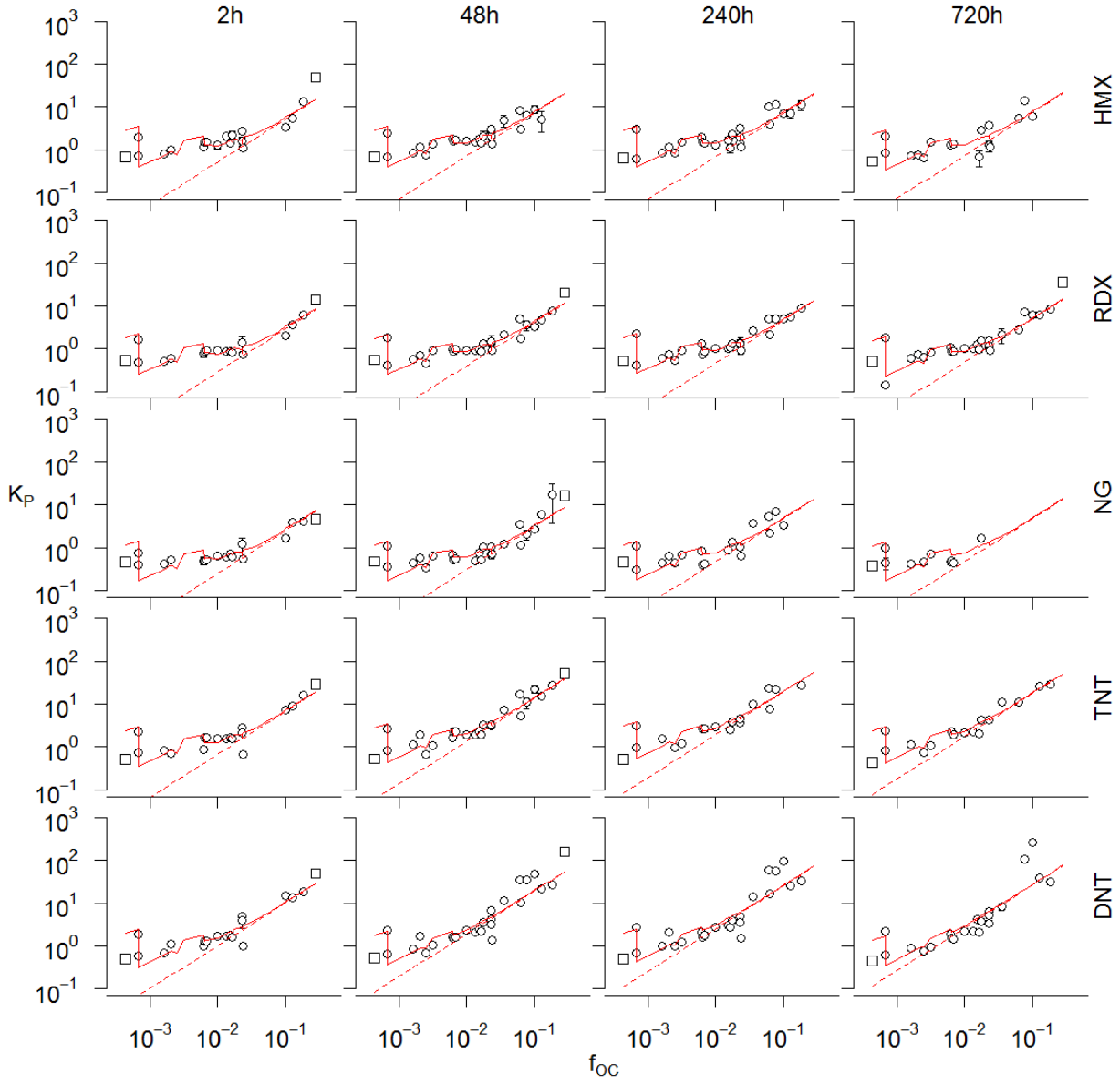

Figure 69. Adsorption partition coefficients (L kg^{-1}) from RR model for soils are shown by mean (point) ± std. error (error bars) if the standard error is greater than the symbol. Red line shows K_P predicted by the two-site multilinear regression, Equation 60. Dashed red line shows K_P predicted by the one-site regression, Equation 61. Square points indicate reference sorbents not used in the multilinear regression.

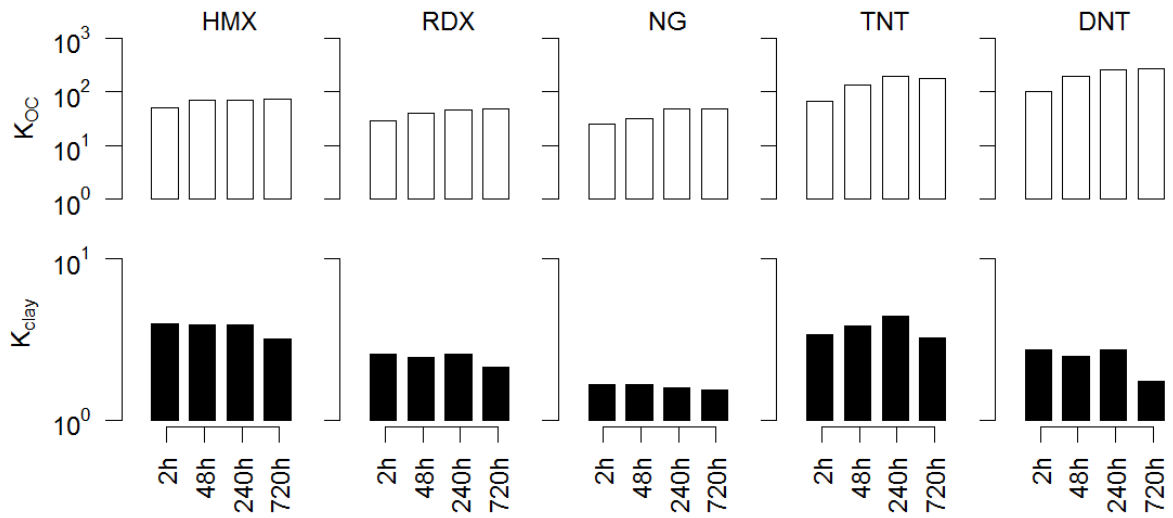

Figure 70. Multilinear component partition coefficients, K_{OC} and K_{clay}, L kg^{-1}, for the adsorption partition coefficients versus adsorption contact time. Hollow bars show $K_{OC,x}(j)$, filled bars show $K_{clay,x}(j)$.

Multilinear model of reversible/resistant partition coefficients. To analyze the RR partition coefficients, a multilinear model for K_{px} and K_{p0} was needed, Equations 62 and 63.

$$K_{px}(i,j) = f_{OC}(i)K_{OC,x}(j) + f_{clay}(i)K_{clay,x}(j) \quad (62)$$

$$K_{\mathrm{p0}}(i,j) = f_{OC}(i)K_{OC,0}(j) + f_{clay}(i)K_{clay,0}(j) \quad (63)$$

where $K_{OC,x}(j)$ and $K_{OC,0}(j)$ are the reversible and resistant partition coefficients associated with MC j binding to OC, $K_{clay,x}(j)$ and $K_{clay,0}(j)$ are the reversible and resistant partition coefficients associated with MC j binding to clay sized particles. Sorbent specific partition coefficients $K_{OC,x}$, $K_{OC,0}$, $K_{clay,x}$, and $K_{clay,0}$ are shown in Tables 43 and 44.

Table 43. Multilinear partition coefficient K_{OC} (L kg^{-1}) for K_p, K_{px}, and K_{p0}.

	MC	$\boldsymbol{K_{OC}^{2h}}$	$\boldsymbol{K_{OC}^{48h}}$	$\boldsymbol{K_{OC}^{240h}}$	$\boldsymbol{K_{OC}^{720h}}$
K_P	HMX	5.15e+01	7.17e+01	6.98e+01	7.34e+01
	RDX	2.92e+01	4.05e+01	4.58e+01	4.94e+01
	NG	2.53e+01	3.13e+01	4.81e+01	4.83e+01
	TNT	6.73e+01	1.37e+02	1.94e+02	1.79e+02
	DNT	1.03e+02	1.95e+02	2.57e+02	2.70e+02
K_{px}	HMX	3.81e+01	5.45e+01	4.79e+01	5.23e+01
	RDX	2.26e+01	2.89e+01	3.18e+01	2.88e+01
	NG	1.71e+01	2.33e+01	2.94e+01	6.22e+01
	TNT	3.37e+01	6.56e+01	8.50e+01	5.46e+01
	DNT	4.58e+01	7.50e+01	9.51e+01	3.69e+01
K_{p0}	HMX	1.03e+01	1.71e+01	2.64e+01	2.48e+01
	RDX	5.22e+00	7.61e+00	1.07e+01	1.14e+01
	NG	4.64e+00	8.19e+00	1.85e+01	1.19e+01
	TNT	3.45e+01	6.62e+01	8.82e+01	7.45e+01
	DNT	4.09e+01	8.73e+01	1.19e+02	8.63e+01

Table 44. Multilinear partition coefficient K_{clay} (L kg^{-1}) for K_p, K_{px}, and K_{p0}.

	MC	K_{clay}^{2h}	K_{clay}^{48h}	K_{clay}^{240h}	K_{clay}^{720h}
K_P	HMX	3.95e+00	3.93e+00	3.92e+00	3.17e+00
	RDX	2.57e+00	2.47e+00	2.59e+00	2.13e+00
	NG	1.66e+00	1.68e+00	1.60e+00	1.53e+00
	TNT	3.42e+00	3.83e+00	4.41e+00	3.24e+00
	DNT	2.74e+00	2.49e+00	2.73e+00	1.75e+00
K_x	HMX	4.67e+00	4.06e+00	3.79e+00	3.52e+00
	RDX	2.72e+00	2.54e+00	2.46e+00	2.53e+00
	NG	1.88e+00	1.78e+00	2.04e+00	2.12e+00
	TNT	4.28e+00	4.15e+00	4.29e+00	4.35e+00
	DNT	3.85e+00	3.55e+00	3.23e+00	3.49e+00
K_0	HMX	2.45e-01	2.36e-01	6.74e-01	3.06e-01
	RDX	1.02e-01	1.54e-01	2.50e-01	2.70e-01
	NG	7.73e-02	1.12e-01	2.59e-01	3.40e-01
	TNT	2.40e-01	4.55e-01	1.01e+00	5.06e-01
	DNT	1.59e-01	2.12e-01	4.17e-01	2.80e-01

Figure 71 is a plot of K_{px} vs. f_{OC} for each MC (rows) and each adsorption contact time (columns) on log-log axes. The partition coefficients are shown as points with error bars of one standard error. The two reference sorbents are shown as squares. The multilinear model is shown as the solid red line. To evaluate the contribution of clay size particles, models with only a single sorption site, OC:

$$K_{px}(i,j) = f_{OC}(i)K_{OC,x}(j) \tag{64}$$

$$K_{\mathrm{p0}}(i,j) = f_{OC}(i)K_{OC,0}(j) \tag{65}$$

are shown as the dashed red lines in Figures 71 and 72.

Multilinear predicted K_x show similar behavior to the adsorption partition coefficients. For $f_{OC} > 0.01$ the reversible partition coefficient is approximately linear with respect to f_{OC}, as shown by the similarity to a K_{OC} only partition coefficient (dashed red line). Below $f_{OC} = 0.01$, deviation from a linear relationship with f_{OC} is again seen.

The multilinear estimated $K_{OC,x}$ and $K_{clay,x}$ (Figure 73) show different behavior than the adsorption K_{OC} and K_{clay} (Figure 70). With the exception of NG, both $K_{OC,x}$ and $K_{clay,x}$ are constant with respect to time. This suggests that there is no change in the reversible component as the duration of adsorption increases.

Resistant partition coefficients show less deviation from a $K_{OC,0}$ model (Equation 65) than K_{px}, Figure 72. This is seen especially for TNT and DNT. K_{p0} for these MC are linear with respect to f_{OC} for f_{OC} values $> 10^{-3}$. However, unlike K_{px}, the magnitude of K_{p0} appears to increase as adsorption contact time increases. This indicates an increase in resistant sorption as contact time increases.

The OC and clay partition coefficients , $K_{OC,x}$ and $K_{OC,0}$, (Figure 74) support these observations. The magnitude of $K_{clay,0}$ for TNT and DNT partition coefficients to OC and clay differ by a factor of approximately 100, an indication that binding to clay is minimal. In these cases, K_{p0} is correlated almost exclusively to binding to organic carbon, as shown by the similarity of the multilinear model in Figure 72 to a $K_{OC,0}$ model (Equation 61). These results strongly suggest that organic matter is the site of resistant sorption, lending support to polymer expansion and other OC modification theories [Chilom and Rice 2005; Sander et al. 2006; Weber et al. 1998]. In addition, $K_{OC,0}$ shows a dependence with sorption time. This suggests that the resistantly bound component increases with increasing adsorption contact time.

Reversibility fraction. To better understand the extent of partitioning due to resistant sorption, the fraction of K_p associated with reversible sorption was calculated:

$$RF = \frac{K_{px}(i,j)}{K_{px}(i,j)+K_{\mathrm{p0}}(i,j)} = \frac{K_{px}(i,j)}{K_P(i,j)} \tag{66}$$

where RF is the reversibility fraction. $RF \simeq 1$ indicates complete reversibility, while decreasing values indicate increasing hysteresis. RF values are plotted vs. f_{OC} for each soil and adsorption contact time in Figure 75. Highly reversible munitions, such as HMX and RDX, display little change in RF with either adsorption contact time or soil, whereas MC with larger resistant component sorption, such as TNT and DNT, show significant changes indicating that not only do high f_{OC} soils display greater hysteresis, but as adsorption contact time increases a larger fraction of soils show hysteretic behavior.

The results of the RF suggest an increase in resistant binding with respect to sorption time and f_{OC} is responsible for the observed increase in hysteretic behavior. The RR model has no mechanistic or empirical explanation for the time dependency. Therefore, development of a model that incorporates this change in binding strength as a function of the adsorption contact time and sorbent properties can further explain observed hysteresis.

Predictive model. The reversible model (Equation 36) requires two sorbate parameters (K_{OC} and K_{clay}) and two sorbent parameters (f_{OC} and f_{clay}) to estimate aqueous and sorbed normalized concentrations. However, the RR model (Equation 53) requires four sorbate parameters (($K_{OC,x}$, $K_{clay,x}$, $K_{OC,0}$ and $K_{clay,0}$) and the same sorbent parameters to estimate aqueous and sorbed

normalized concentrations due to the inclusion of hysteresis. To measure the predictive capabilities of the two models, a comparison was made using the multilinear predicted partition coefficients (Tables 43 and 44).

The log_{10} residuals for normalized aqueous concentrations are shown for each sorbent and MC in Figure 76. The reversible model shows negative biasing for many soils due to the reversible model not incorporating resistant sorption. When compared to the RR model, this bias is corrected. Both models show large residuals for low and high f_{OC} soils. As shown in Figure 68, the RR model should predict significantly more accurate concentrations given precise partition coefficients. Error for multilinear predicted partition coefficients is large in some cases, especially at very low and high f_{OC} (Figures 69, 71, and 72). Increased accuracy in multilinear predictions are expected to show greater improvement when using the RR model.

Conclusions regarding reversible/resistant modeling of MC sorption and the reversibility fraction. From the analysis provided above, a reversible approach to MC sorption can accurately predict behavior for low f_{OC} soils and short adsorption times. As f_{OC} increases, however, a model incorporating hysteresis is required. The reversible resistant model is valid across the range of observed f_{OC} for both fully reversible and highly resistant cases at the cost of an additional fitting parameter.

A reversibility fraction shows how hysteretic behavior changes across multiple soils and sorption times. The time dependent nature of the resistant partition coefficient suggests that a kinetic process is occurring, while the relationship to f_{OC} strongly points to a change in binding strength of organic matter sorption sites. Further investigation is needed to understand the effect of sorption duration, however from the analysis provided, a positive correlation to binding strength is expected.

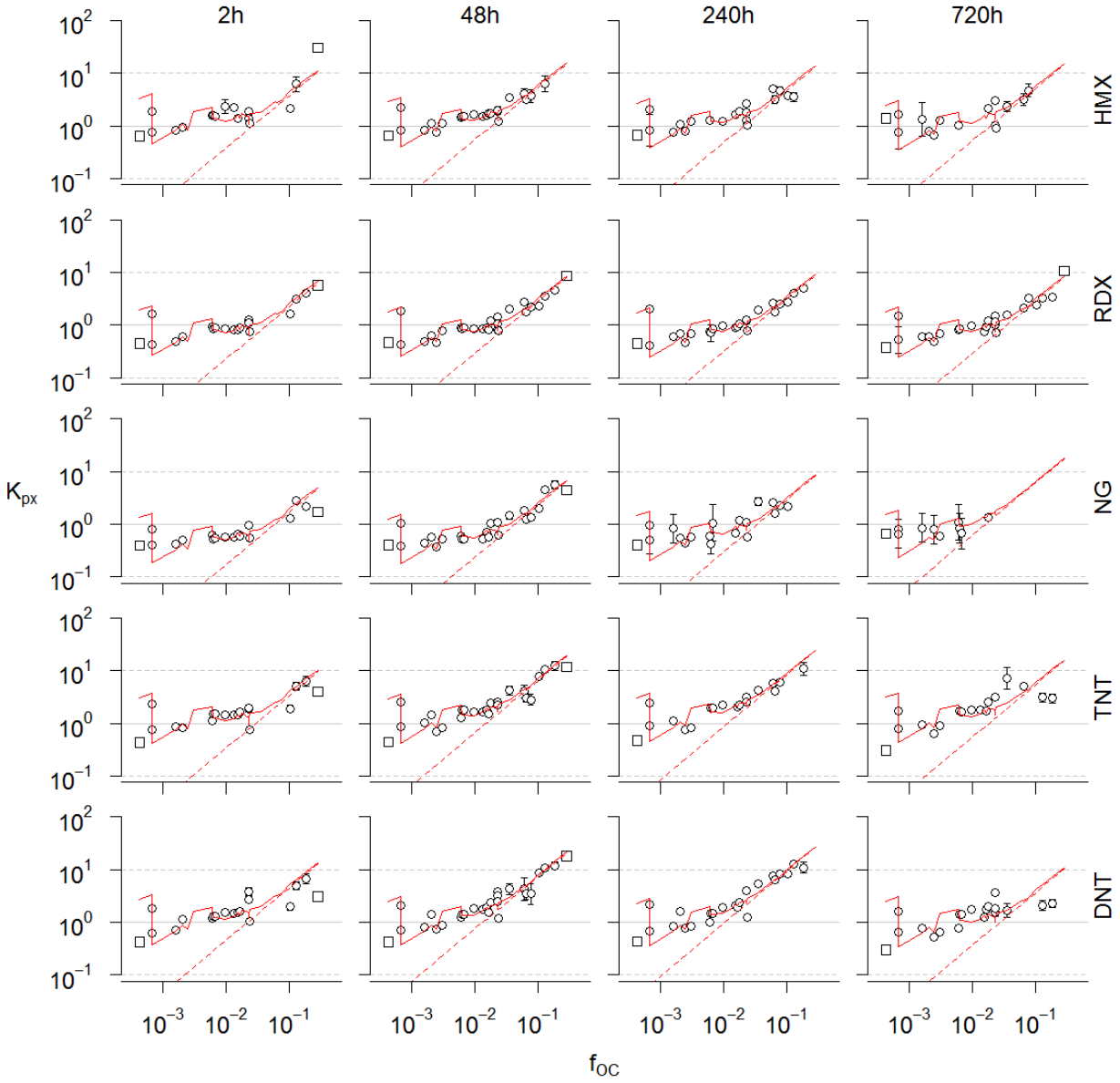

Figure 71. Reversible partition coefficients, K_{px} (L kg^{-1}), from RR model for soils are shown by mean (point) $\pm$ std. error (error bars) if the standard error is greater than the symbol. Solid red line shows K_{px} predicted by the two-site multilinear regression (Equation 62). Dashed red line shows K_{px} predicted by Equation 64. Square points indicate reference sorbents not used in the multilinear regression.

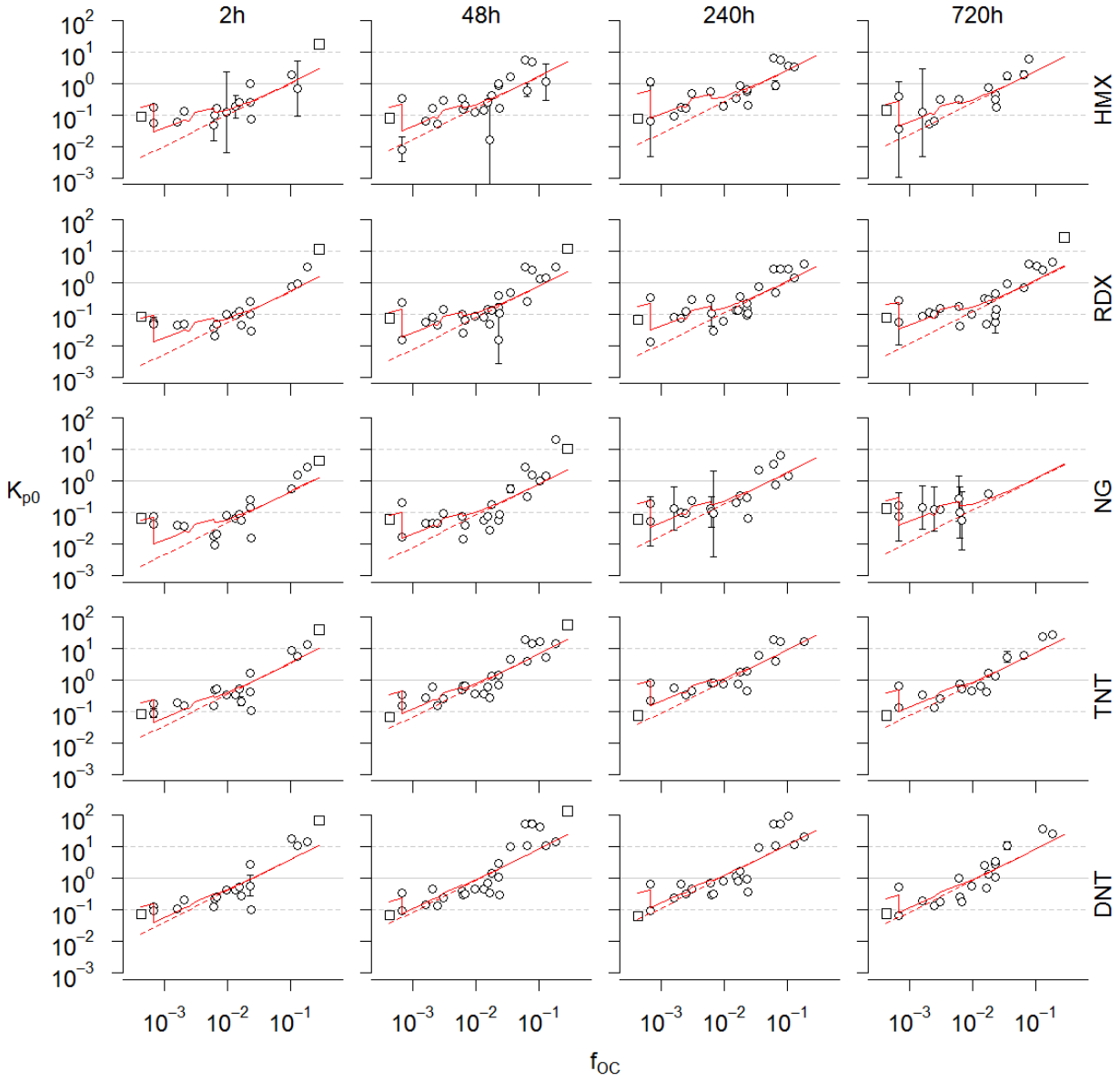

Figure 72. Resistant partition coefficients, K_{p0} (L kg^{-1}), from RR model for soils are shown by mean (point) ± std. error (error bars) if the standard error is greater than the symbol. Solid red line shows K_{p0} predicted by the two-site multilinear regression (Equation 63). Dashed red line shows K_{p0} predicted by Equation 65. Square points indicate reference sorbents not used in the multilinear regression.

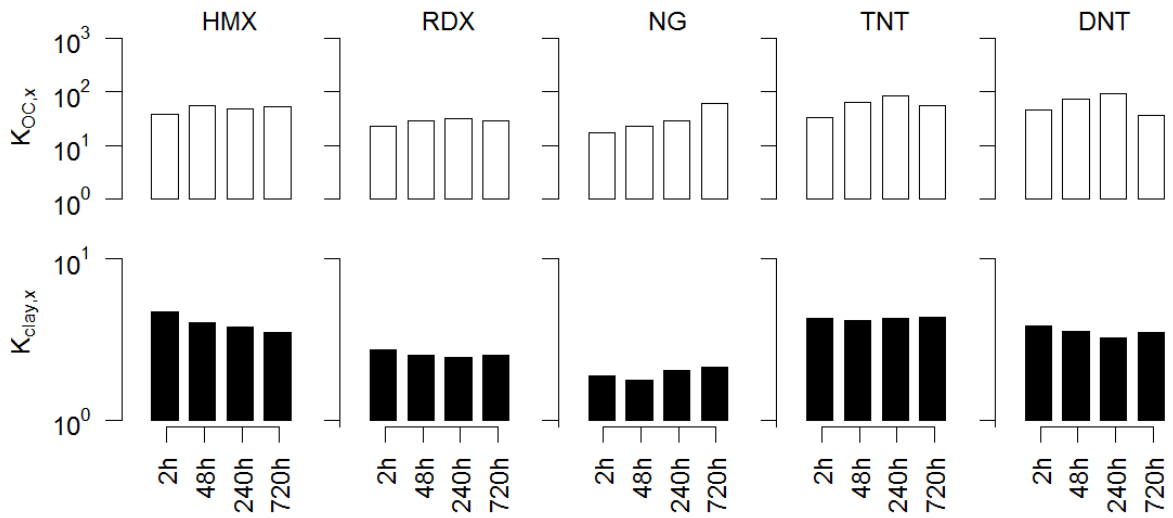

Figure 73. Multilinear component partition coefficients, $K_{OC,x}$ and $K_{clay,x}$ (L kg^{-1}), for the reversible partition coefficients, K_{px}, versus adsorption contact time. Hollow bars show $K_{OC,x}(j)$, filled bars show $K_{clay,x}(j)$.

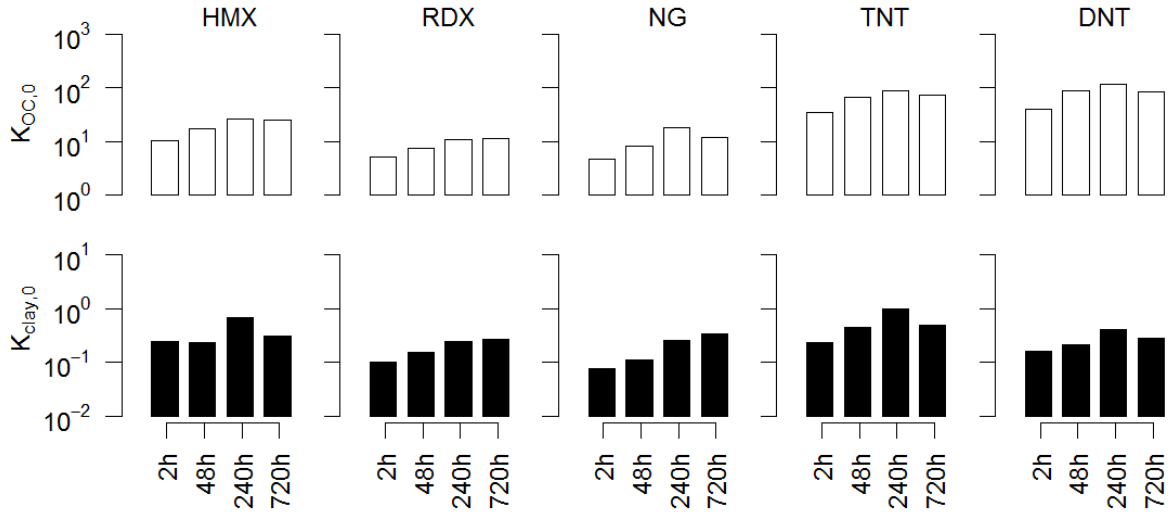

Figure 74. Multilinear component partition coefficients, $K_{OC,0}$ and $K_{clay,0}$ (L kg^{-1}), for the resistant partition coefficients, for K_{p0} versus adsorption contact time. Hollow bars show $K_{OC,0}(j)$, filled bars show $K_{clay,0}(j)$.

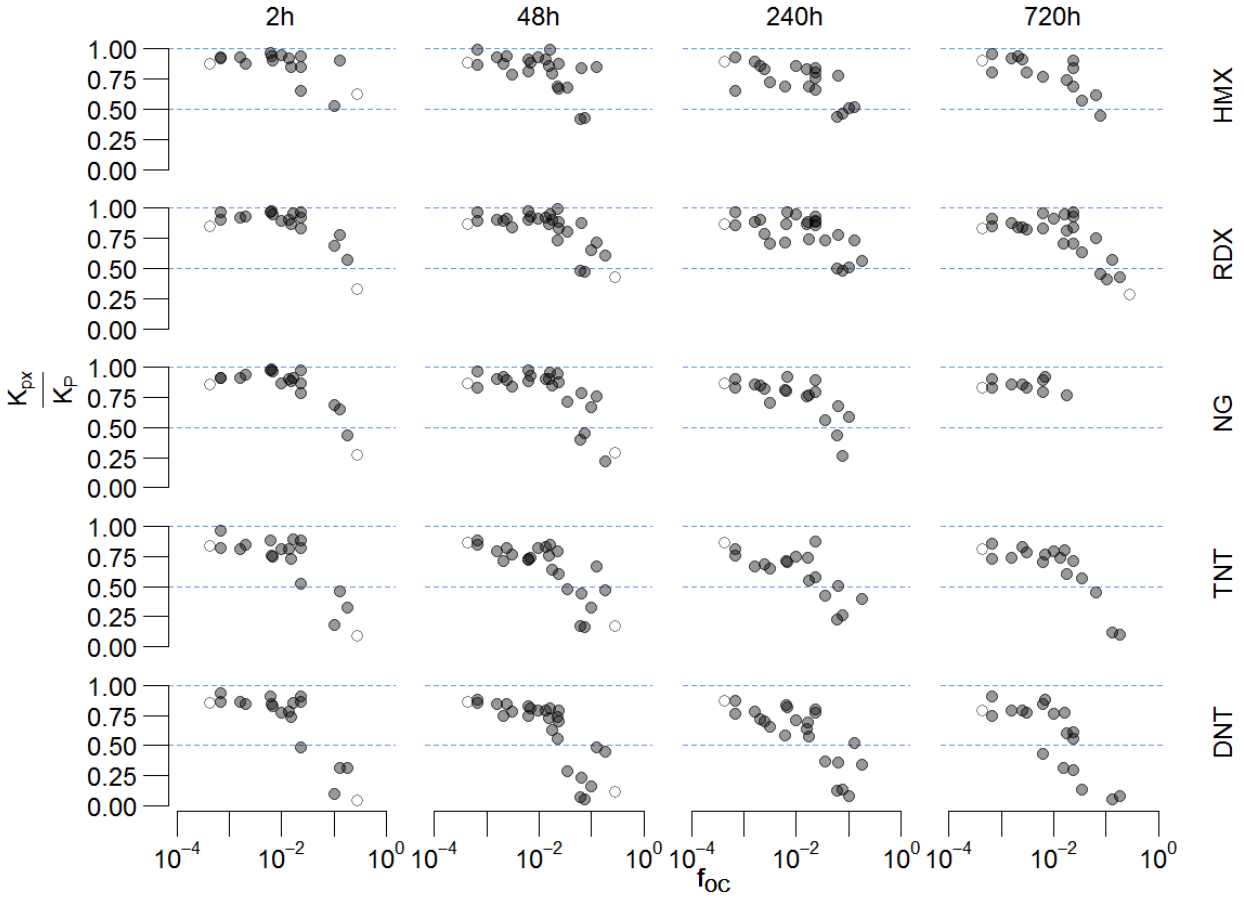

Figure 75. Reversibility Fraction, $\frac{K_{px}}{K_P}$, for RR model. Points are the ratio of the reversible partition coefficient, K_{px} to the total partition coefficient, K_P. Filled points are soils, hollow points are reference sorbents. 2h, 48h, 240h, and 720h refer to the adsorption contact time.

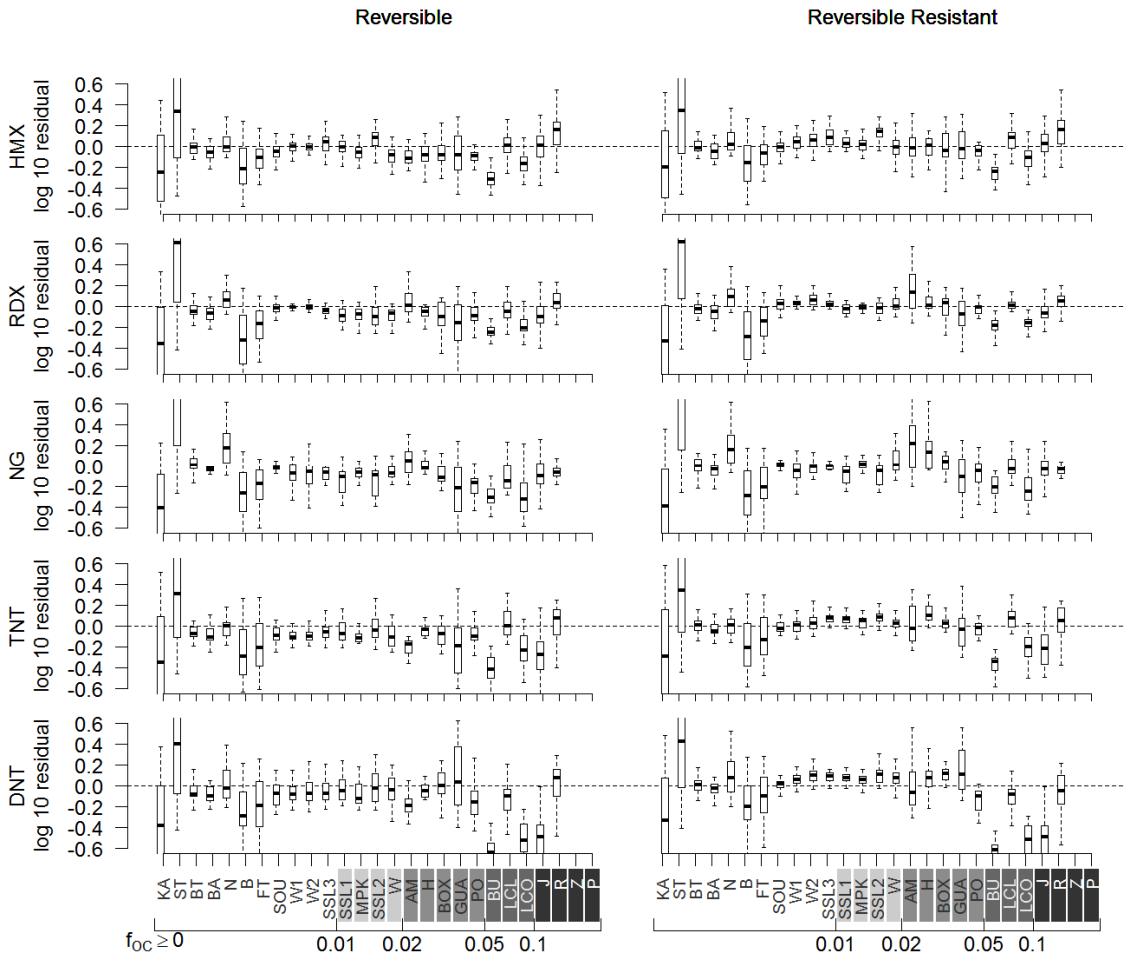

Figure 76. log_{10} residuals (log_{10} observed $-$ log_{10} predicted) of normalized aqueous concentrations for each sorbent and MC for reversible (Equation 41) and RR models (Equation 53) using multilinear predicted partition coefficients (Tables 43 and 44). Shading indicates increasing f_{OC}.

Modeling MC Adsorption and Desorption Hysteresis onto 25 Soils at 4 Durations of Adsorption using the Site Transformation Model. A recently developed model, the Site Transformation Model (STM) (Di Toro 2013), is based on the idea that sites change binding strength as a function of adsorption concentration, resulting in hysteresis. Moreover, the model can be applied to both linear and Langmuir isotherms, enabling modeling of nonlinear sorption. In this work, the STM is applied to the data set of 5 munition constituents and 25 soils during adsorption and sequential desorptions to determine sorbent-model correlations as well as develop predictive tools for the model parameters. Moreover, a relationship between hysteretic behavior, adsorption contact time, and sorbent organic carbon content is made that allows for characterization of hysteresis for new soils.

Data and modeling procedure. In the preceding section, "Normalization and Reversible/ Resistant Modeling of 5 MC onto 25 Soils at 4 Durations of Adsorption", the data were analyzed using linear isotherms. We showed that a reversible model, using the adsorption partition coefficient, could not predict aqueous or sorbed concentrations during desorption. The reversible

model used a partition coefficient estimated for each MC, sorbent and adsorption duration. A comparison between observed and modeled sorbed concentrations is shown as Figure 77. Data are shown as hexagons, with the shade of the hexagon indicating the number of observed-modeled pairs. A 1:1 line (solid red) shows that modeled sorbed concentrations are biased low indicating that the reversible model underpredicts sorbed concentrations. This is due to the inability of the reversible model to incorporate hysteresis since it treats adsorption and desorption using the same isotherm. As a result, a model that applied hysteresis is necessary to model the behavior of MC on soil. The reversible model under predicts sorbed concentrations since it does not include hysteresis. Therefore, a model that includes hysteresis was used to explain the observed behavior.

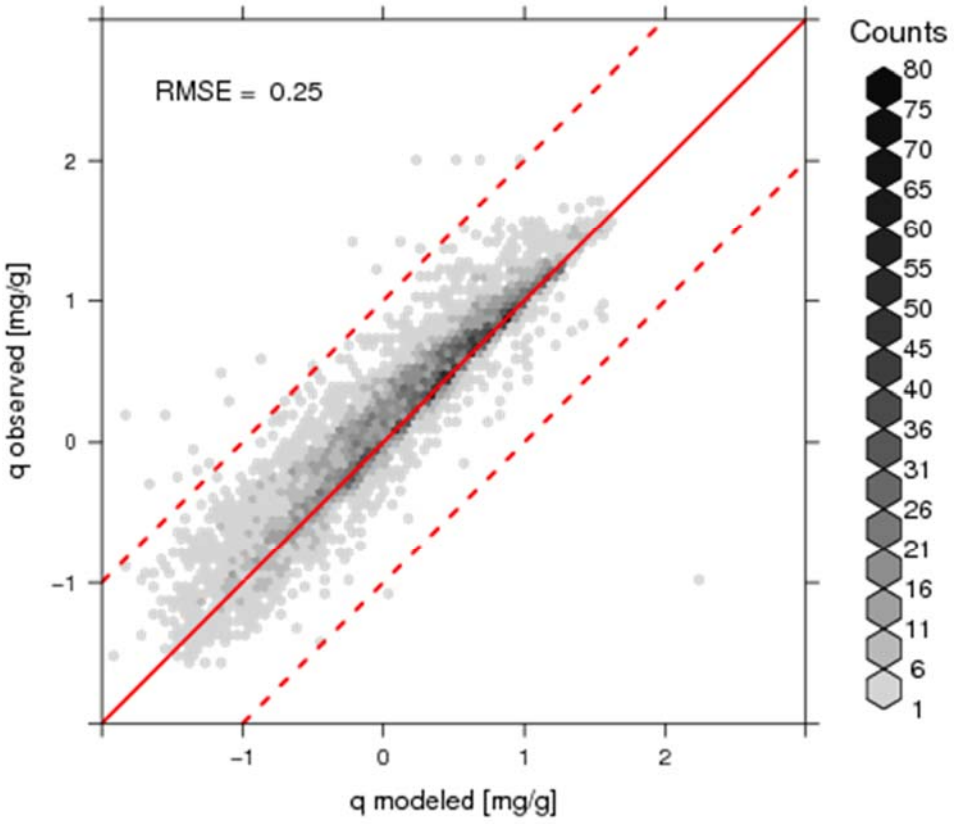

Figure 77. Comparison of modeled and observed sorbed concentrations for a reversible model (fit to the adsorption point). Data is grouped into hexagons, the shading of which indicates the number of data. The red solid line indicates unity, dashed lines are spaced at 1 log unit from unity.

The adsorption and desorption data are modeled using the site transformation model (STM) (Di Toro 2013). Figure 78 shows aqueous concentration plotted vs. sorbed concentration for all MC (rows) and all adsorption times (columns) on Matapeake soil. Adsorption concentrations are shown as the filled red points and desorption concentrations are shown as the hollow points. HMX, RDX, and NG show linear adsorption and desorption, as illustrated by the connected straight lines. TNT and DNT, however, show deviation from linearity. These isotherms appear to

show curvature. A Langmuir STM was therefore proposed to model the observed behavior.

The STM is formulated using a general isotherm model. For application to these data, the isotherm model used is the Langmuir isotherm. The Langmuir isotherm is typically defined as:

$$q = \frac{q_T K_L C}{1+K_L C} \tag{67}$$

where q is the mass of sorbent per unit mass sorbate (mg kg^{-1}), K_L is the Langmuir constant (L mg^{-1}), q_T is the maximum site density (mg (kg soil)$^{-1}$), and C is the aqueous concentration of the sorbate (mg L^{-1}). The STM equations are (derivation is provided in Appendix K):

$$q_A = \frac{q_T K_L C_A}{1+K_L C_A} + f_{ST} \frac{q_T K_L C_A}{1+K_L C_A} \tag{68}$$

$$q_D = \frac{q_T K_L C_D}{1+K_L C_D} + f_{ST} \frac{q_T K_L C_A}{1+K_L C_A} \tag{69}$$

where q_A is the concentration of chemical sorbed on the particles (mg (kg soil)$^{-1}$) after adsorption contact time, q_D is the concentration of chemical sorbed on the particles (mg (kg soil)$^{-1}$) after a single desorption, f_{ST} is the site transformation factor described below $[unitless]$, C_A is the aqueous concentration after adsorption contact time (mg L^{-1}) and C_D is the aqueous concentration after a single desorption (mg L^{-1}).

The adsorption isotherm, Equation 68 is the sum of two Langmuir isotherms. The first term quantifies sorption to weakly sorbing sites. The second quantifies sorption to strong sites. The quantity of strong sites is determined by the magnitude of the site transformation factor, f_{ST}. For adsorption, both terms are a function of C_A, the aqueous concentration. However, for the desorption isotherm, Equation 69, only the first term is a function of the aqueous concentration at desorption, C_D. The second term, defining the resistant component, is fixed at the aqueous adsorption concentration, C_A.

Figure 1 illustrates this behavior, showing sorbed and aqueous concentrations for an example system. During adsorption, the sorbed concentration follows the black line in panel A, the adsorption isotherm (Equation 68). During desorption, the sorbed concentration follows the red line in panel A, the desorption isotherm (Equation 69). Only the weak sites are depleted, the dashed blue line in panel B. In contrast, the strong sorbing sites, the dashed red line in panel B, remain constant. The net result of the differing behavior between strongly and weakly sorbing sites is the total sorbed curve during desorption, as illustrated in panel A. This differing behavior is the cause of hysteresis.

In addition to Langmuir behavior, many soils exhibited linear partitioning. The linear isotherm is a special case of the Langmuir isotherm for which $K_L C \ll 1$. The STM equations reduce to:

$$q_A = q_T K_L C_A + f_{ST} q_T K_L C_A \tag{70}$$

$$q_D = q_T K_L C_D + f_{ST} q_T K_L C_A \tag{71}$$

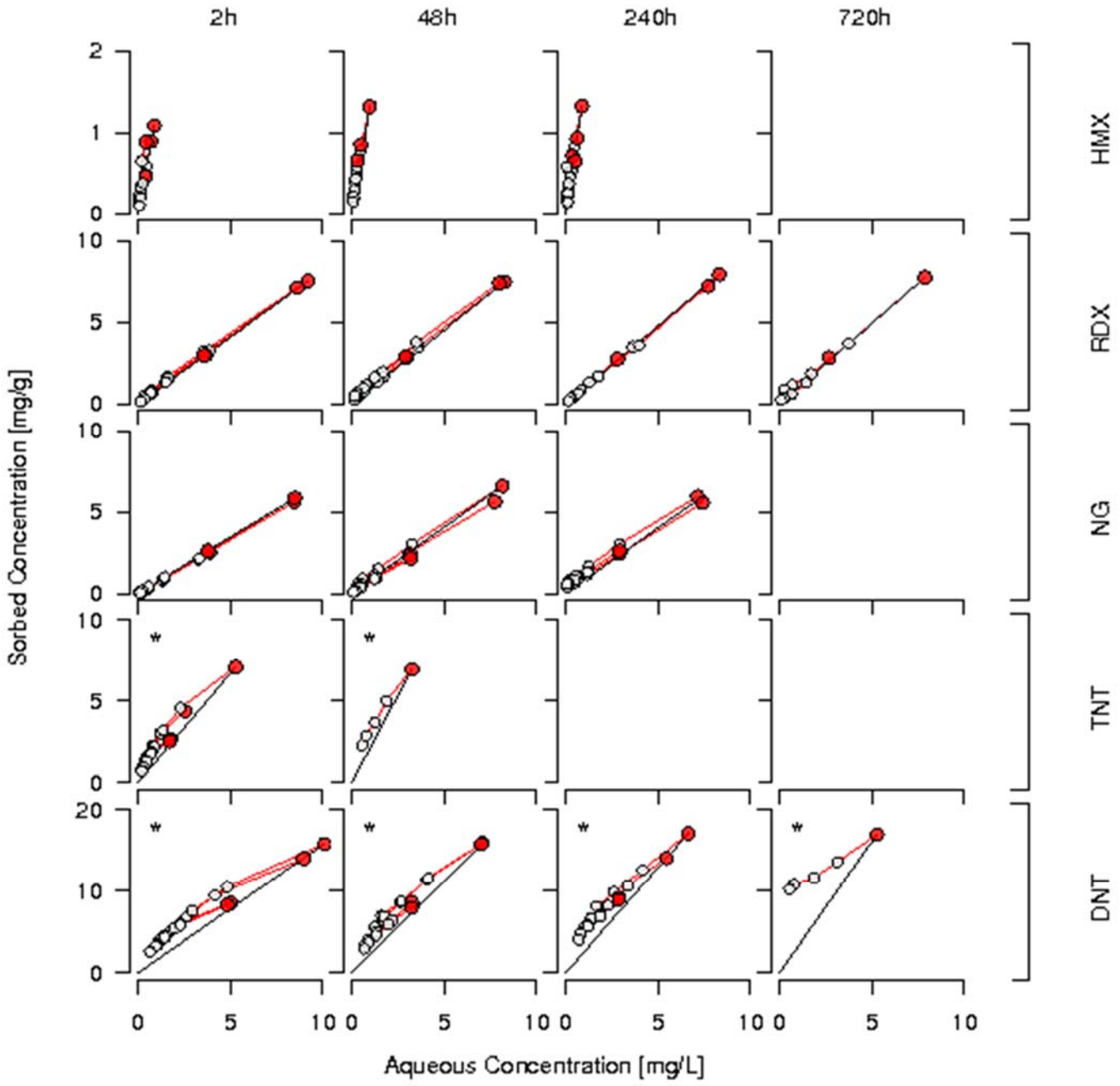

Figure 78. Linear and Langmuir isotherms for MC on Matapeake (MPK) soil. Lines show relationship between observations. Red points are concentrations after adsorption, hollow points are sequential desorption concentrations.

In the linear case, the parameters q_T and K_L cannot be independently determined. Therefore, the product was fit as a single parameter, K_P:

$$q_A = K_P C_A + f_{ST} K_P C_A \quad (72)$$

$$q_D = K_P C_D + f_{ST} K_P C_A \quad (73)$$

The method employed to determine which STM formulation, Equation 67 or 68, is described in the following section.

Isotherm determination. If the Langmuir equations (Equation 67) are applied to linear adsorption and desorption data, q_T and K_L cannot be determined independently since they occur as the product $q_T K_L$ in Equation 68. Fitting a large K_L is offset by fitting a small q_T and vice versa. This is a useful observation since it allows each set of data to be separated into either linear or Langmuir isotherms without introducing potential biases from a visual separation.

Initially a data set is fit using the Langmuir STM (Equation 67). Fitting was performed using R statistical software and the *optim* method [R Core Team 2014] to minimize the root mean square error (RMSE) of sorbed concentrations. The RMSE was calculated using Equation 74.

$$RMSE = \sqrt{\frac{1}{n}\sum_{i=1}^{n}\left(log_{10}q_{i,obs} - log_{10}q_{i,model}\right)^2} \quad (74)$$

where n is the total number of observations in the data set, $q_{i,obs}$ and $q_{i,mod}$ are the sorbed concentrations, subscripts obs and $model$ indicate observed or modeled values, respectively.

After fitting, the correlation coefficient between q_T and K_L was determined from the inverse of the Hessian matrix. If the correlation coefficient exceeded 0.90, the linear STM model (Equation 68) was used, otherwise a Langmuir STM model (Equation 67) was used. The threshold of 0.90 was chosen because using lower values resulted in a sharp increase in soils with clear Langmuir behavior being described as linear. Values above 0.90 were not used because this caused an increasing number of sorbent-sorbate pairs to be fit by Langmuir isotherms which leads to to significant estimation error in K_L.

Model parameter dependencies. It was necessary to determine the dependency of model parameters on sorbate and sorbent properties. The possible parameterizations are shown in Table 45. The first test attempted to determine if the time dependent K_P and K_L could be discerned on a sorbent/sorbate basis. A model with sorbent, sorbate, and adsorption contact time dependence in K_P and K_L was applied to each data set. Figure 78 shows estimated K_P for each MC, sorbent and asdorption contact time. The estimated K_P's were tested using a paired t-test [Walpole et al. 2007] against a null hypothesis that there was no difference between K_P for different adsorption contact times, t_{ads} At an $\alpha = 0.05$ it would be expected that 5% of the test would result in rejection of the null hypothesis by chance. Therefore, a Bonferroni correction [Dunn 1961] was applied to the value of α. For conducting N tests, the correct level of significance is αN. At this level of significance the null hypothesis was rejected for 7.5% of the 509 tests performed. Rejections of the null hypothesis predominantly corresponded to K_P estimated for high f_{OC} soils, but the rejection did not occur in a regular manner. TNT and DNT exhibit the greatest number of rejections of the null hypothesis. The expected behavior would be that K_P increases as adsorption contact time increases or remains constant. Figure 78 shows that several data sets show decreasing, or inconsistent changes in K_P. Thus, it was concluded that K_P and K_L were not changing with t_{ads}, hence the exclusion of an adsorption duration dependency for K_P in Table 45.

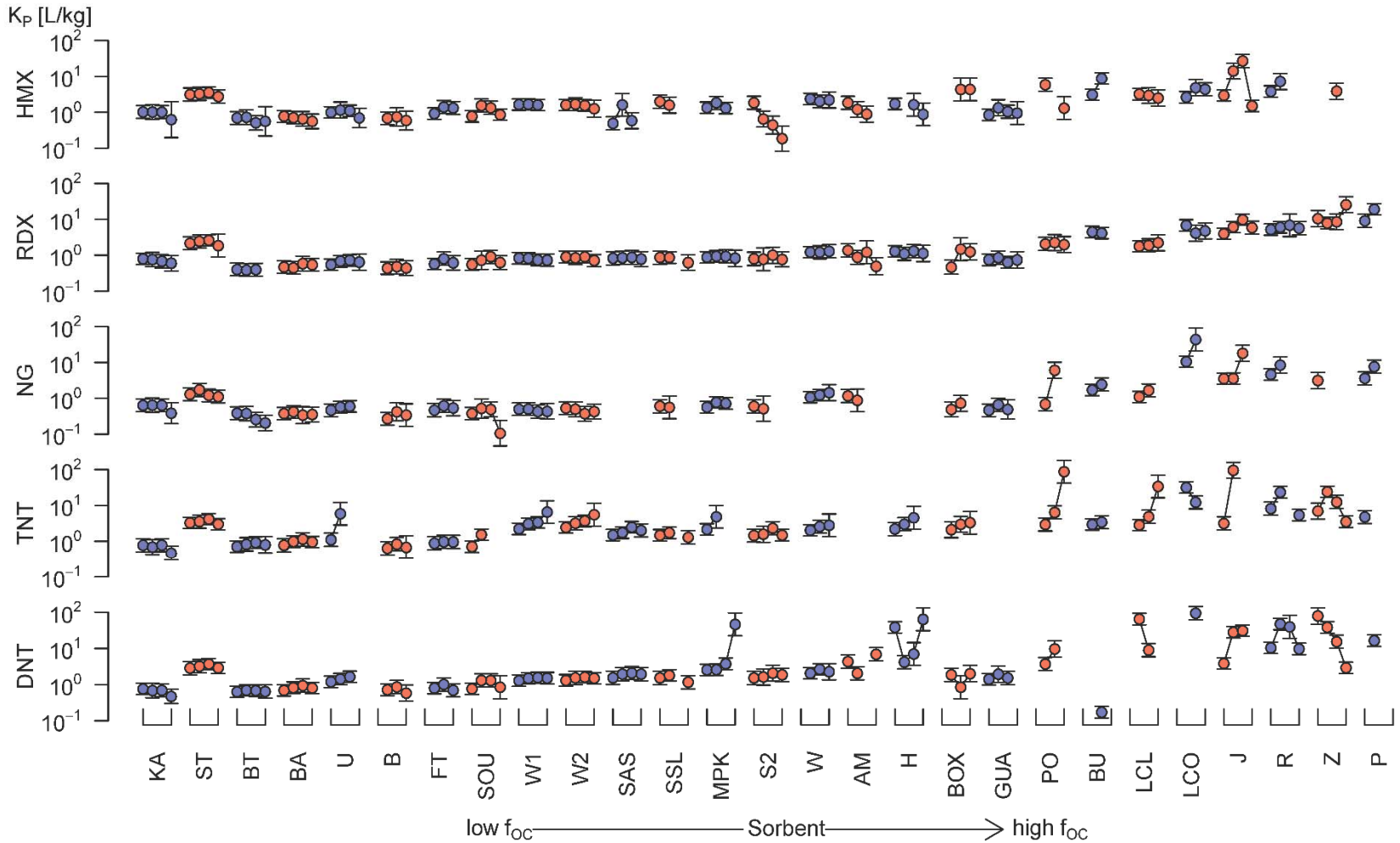

Figure 78. Comparison of K_P (mean $\pm$ std. error) determined for each MC (row) versus sorbent (ordered low to high f_{OC}). Adsorption contact time increases for each data set from left to right. Color alternates between sorbents. Connective line shows values related by data set.

Table 45. Possible STM parameter dependencies.

Parameter	Initial	Final
K_P	M[1], S[2], T[3]	M, S
K_L	M, S, T	M, S
f_{ST}	M, S, T	S, T

[1] Dependency on munition constituent
[2] Dependency on sorbent
[3] Dependency on adsorption contact time

The site transformation factor determines the extent of the conversion of weak sites to strong sites. It has previously been hypothesized that polymeric rearrangement of the sorbent is independent of sorbate (Weber et al. 1992; Lu and Pignatello 2002). This suggests that the site transformation factor may be independent of the sorbate, in this case the MC. Based on this suggestion, f_{ST} determined on a sorbent, sorbate, and adsorption duration were compared. The null hypothesis for this test was that there was no difference between MC specific f_{ST} for sorbent/adsorption duration pairs. The test alpha value, $\alpha = 0.05$ was corrected using the Bonferroni method. A total of 474 tests were performed, none of which resulted in a rejection of the null hypothesis. Therefore, it was concluded that f_{ST} was not changing with respect to MC.

These tests on K_P and f_{ST} yielded parameters dependent on the variables, shown below:

$$K_P = f(M, S) \tag{75}$$

$$K_L = f(M, S) \tag{76}$$

$$f_{ST} = f(S, T) \tag{77}$$

where M is a dependence on sorbate (munition constituent), S is a dependence on soil or reference sorbent, and T is dependent on the adsorption contact time. This parameterization of the model will be used for all further analysis of the data (Table 45).

Analysis of STM parameters. With parameter dependencies and isotherm choices resolved, the appropriate model parameters could be estimated. Data sets were grouped by sorbent and adsorption contact time for analysis. R and the *optim* method (R Core Team 2013) were used for estimating the parameters by minimizing the RMSE (Equation 74) of sorbed concentrations. The observed and modeled sorbed concentrations are shown for all MC and sorbents in Figure 79. The plot shows data grouped by the number of data points in a hexagonal region, with the number in the region indicated by the shade of the hexagon. The figure shows that observed and modeled values are in good agreement, as evident by the proximity of the majority of comparisons to the 1:1 line and the unbiased distribution thereof. Therefore, an analysis of estimated model parameters was conducted.

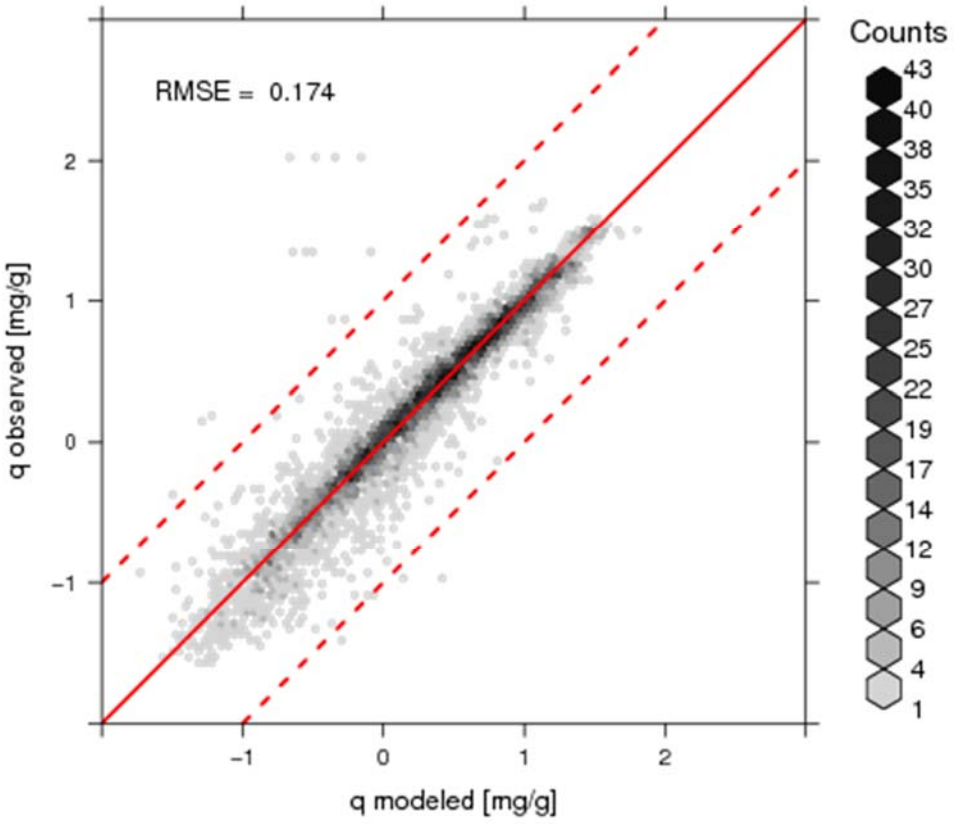

Figure 79. Comparison of STM predicted using estimated parameters and observed sorbed concentrations. Data is grouped into hexagons, the shading of which indicates the number of data. The red solid line indicates unity, dashed lines are spaced at 1 log unit from unity.

Binding constants - K_P and K_L. In the previous analysis, a multilinear model was used to correlate sorbent parameters with estimated partition coefficients. The multilinear model is:

$$K_P(i,j) = f_{OC}(i)K_{OC}(j) + f_{clay}(i)K_{clay}(j) \tag{78}$$

where $f_{OC}(i)$ and $f_{clay}(i)$ are the fractions, $[g/g]$, organic carbon and clay size particles, respectively, for sorbate i, and $K_{OC}(j)$ and $K_{clay}(j)$ are the site specific partition coefficients $[L/kg]$, for MC j. The estimated site specific partition coefficients are listed in Table 46. To contrast the multilinear model, a single site f_{OC} model was also used:

$$K_P(i,j) = f_{OC}(i)K_{OC}(j) \tag{79}$$

The single site model (dashed red line) shows good agreement with STM estimated partition coefficients for $f_{OC} > 0.1$ for HMX and RDX, and $f_{OC} > 0.01$ for NG, TNT and DNT (Figure 80). For soils above these thresholds, the dominant sorption site is organic carbon. Below these threshold values, deviation from a linear relationship is seen. This deviation is well predicted by the multilinear model (solid red line). The observed threshold for non-linear behavior, $f_{OC} < 10^{-2}$ corresponds to a value where $f_{OC}K_{OC}$ is approximately equal to K_{clay}, suggesting that below this threshold binding to clay size particle sites are the dominant sites for sorption. The

derivation of the multilinear model used soils that exhibited no Langmuir behavior. Therefore, an analysis of K_L using the multilinear model could not be performed.

Table 46. Multilinear model parameters for K_P [L/kg] (Equation 2).

MC	$log_{10}K_{OC}$	$log_{10}K_{clay}$
HMX	$1.74(\pm 0.0480)$	$0.596(\pm 0.0512)$
RDX	$1.37(\pm 0.0508)$	$0.315(\pm 0.0506)$
NG	$1.47(\pm 0.0782)$	$0.118(\pm 0.102)$
TNT	$2.07(\pm 0.0823)$	$0.789(\pm 0.102)$
DNT	$2.39(\pm 0.0883)$	$0.470(\pm 0.207)$

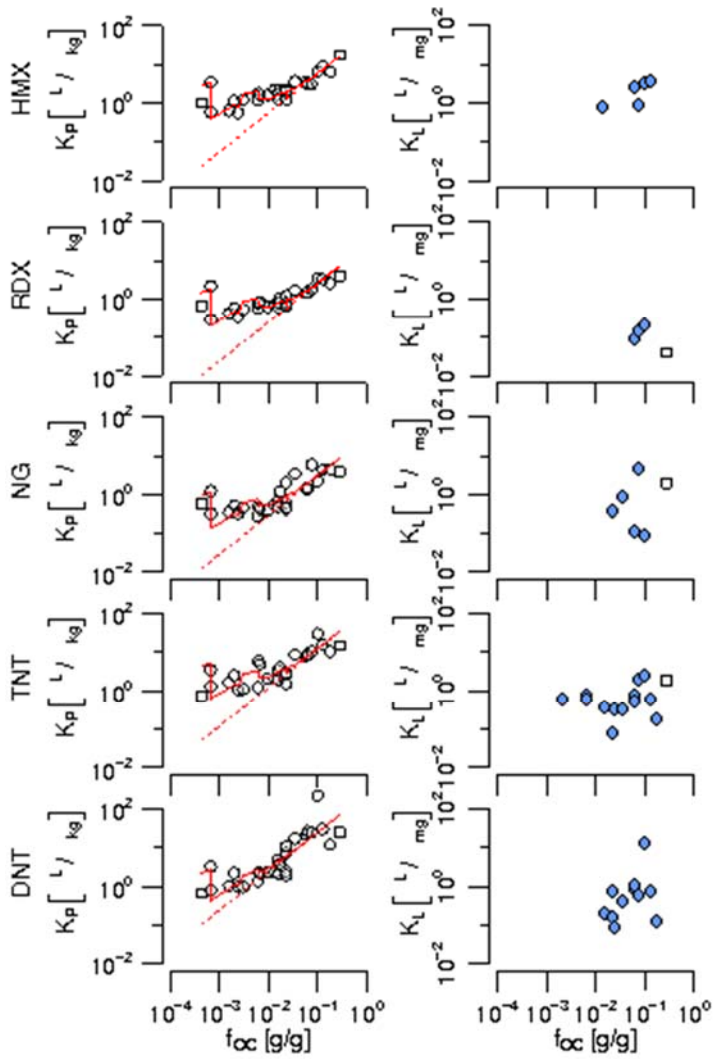

Figure 80. Partition coefficients, K_P, and Langmuir constants, K_L, estimated by STM (points). Solid red line shows K_P as predicted by the two-site multilinear regression, Equation 78. Dashed red line shows K_P predicted by a K_{OC} only model, Equation 79. Squares indicate reference sorbents not used in the multilinear regression.

Site Transformation Factor. Linear and Langmuir partition constants are well researched and used frequently in engineering practices. The site transformation factor, f_{ST}, is novel, however, and an investigation of its sorbent and sorbate relationships was conducted. The behavior was expected to be similar to the previously described Reversibility Fraction (Equation 66) which shows that soils with higher f_{OC} display greater hysteresis and that hysteresis is also a function of adsorption contact time (Figure 75). A plot of f_{ST} vs. fraction organic carbon, Figure 81, shows the relationship of the site transformation factor to f_{OC}. It is clear that the transformation factor is directly related to soil f_{OC} content, and that an increase in f_{OC} corresponds to a proportional increase in f_{ST}:

$$log_{10} f_{ST} = m_{ST} log_{10} f_{OC} + b_{ST} \quad (80)$$

where m_{ST} and b_{ST} are the slope and intercept of the regression.

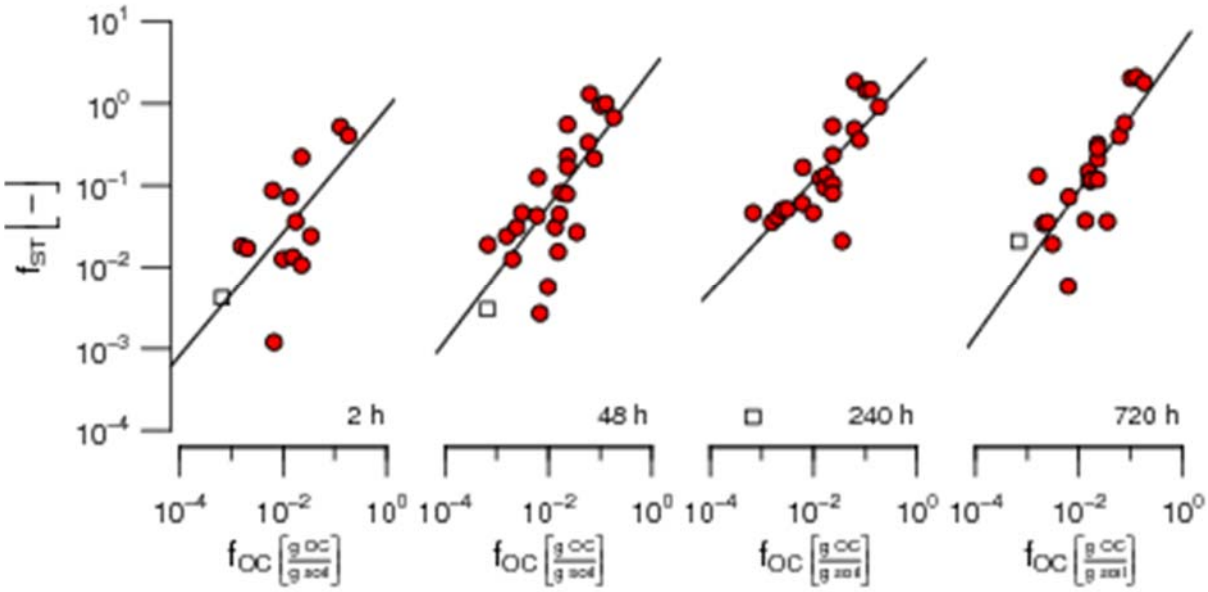

Figure 81. Estimated f_{ST} for each adsorption duration. Points are soils, squares are reference sorbents not used in the log-log regression. Line indicates log-log regression. Parameters listed in Table 47.

Table 47. Coefficients for regression on f_{ST} for 2, 48, 240, and 720 h adsorption contact times (Equation 80).

t_{ads}	m_{ST}	b_{ST}	R^2
2h	0.778 ($\pm$0.248)	0.0851 ($\pm$0.485)	0.457
48h	0.864 ($\pm$0.153)	0.573 ($\pm$0.304)	0.581
240h	0.709 ($\pm$0.109)	0.560 ($\pm$0.218)	0.665
720h	0.892 ($\pm$0.146)	0.837 ($\pm$0.281)	0.664

The four f_{ST} regressions were visually similar. The slope and intercept of a log-log regression for each contact time showed that the slopes were similar, while the intercepts increased as adsorption contact time increased (Table 47). The slopes and intercepts from are plotted against log_{10} (t_{ads}) to develop a model for the time dependence of the transformation, Figure 82.

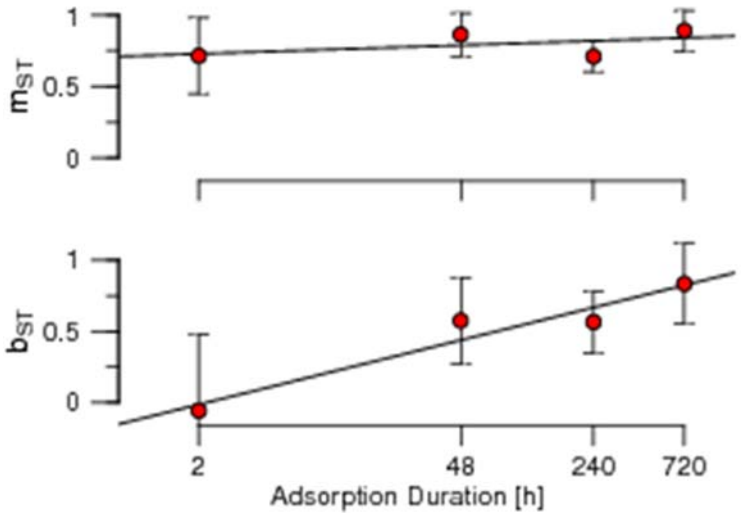

Figure 82. f_{ST} regression estimated slope,m_{ST}, and intercept, b_{ST}.

To develop a model for f_{ST}, regressions on m_{ST} and b_{ST} were developed. The regression of the slope parameter,

$$m_{ST} = 0.0189(\pm 0.0513) log_{10} t_{ads} + 0.777(\pm 0.105) \quad (81)$$

yields a constant value ($p = 0.749$). The intercept regression, however,

$$b_{ST} = 0.270(\pm 0.0549) log_{10} t_{ads} + 0.0256(\pm 0.112) \quad (82)$$

shows dependence in time ($p = 0.0388$), but no constant. Using these results a regression model for f_{ST} is fit to the data in Figure 82.

$$log_{10} f_{ST} = 0.820(\pm 0.0487)\ log_{10}(f_{OC}) + 0.280(\pm 0.0466)\ log_{10}(t_{ads}) \quad (83)$$

The model for f_{ST}, Equation 83, is applicable over the range of f_{OC} observed ($0.0043 \leq f_{OC} \leq 0.281$) and adsorption contact times ($2h \leq t_{ads} \leq 720h$). A plot of the regression predicted f_{ST} vs. STM estimated f_{ST} is presented in Figure 83. The regression (Equation 83) shows good agreement between estimated and predicted f_{ST} values. Reference sorbents were not used in the development of the regression, but show agreement with predicted values, with the exception of the 720h low f_{OC} sorbent.

The f_{ST} regression, Equation 83, indicates that the organic carbon content of the sorbent determines the extent of reversibility. This strongly suggests that organic matter transformation is the dominant mechanism for causing hysteresis in soil. Further, it supports the hypothesis that physical deformation is sorbate independent. Secondly, the strong dependence on adsorption contact time (t_{ads}) shows that a kinetic component may be the transformation of binding site strength. Chemical hysteresis has been suggested in other works as a function of organic carbon and contamination age, i.e. duration of adsorption (Nam et al. 1998).

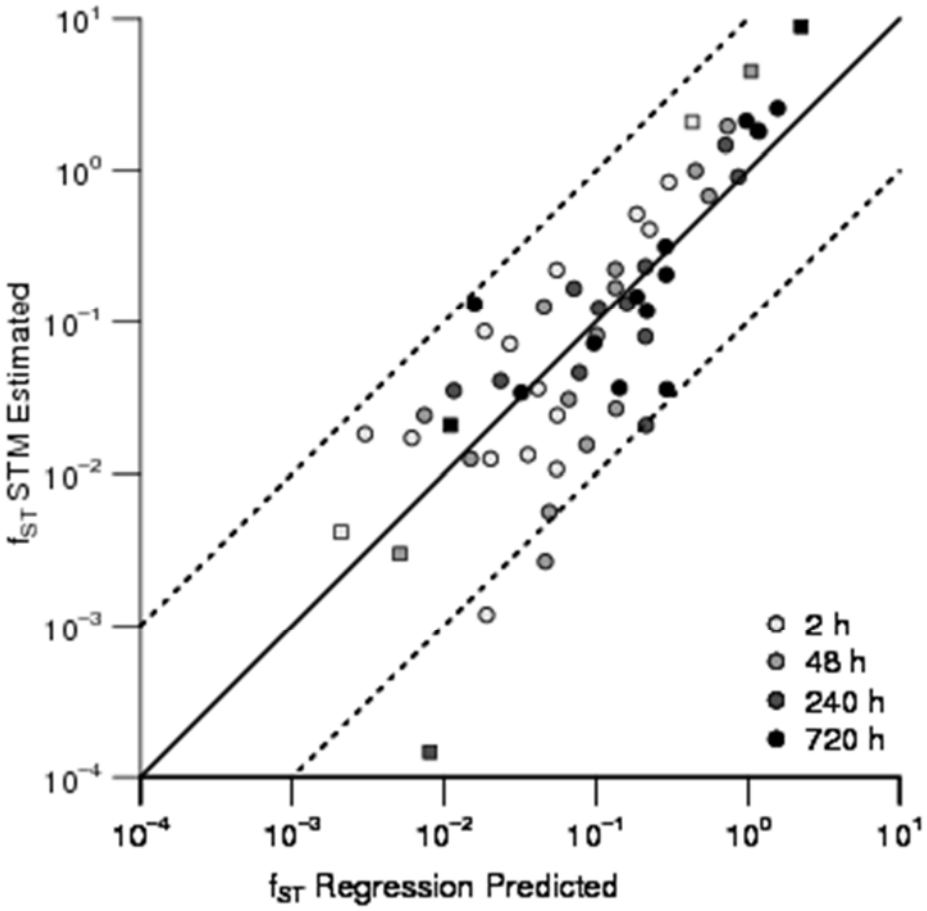

Figure 83. STM estimated f_{ST} vs. regression predicted (Equation 83) f_{ST}. Points are soils, squares are reference sorbents. Darker shading indicates increased adsorption contact time. Solid line indicates a unity comparison. Dashed lines indicate factors of 10.

There is a limitation to the empirical model of f_{ST} (Equation 83). It cannot be determined if there is a maximum f_{ST} as time increases, but since the transformation factor cannot increase indefinitely, it must have a maximum value. Establishing the appropriate dependence will require further investigation.

Comparing Reversible/Resistant and Site Transformation models. Understanding the time dependent behavior of hysteresis is vital to accurate assessment of sorption. In the preceding analysis the reversible/resistant (RR) model was used to describe the data. In the RR model, the time component was not treated explicitly. Rather each adsorption contact time used a different partition coefficient. In contrast, the STM uses only a single partition coefficient for each MC and soil. The time dependence is found only in the site transformation factor, f_{ST} (Equation 83). Therefore the STM can predict both adsorption and desorption hysteretic behavior using only f_{OC} and the adsorption contact time, t_{ads}.

To compare these two models, the RMSE (Equation 74) was calculated for both the RR (Equation 53) and STM (Equations 67 and 68). Both models used estimated parameters (Appendix J for RR partition coefficients, Appendix K for STM parameters) to compare a best case scenario. The log_{10} ratios of RMSE_{RR} and RMSE_{STM} for each MC and sorbent are shown in

Figure 84A. The grey shaded bars correspond to soils for which Langmuir isotherms are used. Positive values indicate reduced RMSE when the STM is applied. In comparison to the RR model the STM is more accurate at predicting sorbed concentrations, as shown by the number of positive RMSE reductions. This is especially true for the higher f_{OC} sorbents which show dramatic improvement for the STM as f_{OC} increases. Several soils showed no improvement, predominantly for RDX which showed greater RMSE_{STM} for the middle third of f_{OC} soils. The RMSE_{STM} for RDX on these soils was an average of 31.4% greater than the corresponding RMSE_{RR} , however for soils with $f_{OC} > 0.03$ predictions improved by an average of 72%. For TNT the improvement was greater. Average improvement for sorbents with $f_{OC} > 0.03$ was 76%.

When comparing the RMSE for different adsorption contact times, error decreases in each case, Figure 84B, indicating that the single time dependent parameter, f_{ST} is sufficient to describe hysteretic behavior independent of sorbent properties.

Multilinear STM predictive model. The RR model requires four sorbate parameters ($K_{OC,x}, K_{OC,0}, K_{clay,x}, K_{clay,0}$) and two sorbent parameters (f_{OC} and f_{clay}) to predict sorbed concentrations. These parameters are adsorption contact time specific and no relationship has been found between them. In contrast, the STM requires two sorbate parameters (K_{OC}, K_{clay}), two sorbent parameters (f_{OC}, f_{clay}), and the adsorption contact time (t_{ads}) to estimate sorbed concentrations. As a measure of the predictive capabilities of the STM, the multilinear model, Equation 78, and f_{ST} regression, Equation 83, were added to the STM.

$$q_A(i,j) = \left(f_{OC}(i)K_{OC}(j) + f_{Clay}(i)K_{Clay}(j)\right)C_A(i,j) + f_{ST}(i)\left(f_{OC}(i)K_{OC}(j) + f_{Clay}(i)K_{Clay}(j)\right)C_A(i,j) \quad (84)$$

$$q_D(i,j) = \left(f_{OC}(i)K_{OC}(j) + f_{Clay}(i)K_{Clay}(j)\right)C_D(i,j) + f_{ST}(i)\left(f_{OC}(i)K_{OC}(j) + f_{Clay}(i)K_{Clay}(j)\right)C_D(i,j) \quad (85)$$

where i and j refer to sorbent i and sorbate j respectively and f_{ST} is given by Equation 83. As there was no suitable method for predicting K_L, the Langmuir data sets were not included. A comparison of observed and modeled sorbed concentrations is shown as Figure 85. The figure shows that the data is well represented by the modeled values. No apparent bias is observed. Further, the RMSE (Equation 74) is low, RMSE = 0.283. This value is a small increase to the fit model RMSE of 0.186.

To determine if there are sorbent specific biases, residuals were calculated between observed and predicted sorbed concentrations, Figure 86. Linear data is well described by the multilinear model, with most data within a factor of 2. It is difficult to determine if the model predicts well for high f_{OC} sorbents since most data were fit using Langmuir isotherms. However, HMX, RDX, and NG show several data sets that are in close agreement with predictions.

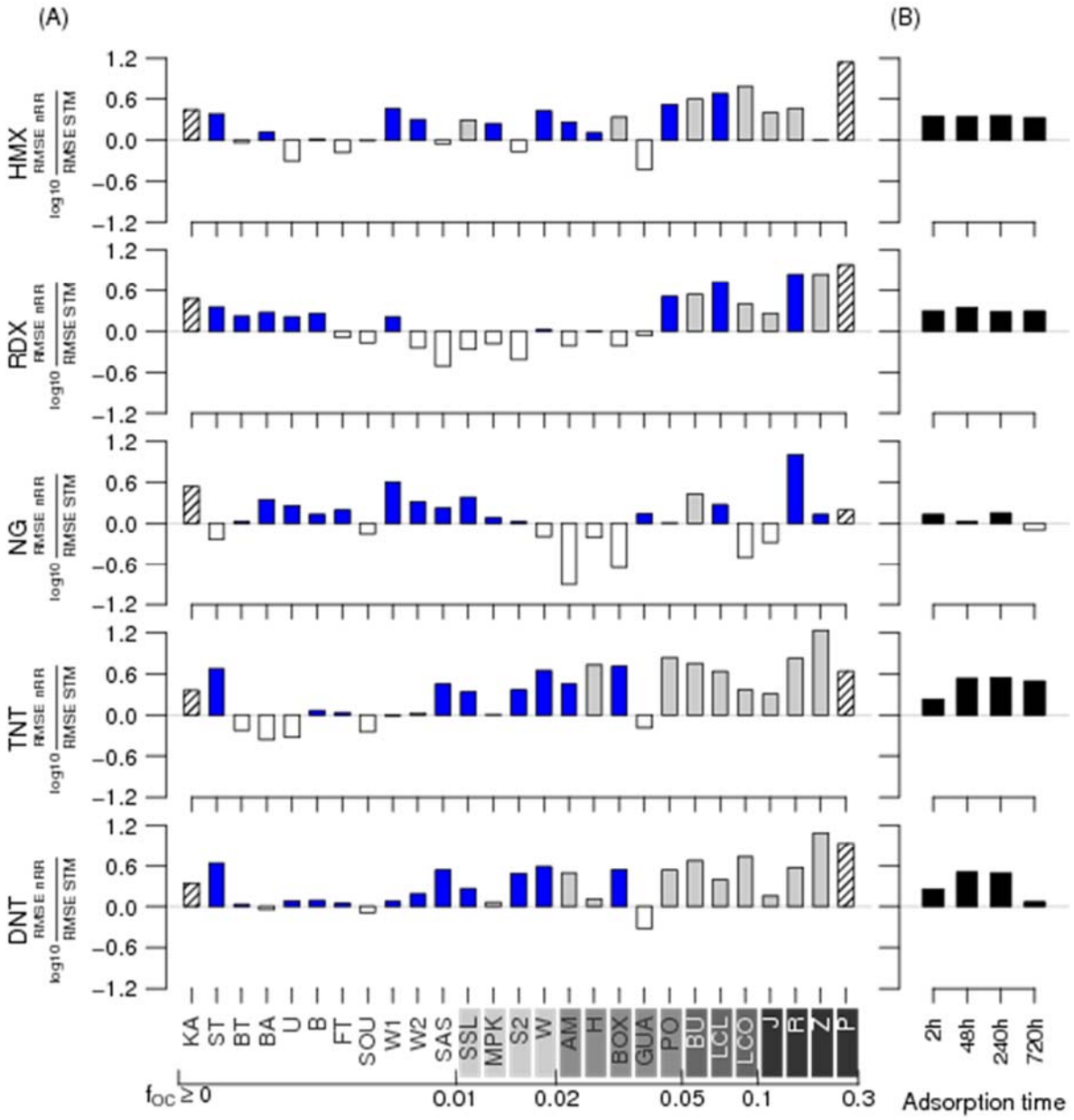

Figure 84. log_{10} ratio of RMSE, RR:STM, for predicted sorbed concentrations. (A) RMSE calculated for each sorbent. (B) RMSE for each adsorption duration. Bars are colored for positive values and hollow for negative values. Filled bars are soils. Hashed bars are reference sorbents. Grey shaded bars correspond to soils for which Langmuir isotherms are used. Axis shading indicates increasing f_{OC}.

Conclusions regarding the Site Transformation Model. The STM incorporates binding strength changes and can reproduce the observed hysteretic sorption. In comparison to other models, the STM requires only one time dependent parameter, the site transformation factor, f_{ST}, significantly reducing the number of parameters that need to be estimated. Moreover, the relationship to f_{OC} and length of adsorption contact time makes physical sense within the framework of glassy/rubbery soil organic carbon sorption. An implication of this observation is that short adsorption contact times and/or low f_{OC} sorbents lead to highly reversible systems,

regardless of the sorbate. This observed sorbate independence supports the hypotheses posed by other researchers and is further evidence for a sorbent transformation process. The new parameter, f_{ST} , requires further analysis to determine if it is bounded, since the current data suggests a log-linear trend in relation to the duration of adsorption. Inclusion of the STM in partitioning models is recommended.

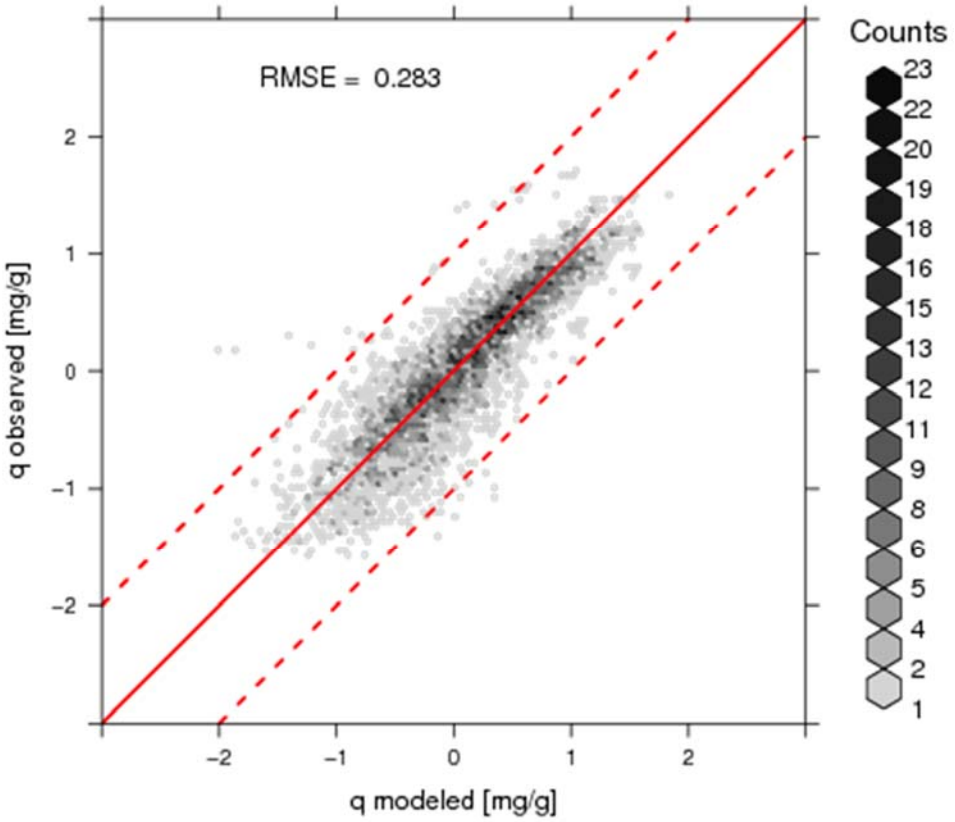

Figure 85. Comparison of STM predicted using predicted parameters and observed sorbed concentrations. Data is grouped into hexagons, the shading of which indicates the number of data. The red solid line indicates unity, dashed lines are spaced at 1 log unit from unity.

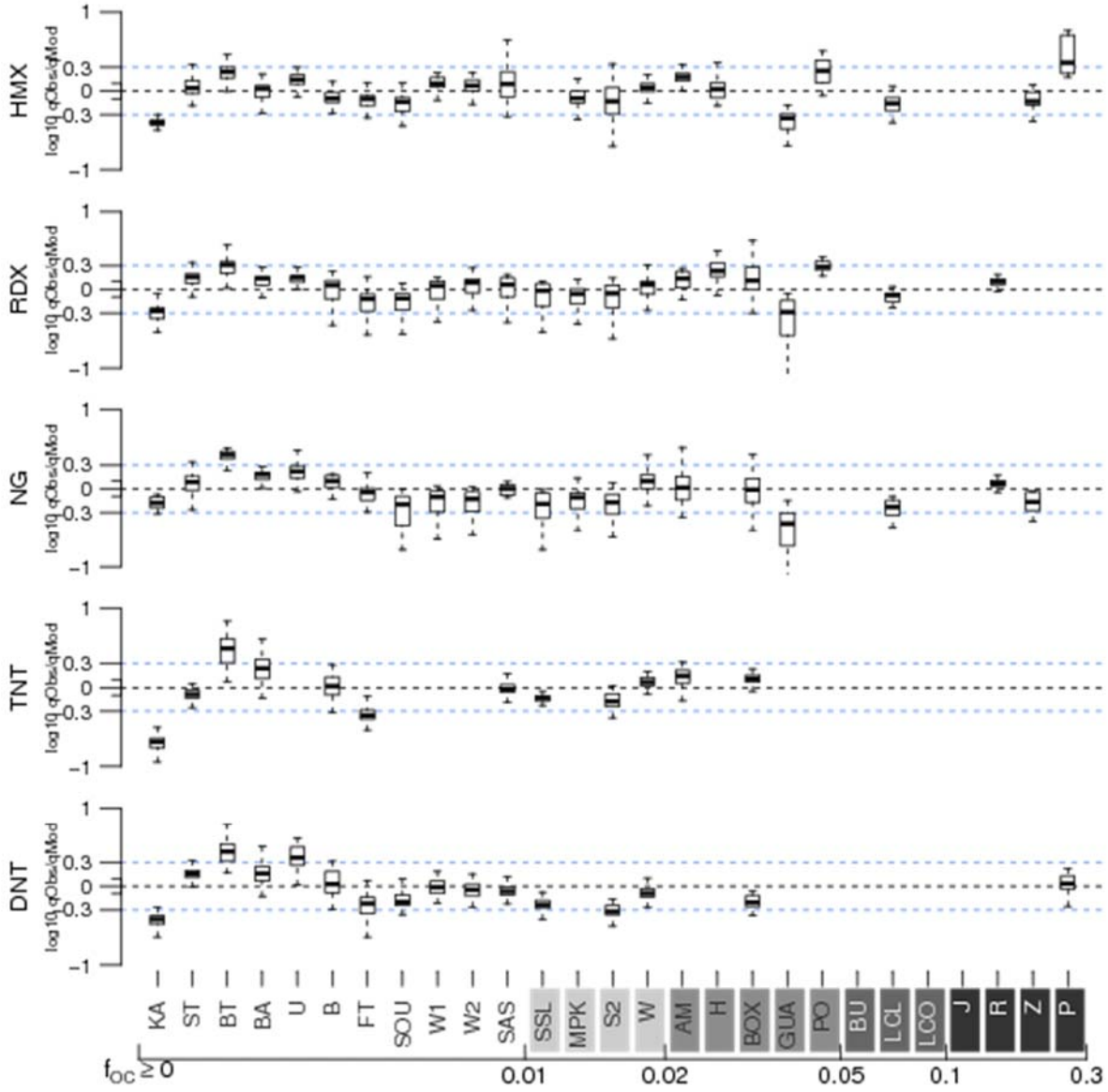

Figure 86. Linear prediction of sorbed concentrations for each MC and sorbent using Eqs 19 - 20 and 18. Langmuir data was not included. Axis shading indicates increasing f_{OC}.

Transport of MC in the Soil Column. The soil column study was designed to provide initial validation of the detailed partitioning study that had been conducted using batch equilibration of soils with MC. This study was conducted using a flow-through column system adapted from Monteil-Rivera et al. [2011] to confirm the reversible and resistant fate and transport model of adsorption and desorption.

Results. After the initial flow-through with electrolyte and biocide only (Solution (1)) with a volume equal to 22 pore volumes, Solution (2) with TNT, RDX, and chloride tracer was introduced to the column as shown in Figure 9. After 24 h, the drip solution was switched back to Solution (1) for an additional 24 h. Breakthrough curves for TNT, RDX and chloride are shown in Figure 87.The RDX outflow curve was similar to that of chloride, lagging behind

slightly but still reaching 100% of the inflow concentration after 10 to 12 h. The chloride concentration peaked at about 4 hrs. Both RDX and chloride remained at 100% through the 26th hour (Figure 87). Conversely, TNT concentration in the outflow lagged far behind, reaching a peak of 58% of the original inflow after 26 h. Following Solution (1) re-initiation, TNT in the outflow declined at a slower rate than RDX and chloride.

Modeling column results. To model the data, an advective, diffusive model was used. The transport model applied the Reversible Resistant Model for partitioning [Di Toro and Horzempa 1982]. The modeled column was composed of 200 segments ($\Delta x = 0.05$ cm) of equal size to mitigate the effects of numerical dispersion. To fit the diffusion coefficient, the model used a single value for all three species. Selected properties of the soil used in the experiment and of others used in simulations are given in Table 48.

Partitioning was controlled using the Reversible Resistant (RR) Model. This model has not been applied to column studies previously. The RR model, Equations 86-88, describes partitioning by allowing sorption to two sorbent sites: a reversible site that is always in equilibrium with the aqueous phase, and a resistant site that is in equilibrium only while adsorbing. In this way, hysteresis is defined by the lack of desorption from the resistant sites. Each site is defined by a partition coefficient, K_{px} for reversible sites and K_{p0} for resistant sites. The corresponding sorbed concentration is q_X or q_0 for reversible and resistant concentrations, respectively.

$$C_{tot} = C_d + m_{sw}q_x + m_{sw}q_0 = C_d + C_x + C_0 \tag{86}$$

$$C_{px} = m_{sw}K_{px} \tag{87}$$

$$C_{p0} = m_{sw}K_{p0} \tag{88}$$

where C_{tot} is the total bulk concentration (mg L^{-1}), C_d is the aqueous phase concentration (mg L^{-1}), m_{sw} is the soil-water ratio (kg L^{-1}), q_X and q_0 are the reversible and resistant sorbed concentrations per unit sorbent, respectively (mg kg^{-1}), C_x and C_0 are the bulk concentrations of the reversible and resistant sorbed concentrations per unit sorbent, respectively (mg L^{-1}), and K_{px} and K_{p0} are the partition coefficients for the reversible and resistant components, respectively (L kg^{-1}).

The resulting advective-diffusive-resistant model depends on whether the sorbent is adsorbing, i.e. adding chemical to the sorbed phase, or desorbing, i.e. depleting the sorbed phase

$$V_i \frac{\mathrm{d}C_{tot,i}}{\mathrm{d}t} = QC_{d,i-1} - QC_{d,i} + \frac{DA}{l}\left(C_{d,i-1} - C_{d,i}\right) + \frac{DA}{l}\left(C_{d,i+1} - C_{d,i}\right) - k_r C_{d,i} V_i \tag{89}$$

$$C_d = \begin{cases} \dfrac{C_{tot}}{1 + m_{sw}K_{px} + m_{sw}K_{p0}} & \text{During adsorption} \\ \dfrac{C_{tot} - C_0}{1 + m_{sw}K_{px}} & \text{During desorption} \end{cases} \tag{90}$$

$$C_0 = m_{sw}K_{p0}C_a \tag{91}$$

where V_i is the volume of layer i [L^3], $C_{tot,i}$ is the total concentration in layer i [mg L^{-1}], Q is the volumetric flow rate of the aqueous phase [L^3 min^{-1}], $C_{d,i}$ is the dissolved concentration for layer

i [mg L^{-1}], D is the effective diffusion coefficient [cm^2 min^{-1}], A is the interfacial area between layers [cm^2], l is the diffusive length [cm], k_r is a first order degradation rate [min^{-1}], K_{px} is the reversible partition coefficient [L kg^{-1}], K_{p0} is the resistant partition coefficient [L kg^{-1}], m_{sw} is the soil-water ratio [kg L^{-1}], C_a is the aqueous concentration at the end of the adsorption period [mg L^{-1}], and C_0 is the resistant concentration [mg L^{-1}].

Fit variables were, D, K_{px}^{RDX}, K_{p0}^{RDX}, k_r^{RDX}, K_{px}^{TNT}, K_{p0}^{TNT}, k_r^{TNT}. Chloride was assumed to only be in the dissolved phase, $m_{sw}K_{px} = m_{sw}K_{p0} = 10^{-9}$ where 10^{-9} is used as a lower limit due to model requirements. The remaining variables were fit by Matlab using a pattern search algorithm that minimized the linear sum of squares between observed and modeled aqueous concentrations.

Figure 88 shows the fit of the advective-diffusive-reversible/resistant model. For all three chemicals, the dissolved concentration is well predicted. Chloride and RDX show no resistant component, while TNT shows the presence of a small amount of resistance. It should be noted that although there is little difference between the reversible/resistant dissolved concentration and the completely reversible case for TNT, the optimization did converge to a non-zero resistant partition coefficient. This suggests that hysteretic processes are occuring within the column. The lack of a resistant component for RDX is not unexpected as the batch studies did not show resistant sorption for SSL soil. Model optimized parameters are shown in Table 49.

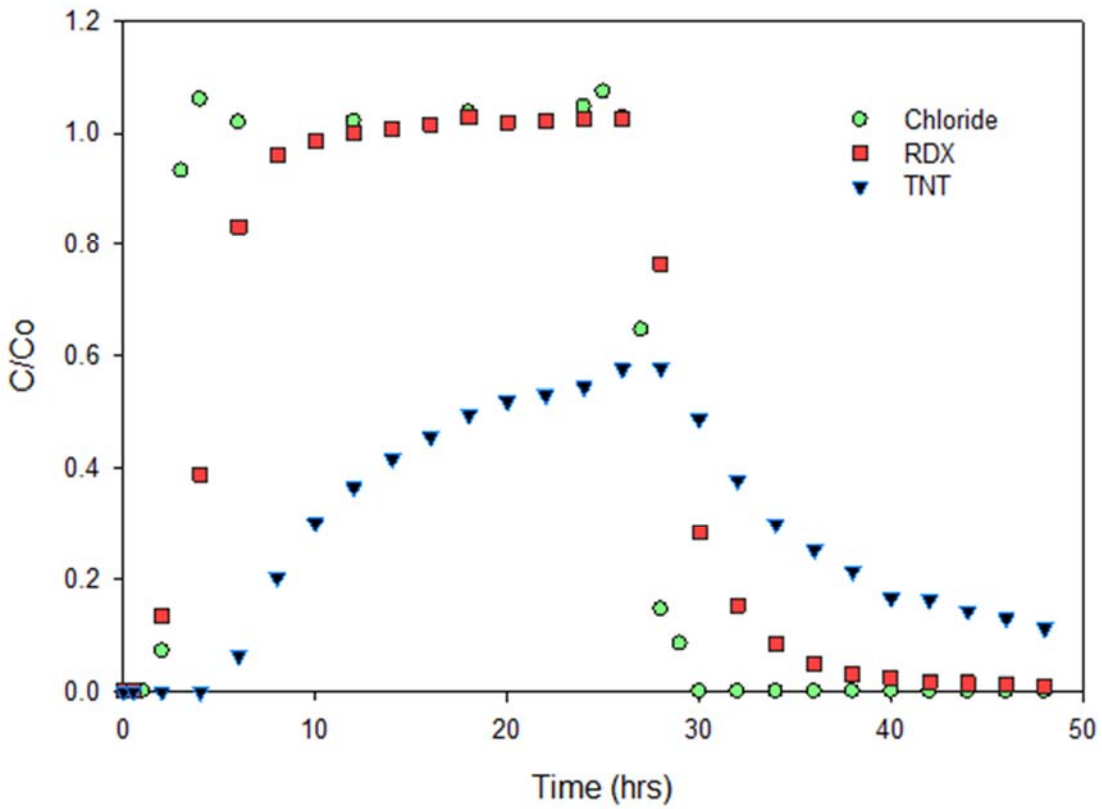

Figure 87. Break-through curves for RDX, TNT, and chloride (tracer).

Table 48. Soils used in the reversible/resistant analysis of column data.

	TOC	Sand	Silt	Clay
	[%]	[%]	[%]	[%]
SSL*	1.33	55	28	18
Aberdeen BT	0.07	83.8	7.1	9.1
Souli	0.61	42.4	14.4	43.2
Houthalein	2.31	85.9	10.1	4
Rhydtalog	12.83	43.8	43.7	12.5
Zegveld	18.23	45.8	32.5	21.7

* indicates the soil used for column experiments

Table 49. Matlab pattern search optimized parameters.

		Species		
		Cl	RDX	TNT
D	($cm^2\ s^{-1}$)	3.98×10^{-3}	3.98×10^{-3}	3.98×10^{-3}
$m_{sw}K_{px}$	(-)	$1\times10^{-9*}$	0.0703	4.68
$m_{sw}K_{p0}$	(-)	$1\times10^{-9*}$	$1\times10^{-9*}$	0.250
k_r	(s^{-1})	0.00	1×10^{-12}	2.2×10^{-5}

* Model lower limits were 1×10^{-9} for $m_{sw}K_{px}$ and $m_{sw}K_{p0}$ and 1×10^{-12} for k_r. These values approximate 0.

To check the validity of the model optimized parameters, the previously discussed multilinear models for reversible and resistant partition coefficients, Equations 14 and 15, were used.

$$K_{px} = f_{OC} K_{OC,x} + f_{clay} K_{clay,x} \tag{14}$$

$$K_{p0} = f_{OC} K_{OC,0} + f_{clay} K_{clay,0} \tag{15}$$

The multilinear derived partition coefficients, as well as sorbent matrix partition coefficients, are shown in Table 50.

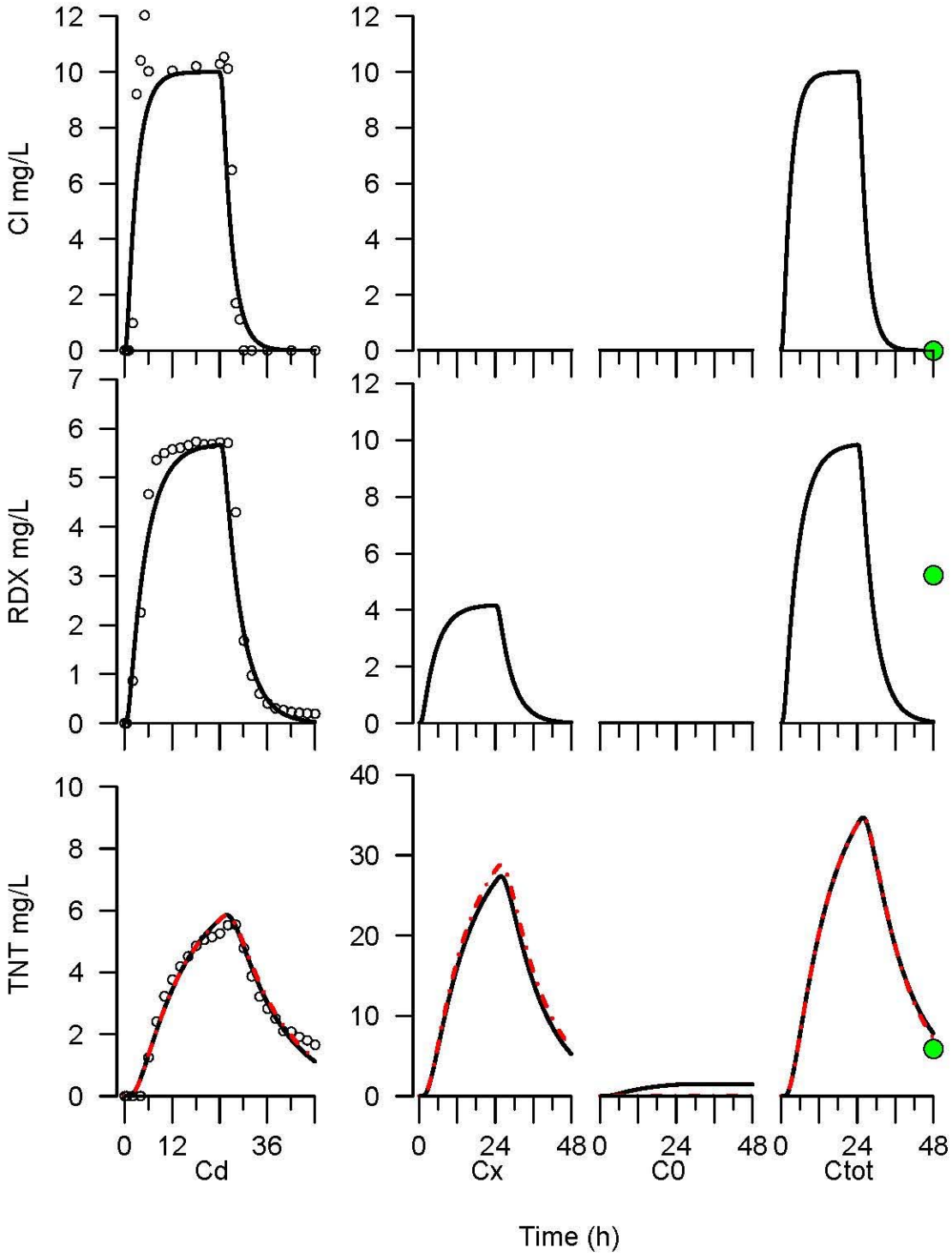

Figure 88: Fit to bottom segment of the column. Black lines are hysteretic model. Red line denotes reversible model. Points on C_d plots are observation concentrations. Green points in C_{tot} plots denote extracted concentrations.

Table 50. Multilinear model coefficients used (from Table 43) and derived partition coefficients for six soils. * indicates the soil used in this experiment.

	$K_{OC,x}$	$K_{OC,0}$	$K_{clay,x}$	$K_{clay,0}$
RDX	28.9	7.61	2.54	0.154
TNT	65.6	66.2	4.15	0.455

		Soil					
		SSL*	BT	SOU	H	R	Z
RDX	$m_{sw}K_{px}$	0.843	0.251	1.274	0.770	4.03	5.82
	$m_{sw}K_{p0}$	0.129	0.0193	0.113	0.182	0.996	1.42
TNT	$m_{sw}K_{px}$	1.62	0.424	2.19	1.68	8.94	12.9
	$m_{sw}K_{p0}$	0.965	0.0877	0.600	1.55	8.55	12.2

Multilinear derived partiton coefficients for TNT compare favorably to those obtained from the pattern fit. RDX pattern fit values for $m_{sw}K_{px}$ compare favorably to multilinear model derived values, however, predicted $m_{sw}K_{p0}$ from each model are markedly different. The pattern optimized partition coefficient for RDX is effectively zero but the mutlilinear resistant partition coefficient is >>0 ($m_{sw}K_{p0}$ = 0.129). It was hypothesized that the pattern fit optimized value was merely an artifact of a small extent of resistant sorption. To test the validity of this hypothesis, a sensitivity analysis was performed. It was found that a value of K_{p0} = 0.0316 showed an increase in the resistant sorption without significantly affecting the observed aqueous concentrations. This sensitivity limit (SL) value is much closer to a multlinear (ML) model predicted partition coefficient ($K_{ML,0}$ = 0.129, $K_{SL,0}$ = 0.0316).

Extractions had been performed on the column to better determine the sorbed phase chemical after a flushing period. Extracted TNT was found at an average concentration of 2.39±0.248 μg g^{-1} wet soil. The advective, diffusive model predicts a concentration of 2.91 μg g^{-1} wet soil indicating that the modeled and observed concentrations are similar. RDX, however, was extracted at a concentration of 0.722±0.0644 μg g^{-1} wet soil for the top 6 cm of the column and 2.12±0.00451 μg g^{-1} wet soil for the bottom 2 cm. No satisfactory explanation for the observed RDX extracted concentrations has been forthcoming. Further research is required to rectify the observed increase in extracted concentrations at the lower portion of the column.

Although the resistant concentrations obtained in the column are low, especially for RDX, it is important to note that field sites show significantly greater depth than a laboratory experiment can conveniently use. The advective, diffusive model would suggest that over longer column depths, a larger fraction of the total mass of MC will sorb to resistant sites. To this end, a simulation of a 3 m column was performed. Model parameters were the same as shown in Table 49 with the exception of $m_{sw}K_0^{RDX}$ which was set to the sensitivity value of 0.0316. Simulation parameters were the same with the exception of the feed periods. The MC solution was allowed to run for 9 days and then a flushing solution was simulated for a further 9 days. The results of this simulation are shown in Figure 89.

Over the 3 m depth of the column, approximately 1.8% of the total RDX mass added remained resistantly bound. If this same behavior were occurring in the 10 cm column, it would be

expected that less than 0.1% of the input mass would be resistantly bound. Using influent and effluent concentrations of RDX will show little if any deviation in total mass recovered due to the associated error in each measurement. Thus, the resistantly sorbed component would be unable to be distinguished from experimental uncertainty. Checkai et al. [1993] has shown that there is a small but measurable soil carrying-capacity for RDX in field contaminated soil.

TNT shows similar behavior to RDX initially, but due to degradation the resistant concentrations decrease as depth increases. However, despite this loss of mass 4% of the total TNT added to the column is retained in the resistant sites. Without a resistant analysis this resistantly bound portion would likely be described as degraded.

As a final simulation, the multilinear model was used to predict the effect of a resistant component in 5 soils that have previously been used for batch testing. These soils were chosen as examples of a range of behavior that would be expected in the field. Soils chosen were, Aberdeen BT, Souli, Houthalein, Rhydalog, and Zegveld. The simulation parameters used are shown in Table 51.

Table 51. Parameters used for simulation of 5 soils using multilinear model derived partition coefficients.

Parameter	Value	Units	Parameter	Value	Units
Adsorption period	36	h	Duration Simulated	120	h
Diameter	2.2	cm	Column Length	20	cm
Flowrate	0.2	mL min^{-1}	Pore volumes per day	0.127	d^{-1}
Porosity	0.482*				

* Estimated from the difference in volume between dry and hydrated soil.

Figures 90 and 91 show the predicted dissolved and resistant components for RDX and TNT respectively, for each of the soils using the multilinear derived partition coefficients or the fully reversible model.

From these figures it can be observed that despite a significant amount of resistant sorption, dissolved concentrations are similar between the reversible and the Reversible/Resistant models regardless of depth or time. Aberdeen BT (f_{OC} = 0.07%) and Zegveld (f_{OC} = 18.23%) soils differ by a factor of 250× in their OC content, yet show little difference in the dissolved concentration exiting the column at any time despite the addition of a much larger resistantly bound concentration in Zegveld soil. This indicates that dissolved concentrations alone are not enough to show if an experiment exhibited resistant sorption.

TNT exhibits depth dependent resistant sorption, whereas RDX does not. This is due to the degradation of TNT. As chemical penetrates the column, the loss in TNT mass allows for less chemical to partition to both the reversible and resistant sites.

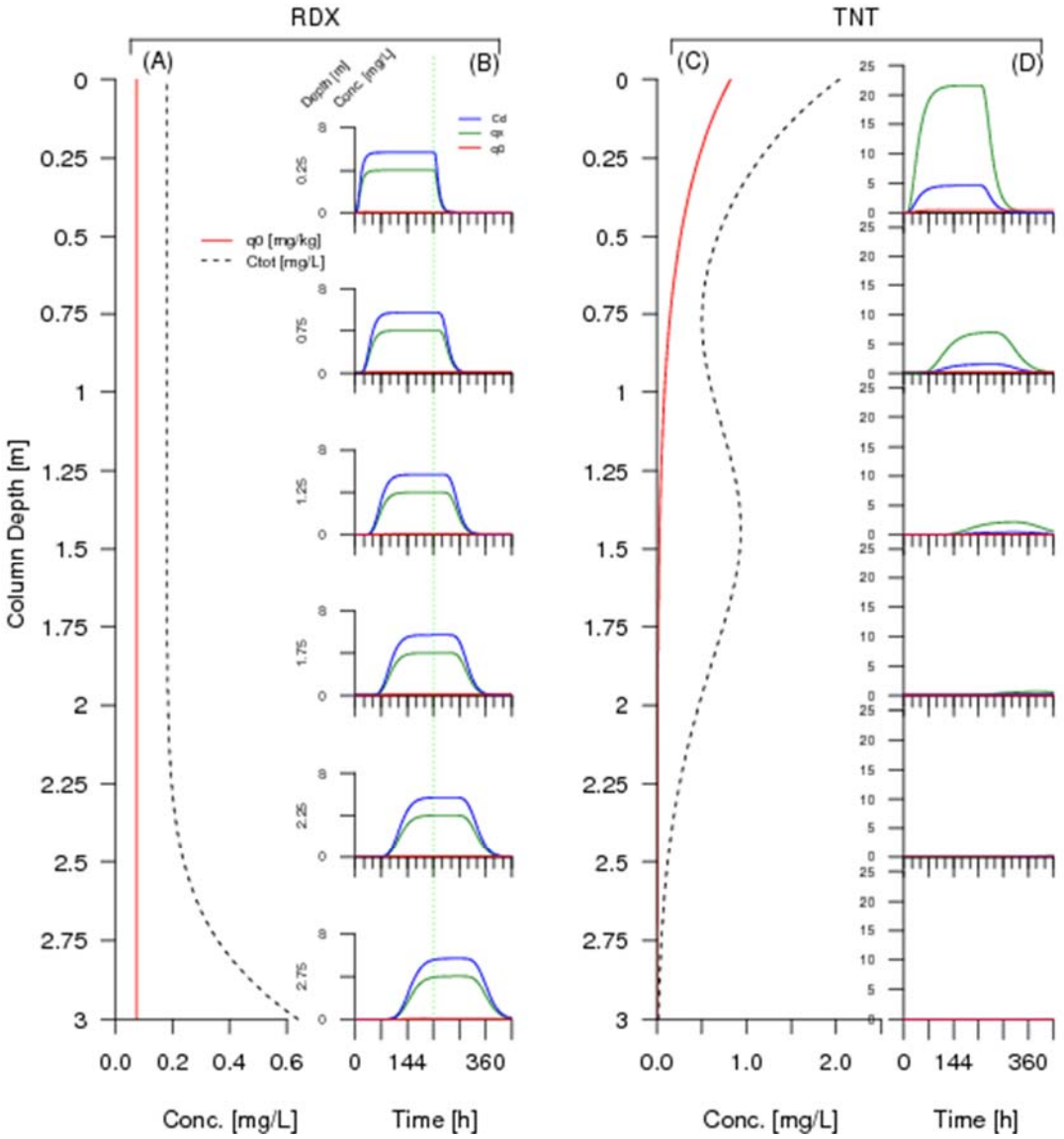

Figure 89. RDX and TNT sorption over a simulated 18 d experiment using the Matlab optimized fit parameters and $K_{px}^{RDX} = 0.0316$. (A) Total concentration RDX ($C_d + C_X + C_0$) as the dashed black line and resistant concentration (q_0) as the red line the end of the flushing cycle (t =432 h) as a function of column depth. (B) Dissolved and resistant RDX concentrations as a function of time for several column depths. (C) Total concentration TNT as the dashed black line and resistant concentration as the red line the end of the flushing cycle as a function of column depth. (D) Dissolved and resistant TNT concentrations as a function of time for several column depths.

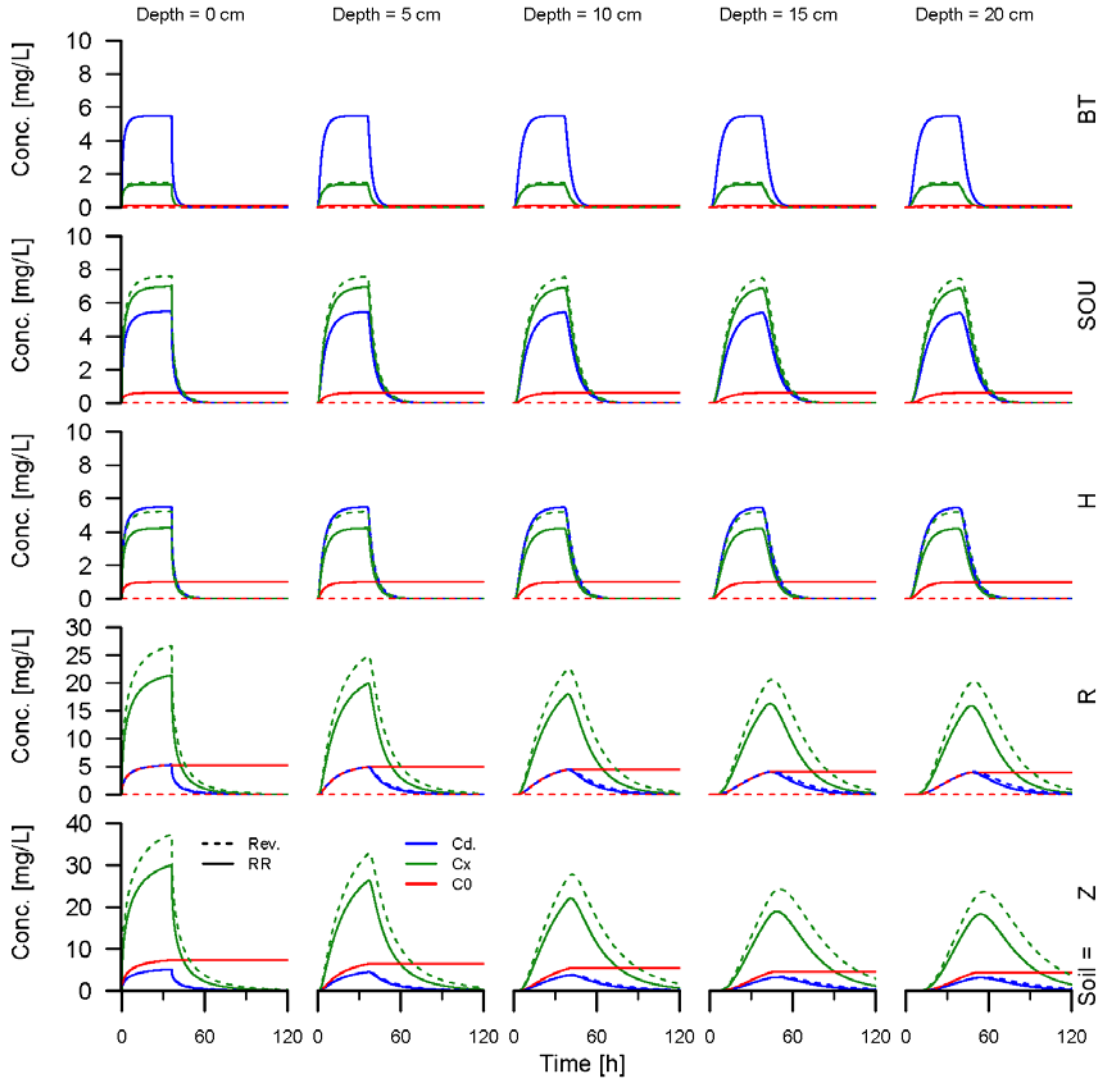

Figure 90. RDX components C_d, C_X and C_0 (blue, green, and red, respectively) for five soils: Aberdeen BT (BT), Souli (SOU), Houthalein (H), Rhydtalog (R), and Zegveld (Z). Soil properties are given in Table 48. Depth increases from left to right. Dashed line indicates a reversible model predicted concentration. Solid lines indicate a reversible resistant model predicted concentration.

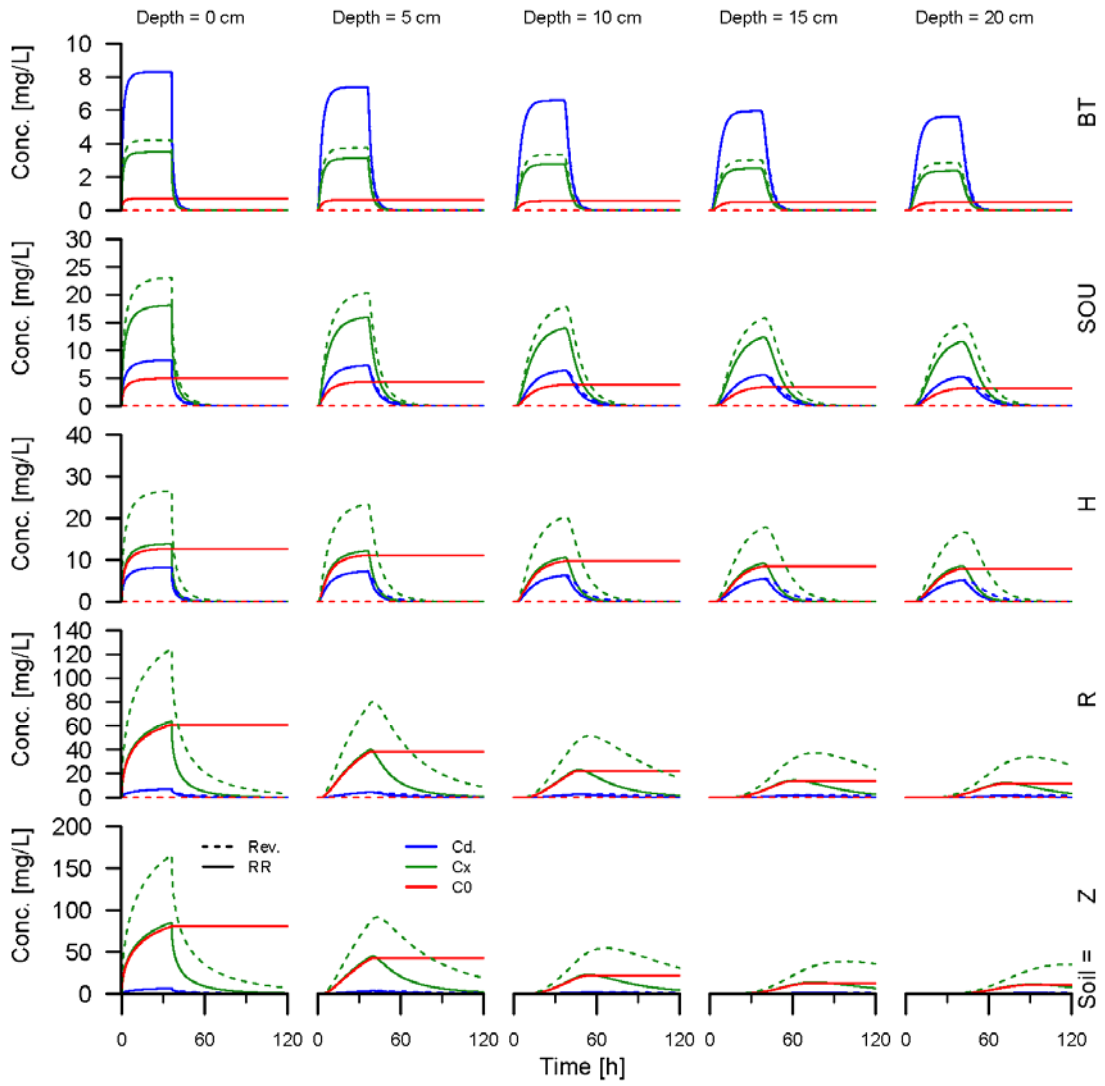

Figure 91. TNT components C_d, C_X and C_0 (blue, green, and red, respectively) for five soils: Aberdeen BT (BT), Souli (SOU), Houthalein (H), Rhydtalog (R), and Zegveld (Z). Soil properties are given in Table 48. Depth increases from left to right. Dashed line indicates a reversible model predicted concentration. Solid lines indicate a reversible resistant model predicted concentration.

For all soils, a large amount of TNT is resistantly sorbed. RDX also resistantly sorbs, though less so, for all except Aberdeen BT soil. The non-zero resistant sorption of both of these chemicals is a point of concern. The effects of resistant sorption may not be detected in laboratory scale columns, without accurate extractions of the sorbed component, due to the small concentrations. If these are overlooked, resistant sorption at field scale depths will go undetected and unaccounted for in laboratory systems.

Conclusions from column study. The implications from this analysis of resistance to desorption are significant. It is evident that extractions are needed to accurately determine the mass

remaining on the column soil. Further, there is a clear need for larger, and especially longer, soil columns in experimental work. This need arises from the small fractions of resistantly sorbed material in a typical laboratory scale experiment. As shown by the simulation of 5 soils, soil characteristics greatly affect the amount of resistant sorption. It is suggested that a soil exhibiting significant resistant properties be used to measure the potential for long term sequestration of MC in the field. Application of more rigorous methods of modeling resistant sorption should aid in determining a mechanism for the observed sorption and whether it is truly irreversible.

Sorption and Release of MC by Nitrocellulose. The sorption and desorption experiments were performed separately for NG and 2,4-DNT. A series of solution concentrations, and time intervals were employed for each MC.

Sorption equilibrium. Before determining the sorption isotherm, it was necessary to demonstrate that sorption steady-state is established. Experiment A was performed to assess the sorption steady-state timescale involving nitrocellulose as sorbent. This was done by varying the sorbent-to-water ratio, which is known to influence the retardation factor for diffusive transport in and out of a sorptive matrix (Wu and Gschwend 1988; Kuo et al. 2007). Figure 92 shows the uptake profiles for NG at five different nitrocellulose-to-water ratios (R_{NC}). The data show that for R_{NC} = 260 or 650 mg_{NC} $(L_{wat})^{-1}$ the dissolved phase concentration, C_{NG}, has stabilized between t = 48 and 96 h. For the higher R_{NC}'s, however, C_{NG} was still declining at t = 96 h. The 260 and 650 R_{NC} samples, however, experienced a low transfer of mass – less than 15% of the total NG had sorbed into nitrocellulose. Low fraction of mass transferred can bias the interpretation of sorption data and the construction of isotherms. This bias can be reduced by adjusting the solid-to-water ratios to achieve a greater fraction of mass transferred. Balancing between uptake kinetics and an optimal fraction of mass transferred, and further assuming that NG and 2,4-DNT had similar sorption affinity and diffusivity (i.e., within the nitrocellulose matrix), sorption isotherms for both solutes were determined at R_{NC} = 3000 - 3700 mg_{NC} $(L_{wat})^{-1}$ with at least 200 - 300 h of equilibration.

With respect to time for equilibration, 500 h of incubation was assumed to be adequate for reaching sorption equilibrium. This was verified by comparing the aqueous phase NG measurements at 500 h and 1200 h after the initiation of sorption (Figure 93a). The figure showed a good match between 500 h and 1200 h data. A similar comparison was also made for sorbed NG concentrations (Figure 93b), which were derived from mass balance based on measured C_{NG}'s.

For batch systems with 2,4-DNT, sorption steady-state was established after approximately 200 to 400 h of incubation/exposure, as shown by the concentration plateau in Figure 94. Comparing the *C-S* data at the end of the sorption experiment (incubation t = 384 h) and the *C-S* data in solutions equilibrated for the desorption experiment (incubation t = 648 h) indicated that sorption steady-state was achieved. Figure 95 shows that the *C-S* data after 384 h (filled circles) and 648 h (plus symbols) of sorption were comparable. The consistency between *C-S* data generated at different exposure times implies that sorption steady-state was established for 2,4-DNT by t = 384 h.

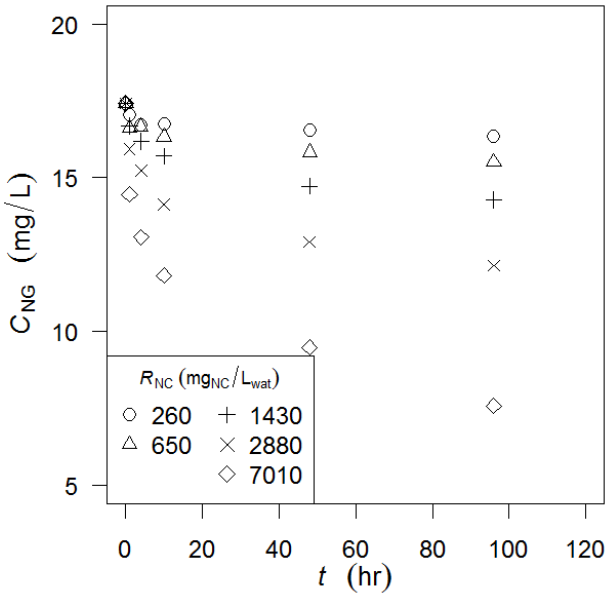

Figure 92. Sorption kinetic profile of NG to nitrocellulose. Aqueous phase NG concentrations were measured at different times in a batch sorption system at five different nitrocellulose-to-water ratios (R_{NC} = 260, 650, 1430, 2880, and 7010 mg_{NC} $(L_{water})^{-1}$).

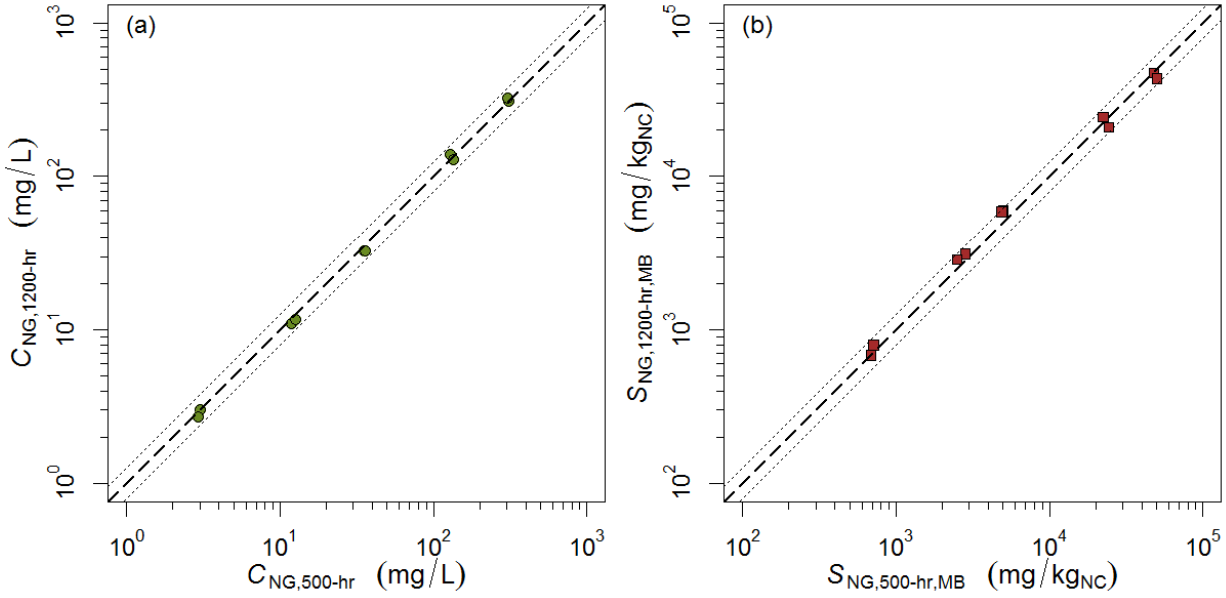

Figure 93. Dissolved phase (C_{NG}) and sorbed phase (S_{NG}) concentrations of NG at 500 and 1200 h. Thick dashed-lines denote perfect match between (a) C_{NG} measurements for 500- and 1200-h after the initiation of sorption and (b) S_{NG} measurements for 500- and 1200-h after the initiation of sorption. Fine dotted-lines denote ± 25% difference in the ratio between the 500- and the 1200-h data (or ± 0.1 log unit).

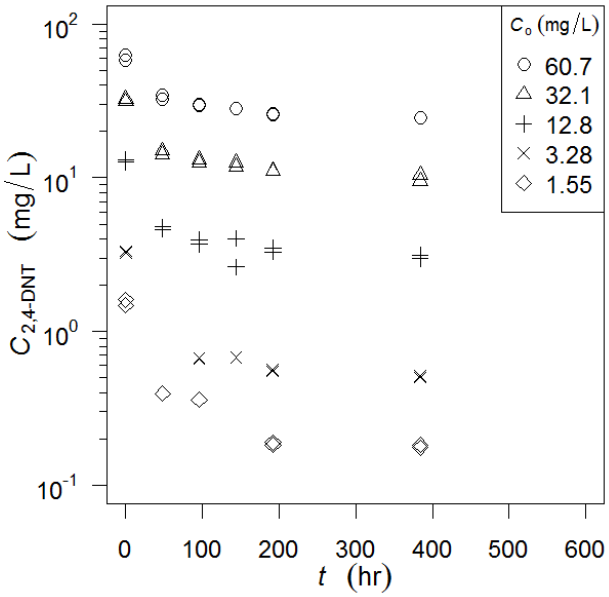

Figure 94. Sorption kinetic profile of 2,4-DNT to nitrocellulose. Aqueous phase 2,4-DNT concentrations were measured at different times in a batch sorption system at five initial concentrations (C_o = 2, 5, 20, 50, and 100 mg $(L_{water})^{-1}$).

Sorption isotherms for 2,4-DNT and NG generally conformed to the Freundlich form as demonstrated in Figure 96. The isotherms were constructed using *C*-*S* data determined after 384 h and 500 h of equilibration for 2,4-DNT and NG, respectively. Isotherm parameters and errors are summarized in Table 52. The derived parameters suggested that 2,4-DNT and NG have similar sorption affinity for nitrocellulose. At C = 1 mg/L, K_{NC} (= S/C) are $10^{3.08}$ and $10^{2.39}$ L/kg_{NC} for 2,4-DNT and NG, respectively. Furthermore, the sorption affinity (K_F) for nitrocellulose increases with the solute's hydrophobicity (reflected by log K_{OW}). This is consistent with the conventional expectation on the sorption of hydrophobic organic compounds.

Table 52. Sorption isotherm parameters in the present study for NG and 2,4-DNT in nitrocellulose-water system at 22 ºC*.

	log K_{OW}	**log K_F**	**n_F**
Nitroglycerin (NG)	1.62	2.39 ± 0.05	0.916 ± 0.032
2,4-dinitrotoluene (2,4-DNT)	1.98	3.08 ± 0.01	0.668 ± 0.010

* $\log S = \log K_F + n_F \log C$. Units of S and C in mg_{solute} $(kg_{NC})^{-1}$ and mg_{solute} $(L_{water})^{-1}$, respectively.

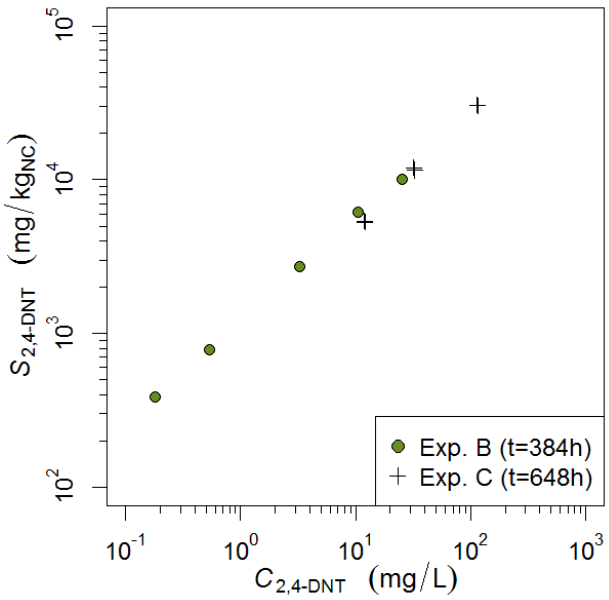

Figure 95. Sorbed (*S*) vs dissolved phase (*C*) concentrations for 2,4-DNT in nitrocellulose-water system after 384 h (filled circles) and 648 h (plus symbols) of uptake exposure.

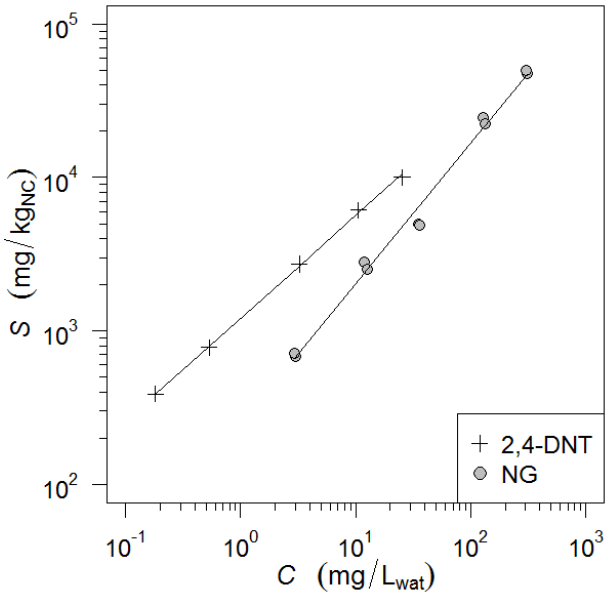

Figure 96. Sorption isotherms for 2,4-dinitrotoluene (plus symbols) and nitroglycerin (filled circles). Isotherms follow the Freundlich form: $S = 10^{3.08\pm0.01}\ C^{0.668\pm0.010}$ for 2,4-dinitrotoluene, $S = 10^{2.39\pm0.05}\ C^{0.916\pm0.032}$ for nitroglycerin, with *S* and *C* in units of mg $(kg_{NC})^{-1}$ and mg $(L_{water})^{-1}$, respectively.

Comparing the measured sorption capacities of nitrocellulose (i.e., K_{NC}) against other similar systems can provide insights regarding the sorptive nature of nitrocellulose and its role in controlling the fate of energetic constituents in field-aged spent munitions on soil. Comparison of partitioning coefficients obtained from this study and those derived for soil organic matter suggested that nitrocellulose is approximately 10 times more sorptive than organic carbon (OC) in binding NG and 2,4-DNT. The OC-normalized partitioning constants (i.e., K_{NC}, K_{OC}) obtained

from this work and those reported in literature are summarized in Table 53. Because the sorption isotherms are often slightly (i.e., $n_F \sim 0.9$) to moderately nonlinear (i.e., $n_F \sim 0.6$ to 0.9), all K's were evaluated at a dissolved phase concentration of 1 mg L^{-1} and normalized by the organic carbon content of the sorbent. From Table 51, soil log K_{OC} for NG and 2,4-DNT were around 1.6-1.7 and 2.2-2.6, respectively, exceeded by log K_{NC}'s by approximately 1 unit (K_{NC} is approximately 10-fold greater than soil K_{OC}) for both solutes. This difference between soil organic matter log K_{OC} and nitrocellulose log K_{NC} is expected to widen as the concentration decreases due to the nonlinear nature of the nitrocellulose isotherms (i.e., $n_F < 1$; Table 52). For example, for 2,4-DNT, log K_{NC} (L $(kg_{OC})^{-1}$) are 3.56, 3.89, and 4.22 at C = 1, 0.1, and 0.01 mg 2,4-DNT/L, respectively. This implies that the bound solute desorbs more slowly with the progressive leaching of the solute from nitrocellulose matrix.

Table 53. Sorption isotherm parameters for NG and 2,4-DNT in nitrocellulose-water system at 22 ºC.

	Nitroglycerin	**2,4-Dinitrotoluene**	**Reference**
log K_{NC}: L $(kg_{OC})^{-1}$	2.70	3.56	this study
Soil studies			
log K_{OC}: L $(kg_{OC})^{-1}$	1.67 ± 0.04	2.59 ± 0.09	this study
	1.70 ± 0.13	2.20 ± 0.08	Clausen et al. 2010
	1.30	2.26	Taylor et al. 2012
	1.91	2.47	Taylor et al. 2012
	1.53	2.61	Taylor et al. 2012
	---	2.25, 2.74	Yamamoto et al. 2004
	1.48	---	Speitel et al. 2002
	1.59	---	Pennington 2002
	---	2.72	Pennington et al. 2001
	---	2.17, 2.51, 2.59	Pennington et al. 2003

These two findings together suggest that nitrocellulose plays an important role in controlling the fate of munition-bound 2,4-DNT or NG in soil. The energetic compounds are initially associated with the nitrocellulose matrix, with K_{NC} approximately 10 times greater than typical soil K_{OC}. Taking an average f_{OC} of 0.03 for soil and an f_{OC} of 0.3 for the nitrocellulose matrix, the K_d in the nitrocellulose matrix would be approximately 100 times greater than the K_d in soil. This implies that the retarded diffusion of the compounds through the nitrocellulose matrix dictates the overall rate of desorption, and is hence the rate limiting step for the release of these chemicals from dispersed munition residuals. Diffusion through the nitrocellulose matrix is retarded in proportion with K_{NC}, so the residual 2,4-DNT or NG, which is more strongly bound to nitrocellulose, will be released from the nitrocellulose to the soil at a rate considerably slower than the material that was released earlier. This may explain the slow release of 2,4-DNT and NG from fired grains in training ranges (Checkai et al. 1993; Dontsova et al. 2009b), the presence of long concentration tails in soil column percolation experiments (Clausen et al. 2010), and the slower dissolution kinetics of munition-bound MCs at the later dissolution phase (Taylor et al. 2012).

Sorption kinetics. Several approaches were taken to analyze the batch sorption kinetics of NG and 2,4-DNT.

A pseudo first-order kinetic model has been used in various studies to describe and summarize kinetic data collected from batch sorption or desorption studies (Pennington et al. 2006; Taylor et al. 2012). It is an approximate model extended from the first-order kinetic model. In a sorption scenario where solute migrates from the dissolved phase into/onto the solid phase, the first-order kinetic model is expressed as follows:

$$\frac{dC}{dt} = -k_1 C + k_2 S \tag{92}$$

where S and C denote the sorbed phase and dissolved phase concentrations [mg kg^{-1} and mg L^{-1}], respectively; t is the time elapsed [h]; k_1 [h^{-1}] and k_2 [kg $(L.h)^{-1}$] are the first-order uptake and release rate constants, respectively. The pseudo first-order model can be obtained with the assumption that the release rate is negligible compared with the uptake rate (i.e., $k_1 C >> k_2 S$):

$$\frac{dC}{dt} = -k_1 C \tag{93a}$$

$$\ln\ (C_t) = -k_1 t + constant \tag{93b}$$

where C_t and C_o are the dissolved phase concentrations at time t and time 0, respectively. This assumption is most appropriate for the early times of sorption when $k_2 S$ is negligible because of small S or small k_2. Such conditions can be found when the system has a very small sorbent-to-water ratio such that C is relatively constant, or when the solute has a much stronger affinity for sorbent than for water (i.e., k_2/K_d is small relative to k_1). The pseudo first-order model fails when the early time assumption is no longer valid.

Transforming the uptake kinetic data of NG according to Equation 93b suggests that NG uptake data may be subdivided into two kinetic domains – a *fast* domain (~ 0 – 10 h) and a *slow* domain (~ 10 – 100 h). Each domain can be modeled separately by the pseudo first-order form, with the rate constants k_{fast} and k_{slow} determined as the negative slope in a ln C_t-vs-t plot (Figure 97). Extending the analysis to all the NG uptake data revealed the same two-domain pattern (Figure 98). Data-fitting with the two-domain model was generally satisfactory, with R^2 ranging from 0.80 – 1.00 except in one instance (R_{NC} = 650 mg_{NC} L^{-1}; Table 54). In general, k_{fast} was approximately 10 – 30 times greater than k_{slow}.

Table 54. R^2 for two-domain pseudo first-order fitting of batch NG sorption kinetic data.

R_{NC} (mg NC L^{-1})	Fast domain	Slow domain
260	0.91	1.00
650	0.59	0.97
1430	0.86	0.93
2880	0.80	0.97
7010	0.81	1.00

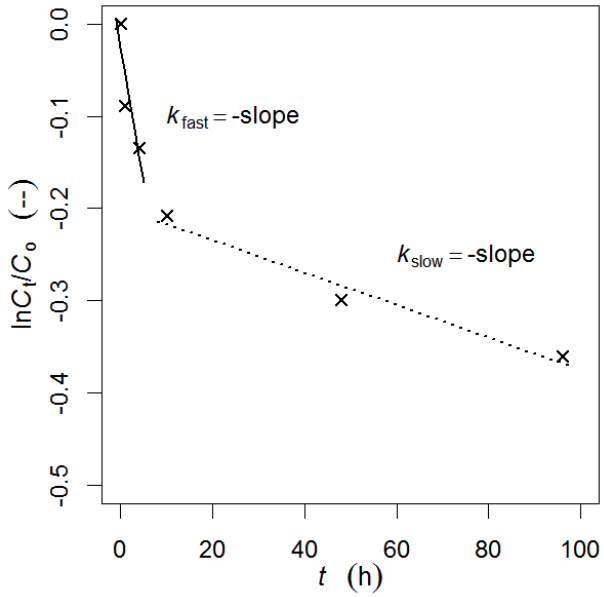

Figure 97. Kinetic data of batch uptake of NG to nitrocellulose (at R_{NC} = 2880 mg_{NC} L^{-1}) as modeled by a two-domain framework: the *fast* domain (~ 0 – 10 h) and the *slow* domain (~ 10 – 100 h). The rate constants of the two domains, k_{fast} and k_{slow}, were determined as the negative slopes of the regression curves for ln C_t/C_o vs t. Solid-line denotes the regression line for the fast domain; dotted-line denotes the regression line for the slow domain.

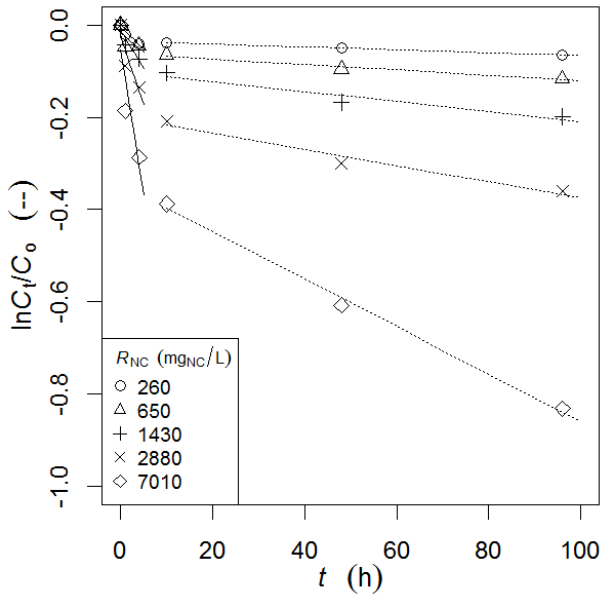

Figure 98. Kinetic data of batch uptake of NG to nitrocellulose as modeled by a two-domain framework at all five nitrocellulose-to-water ratios (R_{NC}). Solid-line denotes the regression line for the fast domain; dotted-line denotes the regression line for the slow domain.

Both k_{fast} and k_{slow} were found to vary linearly with the nitrocellulose-to-water ratio as shown in Figure 99. The regression was very strong as both plots showed $R^2 > 0.99$. The observed dependence is consistent with the theoretical expectation that rate of uptake generally increases with the concentration of sorbing solids (Crank 1979; Wu et al. 1988). This means that the overall uptake rate of NG may be predicted if the system R_{NC} is known.

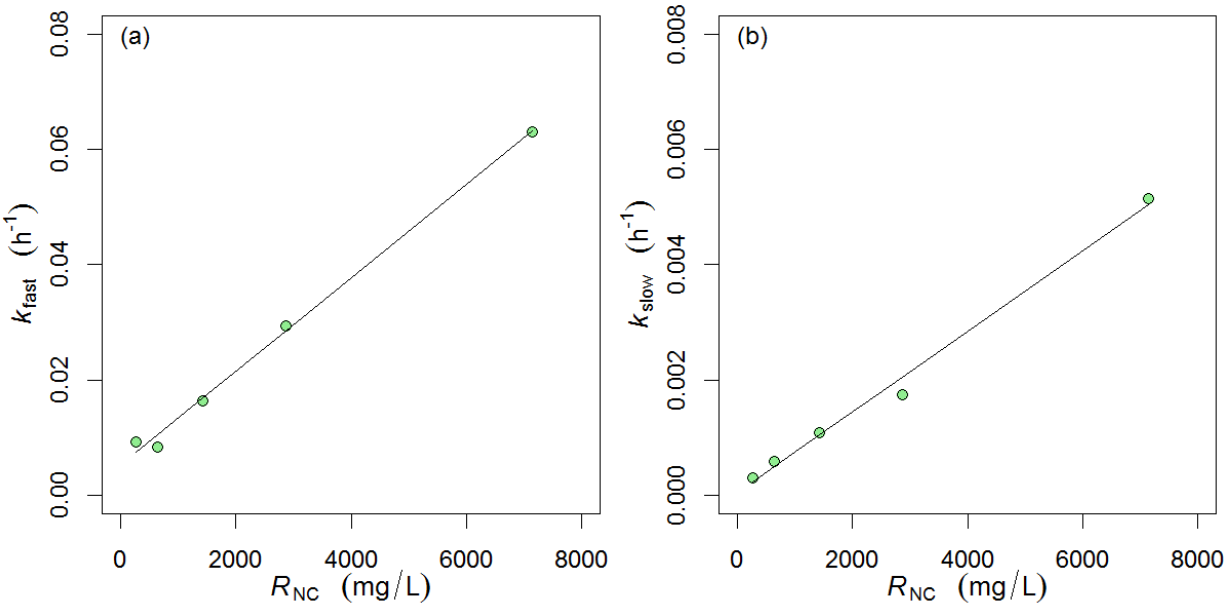

Figure 99. Sorptive uptake of NG by nitrocellulose. Linear dependence of k_{fast} and k_{slow} to nitrocellulose-to-water ratio (R_{NC}): (a) the *fast* domain ($k_{fast} = 8.1\times10^{-6}\ R_{NC} + 5.3\times10^{-3}$; $R^2 = 0.996$), and (b) the *slow* domain ($k_{slow} = 7.0\times10^{-7}\ R_{NC} + 5.0\times10^{-5}$; $R^2 = 0.993$).

The application of the two-domain model to the 2,4-DNT sorption data, however, revealed the limitations of the pseudo first-order approach. Figure 100 shows the determination of the *fast* (~ 0 – 50 h) and the *slow* (~ 50 – 400 h) domains in the 2,4-DNT uptake data. The coefficients of determination, R^2 (Table 55), for the data-fits were generally poorer than were those for NG (R^2 = 0.68 – 0.88 for k_{slow}; note that R^2 was not defined for k_{fast} regressions because only 2 data points were present). One limitation is the arbitrary definition of the domain boundary. Here, t = 50 h was arbitrarily selected as the boundary between the fast and slow domain. Visual inspection of the 50 – 400 h data also suggested a change in slope at around 200 h, hinting that a third kinetic domain probably exists. Regression analysis with this "third" domain (i.e., t = 200 – 400 h) suggested that a three-domain framework may be more appropriate for 2,4-DNT. It is likely that an additional kinetic domain will be needed for NG data if further observations beyond the 100 h were available. The arbitrariness in defining the number of domains and the domain boundaries greatly limit the usefulness of extending the domain-based kinetic model beyond the time frame examined.

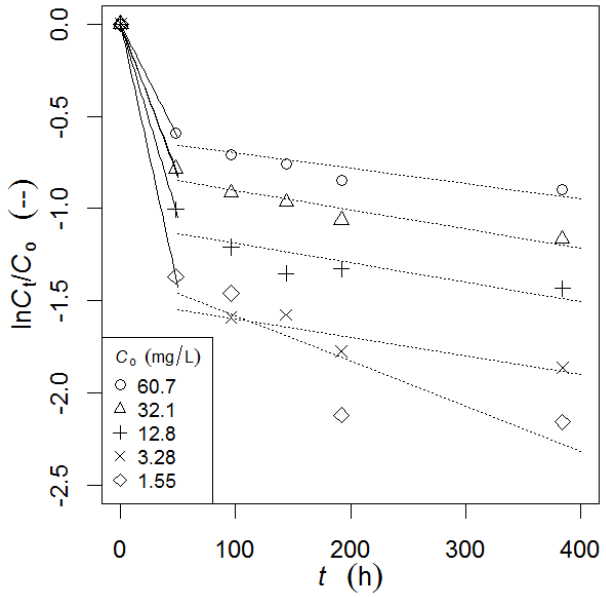

Figure 100. Kinetic data of batch uptake of 2,4-DNT to nitrocellulose as modeled by a two-domain framework. Solid-line denotes the regression line for the fast domain; dotted-line denotes the regression line for the slow domain. R^2 for the fast and slow domain regressions are summarized in Table 55.

Table 55. R^2 for two-domain pseudo first-order fitting of batch 2,4-DNT sorption kinetic data.

$C_{o,\ 24\text{-DNT}}$ (mg L^{-1})	**Fast domain (0 – 50 h)**	**Slow domain (50 – 400 h)**
60.7	--	0.81
32.1	--	0.88
12.8	--	0.68
3.28	--	0.80
1.55	--	0.75

$C_{o,\ 24\text{-DNT}}$ (mg L^{-1})	**Fast domain (0 – 50 h)**	**Slow domain #1 (50 – 200 h)**	**Slow domain #2 (200 – 400 h)**
60.7	--	0.98	--
32.1	--	0.98	--
12.8	--	0.82	--
3.28	--	0.69	--
1.55	--	0.95	--

Alternatively, NG and 2,4-DNT sorption kinetic data can also be fitted to a power-law model in the following form:

$$C_t = a\log(t) + b \tag{94}$$

where C_t is the dissolved phase concentration at time t with unit [h], and a and b are the regression constants with units [mg L^{-1}]. As an illustration, the application of the power-law model to one of the NG sorption experiments is shown in Figure 101. The power-law model has the advantage of being capable of fitting all kinetic data through the entire observation period, and thus circumventing the issue of defining different kinetic domains (i.e., *fast* vs *slow*). The power-law form was successfully applied to all kinetic data for both NG and 2,4-DNT uptake experiments (Figure 102). The power-law regression was generally satisfactory, with R^2 ranging from 0.89 to 0.99 and 0.81 to 0.99 for NG and 2,4-DNT uptake data, respectively (Table 56).

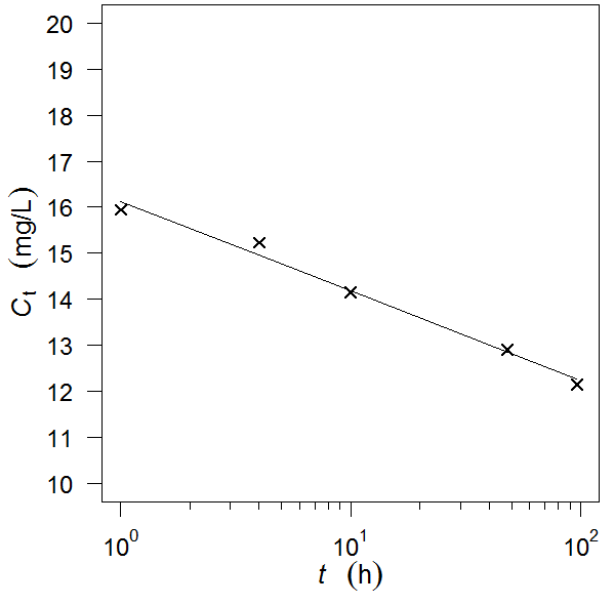

Figure 101. Regression of sorption kinetic data of batch NG uptake by nitrocellulose (at R_{NC} = 2880 mg_{NC}/L) by the power-law model $C_t = a \log(t) + b$.

Table 56. R^2 for power-law fitting of batch NG and 2,4-DNT sorption kinetic data.

R_{NC} (mg NC L^{-1})	R^2 for NG	C_o (mg L^{-1})	R^2 for 2,4-DNT
260	0.91	60.7	0.96
650	0.89	32.1	0.99
1430	0.99	12.8	0.88
2880	0.99	3.28	0.81
7010	0.98	1.55	0.87

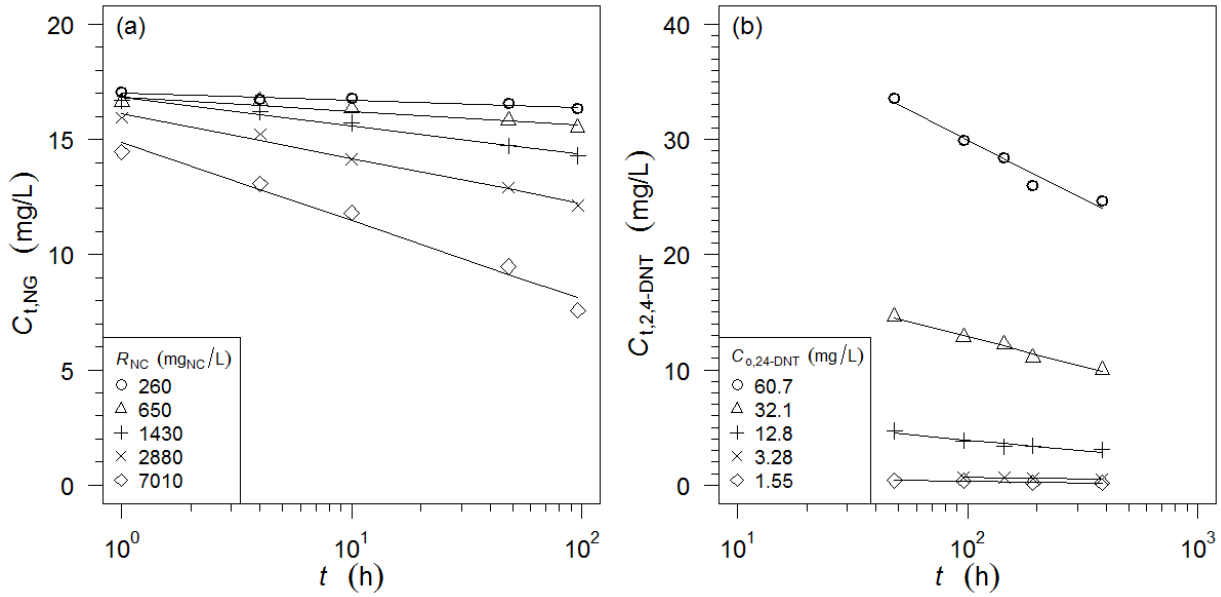

Figure 102. Power-law regression of NG and 2,4-DNT uptake kinetic data in batch nitrocellulose-water system: (a) NG at five nitrocellulose-to-water ratios (R_{NC}), and (b) 2,4-DNT at five initial concentrations. Solid lines are the power-law regression lines. R^2 for NG and 2,4-DNT ranges were 0.89 to 0.99 and 0.81 to 0.99, respectively.

Lastly, the sorption kinetic data were fitted to the analytical solution for transient solute uptake by particles in batch system developed by Crank (1979) for diffusion problems involving different geometries and conditions. Microscopic images (Figure 103) show that nitrocellulose "cotton" easily "disintegrates" into the constituent fibers. While the fibers have variable length and diameter, as a first approximation, the individual fiber may be approximated as a long cylinder. This implies that the analytical solution involving cylindrical particles should be applied. For the uptake of solute by a cylindrical sorbent with diameter a from a limited/closed volume of aqueous phase, the normalized solute gain by the sorbent is depicted by the following expression (Crank 1979):

$$\frac{M_t}{M_\infty} = 1 - \sum_{n=1}^{\infty} \frac{4\alpha(1+\alpha)}{4 + 4\alpha + \alpha^2 q_n^2} \exp\left(-\frac{D q_n^2 t}{a^2}\right) \tag{95}$$

where M_t and M_∞ are the mass of solute associated or sorbed by the sorbent at time t and infinite time, respectively; α is a dimensionless ratio (see Equation 97); D is the effective diffusivity within the sorbent [cm^2 s^{-1}]; a is the radius of the cylinder [cm]; t is time [s]; q_n is the nth root to the Equation 96 ($J_o(q_n)$ and $J_1(q_n)$ are the Bessel functions of the first kind evaluated at q_n):

$$\alpha q_n J_o(q_n) + 2J_1(q_n) = 0 \tag{96}$$

α accounts for sorbent-aqueous phase partitioning and sorbent mass-to-water ratio. In Crank, α was defined in terms of the aqueous phase to sorbent volume ratio and is a volume based partition coefficient K:

$$\alpha = \frac{A}{\pi a^2 K} \tag{97}$$

However, for consistency with the unit and partitioning convention adopted in contaminant transport literature, α is rephrased in terms of the sorbent-to-water ratio R_{NC} [kg_{NC} $(L_{water})^{-1}$] and the partition coefficient K_d [L_{water} $(kg_{NC})^{-1}$]:

$$\alpha = \frac{1}{R_{NC}K_d} \tag{98}$$

The diffusivity, D, in Equation 95 represents the effective diffusion coefficient of the solute through the sorbent medium, including the void/pore space enclosed. D is related to the intrinsic diffusivity in the sorbing medium (i.e., the nitrocellulose fiber itself) D_m as developed by Wu and Gschwend [1988]:

$$D\ (or\ D_{eff}) = \frac{D_m n^2}{(1-n)\rho_s K_d + n} \tag{99}$$

where D_m is the molecular diffusivity through the medium [$cm^2\ s^{-1}$]; n is the porosity of the hydrated fiber or fiber aggregate; ρ_s is the density of the dry fiber [$kg\ L^{-1}$]; K_d is the partition coefficient of the solute between the fiber and the aqueous phase [$L\ kg^{-1}$].

Figure 103. Microscopic image of nitrocellulose aggregates and fibers.

The analytical solution or model (Equation 95 to 99) has the advantage of linking kinetic observations to physicochemical properties of the sorbent and the system, providing a mechanistic and rational account of the uptake profile. Furthermore, it also allows the diffusion coefficient of the sorbent, here as hydrated nitrocellulose matter, to be back-derived through data-fitting. However, applying the analytical model would require accurate information about the sorbent: the geometry of constituent fibers, the size distribution of fibers, and the dynamics of aggregation during tumbling, etc. Such information was not determined in this work, and instead "average" geometry and aggregation behavior were used.

A number of other assumptions and approximations were also adopted. The analytical solution

assumed a constant K_d throughout the uptake process. This was not true for NG or 2,4-DNT as the isotherms for both chemicals were found to be nonlinear. In order to apply the analytical model, a mean K_d averaged between the initial concentration (i.e., C_o) and the theoretical equilibrium dissolved concentration (C_∞) was used to fit the data of a particular sorption experiment. For NG, the initial and final K_d's differed by no more than 10%. For 2,4-DNT, however, the final K_d could exceed the initial value from 35 to 100%. Although the mean K_d approximation was more appropriate for NG, the resulting error in the case of 2,4-DNT would amount to no more than 0.2 log unit in K_d. Furthermore, it is also assumed that the structure of nitrocellulose had stabilized after the hydration period. It is also understood that the length of the individual fiber is adequately long relative to its radius that the 2-D cylindrical solution is a reasonable approximation. A more rigorous approach would be to model the uptake of solute at incremental time-steps and discretized space, considering the nonlinear partitioning and the distributed geometry of the fibers.

The fitting of NG and 2,4-DNT uptake kinetic data to the analytical model is shown in Figure 104 and 105. Optimal fit was determined by the least sum of squares of errors with the effective diffusivity, D, as the only fitting parameter. All other sorbent and system parameters were specified *a priori*. A 5×10^{-3} cm radius for the individual fiber was estimated from the microscopic images of nitrocellulose aggregates. A density of 1.5 kg L^{-1} was assumed for the dry nitrocellulose. The intrinsic molecular diffusivity in wetted nitrocellulose, D_m, was estimated from the individual fitted curves. (D_m was the only fitting parameter in Equation 99). The estimated individual and mean D_m's are summarized in Table 57. The mean D_m for NG and 2,4-DNT were estimated to be 1.5×10^{-9} ($\pm7.8\times10^{-10}$) and 2.6×10^{-9} ($\pm9.0\times10^{-10}$) $cm^2\ s^{-1}$, respectively.

Table 57. D_m for NG and 2,4-DNT in nitrocellulose matrix as determined from fitting uptake kinetic data to the cylindrical transient diffusion solution (Equation 95 to 99).

R_{NC} ($mg_{NC}\ L^{-1}$)	D_m for NG ($cm^2\ s^{-1}$)	C_o ($mg\ L^{-1}$)	D_m for 2,4-DNT ($cm^2\ s^{-1}$)
260	9.4×10^{-10}	60.7	2.9×10^{-9}
650	8.6×10^{-10}	32.1	3.4×10^{-9}
1430	8.5×10^{-10}	12.8	3.2×10^{-9}
2880	2.1×10^{-9}	3.28	2.1×10^{-9}
7010	2.5×10^{-9}	1.55	1.2×10^{-9}
mean	1.5×10^{-9} ($\pm7.8\times10^{-10}$)	mean	2.6×10^{-9} ($\pm9.0\times10^{-10}$)

A question of key importance is whether or not the derived D_m's for NG and 2,4-DNT in nitrocellulose are realistic. This can be examined by considering if the estimated D_m's yield kinetic expectations consistent with other experimental studies, and if the D_m's are comparable with those of organic compounds with similar physicochemical properties.

For the question of consistency in kinetic behavior, the propellant dissolution study by Taylor et al. [2012] was used as a test case. In their study, Taylor et al. investigated and modeled the dissolution rates of NG from four types of propellants. The dissolution process was modeled with an analytical model for 1-D diffusion. Effective diffusivities for the dissolution of propellant-associated NG were found to range between 3.2×10^{-14} $cm^2\ s^{-1}$ to 280×10^{-14} $cm^2\ s^{-1}$ for weaponry covering pistol and machine guns. The examined propellant grains contained approximately 80–90% of nitrocellulose by mass with the rest being NG solids. The propellant

grain system would be "comparable" to the sorption/desorption cases in this work when all crystalline mass of NG has dissolved away and that the residual sorbed NG is desorbing from the porous nitrocellulose matrix. The predicted effective diffusivity of NG in the propellant grains can be estimated from Equation 94. Assuming a mean K_d of 200 L kg^{-1} for NG, a ρ_s of 1.5 kg L^{-1} for nitrocellulose, a porosity of 0.1 – 0.2 (i.e., 100% – 80/90%), and D_m as 1.5×10^{-9} cm^2 s^{-1}, effective diffusivity was estimated to be 5.6 and 25×10^{-14} cm^2 s^{-1} for porosities of 0.1 and 0.2, respectively. The estimation is of the same order as the reported effective diffusivities (i.e., 3.2×10^{-14} cm^2 s^{-1} to 280×10^{-14} cm^2 s^{-1}; Taylor et al. 2012). The predicted values are even closer when compared against the diffusivities fitted to the tail slope (i.e., diffusion rather than dissolution dominant) of the propellant dissolution profiles: 3.2×10^{-14} cm^2 s^{-1} to 12×10^{-14} cm^2 s^{-1} (Table 6 in Taylor et al. 2012). This comparison exercise clearly suggests that the D_m's obtained from the current study are behaviorally consistent with those observed in earlier works.

Comparison with diffusivities measured for other organic compounds in natural or manufactured polymeric systems also suggested that the derived D_m's are reasonable. The D_m's for NG and 2,4-DNT were estimated to be of the order 10^{-9} cm^2 s^{-1} (Table 57). This is similar to those of organic compounds in humic acid ($D \sim 10^{-9}$ cm^2 s^{-1}) [Chang et al. 1997; Fomba et al. 2009], biofilm ($\sim10^{-10} – 10^{-9}$ cm^2 s^{-1}) [Wicke et al. 2008], and petrolatum ($\sim10^{-11} – 10^{-8}$ cm^2 s^{-1}) [Ortiz et al. 1999]. Diffusion appears to be faster in nitrocellulose than in polyoxymethylene ($10^{-11} – 10^{-10}$ cm^2 s^{-1}) [Ahn et al. 2005], slightly slower in tire rubber ($\sim10^{-8}$ cm^2 s^{-1}) [Kim et al. 1997], and approximately 2 – 3 orders of magnitude slower in polydimethylsiloxane ($\sim10^{-6}$ cm^2 s^{-1}) [Chandak et al. 1998]. It should be noted that diffusivity can vary by 2–3 orders of magnitude in different polymeric systems. For instance, D_m for trichloroethylene was found to be as high as 1.4×10^{-6} cm^2 s^{-1} when diffusing into polydimethylsiloxane (PDMS) [Chandak et al. 1998] but decreased to 5.5×10^{-8} cm^2 s^{-1} in tire rubber [Kim et al. 1997]. Similarly, for pyrene, D_m was estimated to be 2.6×10^{-10} cm^2 s^{-1} in biofilm [Wicke et al. 2008] and 7.2×10^{-12} cm^2 s^{-1} in paraffin sheet [Ortiz et al. 1999]. Considering the degree of variability in diffusivity across different chemicals in a given medium, the estimated D_m's are well within the expected range of $10^{-9} – 10^{-11}$ cm^2 s^{-1}.

Desorption kinetics. Desorption kinetic data were modeled with the power-law model and the analytical diffusion model only. The two-domain model was not applied here as it was considered as an alternative empirical model without necessarily better performance than the power-law model. Regression results from the analytical model fitting will be discussed first followed by the power-law model.

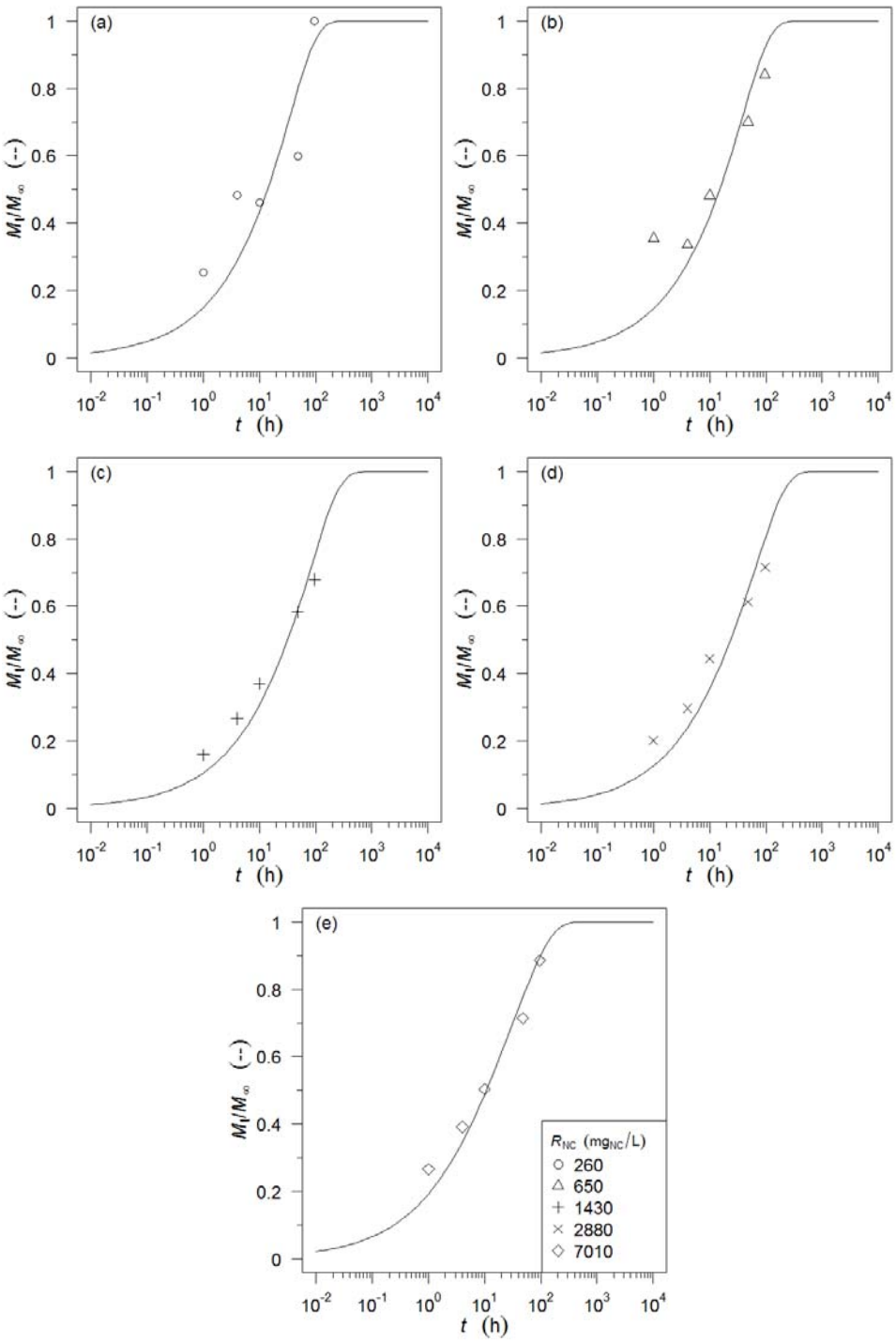

Figure 104. Batch uptake kinetics of NG by nitrocellulose fit to analytical diffusion solution (cylindrical solids, limited volume diffusion). The ratio of solute sorbed at time t (M_t) to solute sorbed at equilibrium (M_∞) is plotted against time at five nitrocellulose-to-water ratios R_{NC}: (a) 260, (b) 650, (c) 1430, (d) 2880, and (e) 7010 mg$_{NC}$ L^{-1}. A ratio of $M_t/M_\infty = 1$ implies equilibrium has been established within the batch system.

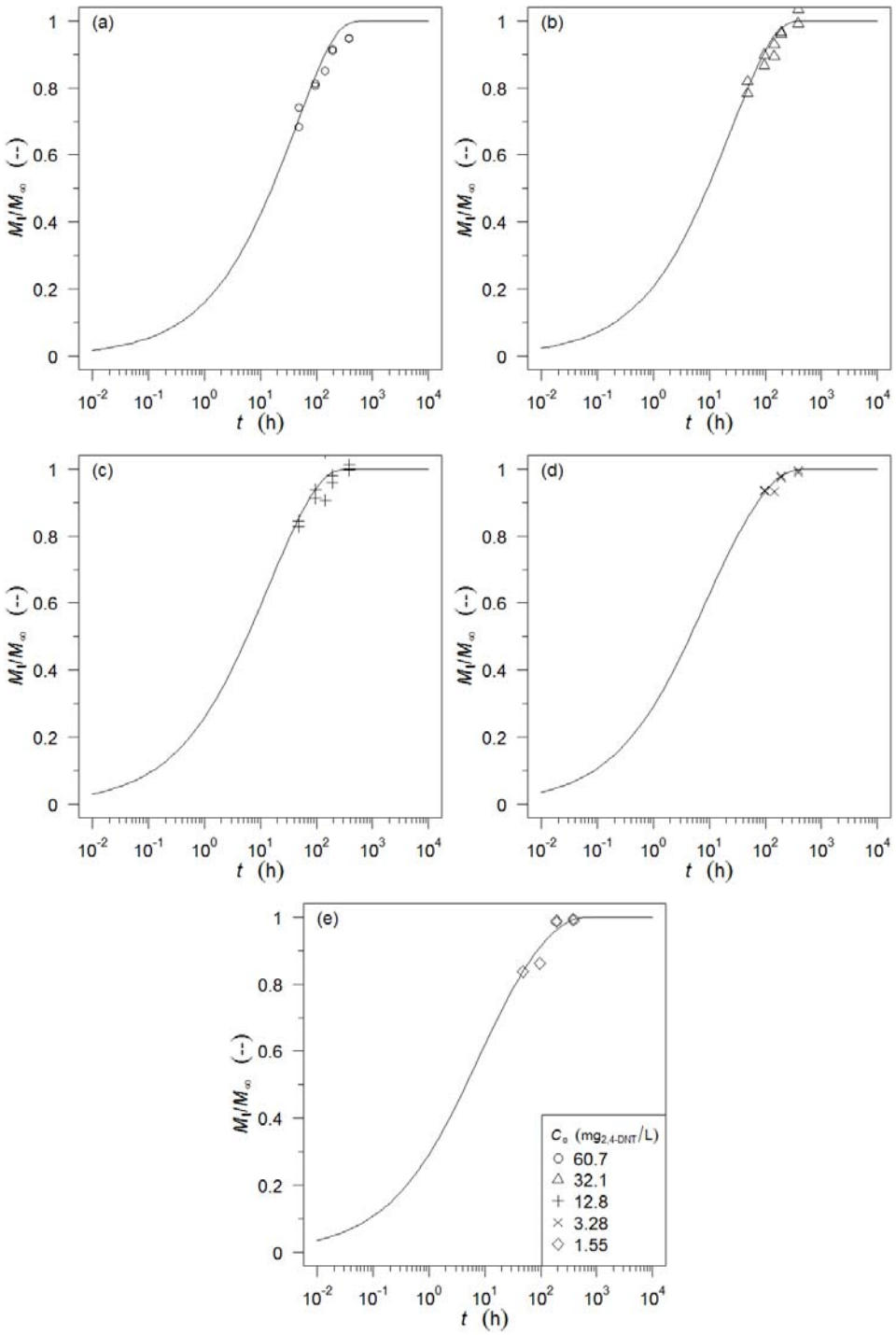

Figure 105. Batch uptake kinetics of 2,4-DNT by nitrocellulose fit to analytical diffusion solution (cylindrical solids, limited volume diffusion). The ratio of solute sorbed at time t (M_t) to solute sorbed at equilibrium (M_∞) is plotted against time at five initial dissolved phase concentrations C_o: (a) 60.7, (b) 32.1, (c) 12.8, (d) 3.28, and (e) 1.55 mg L^{-1}. A ratio of $M_t/M_\infty = 1$ implies equilibrium has been established within the batch system.

Regressing the desorption data for all C_{init}-R_{NC} combinations with the analytical model [Crank 1979] yielded an estimated D_m of 2.9×10^{-9} ($\pm1.4\times10^{-9}$) $cm^2\ s^{-1}$ and 2.0×10^{-8} ($\pm7.8\times10^{-9}$) $cm^2\ s^{-1}$ for NG and 2,4-DNT, respectively. For NG, the D_m derived from sorption and desorption kinetics are 1.5×10^{-9} ($\pm7.8\times10^{-10}$) and 2.9×10^{-9} ($\pm1.4\times10^{-9}$) $cm^2\ s^{-1}$, respectively, suggesting a similar D_m regardless of the direction of movement. For 2,4-DNT, however, the sorption derived D_m was approximately 10 times lower than the D_m estimated from desorption. It was unclear what contributed to the 10-fold discrepancy in the D_m of 2,4-DNT. A difference in sorption/desorption diffusivities by as much as a factor of 4-6 have been reported for diffusion of hexane and toluene in humic acid disks [Chang et al. 1997], with, however, the uptake-based D_m faster than the desorption-based D_m. A slower out-going/desorbing diffusivity can be observed if adsorption of solute is still taking place in the inner layers of the sorbent while solute associated with the outer layers desorbs into the bulk aqueous phase. A noteworthy point for 2,4-DNT was that the mean K_d during its sorption was approximately 2-3 times greater than that during its desorption. This means that the diffusion would be less retarded during desorption; however, since D_m represents the intrinsic diffusivity within wetted nitrocellulose, the difference in K_d is not a valid explanation for the greater desorption-case D_m. In the absence of good or even probable explanations, the desorption-derived D_m for 2,4-DNT should be used with caution.

Desorption kinetic data for NG and 2,4-DNT experiments were satisfactorily regressed with the power-law model, with R^2 ranging from 0.92 to 1.0. Since desorption experiments were conducted at varying initial exposure concentration (C_{init}) and solution volume (V), the regression parameters a and b are presented as a function of both variables (Figure 106 and 107). Both plots show that a and b increase with greater C_{init} and smaller V. The figures also indicate an interaction between C_{init} and V while affecting a and b. For instance, both parameters are much more sensitive to variation in C_{init} at small V (i.e., 10 mL) than at large V (i.e., 200 mL). This interaction must be considered when trying to understand and/or predict a and b.

Conclusions regarding sorption and release of MC by nitrocellulose. The sorptive interaction between the MCs (NG and 2,4-DNT) and the propellant matrix nitrocellulose has been characterized. Batch sorption experiments revealed that the sorption of NG and 2,4-DNT to nitrocellulose to be slightly non-linear. The isotherms for NG and 2,4-DNT to nitrocellulose were found to be $S_{NG} = 10^{2.39(\pm0.05)}\ C_{NG}^{0.916(\pm0.032)}$ and $S_{24DNT} = 10^{3.08(\pm0.01)}\ C_{24DNT}^{0.668(\pm0.010)}$, respectively (with units of S in mg/kg_{NC} and C in mg/L). The nitrocellulose-water partitioning coefficient, K_{NC}, when normalized to organic carbon content, was found to be approximately 10 times greater than K_{OC} of soils. Considering that the typical soil organic carbon content to be approximately 1/10 of that in the nitrocellulose-dominated propellant matrix, the propellant is expected to be approximately 100 times more sorptive than soil particles. This implies that the dispersed propellant residues or grains, if left on the field, may serve as a source for the continuous release of munition constituents, with the rate of release largely controlled by the sorptive strength of the compound to the nitrocellulose matrix.

The sorption and desorption kinetic behavior of both NG and 2,4-DNT could be fit using an analytical diffusion model with cylindrical geometry for the nitrocellulose fibers. The molecular diffusivities of the MCs in nitrocellulose (i.e., D_m) could be derived and were found to be in the order of 1×10^{-9} cm^2/s. The magnitude of the derived D_m's were comparable to the diffusivities of other organic compounds in various polymeric systems. Furthermore, the estimated D_m's were also consistent with the chemical release behavior of MC from propellant grains in previous dissolution studies.

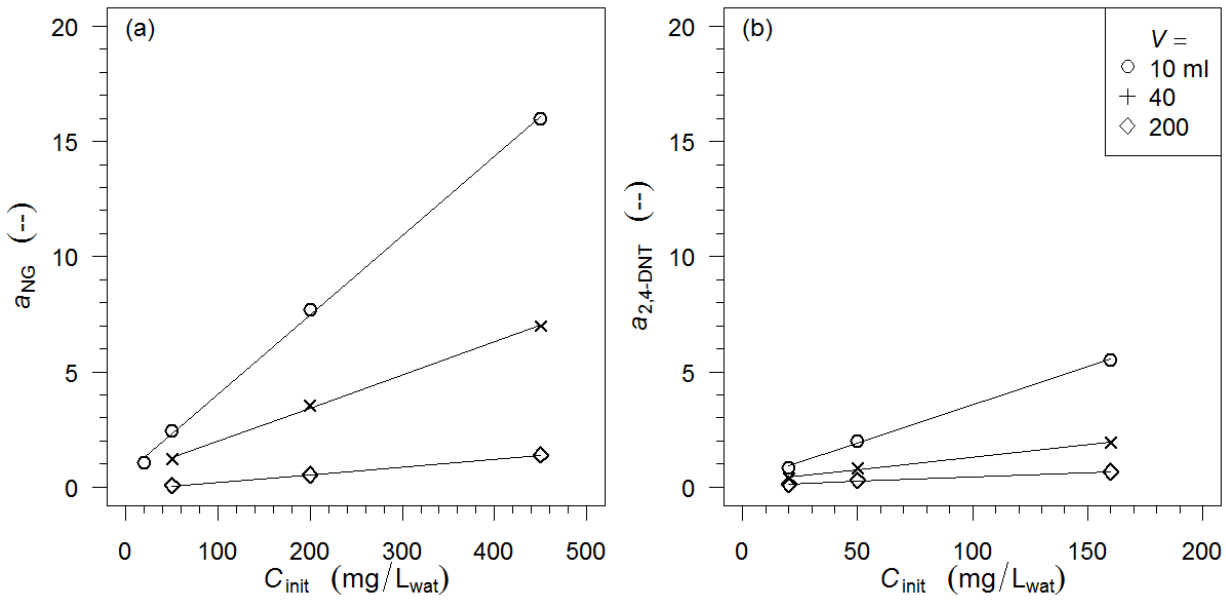

Figure 106. Dependence of *a* parameter regressed from the batch desorption of nitrocellulose-associated NG and 2,4-DNT into water: (a) NG data, (b) 2,4-DNT data.

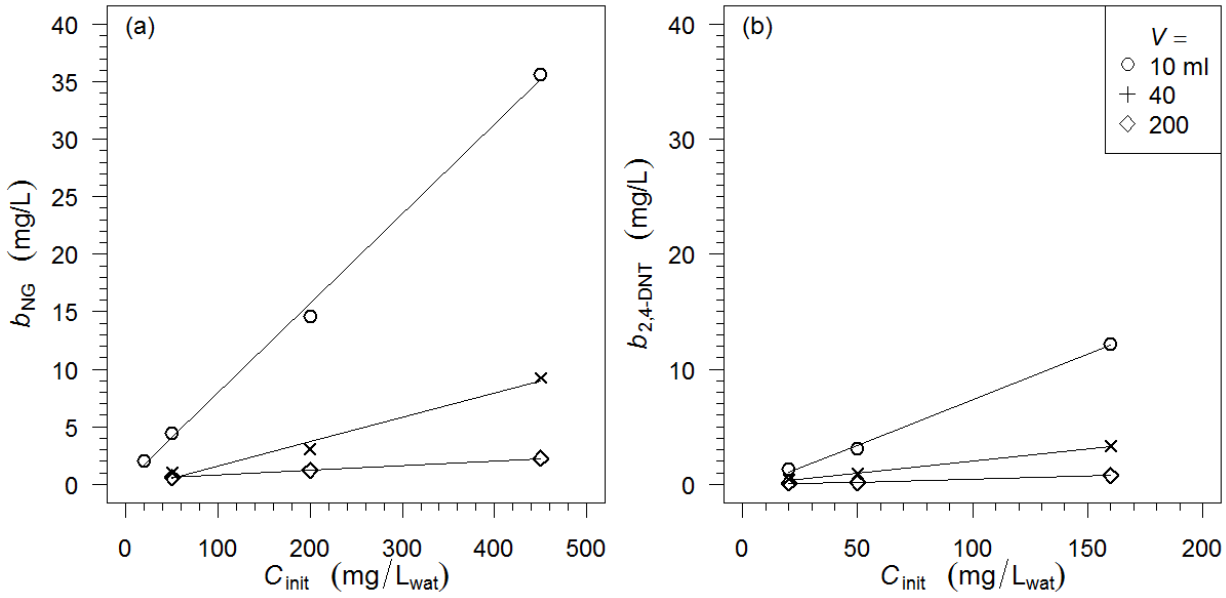

Figure 107. Dependence of *b* parameter regressed from the batch desorption of nitrocellulose-associated NG and 2,4-DNT into water: (a) NG data, (b) 2,4-DNT data.

Conclusions and Implications for Future Research/Implementation

Conclusions Regarding Partitioning of MC to Soils. The partitioning of RDX, HMX, TNT, NG, 2,4-DNT, and NQ to 25 soils was studied. The soils had a wide range of physical and chemical properties. The clay size particle content was between 4.0 to 43.2%, total organic carbon content was 0.07 to 18.23%, and oxalate-extractable Fe content was 0.0053 to 1.20%. Use of a large number of samples of diverse character is necessary to ensure the applicability of models developed to other sites that fall within the domain of the characteristics, and to enhance the possibility of using experimental results extrapolated to additional sites. Future projects should also study many soils to ensure that the results will be widely applicable.

The objective of this project was the development of models for the partitioning of the MC to soils. The objective was met. The number of soils studied exceeded the number that had been proposed. A new model that had not been proposed was developed and applied to the data. We found that the sorption of the MC to the soils was dominated by partitioning to the organic matter faction of the soil. For soils with OM greater than a few percent, the sorption of all MC was related virtually solely to the OM content. The sorption of NG was dominated by the OM content of the soil for all OM contents studied. For the other MC, as the content of OM decreased, partitioning to additional soil components became increasingly important. The additional partitioning was largely due to clay minerals. We developed multilinear models that included clay mineral content as paramaterized by both clay size particles and the cation exchange capacity of the soils. Inclusion of either of these parameters provided approximately equal predictive capability in a multilinear model in which both clay and organic matter were included. We had proposed using a specific characterization of clay exchange site by measuring the exchange of cesium ions. These values provided only a small improvement in the model. Because the Cs method is very labor intensive, we do not recommend its use. The content of oxalate extractable iron was also incorporated as a third sorption site. This refinement would not be needed except for very low organic matter content soils.

Desorption of the MC showed hysteresis as was expected. As proposed, we applied the Reversible/Resistant (RR) Model to the desorption results. The model was extended to the multilinear models. Increasing the duration of sorption increased the resistant fraction. Resistance to desorption was related to the sorption of the MC by OM, not by clay. The Site Transformation Model (STM), a new model developed as a part of this project, was created. The STM provides a mechanistic basis for the process by which the sorbed MC is made resistant to desorption. Preliminary work provides a model of the kinetics. The results of the project have provided RR constants that can be applied to soils. Use of the STM is recommended as we believe this model will be adopted in preference to the established RR Model. The research objective related to modeling resistance to desortion using the RR model has been met. The development of the STM was not anticipated in the proposed research. With its development the research objective has been exceeded.

It was envisioned that the partitioning results would be validated by investigating MC sorption and desorption in a soil column study. This would also provide a transition from the batch partitioning results to the field situation. For this objective, we were only partially successful. The residual sorbed RDX did not follow the anticipated concentration profile. However, the results did provide very important information. Batch studies had indicated that RDX was sorbed reversibly. However, the presence of residual RDX on the column after the column had been

flushed showed that a very small portion of the RDX was sorbed resistantly. This unanticipated finding was subjected to sensitivity analysis which clearly indicted that following the solution phase MC concentration without also monitoring the amount of MC retained on the soil is insufficient. The time available did not allow for conducting additional column studies to further resolve the extent of partitioning.

Conclusions Regarding Partitioning of MC to Nitrocellulose. The partitioning of MC to NC was confirmed in this study as had been suggested in the proposal. Its release from NC in the field will be slow, thus providing tailing in the concentration profile and is a mechanism explaining the observed slow release from incomplete detonations. This mechanism should be incorporated into models of MC release from propellant NC to provide a more mechanistic reality in contaminant models.

Implications for Future Work. The research on partitioning of MC to soil should be followed up with additional studies. Research should be conducted on MC partitioning in soil columns. These studies should follow the approaches used in this research project, but should employ longer soil columns with soils having greater organic matter content. That would accentuate partitioning of MC in comparison to that seen for the Sassafras Sandy Loam used in this project. This would provide a powerful means to determine the extent to which MC would remain in the soil and the degree of its resistance to leaching.

Desorption of MC from field contaminated soils should be studied for the validation of the laboratory partitioning results. That information should be used in the refinement of soil leaching models to incorporate reversible/resistant or site transformation.

Additional research should be conducted on development of the Site Transformation Model. This should be directed toward study of compounds for which the log K_p is 2 to 4, somewhat greater than are the MC studied in the present project. The application of the Site Transformation Model to systems exhibiting Langmuirian sorption should be further evaluated with a focus toward further development of a predictive model. These studies should also be directed toward understanding the mechanisms responsible for the observed hysteresis.

This study has provided results that can be used to predict partitioning of six MC to soils as a function of soil composition. Chemical descriptors that are being developed in the SERDP Project ER-1734 could be applied to provide prediction of partitioning of additional compounds to soils for which partitioning is dominated by the interaction of the compound to organic matter. This predictive capability should be validated for additional compounds using a smaller number of soils than has been employed in this study. Additionally, the partitioning of MC, including new compounds, to clay and iron oxides should be further investigated to provide a generalized partitioning model to clay and ironides as these two components dominate partitioning in groundwater aquifers where the content of organic matter is low.

Recommendations for Implementation. Results for the adsorption and desorption of MC should be used in models for the fate of MC. We recommend the use of the values provided by the Site Transformation Model as this model explicitly accounts for time. However, results that have been provided by the Reversible/Resistant Madel can also be used. Incorporating hysteresis in partitioning models of fate is important and a single partition coefficient to represent both the adsorption and the desorption of a compound is not warranted; hysteresis should be dealt with explicitly. If the soil to be modeled for prediction has a content of organic matter exceeding 2%, only parammeters for the organic matter content of the soil needs to be incorporated into the

partitioning model. However, for soils that have little organic matter content, particularly for soils containing less than 1% organic matter, both organic matter and the clay component of the soil should be included as sorbents.

Desorption of sorbed MC from nitrocellulose was demonstated as providing a mechanism for the slow release of MC from propellant residues in the field. This process should be explicitly considered in models of the release of MC from NC.

References

Ahn S, Werner D, Karapanagioti HK, McGlothlin DR, Zare RN, Luthy RG. 2005. Phenanthrene and pyrene sorption and intraparticle diffusion in polyoxymethylene, coke, and activated carbon. *Environmental Science & Technology.* 39: 6516-6526.

Ainsworth CC, Harvey SD, Szecsody JE, Simmons MA, Cullinan VI, Resch CT, Mong GH. 1993. Relationship between the leachability characteristics of unique energetic compounds and soil properties. Final Report. Project Order No. 91PP1800, U.S. Army Biomedical Research and Development Laboratory, Fort Detrick, Frederick, MD.

Altfelder S, Streck T, Richter J. 2000. Nonsingular sorption of organic compounds in soil: The role of slow kinetics. *Journal of Environmental Quality*. 29: 917-925.

Anderson SJ, Sposito G. 1991. Cesium-adsorption method for measuring accessible structural surface-charge. *Soil Science Society of America Journal.* 55: 1569-1576.

ARDEC. 2008. US Army RDECOM Armament Research, Development & Engineering Center, AMSRD-AAR-AEE-P, Picatinny Arsenal, NJ.

Barshad I. 1948. Vermiculite and its relation to biotite as revealed by base exchange reactions, x-ray analyses, differential thermal curves, and water content. *American Mineralogist.* 33:655-678.

Benson LV. 1982. A tabulation and evaluation of ion-exchange data on smectites. *Environmental Geology*. 4: 23-29.

Birdwell J, Cook RL, Thibodeaux LJ. 2007. Desorption kinetics of hydrophobic organic chemicals from sediment to water: A review of data and models. *Environmental Toxicology and Chemistry*. 26: 424-434.

Blume HP, Schwertmann U. 1969. Genetic evaluation of profile distribution of aluminium, iron, and manganese oxides. *Soil Science Society of American Journal.* 33: 438-444.

Bouyoucos GJ. 1962. Hydrometer method improved for making particle size analysis of soils. *Agronomy Journal*. 54: 464-465.

Brannon JM, Pennington JC. 2002. Environmental Fate and Transport Process Descriptors for Explosives. U.S. Army Corps of Engineers, ERDC. TR-02-10.

Brodman BW, Lampner N, Eng J. 1982. Hydrogen bonding of dinitrotoluene isomers to unesterified hydroxyl groups in nitrocellulose. *Journal of Applied Polymer Science.* 27: 3621-3623.

Brodman BW, Sipia JA, Schwartz S. 1975. Diffusion of deterrents into a nitrocellulose matrix. An example of diffusion with interaction. *Journal of Applied Polymer Science.* 19: 1905-1909.

Brusseau M, Jessup R, Rao P. 1991. Nonequilibrium sorption of organic chemicals - Elucidation of rate-limiting processes. *Environmental Science & Technology*. 25: 134-142.

Cebula DJ, Ottewill RH. 1981. Neutron-diffraction studies on lithium montmorillonite-water dispersions. *Clays and Clay Minerals.* 29: 73-75.

Chandak MV, Lin YS, Ji W, Higgins RJ. 1998. Sorption and diffusion of volatile organic compounds in polydimethylsiloxane membranes. *Journal of Applied Polymer Science.* 67: 165-175.

Chang ML, Wu SC, Chen CY. 1997. Diffusion of volatile organic compounds in pressed humic acid disks. *Environmental Science & Technology*. 31: 2307-2312.

Chappell MA. 2011. Solid-Phase Considerations for the Environmental Fate of TNT and RDX in Soil Soil and Sediment Geochemistry. Team Lead, Environmental Laboratory, U.S. Army Engineer Research and Development Center, (ERDC), 3909 Halls Ferry Road, Vicksburg, MS.

Charles SM, Teppen BJ, Li H, Boyd SA. 2008. Fractional availability of smectite surfaces in soils for adsorption of nitroaromatic compounds in relation to soil and solute properties. *Soil Science Society of America Journal.* 72: 586-594.

Chemical Properties Database. Groundwater Services, Inc., Houston, TX. 2010. Retrieved from http://www.gsi-net.com/UsefulTools/ChemPropDatabaseHome.asp. (accessed April 2012).

ChemIDPlus Lite, National Library of Medicine, Bethesda, MD. 2006. Retrieved from http://toxnet.nlm.nih.gov. (accessed April 2012).

Chen SH, Nyman MC. 2005. Slow desorption behavior of one highly resistant aromatic amine in Lake Macatawa, Michigan, USA, sediment. *Environmental Toxicology and Chemistry*. 24: 3020-3029.

Chilom G, Rice JA. 2005. Glass transition and crystallite melting in natural organic matter. *Organic Geochemistry*. 36: 1339–1346.

Clausen JL, Scott C, Mulherin N, Bilg S, Gooch G, Douglas T, Osgerby I, Palm B. 2010. Adsorption/desorption measurements of nitroglycerin and dinitrotoluene in Camp Edwards, Massachusetts soil. Final Report ADA520200. U.S. Engineer Research and Development Center Hanover NH. Cold Regions Research and Engineering Lab.

Checkai RT, Major MA, Nwanguma RO, Phillips CT, Sadusky MC. 1993. Transport and fate of nitroaromatic and nitramine explosives in soils from open burning/open detonation operations: Milan Army Ammunition Plant (MAAP). ERDEC-TR-136. Edgewood Research, Development and Engineering Center, Aberdeen Proving Ground, MD.

Coleman NT, Craig D, Lewis RJ. 1963a. Ion-exchange reactions of cesium. *Soil Science Society of America Journal.* 27: 287-289.

Coleman NT, Lewis RJ, Craig D. 1963b. Sorption of cesium by soils and its displacement by salt solutions. *Soil Science Society of America Journal.* 27: 290-294.

Comfort SD, Shea PJ, Hundal LS, Li Z, Woodbury BL, Martin JL, Powers WL. 1995. TNT transport and fate in contaminated soil. *Journal of Environment Quality*. 24:1174-1182.

Cornelissen, G, Rigterink H, Vrind, BA, tenHulscher, TEM, Ferdinandy, MMA, vanNoort, PCM. 1997. Two-stage desorption kinetics and in situ partitioning of hexachlorobenzene and dichlorobenzenes in a contaminated sediment. *Chemosphere*. 35: 2405-2416.

Crank J. 1979. *The Mathematics of Diffusion.* 2nd ed. Clarendon Press, Oxford.

Cuissinat C, Navard P, Heinze T. 2008. Swelling and dissolution of cellulose, Part V: Cellulose derivatives fibres in aqueous systems and ionic liquids. *Cellulose*. 15: 75-80.

Culver TB, Hallisey SP, Sahoo D, Deitsch JJ, Smith JA. 1997. Modeling the desorption of organic contaminants from long-term contaminated soil using distributed mass transfer rates. *Environmental Science & Technology*. 31: 1581-1588.

De Kimpe, ER, Laverdiere MR, Martel YA. 1979. Surface area and exchange capacity of clay in relation to mineralogical composition of gleysolic soils. *Canadian Soil Science Journal*. 59: 341-347.

Del Campillo MC, Torrent J. 1992. A rapid acid-oxalate extraction procedure for the determination of active Fe-oxide forms in calcareous soils. *Angenommen*. 28: 437-440.

Delle SA. 2001. Factors affecting sorption of organic compounds in natural sorbent/water systems and sorption coefficients for selected pollutants. A review. *Journal of Physical and Chemical Reference Data.* 30: 187-439.

Dinelli E, Tateo F, Summa V. 2007. Geochemical and mineralogical proxies for grain size in mudstones and siltstones from the Pleistocene and Holocene of the Po alluvial plain, Italy. *Perspectives from Petrography and Geochemistry.* 420: 25-36.

Di Toro DM. 1985. A particle interaction-model of reversible organic-chemical sorption. *Chemosphere.* 14: 1503-1538.

Di Toro DM. 2013. Site transformation model of adsorption-desorption hysteresis. Abstracts of Papers of the American Chemical Society. 245: Meeting Abstract 77-ENVR.

Di Toro DM, Horzempa LM. 1982. Reversible and resistant components of PCB adsorption desorption - isotherms. *Environmental Science & Technology.* 16: 594-602.

Di Toro DM, Jeris JS, Ciarcia D. 1985. Diffusion and partitioning of hexachlorobiphenyl in sediments. *Environmental Science & Technology*. 19: 1169-1176.

Di Toro DM, Mahony JD, Kirchgraber PR, Obyrne AL, Pasquale LR, Piccirilli DC. 1986. Effects of nonreversibility, particle concentration, and ionic-strength on heavy-metal sorption. *Environmental Science & Technology.* 20: 55-61.

Dontsova KM, Hayes C, Pennington JC, Porter B. 2009a. Sorption of high explosives to water-dispersible clay: influence of organic carbon, aluminosilicate clay, and extractable iron. *Journal of Environmental Quality.* 38: 1458-1465.

Dontsova KM, Pennington JC, Hayes C, Simunek J, Williford CW. 2009b. Dissolution and transport of 2,4-DNT and 2,6-DNT from M1 propellant in soil. *Chemosphere* 77:597-603.

Dontsova KM, Yost SL, Simunek J, Pennington JC, Williford CW. 2006. Dissolution and Transport of TNT, RDX, and Composition B in saturated soil columns. *Journal of Environmental Quality.* 35: 2043–2054.

Douglas TA, Walsh ME, McGrath CJ, Weiss CA, Jaramillo AM, Trainor TP. 2011. Desorption of nitramine and nitroaromatic explosive residues from soils detonated under controlled conditions. *Environmental Toxicology and Chemistry.* 30: 345-353.

Dunn OJ. 1961. Multiple comparisons among means. *Journal of the American Statistical Association* 56: 52-64.

Edwards DG, Posner AM, Quirk JP. 1965. Repulsion of chloride ions by negatively charged clay surfaces .1. Monovalent cation fithian illites. *Transactions of the Faraday Society.* 61: 2808-2815.

Eriksson J, Frankki S, Shchukarev A, Skyllberg U. 2004. Binding of 2,4,6-trinitrotoluene, aniline, and nitrobenzene to dissolved and particulate soil organic matter. *Environmental Science & Technology*. 38: 3074-3080.

Falone SZ, Vieira EM, Onuska FI. 2006. Adsorption study of RDX and TNT explosives in soils by HPLC. *Journal of Liquid Chromatography & Related Technologies*. 29: 1645-1662.

Farrell J, Grassian D, Jones M. 1999 Investigation of mechanisms contributing to slow desorption of hydrophobic organic compounds from mineral solids. *Environmental Science & Technology*. 33: 1237-1243.

Ferris AP and Jepson WP. 1975. The exchange capacities of kaolinite and the preparation of homoionic clays. *Journal of Colloids Interface Science.* 51: 245-259.

Fomba KW, Galvosas P, Roland U, Karger J, Kopinke FD. 2009. New option for characterizing the mobility of organic compounds in humic acids. *Environmental Science & Technology.* 43: 8264-8269.

Gebremariam S.Y, Beutel MW, Flury M, Harsh JB, Yonge DR. 2012. Nonsingular adsorption/desorption of chlorpyrifos in soils and sediments: Experimental results and modeling. *Environmental Science & Technology*. 46: 869-875.

Gong P, Siciliano SD, Greer CW, Paquet L, Hawari J, Sunahara GI. 1999. Effects and bioavailability of 2,4,6-trinitrotoluene in spiked and field-contaminated soils to indigenous microorganisms. *Environmental Toxicology and Chemistry.* 18: 2681-2688.

González Forero R. 2013. Factors Controlling the Reversible and Resistant Adsorption and Desorption of Munitions Constituents on Soils. University of Delaware, Department of Civil and Environmental Engineering. Ph.D. Dissertation.

Haderlein SB, Weissmahr KW, Schwarzenbach RP. 1996. Specific adsorption of nitroaromatic: Explosives and pesticides to clay minerals. *Environmental Science & Technology* 30: 612-622.

Hatzinger PB, Fuller ME, Rungmakol D, Schuster RL, Steffan RJ. 2004. Enhancing the attenuation of explosives in surface soils at military facilities: Sorption-desorption isotherms. *Environmental Toxicology and Chemistry.* 23: 306-312.

Hawari J, Halasz A. 2002. Microbial degradation of explosives, in *The Encyclopedia of Environmental Microbiology*, Bitton G, Ed., John Wiley & Sons Ltd., Amsterdam, Netherlands.

Hewson, RD, Cudahy, TJ, Jones M, Thomas, M. 2012. Investigations into soil composition and texture using infrared spectroscopy (2–14μm). *Applied and Environmental Soil Science.* 2012: 12 p.

Ho YS, McKay G. 1998. A comparison of chemisorption kinetic models applied to pollutant removal on various sorbents. *Process Safety and Environmental Protection*. **76**: 332-340.

HSDB Hazardous Substances Data Bank, National Library of Medicine, Bethesda, MD. 2008. Retrieved from http://toxnet.nlm.nih.gov. (accessed April 2012).

Huang WL, Yu H, Weber WJ. 1998. Hysteresis in the sorption and desorption of hydrophobic organic contaminants by soils and sediments - 1. A comparative analysis of experimental protocols. *Journal of Contaminant Hydrology*. 31: 129-148.

Huang WL, Weber WJ, A distributed reactivity model for sorption by soils and sediments .10. Relationships between desorption, hysteresis, and the chemical characteristics of organic domains. *Environmental Science & Technology*. 31: 2562-2569.

Jenkins TF, Grant CL, Brar GS, Thorne PG, Schumacher PW, Ranney TA. 1997. Sampling error associated with collection and analysis of soil samples at TNT-contaminated sites. *Field Analytical Chemistry and Technology.* 1: 151-163.

Johnston CT, De Oliveira MF, Teppen BJ, Sheng GY, Boyd SA. 2001. Spectroscopic study of nitroaromatic-smectite sorption mechanisms. *Environmental Science & Technology.* 35: 4767-4772.

Johnson OH, 1956. HMX as a Military Explosive. Technical Report AD114067. U.S. Naval Ordnance Laboratory. White Oak, MD.

Kan AT, Fu G, Hunter M, Chen W, Ward CH, Tomson MB. 1998. Irreversible sorption of neutral hydrocarbons to sediments: Experimental observations and model predictions. *Environmental Science & Technology*. 32: 892-902.

Kaplan DL, Kaplan AM. 1982. 2,4,6-Trinitrotoluene surfactant complexes - decomposition, mutagenicity, and soil leaching studies. *Environmental Science & Technology.* 16: 566-571.

Karickhoff SW, Brown DS, Scott TA. 1979. Sorption of hydrophobic pollutants on natural sediments. *Water Research.* 13: 241-248.

Karickhoff, SW, Morris KR. 1985. Sorption dynamics of hydrophobic pollutants in sediment suspensions. *Environmental Toxicology and Chemistry*. 4: 469-479.

Keng JKC, Uehara G. 1973. Chemistry, mineralogy, and taxonomy of oxisols and ultisols. *Soil & Crop Science Society* of *Florida.* 33: 119–126.

Kim JY, Park JK, Edil TB. 1997. Sorption of organic compounds in the aqueous phase onto tire rubber. *Journal of Environmental Engineering.* 123: 827–835.

Kuo DTF, Adams RG, Rudnick SM, Chen RF, Gschwend PM. 2007. Investigating desorption of native pyrene from sediment on minute- to month-timescales by time-gated fluorescence spectroscopy. *Environmental Science & Technology.* 41: 7752–7758.

Lambooy AM. 1984. Relationship between cation exchange capacity, clay size particle and water retention of Highveld soils. *South African Journal of Plant and Soil.* 1: 33-38.

Lapakko KA, Haub J, Antonson DA. 1998. Effect of dissolution time and particle size on kinetic test results. *Society for Mining, Metallurgy, and Exploration, SME*. Littleton, CO, preprint 98-114.

Larson SL, Martin WA, Escalon BL, Thompson M. 2008. Dissolution, sorption, and kinetics involved in systems containing explosives, water, and soil. *Environmental Science & Technology.* 42: 786-792.

Lesan HM, Bhandari A. 2003. Atrazine sorption on surface soils: Time-dependent phase distribution and apparent desorption hysteresis. *Water Research*. 37: 1644-1654.

Lu YF, Pignatello JJ. 2002. Demonstration of the "Conditioning effect" in soil organic matter in support of a pore deformation mechanism for sorption hysteresis. *Environmental Science & Technology*. 36: 4553-4561.

Martel YA, De Kimpe ER, Laverdiere MR. 1978. Cation-exchange capacity of clay-rich soils in relation to organic matter, mineral composition and surface area. *Soil Science Society of American Journal.* 42: 764-767.

McKeague JA, Day JH. 1993. Ammonium oxalate extraction. p. 241. *In* M.R. Carter (ed.) *Soil sampling and methods of analysis.* Lewis Publishers, Boca Raton, FL.

Michalkova A, Szymczak JJ, Leszczynski J. 2005. Adsorption of 2,4-dinitrotoluene on dickite: The role of H-bonding. *Structural Chemistry.* 16: 325-337.

Miller WF. 1970. Inter-regional predictability of cation-exchange capacity by multiple regression. *Plant and Soil*. 33: 721-725.

Monteil-Rivera F, Groom C, Hawari J. 2003. Sorption and degradation of octahydro-1,3,5,7-tetranitro-1,3,5,7-tetrazocine in soil. *Environmental Science & Technology.* 37: 3878-3884.

Monteil-Rivera F, Paquet L, Deschamps S, Balakrishnan VK, Beaulieu C, Hawari J. 2004. Physico-chemical measurements of CL-20 for environmental applications. Comparison with RDX and HMX. *Journal of Chromatography A*. 1025: 125-132.

Monteil-Rivera F, Radovic-Hrapovic Z, Halasz A, Paquet L, Ampleman G, Thiboutot S, Hawari J. 2011. Environmental Fate of Triethylene Glycol Dinitrate. *Environmental Engineering Science*. 28: 71-79.

Morkeh J, McClemore VT. 2012. The effect of particle size fractions on chemistry, mineralogy, and acid potential of the Questa Rock Piles, Taos County, New Mexico. Open-file Report 545. Questa Rock Pile Weathering and Stability Project. Socorro, New Mexico 87801.

Morley MC, Henke JL, Speitel GE. 2005. Adsorption of RDX and HMX in rapid small-scale column tests: Implications for full-scale adsorbers. *Journal of Environmental Engineering-ASCE.* 131: 29-37.

Nam K, Chung N, Alexander M. 1998. Relationship between organic matter content of soil and the sequestration of phenanthrene. *Environmental Science & Technology*. 32: 3785-3788.

Nefso EK, Burns SE, McGrath CJ. 2005. Degradation kinetics of TNT in the presence of six mineral surfaces and ferrous iron. *Journal of Hazardous Materials*. 123: 79-88.

Ortiz E, Kraatz M, Luthy RG. 1999. Organic phase resistance to dissolution of polycyclic aromatic hydrocarbon compounds. *Environmental Science & Technology.* 33: 235–242.

Palomo M, Bhandari A. 2006. Impact of aging on the formation of bound residues after peroxidase-mediated treatment of 2,4-DCP contaminated soils. *Environmental Science & Technology.* 40: 3402-3408.

Pennington JC. 2002. Distribution and Fate of Energetics on DoD Test and Training Ranges: Interim Report 2, ERDC TR-02-08. Engineer Research and Development Center, prepared for US Army Corps of Engineers, Washington, DC.

Pennington JC, Brannon JM, Berry TE, Jenkins TF, Miyares PH, Walsh ME, Hewitt AD, Perron N, Ranney TA, Lynch J, Delfino JJ, Hayes CA. 2001. Distribution and fate of energetics on DoD test and training ranges: Interim report 1. U.S. Army Engineer Research and Development Center, ERDC TR-01-13-1. Army Corps of Engineers, Waterways Experiment Station, Vicksburg, MS.

Pennington JC, Jenkins TF, Ampleman G, Thiboutot S, Brannon JM, Hewitt AD, Lewis J, Brochu S, Diaz E, Walsh MR, Walsh ME, Taylor S, Lynch JC, Clausen J, Ranney TA, Ramsey CA, Hayes CA, Grant CL, Collins CM, Bigi SR, Yost S, Dontsova K. 2006. Distribution and fate of energetics on DoD test and training ranges: Final report. U.S. Army Engineer Research and Deveopment Center, Environmental Laboratory, ERDC/EL TR-06-13. Army Corps of Engineers, Waterways Experiment Station, Vicksburg, MS.

Pennington JC, Patrick WH. 1990. Adsorption and desorption of 2,4,6-trinitrotoluene by soils. *Journal of Environmental Quality*. 19: 559–567.

Pennington JC, Thorn KA, Hayes CA, Porter BE, Kennedy KR. 2003. Immobilization of 2,4- and 2,6- Dinitrotoluenes in Soils and Compost. Technical Report ERDC/EL. TR-03-2. U.S. Army Corps of Engineers, Waterways Experiment Station, Vicksburg, MS.

Pignatello JJ. 2000. The measurement and interpretation of sorption and desorption rates for organic compounds in soil media. *Advances in Agronomy*. 69: 1-73.

Pignatello, JJ and Xing B. 1996. Mechanisms of slow sorption of organic chemicals to natural particles. *Environmental Science & Technology*. 30: 1-11.

Posner AM, Quirk JP. 1964. The adsorption of water from concentrated electrolyte solutions by montmorillonite and illite. *Proceedings of the Royal Society.* 278: 35-56.

Rashidi M, Seilsepour M. 2008. Modeling of soil cation exchange capacity based on soil organic carbon. *Journal of Agricultural and Biological Science*. 3: 1-5.

R Core Team. 2013. *R: A Language and Environment for Statistical Computing*. R Foundation for Statistical Computing, Vienna, Austria.

R Core Team. 2014. *R: A Language and Environment for Statistical Computing*. R Foundation for Statistical Computing, Vienna, Austria.

Roberts MG, Rugh CL, Li H, Teppen BJ, Boyd SA. 2007. Reducing bioavailability and phytotoxicity of 2,4-dinitrotoluene by sorption on K-smectite clay. *Environmental Toxicology and Chemistry.* 26: 358-360.

Robidoux PY, Hawari J, Thiboutot S, Ampleman G, Sunahara GI. 2001. Chronic toxicity of octahydro-1,3,5,7-tetranitro-1,3,5,7-tetrazocine (HMX) in soil determined using the earthworm (Eisenia andrei) reproduction test. *Environmental Pollution* 111: 283-292.

Sabbah I, Ball, WP, Young, DF, Bouwer EJ. 2005. Misinterpretations in the modeling of contaminant desorption from environmental solids when equilibrium conditions are not fully understood. *Environmental Engineering Science*. 22: 350-366.

Sander M, Lu YF, Pignatello JJ. 2006. Conditioning-annealing studies of natural organic matter solids linking irreversible sorption to irreversible structural expansion. *Environmental Science & Technology*, 40: 170–178.

Sander M, Pignatello JJ. 2005. An isotope exchange technique to assess mechanisms of sorption hysteresis applied to naphthalene in kerogenous organic matter. *Environmental Science & Technology*. 39: 7476-7484.

Sander M, Pignatello JJ. 2009. Sorption irreversibility of 1,4-dichlorobenzene in two natural organic matter-rich geosorbents. *Environmental Toxicology and Chemistry*. 28: 447-457.

Schultz RK, Overstreet R, Barshad I. 1960. On the soil chemistry of cesium^{137}. *Soil Science.* 89: 16-27.

Schwarzenbach RP, Gschwend PM, Imboden DM. 2003. *Environmental Organic Chemistry*. John Wiley & Sons, Hoboken, NJ.

Schwertmann U. 1964. Differenzierung der eisenoxide des bodens durch extraktion mit ammoniumoxalat-losung. *Zeitschrift für Pflanzenernahrung und Bodenkunde*. 105: 194-202.

Schwertmann, U. 1973. Use of oxalate for Fe extraction from soils. *Canadian Journal of Soil Science.* 53: 244-246.

Sheng GY, Johnston CT, Teppen BJ, Boyd SA. 2001. Potential contributions of smectite clays and organic matter to pesticide retention in soils. *Journal of Agricultural and Food Chemistry.* 49: 2899-2907.

Sheremata TW, Halasz A, Paquet L, Thiboutot S, Ampleman G, Hawari J. 2001. The fate of the cyclic nitramine explosive RDX in natural soil. *Environmental Science & Technology.* 35: 1037-1040.

Siciliano SD, Roy R, Greer CW. 2000. Reduction in denitrification activity in field soils exposed to long term contamination by 2,4,6-trinitrotoluene (TNT). *Fems Microbiology Ecology.* 32: 61-68.

Singh N, Berns AE, Hennecke D, Hoerner J, Koerdel W, Schaeffer A. 2010. Effect of soil organic matter chemistry on sorption of trinitrotoluene and 2,4-dinitrotoluene. *Journal of Hazardous Materials.* 173: 343-348.

Soil Colloids Course. University of Tennessee. 2007. Retrieved from http://web.utk.edu/~drtd0c/Soil%20Colloids.pdf. (accessed October 2013).

Sparks DL. 2003. *Environmental Soil Chemistry,* Academic Press, San Diego, CA.

Sunahara GI, Lotufo G, Kuperman RG, Hawari J. 2009. *Ecotoxicology of Explosives*. CRC Press, Boca Raton, FL.

Taylor S, Dontsova K, Bigl S, Richardson C, Lever J, Pitt J, Bradley JP, Walsh M, Simunek J. 2012. Dissolution Rate of Propellant Energetics from Nitrocellulose Matrices. U.S. Army Engineer Research and Development Center, ERDC TR-12-9.

Thiboutot S, Ampleman G, Lewis J, Faucher D, Marois A, Martel R, Ballard JM, Jenkins T, Hewitt A. 2003. Environmental Conditions of Surface Soils and Biomass Prevailing in the Training Area at CFB Gagetown, New Brunswick, Report DRDC-TR 2003-152, Valcartier, PQ.

U.S. EPA (Environmental Protection Agency). 2006. Nitroaromatics, Nitramines and Nitrate Esters by High Performance Liquid Chromatography (HPLC). Method 8330B. SW846. Office of Solid Waste, Washington, DC.

US EPA (Environmental Protection Agency). 2008. Fate, Transport and Transformation Test Guidelines: OPPTS.835.1230. Adsorption/Desorption (Batch Equilibrium). United States Environmental Protection Agency, Washington, DC. EPA 712-C-08-009. Available at http://www.epa.gov/nscep/.

U.S. General Accounting Office. 2003. Military Munitions: DOD Needs to Develop a Comprehensive Approach for Cleaning Up Contaminated Sites. Report to the Honorable John D. Dingell Ranking Minority Member, Committee on Energy and Commerce, House of Representatives. GAO-04-147, December 2003.

van Beinum W, Beulke S, Brown CD. 2006. Pesticide sorption and desorption by lignin described by an intraparticle diffusion model. *Environmental Science & Technology*. 40: 494-500.

Van Loon LR, Baeyens B, Bradbury MH. 2009. The sorption behaviour of caesium on Opalinus clay: A comparison between intact and crushed material. *Applied Geochemistry.* 24: 999-1004.

Walpole RE, R. Myers RH, Myers SL, Ye K. 2007. *Probability and Statistics for Engineers and Scientists*, Pearson Prentice Hall.

Wang Z, Chen S, Xu Y, Tang J. 2012. Aging effects on sorption-desorption behaviors of PAHs in different natural organic matters. *Journal of Colloid and Interface Science*. 382: 117-122.

Wanner H, Albinsson Y, Wieland E. 1996. A thermodynamic surface model for caesium sorption on bentonite. *Fresenius Journal of Analytical Chemistry.* 354: 763-769.

Weber W, McGinley P, Katz L. 1992. A distributed reactivity model for sorption by soils and sediments .1. Conceptual basis and equilibrium assessments. *Environmental Science & Technology*. 26: 1955-1962.

Weber WJ Jr, Huang W, Yu H. 1998. Hysteresis in the sorption and desorption of hydrophobic organic contaminants by soils and sediments: 2. Effects of soil organic matter heterogeneity. *Journal of Contaminant Hydrology*. 31: 149–165.

Weiss CA, Kirkpatrick RJ, Altaner SP. 1990. The structural environments of cations adsorbed onto clays: ^{133}Cs variable- temperature MAS NMR spectroscopic study of hectorite. *Geochimica et Cosmochimica Acta* 54:1655-1669.

Weissmahr KW, Haderlein SB, Schwarzenbach RP, Haderlein SB. 1998. Complex formation of soil minerals with nitroaromatic explosives and other pi-acceptors. *Soil Science Society of America Journal.* 62: 369-378.

White JD, Akin FA, Oser H, Crosley DR. 2011. Production of the NO photofragment in the desorption of RDX and HMX from surfaces. *Applied Optics.* 50: 74-81.

Wicke D, Bockelmann U, Reemtsma T. 2008. Environmental influences on the partitioning and diffusion of hydrophobic organic contaminants in microbial biofilms. *Environmental Science & Technology.* 42: 1990-1996.

Winkler DA, Starks A. 1988. The non-Fickian diffusion of deterrents into a nitrocellulose-based propellant. *Journal of Applied Polymer Science* 35: 51–62.

Wu SC, Gschwend PM. 1986. Sorption kinetics of hydrophobic organic-compounds to natural sediments and soils. *Environmental Science & Technology*. 20: 717-725.

Xue SK, Iskandar IK, Selim HM. 1995. Adsorption-desorption of 2,4,6-trinitrotoluene and hexahydro-1,3,5-trinitro-1,3,5-triazine in soils. *Soil Science.* 160: 317-327.

Yamamoto H, Morley MC, Speitel GE, Clausen J. 2004. Fate and transport of high explosives in a sandy soil: Adsorption and desorption. *Soil & Sediment Contamination* 13: 459-477.

Yang WC, Duan L, Zhang N, Zhang CD, Shipley HJ, Kan AT, Tomson MB, Chen W. 2008. Resistant desorption of hydrophobic organic contaminants in typical Chinese soils: Implications for long-term fate and soil quality standards. *Environmental Toxicology and Chemistry*. 27: 235-242.

You SJ, Yin Y, Allen HE. 1999. Partitioning of organic matter in soils: effects of pH and water/soil ratio. *The Science of the Total Environment.* 227: 155-160.

Young DF, Ball WP. 1999. Two-region linear/nonlinear sorption modeling: Batch and column experiments. *Environmental Toxicology and Chemistry*. 18: 1686-1693.

Zhang DM, Zhu DQ, Chen W. 2009. Sorption of nitroaromatics to soils: Comparison of the importance of soil organic matter versus clay. *Environmental Toxicology and Chemistry.* 28: 1447-1454.

Zhu HW, Wang YJ, Zhou J, Jiang J, Li CB, Zhou DM, Friedman P. 2009. Wien effect characterization of interactions between ions and charged sites on clay surfaces of variable-charge soils. *Pedosphere.* 19: 545–553.

Zubkov MY. 2008. Assessment of clay content from the analysis of K, U, and Th distribution in different grain-size fractions of the productive sediments of the Lovin Field, Western Siberia. *Geochemistry International.* 46: 465–481.

Appendix I – List of Scientific/Technical Publications

Scientific Publications

Gonzalez, R., Michelson, K., Di Toro, D.M., Allen, H.E. Modeling the Time Variable Reversible and Resistant Components of Munitions Constituents of Adsorption and Desorption on Soils. Water, Air, and Soil Pollution (in review).

González-Forero, R. Partitioning model of the adsorption of explosives from soils to determine its environmental fate. Revista Criminalidad, 56 (3): 139-152.

Di Toro, D.M. Site Transformation Model of Sorption Hysteresis. Environmental Science & Technology (in review).

Theses

González Forero, R. (2013) Factors Controlling the Reversible and Resistant Adsorption and Desorption of Munitions Constituents on Soils. University of Delaware, Department of Civil and Environmental Engineering. Ph.D. Dissertation.

Michelson, K.E. (2011) Application of the Reversible / Resistant Model to Explosives Sorption in Natural Soils. University of Delaware, Department of Civil and Environmental Engineering. M.S. Thesis.

Miglino, A. (2015) Modeling the Adsorption and Desorption of Munition Constituents on Soils using Reversible and Resistant Components. University of Delaware, Department of Civil and Environmental Engineering. Ph.D. Dissertation.

Presentations (Oral and Poster)

Allen, H.E., Di Toro, D.M. Checkai, R.T., Kuperman, R.G., Simini, M., Phillips, C., Hawari, J., Gonzalez, R., Michelson, K., Improving the Understanding of the Fate and Transport of Munitions Constituents to Enhance Sustainability of Operational Ranges, Partners in Environmental Technology Technical Symposium & Workshop, Washington, DC. 2009.

Allen, H.E., Di Toro, D.M. Checkai, R.T., Kuperman, R.G., Simini, M., Phillips, C., Hawari, J., Gonzalez, R., Michelson, K., Miglino, A., Daviau, C. Reversibility and Resistance to Sorption of Munitions Constituents onto Soil, Partners in Environmental Technology Technical Symposium & Workshop, Washington, DC. 2010.

Di Toro, D.M., Predicting Chemical Partitioning to Natural Organic Matter Using Organic Matter Molecular Structure, Colby College Chemistry Department, Waterville ME, March 15, 2011.

Di Toro, D.M., A Site Transformation Model of Adsorption-Desorption Hysteresis. Society for Environmental Toxicology and Chemistry, Boston, November 2011.

Di Toro, D.M., Predicting Chemical Partitioning to Natural Organic Matter Using Organic Matter Molecular Structure, 243rd ACS National Meeting, March 2012.

Di Toro, D.M. 2013. Site Transformation Model of Adsorption-Desorption Hysteresis. 245th ACS National Meeting, March 2013.

Gonzalez, R., Di Toro, D.M., Allen, H.E. Effect of Electrolyte on the Resistance to Desorption

of Munitions Constituents from Soils with a Wide Range of Soil Properties. The 2011 SERDP Partners in Environmental Technology Technical Symposium & Workshop, Washington, DC. 29-Nov to 01-Dec 2011. (published abstract T-349)

Gonzalez, R., Michelson, K., Di Toro, D.M., Allen, H.E. Effect of Kinetics on the Resistance to Desorption of Munitions Constituents (MC) from Soil. Society for Environmental Toxicology and Chemistry, Boston, November 2011.

Gonzalez, R., Miglino, A., Di Toro, D.M., Allen, H.E. Understanding Partitioning of Munitions Constituents to Soil. 3rd International Congress of Environment, Xi'an, China, September 27, 2013.

Gonzalez, R., Di Toro, D.M., Allen, H.E. Sorption of Munitions Constituents by Soil. Society of Environmental Toxicology and Chemistry (SETAC) North America 33nd Annual Meeting, Long Beach, CA. November 12, 2012

Gonzalez, R., Miglino, A., Di Toro, D.M., Allen, H.E. Partitioning of Munitions Constituents to Soil. American Chemical Society. New Orleans. April 7, 2013.

Gonzalez, R., Miglino, A., Di Toro, D.M., Allen, H.E. Factors Controlling Partitioning of Munitions Constituents to Soil. Joint Army-Navy-NASA-Air Force (JANNAF) Meeting. Charleston, SC. May 19-23, 2014.

Miligno A., Gonzalez, R., Michelson, K., Allen, H.E., Di Toro, D.M. A Kinetic Model for Munitions Constituents Adsorption and Desorption. Society for Environmental Toxicology and Chemistry, Boston, November 2011.

Miglino, M., Gonzalez, R., Allen, H.E., Di Toro, D.M., Modeling Adsorption and Desorption Partitioning of Munitions Constituents to Soil. Society of Environmental Toxicology and Chemistry 33rd Annual Meeting, Long Beach, CA, November 2012.

Miglino A., Gonzalez, R., Allen, H.E., Di Toro, D.M. Prediction of Adsorption and Hysteretic Desorption Isotherms for Munition Constituents on Soils. Society of Environmental Toxicology and Chemistry 35th Annual Meeting, Vancouver, BC, 9-13 November 2014 (published abstract).

Simini, M., Minyard, M., Checkai, R.T., Kuperman, R.T., Allen, H.E., Di Toro, D.M. 2011. Diffusion Kinetics of Lithium Bromide Tracer Into And Out of Nitrocellulose: A Distinguishing-Model for Nitroglycerin and 2,4-Dinitrotoluene. Partners in Environmental Technology Technical Symposium & Workshop, Washington, DC, 29 November - 1 December, 2011 (published abstract).

Simini, M., Minyard, M., Checkai, R.T., Kuperman, R.T., Allen, H.E., Di Toro, D.M. 2011. Determining Diffusion Kinetics of Lithium Bromide Tracer into Nitrocellulose as a Distinguishing-Model for Nitroglycerin and 2,4-Dinitrotoluene. Society of Environmental Toxicology and Chemistry 32nd Annual Meeting, Boston, MA, 13-17 November 2011 (published abstract).

Simini, M., Checkai, R.T., Gonzalez, R., Kuo, D., Allen, H., and Di Toro, D.M. 2014. Fate and Transport of RDX and TNT in Soils – Initial Validation of Predictive Model. Society of Environmental Toxicology and Chemistry 35th Annual Meeting, Vancouver, BC, 9-13 November 2014 (published abstract).

Appendix II – Supporting Data